Alkane Metathesis via Tandem Catalysis

Zheng Huang

A dissertation submitted to the faculty of the University of North Carolina at Chapel Hill in partial fulfillment of the requirements for the degree of Doctor of Philosophy in the Department of Chemistry

Chapel Hill

2009

Approved by:

Advisor: Professor M. S. Brookhart

Reader: Professor J. L. Templeton

Reader: Professor M. R. Gagné

Professor J. S. Johnson

Professor E. J. Alexanian

ABSTRACT

Zheng Huang: Alkane Metathesis via Tandem Catalysis
(Under the direction of Professor Maurice Brookhart)

Alkane metathesis (AM) has potentially tremendous applicability via converting low-value alkanes (C_3-C_9) from the Fisher-Tropsch process into linear alkanes in the diesel fuel range (C_{10}-C_{19}). A well-defined and highly efficient tandem catalytic system for the metathesis of n-alkanes has been developed. The system is comprised of one pincer Ir catalyst that effects alkane dehydrogenation and olefin hydrogenation, and a second catalyst for olefin metathesis. The catalytic system shows complete selectivity for linear alkane products.

Chapter 2 presents the mechanistic studies of AM. The (^{t}Bu-PCP)Ir [^{t}Bu-PCP = $C_6H_3(CH_2P^tBu_2)_2$-1,3] system shows higher product selectivity than the (^{t}Bu-POCOP)Ir [^{t}Bu-POCOP = $C_6H_3(OP^tBu_2)_2$-1,3] system because of the different resting states under AM. Both of steric and electronic factors favor the formation of (^{t}Bu-PCP)IrH$_2$ and (^{t}Bu-POCOP)Ir-olefin as the catalytic resting states. Experimental evidence and DFT calculations suggest that olefin isomerization by the Ir complex occurs from a (pincer)Ir(I)-olefin complex via formation of a (pincer)Ir(III)(allyl)(H) intermediate, not via a (pincer)Ir(H)$_2$(olefin) intermediate.

Syntheses of eight new Ir pincer complexes for transfer dehydrogenation and alkane metathesis are outlined in chapter 3. Among these iridium complexes, the least bulky,

(^{i}Pr-POCOP)Ir-C$_2$H$_4$, exhibits the highest activity in both transfer dehydrogenation and alkane metathesis. Compared to the parent (^{t}Bu-POCOP)Ir-C$_2$H$_4$, the sterically more hindered complex (^{t}Bu-PSCOP)Ir-C$_2$H$_4$ shows lower transfer dehydrogenation and alkane metathesis activity, but the product selectivity in alkane metathesis was improved as a result of a dihydride resting state ((^{t}Bu-PSCOP)Ir-H$_2$).

Chapters 4 and 5 describe the synthesis of alumina-supported Ir pincer complexes which are recyclable and highly active in transfer dehydrogenation reactions. In addition, use of this supported catalyst in combination with Re$_2$O$_7$/Al$_2$O$_3$ or MoO$_3$/CoO/Al$_2$O$_3$ catalyst provides an efficient alkane metathesis catalytic system in which both catalytic components are heterogeneous.

Chapter 6 presents a series of unprecedented single-crystal-to-single-crystal transformations involving interchange of multiple small gaseous ligands (N$_2$, CO, NH$_3$, C$_2$H$_4$, H$_2$, O$_2$) at an iridium center of a pincer iridium(I) complex. The single crystal remains intact during these ligand exchange reactions which occur *within* the crystal and do not require prior ligand extrusion. Single crystals bearing nitrogen, ethylene or hydrogen exhibit highly selective hydrogenation of ethylene relative to propylene (25:1) when surface sites are passified by CO.

ACKNOWLEDGMENTS

The faculty and staff in the chemistry department are great. I would like to acknowledge Dr. Joe Templeton, Dr. Mike Gagne, Dr. Wenbin Lin, Dr. Jeff Johnson, Dr. Erik Alexanian, and Dr. James Morken who served on my committee at some point in my career at UNC. Joe, your jokes and big smile made me not so nervous about my presentations and defenses. I would like to thank Dr. Peter White for solving numerous difficult single crystal structures. I would like to acknowledge our secretary Ann for all the things that she has helped me out. I would also like to acknowledge Dr. Marc ter Horst and Dr. David Harris for helping me with NMR experiments, and Mr. Walt Boger for constructing a "two-pot" glass device for my reactions.

I would like to thank my family, my parents and my sisters for their continue support throughout my undergraduate and postgraduate years. I feel so fortunate that I have such understanding and supportive families. I am really grateful to my parents and brother in law. Xiaofang and I have been so far way from you (on the other side of the Pacific Ocean) during my Ph.D study. I know this is very difficult for you.

Finally, a special thanks to my wife, Xiaofang. Thank you for sacrificing so much to be with me during these years. I guess you have to move with me at least two more times. The next stop is Urban & Champaign in Illinois, and I hope I can let you know the place after that soon☺

To Xiaofang

TABLE OF CONTENTS

LIST OF TABLES

LIST OF SCHEMES

LIST OF FIGURES

LIST OF ABBREVIATIONS AND SYMBOLS

°C	degrees Celsius
δ	chemical shift
ΔG	change in Gibbs' free energy
μ	bridging
ν	frequency, in hertz
AM	alkane metathesis
Ar	$1,3,5\text{-}(CF_3)_3C_6H_2$
atm	atmosphere
d	doublet
DFT	density functional theory
eq	equation
equiv	equivalents
g	grams
GC	gas chromatography
h	hours
Hz	hertz
^{i}Pr	isopropyl, $\text{-}CH(CH_3)_2$
J	scalar coupling constant, in Hz
k	rate constant
kcal	kilocalorie
M	molar (moles solute/liter solution)

m	multiplet
Me	methyl, CH_3
mL	milliliter
mol	moles
MW	molecular weight
NMR	nuclear magnetic resonance
ppm	parts per million
q	quartet
RT	room temperature
s	singlet (used in NMR data)
sep	septet
t	triplet
TD	transfer dehydrogenation
TONs	turnover numbers
^tBu	tertiary butyl, $-C(CH_3)_3$

CHAPTER ONE

Alkane Metathesis by Tandem Catalysis:

Introduction and Initial Results

Introduction

The interconversion of alkanes via alkane metathesis (Eq 1) is a reaction with enormous potential applicability.

$$H_3C\text{-}(CH_2)_n\text{-}CH_3 \ + \ H_3C\text{-}(CH_2)_m\text{-}CH_3 \ \rightarrow \ H_3C\text{-}(CH_2)_{m+n-x}\text{-}CH_3 + \ H_3C\text{-}(CH_2)_x\text{-}CH_3 \quad (Eq\ 1)$$
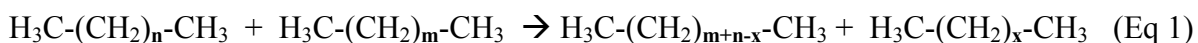
Alkanes are the major constituents of petroleum. As oil reserves dwindle, application of the Fischer-Tropsch (F-T) process to produce synthetic petroleum will likely become increasingly important. The feedstock of the F-T process, syngas (a mixture of carbon monoxide and hydrogen), can be derived from various carbon sources including coal, natural gas, shale oil and biomass. Conversion of coal to liquid hydrocarbons is of current interest

due to the world's vast coal reserves.[1] Production of diesel fuel using the F-T process is attractive since it is highly paraffinic with very low sulphur content (< 1ppm) and thus burns more cleanly than oil-based diesel.[2,3] Furthermore, diesel engines run ~30% more efficiently than gasoline engines.

Though F-T technology has been in use for nearly a century, diesel production is still limited due to its high cost. A major problem is that the F-T process yields alkane mixtures with no molecular weight (MW) control and only linear hydrocarbons in the C_9–C_{19} range are useful as diesel fuel. *n*-Alkanes lower than ca. C_9, however, suffer from high volatility and lower ignition quality (cetane number).[4] In addition to F-T product mixtures, low-carbon number, low-MW alkanes are also major constituents of a variety of refinery and petrochemical streams. Heavy hydrocarbons can (unselectively) be broken into liquid alkanes via the hydrocracking process. Unfortunately, there is no practical method to upgrade the low-MW alkanes to transportation fuel. Alkane metathesis (AM) can potentially be employed to selectively convert low-MW hydrocarbons into diesel and thus improve the diesel yields via F-T synthesis.

Two examples of AM have been previously reported. In 1971, Burnett and Hughes[5] showed that passage of *n*-butane over a mixture of an alumina-supported platinum (a hydrogen transfer catalyst) and a silica-supported WO_3 (an olefin metathesis catalyst) resulted in the formation of hydrocarbons in the C_1–C_{8+} range with propane and pentane as the major products (25 wt% and 16 wt%, respectively). The process operated at high temperature (399 °C), resulting in poor product selectivity. Methane, branched hydrocarbons, and olefins were produced in addition to the linear alkanes. The yield of the process was good (62 wt %), but the alumina-supported platinum catalyst is sensitive to impurities. More

recently, Basset *et al.*[6-9] reported single component Ta or W catalysts for AM which function at much lower temperatures. For example, propane can be converted at 150 °C to a mixture of C_1 to C_6 alkanes in 18% yield (121 turnovers, 120 h) by using an alumina-supported W hydride catalyst.[7] These systems are proposed to operate via the reaction of metal with alkanes to form alkylidene complexes and olefins.[9] As a result, both branched and linear hydrocarbons, as well as methane, are generated.

In this study, we report a tandem system in which the metathesis of *n*-alkanes is achieved efficiently with complete selectivity for linear alkanes at moderate temperatures. The basic tandem catalytic process is outlined in Fig. 1.1 for metathesis of *n*-hexane, to give ethane and *n*-decane. A dehydrogenation catalyst, M, reacts with hexane to give 1-hexene and MH_2. Olefin metathesis of 1-hexene generates ethylene and 5-decene. The alkenes thus produced serve as hydrogen acceptors and generate ethane and *n*-decane via reaction with MH_2, regenerating M and closing the catalytic cycle. The transfer dehydrogenation catalysts chosen for investigation were Ir-based pincer complexes, first reported by Jensen and Kaska[10,11] and explored extensively in these laboratories.[12-16] Complexes **1a**, **2a** and **2b** were employed in this study (Fig. 1.2). These systems exhibit high stability, but activity is inhibited by build-up of even moderate concentrations of alkene product. The dual catalytic system as envisioned in Fig. 1.1 would require only a very low steady-state concentration of alkenes during catalysis; thus, inhibition of catalysis by product could be avoided. Numerous olefin metathesis catalysts are available;[17-19] for studies in homogeneous systems, the Schrock-type catalyst, **3**, was initially examined.[20-21]
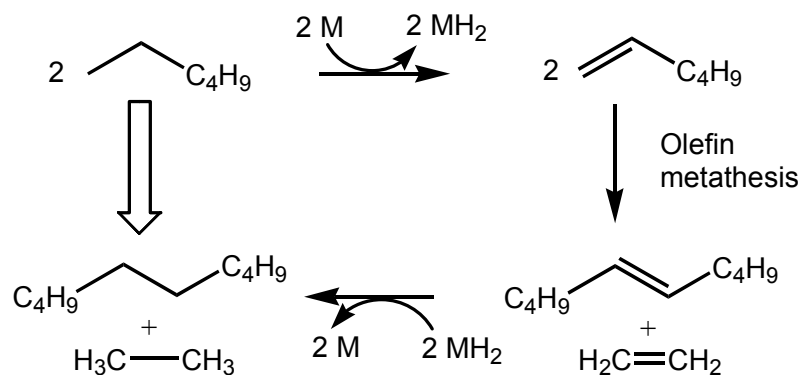
Fig. 1.1 Alkane metathesis via tandem transfer dehydrogenation/olefin metathesis illustrated with the formation and metathesis of two mol 1-hexene. M = active fragment in the transfer-dehydrogenation cycle (e.g. (pincer)Ir).

1a-C$_2$H$_4$ L = C$_2$H$_4$
1a-H$_2$ L = H$_2$

2a: R= ^{t}Bu, X = H
2b: R= ^{i}Pr, X = OMe
L = H$_2$ or/and H$_4$

3
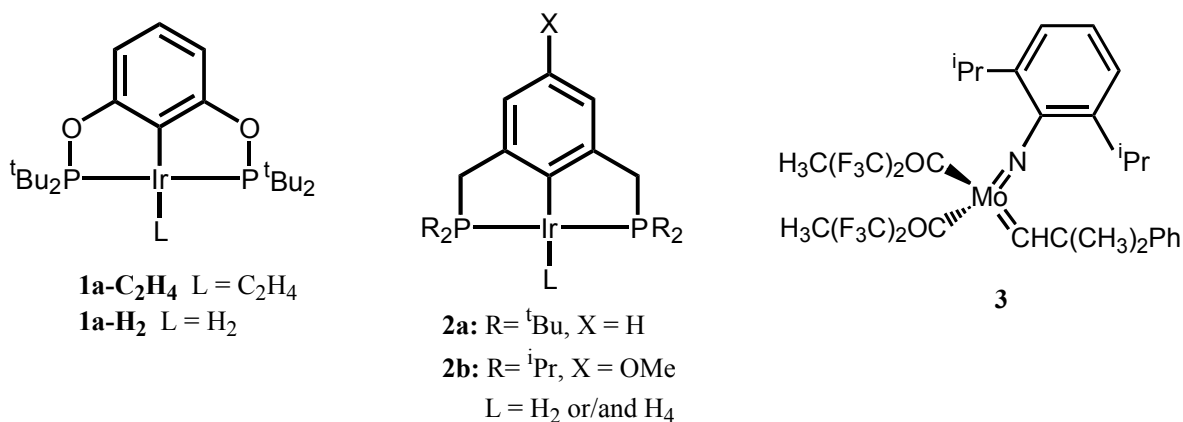
Fig. 1.2 Dehydrogenation catalysts (R-PCP)IrL and (^{t}Bu-POCOP)IrL; and Schrock-type metathesis catalyst, **3**.

Results and Discussion

Initial experiments employing the combination of **3** with Ir-based dehydrogenation catalysts in solution proved successful. Heating an *n*-hexane solution at 125 °C under argon in a sealed glass vessel containing 10 mM dehydrogenation-catalyst precursor **1a-C$_2$H$_4$** (0.14 mol% relative to hexane) and 16 mM Schrock catalyst **3,** for 24 h, converts ca. 135 equivalents (relative to Ir) of *n*-hexane to a range of C$_2$ to C$_{15}$ *n*-alkanes. No branched or cyclic alkanes were detected. Products were monitored by gas chromatography (GC) using

mesitylene as an internal standard. Major amounts of products lie in the C_2-C_5 and C_7-C_{10} range. Results are summarized in Table 1.1, entry 1. Heating for longer times results in few additional turnovers. However, upon addition of additional olefin metathesis catalyst **3**, alkane metathesis catalysis reinitiated, indicating that decomposition of **3** is responsible for deactivation of the system under these conditions. Using **1a-H₂** and 2 equiv *tert*-butylethylene (TBE) as a hydrogen-acceptor, along with catalyst **3**, similar results were obtained and are summarized in entry 2, Table 1.1.

Table 1.1 Representative examples of the metathesis of *n*-hexane by **1a** or **2** (10 mM) and **3** (16 mM): distribution of C_2-C_{15} *n*-alkane products (mM).

entry	Ir-catalyst	[TBE] /mM	temp. /°C	time	C_2	C_3	C_4	C_5	C_7	C_8	C_9	C_{10}	C_{11}	C_{12}	C_{13}	C_{14}	$C_{\geq 15}$	total (M)
1	**1a-C₂H₄**	0	125	6 h	123		105	183	131	73	70	47	10	4	2	1	0.3	0.75
				24 h	233		191	319	234	133	122	81	22	9	5	2	1	1.35
				2 d	261		215	362	265	147	138	89	25	11	6	3	1	1.52
				4 d	264		218	372	276	154	146	95	26	12	6	3	1	1.57
			Added additional **3** (8 mM)															
				5d	502		436	721	420	239	223	153	56	30	18	10	5	2.81
2	**1a-H₂**	20	125	1d	458		345	547	258	151	139	95	29	13	6	3	2	2.05
3	**2a-H₂**ᵃ	20	125	26 h	(140)	155	119	262	125	37	49	240	15	4	4	10	1	1.16
			Added additional **3** (6.4 mM)															
				49 h	(300)	190	174	376	180	62	82	356	30	10	10	24	7	1.80

a) 6.4 mM catalyst **3** added initially. Ethane concentrations for entry 3 are extrapolated as explained in the text. For entries 1 and 2 no separation of C_2 and C_3 peaks was obtained (values shown are not extrapolated).

Pincer-ligated iridium complexes have been reported to dehydrogenate *n*-alkanes with high kinetic selectivity for the formation of the corresponding 1-alkene.[14] Thus, the product distributions indicated in entries 1 and 2 in Table 1.1 presumably reflect a substantial degree of olefin isomerization prior to olefin metathesis under these conditions. Thus for example, isomerization of 1-hexene to 2-hexene, followed by cross-metathesis between 2-hexene and 1-hexene, could give 1-pentene plus 2-heptene.[17-19] Alternatively, or in addition, 5-decene (from the cross metathesis of 2 mol 1-hexene) could be isomerized to give 4-decene;

metathesis with ethylene would then give 1-pentene and 1-heptene. Thus, terminal dehydrogenation of *n*-hexane in tandem with olefin metathesis, when coupled with rapid olefin isomerization, can account for the C_3-C_5 and C_7-C_9 alkanes; this is illustrated for production of *n*-pentane and *n*-heptane in Fig. 1.3.
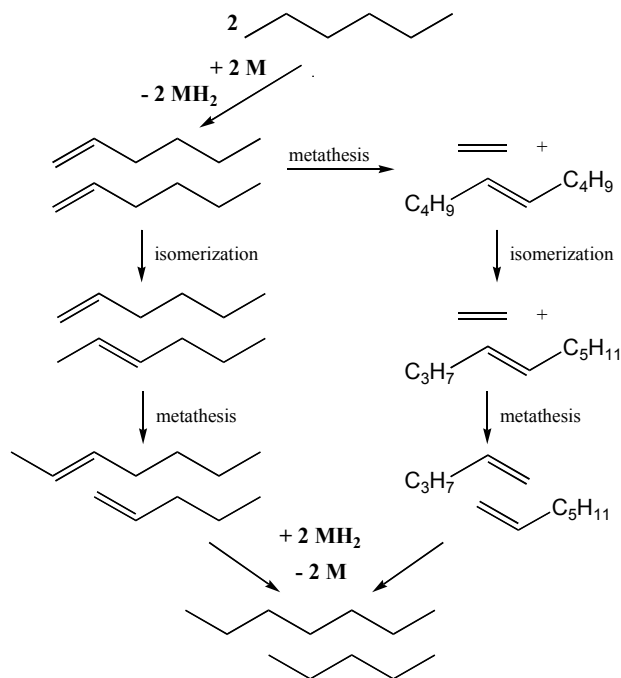
Fig. 1.3 Two possible pathways for the metathesis of *n*-hexane to give *n*-pentane and *n*-heptane, initiated by dehydrogenation at the *n*-hexane terminal position.

Alkanes with carbon number greater than 10, produced from hexane, must derive from olefin metathesis of at least one alkene of $C_{n>6}$. The $C_{n>6}$ alkene may derive from dehydrogenation of the corresponding *n*-alkane primary product, or it may be obtained directly via cross-metathesis of hexenes, before the resulting olefin (e.g. 5-decene) is hydrogenated.

6

Consistent with the hypothesis that 1-alkenes are the initial dehydrogenation products, under certain conditions, presumably when olefin isomerization is slow relative to olefin metathesis, n-decane is the major heavy ($C_{n>6}$) product of n-hexane metathesis. (The non-degenerate cross-metathesis of 1-hexene can only yield ethene and 5-decene). The results of an experiment with dehydrogenation-catalyst **2a** and metathesis-catalyst **3** are shown in entry 3, Table 1.1. Notably, n-decane is the major heavy product under these conditions. (The formation of n-tetradecane presumably results from the secondary metathesis reaction of n-decane with n-hexane.) This reaction was also monitored by ^{13}C NMR, a method that yields results that are less precise than GC, but facilitates continuous monitoring in a sealed reaction vessel. The NMR results were generally consistent with those obtained by GC, and in particular revealed that the ratio of the major n-alkane products did not significantly change with time.

While it is difficult to precisely quantify ethane production under our conditions, the concentration for the first run in entry 3 was measured by GC as 85 mM. Assuming that the average carbon-number of all products is equal to 6, and assuming that ethane is the major alkane product lost from solution, the concentration of ethane produced (if none had escaped from solution) would be 140 mM. This value is an upper limit since any escaped propane would also partially account for the high (>6) average carbon-number of the observed products;[22] however, it is substantially lower than the concentration of n-decane observed (240 mM). This discrepancy between ethane and n-decane production is probably largely attributable to secondary metathesis of the ethene product with 2- or 3- hexenes (which would then contribute to the formation of propene, butene, and pentene).

As well as for alkane disproportionation (i.e. self-metathesis) as illustrated above, the catalyst system may be used for alkane conproportionation (cross-metathesis), i.e., the production of intermediate-MW alkanes from low-MW and high-MW reactants. Table 1.2 shows the result of carrying out alkane metathesis on a mixture of 4:1 (mol:mol) n-hexane and the C_{20} alkane, eicosane.

Table 1.2 Distribution of C_2-C_{38} n-alkane products (M) from the metathesis of n-hexane and eicosane (n-$C_{20}H_{42}$) by **1a-C_2H_4** (7.14 mM) and **3** (11.43 mM) at 125 °C.

time	C_{2-5}	C_{7-10}	C_{11-14}	C_{15-19}	C_{21-24}	C_{25-38}	Total
1d	0.44	0.36	0.24	0.31	0.14	0.066	1.56
6d	0.56	0.64	0.31	0.27	0.12	0.070	1.97

Given the instability of the molybdenum alkylidene catalysts, the supported Re metathesis-catalyst Re_2O_7/Al_2O_3 which exhibits greater stability at high temperature, was investigated.[23] These reactions were conducted at 175 °C with n-decane as the solvent/substrate (Table 1.3).[24] The (PCP)Ir catalysts (**2**) proved more effective than the (POCOP)Ir systems (**1**). In a typical experiment, a n-decane (2.5 mL, 12.8 mmol) solution of **2b-H_4** (12.8 mg, 0.0227 mmol), TBE (10 μL, 0.078 mmol), and hexamethylbenzene (10 mg, internal standard) was heated over Re_2O_7/Al_2O_3 (535 mg, 5 wt% Re_2O_7) at 175 °C under argon and monitored by GC. After 3 h, C_2-C_{28} alkanes were observed with total product concentration estimated as 1.6 M (corresponding to 180 turnovers based on Ir). Catalysis slows, but after 9 days, product concentrations reached 4.4 M. Remarkably, at 9 days, n-decane is comparable in molar quantity to n-nonane and n-undecane with measured molar ratios of C_9:C_{10}:C_{11} of 0.6 : 1 : 0.6 (Fig. 1.4).

Table 1.3 Distribution of C_2-C_{34} n-alkane products (mM) from the metathesis of n-decane by Ir-based catalysts (9.0-9.5 mM) and Re_2O_7/Al_2O_3 (16 mM effective Re_2O_7 concentration) at 175 °C.

Ir-cat.	[TBE]/mM	time	C_2	C_3	C_4	C_5	C_6	C_7	C_8	C_9	C_{10}	C_{11}	C_{12}	C_{13}	C_{14}	C_{15}	C_{16}	C_{17}	C_{18}	[> C_{18}]	total/M
1a-C_2H_4	0	3h	3.9	2.8	8.3	10	12	12	13	16	4980	15	11	9.3	7.2	6.0	4.6	2.1	1.3	1.9	0.14
(9.5 mM)		18h	5.4	9.7	39	43	43	48	55	64	4580	61	46	38	28	23	17	6.9	3.7	5.4	0.54
		7d	26		101	117	118	115	140	163	3760	154	115	94	71	58	43	18	9.8	16.3	1.36
2a-H_2	18	3h	16		61	86	98	122	142	152	3990	137	104	78	53	37	23	9.3	5.2	6.3	1.13
(9.0 mM)		11d	39		207	299	327	382	427	446	1500	408	314	245	174	129	87	48	32	58	3.62
2b-H_4	35	3h	15		81	117	134	146	172	181	3490	177	147	120	91	72	52	34	26	63	1.63
(9.1 mM)		18h	39		160	234	265	280	318	324	1870	317	271	226	176	145	110	76	61	194	3.20
		9d	44		220	332	346	405	456	457	753	429	362	300	233	195	151	108	88	241	4.37
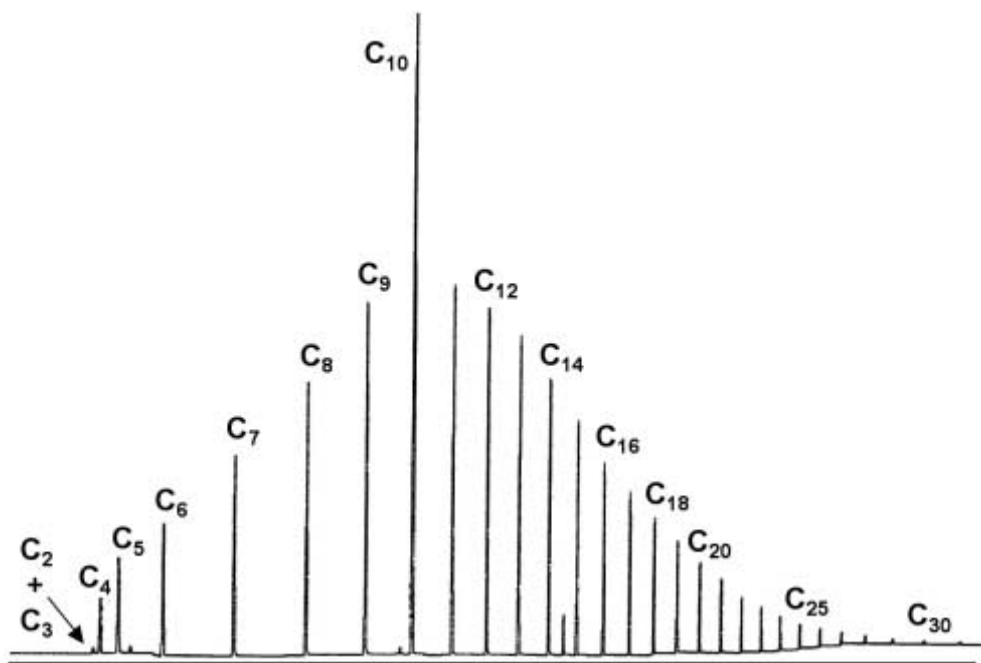
Fig. 1.4 GC trace of product mixture resulting from the metathesis of n-decane (solvent) by **2b-H_4** and Re_2O_7/Al_2O_3 after 9 days at 175 °C (see Table 1.3).

9

Conclusions

In summary, the catalytic metathesis of *n*-alkanes has been achieved through the use of a tandem system comprising catalysts for alkane dehydrogenation and olefin metathesis. Conversions as high as 84% have been obtained. The system is completely selective for linear alkane products in contrast to the Basset systems which produce both linear and branched alkanes. The product can display a roughly stochastic distribution of carbon-numbers, but under certain conditions the system shows significant (and unprecedented) selectivity for the $C_{(2n-2)}$ alkane (i.e. *n*-decane from *n*-hexane).

Experimental Section

General Considerations. All manipulations were carried out using standard Schlenk and glovebox techniques. Argon was purified by passage through columns of BASF R3-11 (Chemalog) and 4 Å molecular sieves. Toluene and pentane were passed through columns of activated alumina. Hexane was purchased from Aldrich, dried over CaH_2, degassed via several freeze-pump-thaw cycles, and stored under argon. Anhydrous decane was purchased from Aldrich, degassed, and stored under argon. Eicosane and ammonium perrhenate was purchased from Aldrich and used as received. γ-Alumina and $[Mo(C_{10}H_{12})(C_{12}H_{17}N)[OC(CH_3)(CF_3)_2]_2$, **3**, were purchased from Strem and used as received. $\{C_6H_3$-2,6-$[CH_2P(t\text{-}Bu)_2]_2\}Ir(H)_2$, **2a-H₂**,[10] and $\{C_6H_3$-2,6-$[OP(t\text{-}Bu)_2]_2\}Ir(H)(Cl)$[12] were prepared according to literature procedures. NMR spectra were recorded on Bruker DRX 400 and AMX 300 MHz instruments and are referenced to residual protio solvent. $^{31}P\{^1H\}$ NMR chemical shifts are referenced to an external 85% H_3PO_4 standard. GC

analysis was performed on an Agilent 6850 Series GC with a dimethylpolysiloxane column (Agilent HP-1).

Synthesis of Re₂O₇ supported on alumina. The following procedure was adapted from literature procedure.[3] In a vial, 1.20 g (4.47 mmol) of NH_4ReO_4 was dissolved in 30 mL distilled water. This solution was added to 10 g (98 mmol) of γ-Al_2O_3. The suspension was swirled by hand for about a minute, then allowed to stand undisturbed at room temperature for 30 min. This cycle of swirling and standing was repeated until all of the water was absorbed by the alumina. The solid was dried in a 120 °C oven overnight, then calcined at 550 °C for 3 hours under a flow of O_2 cooled to room temperature under O_2. The solid was brought into the drybox under vacuum to avoid exposure to moisture, and was stored under argon.

Synthesis of {C₆H₃-2,6-[OP(*t*-Bu)₂]₂}Ir(C₂H₄), 1a-C₂H₄. {C₆H₃-2,6-[OP(*t*-Bu)₂]₂}Ir(H)(Cl) (1.5 g, 2.4 mmol) and NaO-*t*-Bu (277 mg, 2.89 mmol) were weighed into a flame-dried Schlenk flask and put under a flow of argon. Toluene (40 mL) was added to the flask via syringe, and the resulting suspension was stirred for 10 min at room temperature. Ethylene was bubbled through the solution for 1-2 hours. The solution was cannula-filtered through a pad of Celite, volatiles were evaporated under vacuum, and the resulting red solid was dried under vacuum overnight to give 867 mg (59% yield) of pure product. ^{1}H NMR (C_6D_6): δ 1.24 (t, J=6.8 Hz, 36H), 3.10 (t, J=2.4 Hz, 4H), 6.91-6.94 (m, 2H), 7.01-7.06 (m, 1H). ^{13}C NMR (C_6D_6): δ 28.93 (m, 12C), 36.13 (s, 2C), 41.92 (t, J=11.2 Hz, 4C), 103.98 (t, J=6.0 Hz, 2C), 127.45 (s), 145.19 (t, J=8.5 Hz), 168.17 (t, J=8.4 Hz, 2C). ^{31}P{^{1}H} NMR (C_6D_6): δ 181.7 (s). Anal. Calc'd for $C_{24}H_{43}O_2P_2Ir$: C, 46.65; H, 7.03. Found: C, 46.64; H, 7.15.

Procedures for alkane metathesis reactions:

Table 1.1, entry 1: A flask was charged with 12.8 mg (0.021 mmol) of **1a-C₂H₄**, 26 mg (0.034 mmol) of the hexafluorinated Schrock catalyst **3**, 2 mL (15.1 mmol) of *n*-hexane, and 8.8 μL (0.063 mmol) of mesitylene as internal standard. The flask was sealed tightly with a teflon plug under an argon atmosphere, and the solution stirred in a 125 °C oil bath. Periodically, the flask was removed from the bath and cooled in an ice bath. An aliquot was removed from the flask, and analyzed by GC. Product concentrations were calculated for each aliquot.

GC Method Details:

Column: HP-1, 100% dimethylpolysiloxane
     Length: 30 m
     ID: 0.32 mm
     Film thickness: 0.25 μm
Detector: FID
Starting temperature: 33 °C
Time at starting temp: 5 min
Ramp: 20 °C/min
Ending temperature: 300 °C
Time at ending temperature: 10 min
Flow rate: 1 mL/min
Split ratio: 400
Inlet temperature: 250 °C
Detector temperature: 250 °C

Method to measure/calculate GC response factors: The response factors of *n*-alkanes from pentane to pentadecane with respective to mesitylene were obtained from experimental data. The area percent ratios of each alkane with respective to mesitylene were obtained by GC analysis from three independent *n*-hexane solutions which contained a 1:1 molar ratio of alkane to mesitylene. The final response factor of each alkane with respective to mesitylene were an average of three independent runs. A plot for response factors *vs* molecular weights

of alkanes was made. The response factors of ethane, propane, butane, and alkanes after pentadecane were extrapolated from the plot.

Table 1.1, **entry 2** and **3**: A flask was charged with 12.3 mg (0.021 mmol) of **1a-H$_2$** or **2a-H$_2$**, 5.4 μL (0.042 mmol) of *tert*-butyl ethylene, 26 mg (0.034 mmol) of the hexafluorinated Schrock catalyst **3**, 2 mL (15.1 mmol) of *n*-hexane, and 8.8 μL (0.063 mmol) of mesitylene as internal standard. The flask was sealed tightly with a teflon plug under an argon atmosphere, and the solution stirred in a 125 °C oil bath. Periodically, the flask was removed from the bath and cooled in an ice bath. An aliquot was removed from the flask, and analyzed by GC. Product concentrations were calculated for each aliquot.

Table 1.2: A flask was charged with 12.8 mg (0.021 mmol) of **1a-C$_2$H$_4$**, 26 mg (0.034 mmol) of the hexafluorinated Schrock catalyst **3**, 1.6 mL (12.07 mmol) of *n*-hexane, 0.852 g (3.02 mmol) of eicosane, and 10.2 mg (0.063 mmol) of hexamethylbenzene as internal standard. The flask was sealed tightly with a teflon plug under an argon atmosphere, and the solution stirred in a 125 °C oil bath. Periodically, the flask was removed from the bath and cooled in an ice bath. An aliquot was removed from the flask, and analyzed by GC. Product concentrations were calculated for each aliquot.

Table 1.3, **entry 1**: A flask was charged with 14.7 mg (0.024 mmol) of **1a-C$_2$H$_4$**, 546 mg of Re$_2$O$_7$ supported on alumina (5% Re$_2$O$_7$ by weight), 2.5 mL (12.8 mmol) of *n*-decane, and 9.6 mg (0.059 mmol) of hexamethylbenzene as internal standard. The iridium complex immediately adsorbed itself onto the Re$_2$O$_7$ alumina support, as observed by the colorless solution and rust-colored solid. The flask was sealed tightly with a teflon plug under an argon atmosphere, and the solution stirred in a 175 °C oil bath. Periodically, the flask was removed

from the bath and cooled in an ice bath. An aliquot was removed from the flask, and analyzed by GC. Turnover numbers were calculated for each aliquot.

Table 1.3, **entry 2**: A flask was charged with 13.3 mg (0.023 mmol) of **2a-H$_2$**, 5.8 µL (0.045 mmol) of *tert*-butyl ethylene as hydrogen acceptor, 543 mg of Re$_2$O$_7$ supported on alumina (5% Re$_2$O$_7$ by weight), 2.5 mL (12.8 mmol) of *n*-decane, and 10.2 mg (0.063 mmol) of hexamethylbenzene as internal standard. The iridium complex immediately adsorbed itself onto the Re$_2$O$_7$ alumina support, as observed by the colorless solution and rust-colored solid. The flask was sealed tightly with a teflon plug under an argon atmosphere, and the solution stirred in a 175 °C oil bath. Periodically, the flask was removed from the bath and cooled in an ice bath. An aliquot was removed from the flask, and analyzed by GC. Turnover numbers were calculated for each aliquot.

Table 1.3, **entry 3**: A flask was charged with 12.8 mg (0.023 mmol) of **2b-(H)$_4$**, 10 µL (0.078 mmol) of *tert*-butyl ethylene, 536 mg of Re$_2$O$_7$ supported on alumina (5% Re$_2$O$_7$ by weight), 2.5 mL (12.8 mmol) of *n*-decane, and 20.2 mg (0.124 mmol) of hexamethylbenzene as internal standard. The iridium complex immediately adsorbed itself onto the Re$_2$O$_7$ alumina support, as observed by the colorless solution and rust-colored solid. The flask was sealed tightly with a teflon plug under an argon atmosphere, and the solution stirred in a 175 °C oil bath. Periodically, the flask was removed from the bath and cooled in an ice bath. An aliquot was removed from the flask, and analyzed by GC. Turnover numbers were calculated for each aliquot.

References and Notes

(1) Levenspiel, O. *Ind. Eng. Chem. Res.* **2005**, *44*, 5073.

(2) Dry, M. E. *J. Chem. Tech. Biotech.* **2001**, *77*, 43.

(3) Szybist, J. P.; Kirby, S. R.; Boehman, A. L. *Energy & Fuels* **2005**, *19*, 1484.

(4) Murphy, M. J.; Taylor, J. D.; McCormick, R. L. Compendium of Experimental Cetane Number Data: NREL/SR-540-36805, National Renewable Energy Laboratory, Golden, CO, 2004, http://www.nrel.gov/vehiclesandfuels/pdfs/sr368051.pdf.

(5) Burnett, R. L.; Hughes, T. R. *J. Catal.* **1973**, *31*, 55.

(6) Vidal,V.; Theolier, A.; Thivolle-Cazat, J.; Basset, J.-M. *Science* **1997**, *276*, 99.

(7) Roux, E. L.; Taoufik, M.; Baudouin, A.; Copéret, C.; Thivolle-Cazat, J.; Basset, J.-M. *Adv. Synth. Catal.* **2007**, *349*, 231.

(8) Roux, E. L.; Taoufik, M.; Copéret, C.; Mallmann, A.; Thivolle-Cazat, J.; Baudouin, A.; Basset, J.-M.; Maunders, B. M.; Sunley, G. J. *Angew. Chem.* **2005**, *44*, 6755.

(9) Basset, J. M.; Copéret, C.; Lefort, L.; Maunders, B. M.; Maury, O.; Roux, E. L.; Saggio, G.; Soignier, S.; Soulivong, D.; Sunley, G. J.; Taoufik, M.; Thivolle-Cazat, J. *J. Am. Chem. Soc.* **2005**, *127*, 8604.

(10) Gupta, M.; Hagen, C.; Flesher, R. J.; Kaska, W. C.; Jensen, C. M. *Chem. Commun.*, **1996**, 2083.

(11) Gupta, M.; Hagen, C.; Kaska, W. C.; Cramer, R. E.; Jensen, C. M. *J. Am. Chem. Soc.* **1997**, *119*, 840.

(12) Göttker-Schnetmann, I.; White, P.; Brookhart, M. *J. Am. Chem. Soc.* **2004**, *126*, 1804.

(13) Göttker-Schnetmann, I.; Brookhart, M. *J. Am. Chem. Soc.* **2004**, *126*, 9330.

(14) Liu, F.; Pak, E. B.; Singh, B.; Jensen, C. M.; Goldman, A. S. *J. Am. Chem. Soc.* **1999**, *121*, 4086.

(15) Xu, W.-W.; Rosini, G. P.; Gupta, M.; Jensen, C. M.; Kaska, W. C.; Krogh-Jespersen, K.; Goldman, A. S. *Chem. Commun.* **1997**, 2273.

(16) Zhu, K.; Achord, P. D.; Zhang, X.; Krogh-Jespersen, K.; Goldman, A. S. *J. Am. Chem. Soc.* **2004**, *126***, 13044.

(17) Astruc, D. *New. J. Chem.* **2005**, *29*, 42.

(18) Grubbs, R. H. *Tetrahedron* **2004**, *60*, 7117.

(19) Schrock, R. R.; Hoveyda, A. H. *Angew. Chem. Intl. Ed.* **2003**, *42*, 4592.

(20) Schrock, R. R. *Chem. Comm.* **2005**, 2773.

(21) Schrock, R. R.; Murdzek, J. S.; Bazan, G. C.; Robbins, J.; Dimare, M.; O'Regan, M. *J. Am. Chem. Soc.* **1990**, *112*, 3875.

(22) By approximating that ethane is the only escaped volatile, we obtain a lower limit for the total concentration of alkane metathesis products (since, for example, more moles propane than ethane would need to escape in order to yield an equally high average carbon-number of the remaining product).

(23) Pariya, C.; Jayaprakash, K. N.; Sarkar, A. *Coord. Chem. Rev.* **1998**, *168*, 1.

(24) The iridium-based dehydrogenation catalysts appear to be adsorbed on alumina. Accordingly, when alumina is treated with pentane solutions of the iridium complexes, the solutions turn colorless and the support acquires the red color of the catalyst. However, we have yet to determine if dehydrogenation is actually catalyzed by supported-phase iridium complexes, or if it is effected by a low concentration of catalyst that may slowly leach into solution.

CHAPTER TWO

Mechanistic Studies of Alkane Metathesis

Introduction

In homogeneous alkane metathesis (AM) reactions (Scheme 2.1), we observed that a) the Schrock olefin metathesis catalyst (Mo-F_6) is short-lived relative to the pincer iridium dehydrogenation catalyst under AM conditions;[1,2] b) the POCOP system (**1a**) is more productive than the PCP system (**2**);[2] and c) the PCP system is more selective for the formation of *n*-decane from the metathesis of *n*-hexane than the POCOP system.[1,2]

Moreover, the PCP and POCOP Ir catalysts show different resting states in AM.[1] For the PCP system, the Ir(III) dihydride complex (**2-H₂**) is the resting state. Starting from the **1a-H₂**, the POCOP-Ir catalyst forms Ir(I) olefin complexes as the resting states. It is interesting that a slight variation of the linkers in the pincer ligand ("O" *vs* "CH₂") leads to such a significant difference between POCOP and PCP in AM. In collaboration with the Goldman group (Rutgers University), we investigated the role that pincer complexes play in AM with respect to olefin isomerization and transfer dehydrogenation.

Results described in this chapter establish that the POCOP system shows a higher olefin binding affinity relative to the PCP system from both steric and electronic effects. Results presented here support a new iridium-catalyzed olefin isomerization pathway involving formation of an iridium π–allyl hydride from an iridium olefin complex. DFT

calculations conducted by Goldman *et al.* indicate this "π–allyl" pathway is favored over the previously presumed "hydride insertion" olefin isomerization pathway.[3] Goldman demonstrated that there is no solvent effect (*n*-alkane vs mesitylene) on the rate of olefin isomerization, suggesting the iridium dihydride is not the major isomerization catalyst. Results reported in this chapter demonstrate the H/D scrambling in the coordinated propylene ligand of an iridium complex which must occur via the "π–allyl" isomerization pathway. Furthermore, the π–allyl hydride intermediate in the "π–allyl" olefin isomerization mechanism has been observed using low-temperature NMR spectroscopy. Kinetic investigations of the hydrogen transfer and the isomerization of 1-octene using the POCOP ethylene complex, **1a-C₂H₄**, were carried out. 1-octene isomeraztion via the "π–allyl" mechanism is hindered in the presence of ethylene. Furthermore, the high binding affinities of ethylene and 1-octene to the iridium center inhibit the transfer hydrogenation.

Scheme 2.1 Tandem catalytic alkane metathesis with pincer iridium and Schrock-type catalysts

18
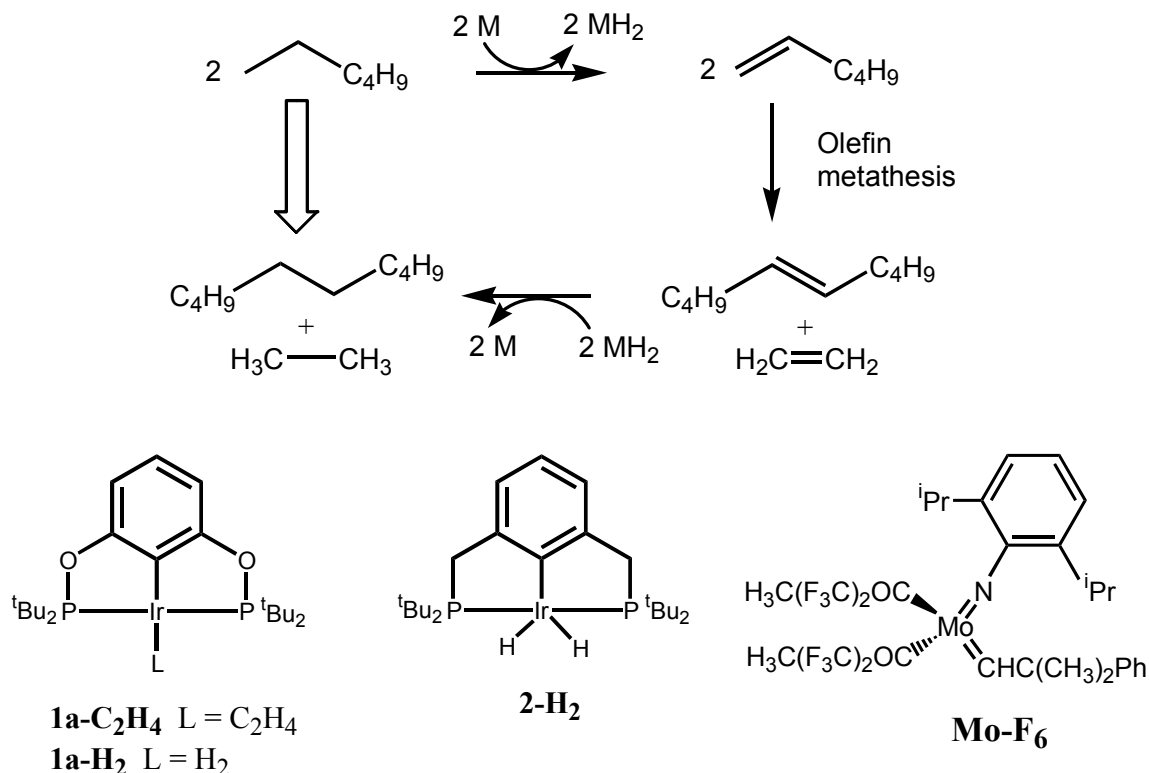
Results and discussion

1. Olefin metathesis catalyst in alkane metathesis.

Schrock-type catalysts are highly active, but not very stable and typically operate at room temperature for olefin metathesis. Two decomposition pathways have been proposed by Schrock *et al.*: a bimolecular coupling of alkylidenes, especially methylidene, and rearrangement of metallacyclobutanes.[2,4-6] Under the AM condition (125 °C), though the **Mo-F₆** catalyst is relatively unstable compared to the iridium catalyst, it maintains metathesis activity over the course of a day (see Table 1.1, Chapter 1).[1,2] The low concentration of olefins (especially ethylene) in AM limits the concentration of metallacyclobutanes in solution.[2,4-6] Additionally, low concentrations of Schrock catalyst will result in a low rate of the bimolecular coupling of alkylidenes in AM, which may also extend the lifetime of Schrock catalyst. In a cross metathesis reaction of *n*-hexane and eicosane (Eq 1), increasing the concentration of **Mo-F₆** from 2.86 mM to 11.44 mM had a negligible effect on the total productivity (1.36 vs 1.40 M of total product, Table 2.1). The results imply that the decomposition rate via bimolecular coupling increases as the metathesis catalyst concentration increases. The experiments also show that the productivity is limited mainly by decomposition of the Schrock catalyst, as addition of more **Mo-F₆** reinitiated the reaction (Table 2.1, entry 1).

$$1a\text{-}C_2H_4 \quad + \quad n\text{-}C_6H_{14} \quad + \quad n\text{-}C_{20}H_{42} \quad + \quad Mo\text{-}F_6 \quad \xrightarrow{\;125\,^{\circ}C\;} \quad n\text{-alkanes}$$

1 equiv   610 equiv   153 equiv   0.4/1.6 equiv   (Eq 1)
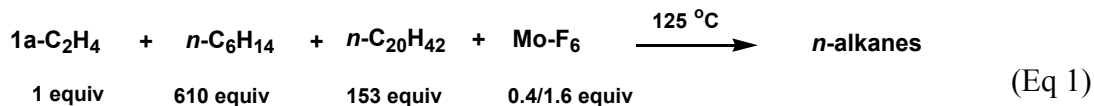
Table 2.1. Distribution of *n*-alkanes products from the metathesis of *n*-hexane (4.36 M) and eicosane (1.09 M) by **1a-C₂H₄** (7.14 mM) and **Mo-F₆** (2.86 to 11.44 mM) at 125 °C.

Entry	Mo (mM)	Time (d)	Product distribution (mM)					Total Product (M)
			C_{2-5}	C_{7-10}	C_{11-14}	C_{15-19}	C_{21-36}	
1	2.86	1	404	386	179	225	164	1.36
		2	396	376	190	233	163	1.36
	Additional 2.86 mM of **Mo-F₆** added							
	5.72	1	556	548	311	317	203	1.93
2	11.44	2	422	438	209	200	130	1.40

2. Product selectivity and resting states in AM with POCOP and PCP systems.

Under the same reaction conditions, the PCP system shows higher selectivity for C_2H_6 and $C_{n-2}H_{2n-2}$ from metathesis of C_nH_{2n+2} (see Chapter 1).[1,2] For example, metathesis of C_6H_{14} using **1a-H₂** formed 15 mol% of *n*-$C_{10}H_{22}$ relative to the production of total heavy alkanes (C_7H_{16} – $C_{10}H_{22}$). As a comparison, the reaction with **2-H₂** produced 49% of *n*-$C_{10}H_{22}$.[1]

Notably, the PCP and POCOP iridium systems exhibit different resting states in AM. For the PCP system, Goldman *et al.* found that the dihydride complex, **2-H₂**, is the primarily iridium resting state in the AM reaction with catalysts **2-H₂** and **Mo-F₆**.[1] In AM with the POCOP system, under working catalytic condition only **1a-olefin** species were observed. As shown in Fig. 2.1, monitoring a *n*-hexane solution of **1a-H₂**, **Mo-F₆** and *tert*-butylethylene (hydrogen acceptor, 2 equiv.) by ^{31}P NMR spectroscopy indicated that at the early stage (4 h at 125 °C), **1a-C₂H₄** was the major resting state, with small amounts of **1a-propylene, 1a-(1-butene)**, **1a-(1-pentene)**, **1a-(1-hexene)**, and **1a-(internal-hexenes)** present (all the **1a-olefin** complexes were synthesized independently and characterized by ^{31}P NMR, see Experimental Section). At the later stage (4 d at 125 °C), however, **1a-(1-hexene)** was

observed as the primarily iridium species. The iridium resting state reflects the activity of the olefin metathesis catalyst. As **Mo-F$_6$** decays over time, ethylene is no longer produced via olefin metathesis. Meanwhile, it continues to be consumed by dehydrogenation of hexane, resulting in the conversion of **1a-C$_2$H$_4$** to **1a-(1-hexene)**. In a control experiment, heating a hexane solution of **1a-C$_2$H$_4$** at 125 °C led to the formation of **1a-(1-hexene)** (> 90%) and **1a-(internal-hexenes)** (< 10%) in 24 h.
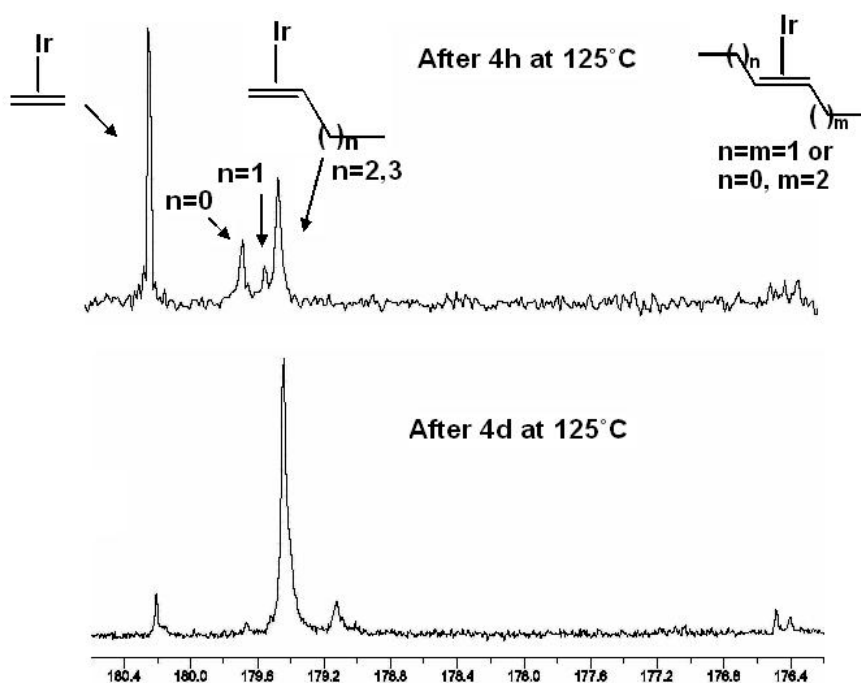
Fig. 2.1 The resting states of (^{t}Bu-POCOP)Ir catalyst in AM.

3. Olefin binding affinities of iridium complex.

It's interesting that the apparently similar POCOP and PCP iridium systems have different resting states in AM. Indeed, from both steric and electronic considerations, the POCOP is more likely to form the olefin complexes than the PCP.

First, the PCP iridium complex is more sterically crowded than the POCOP iridium complex. Fig. 2.2 shows the crystal structures of (^{t}Bu-POCOP)Ir-CO (**1a-CO**) and (^{t}Bu-PCP)Ir-CO (**2-CO**). The C-C and C-P bond distances are longer than C-O and O-P bond distances and most significantly the P-Ir-P bond angle in **2-CO** is larger than that in **1a-CO** (163 vs 158°). Consequently, the *tert*-butyl groups on different phosphorus atoms in the PCP system are closer to each other compared to those in the POCOP system. As shown in the spacefilling structures (Fig. 2.2), the average distance between the *tert*-butyl groups in **2-CO** is 4.33 Å, closer than that of 4.67 Å in **1a-CO**. The steric overcrowding in the PCP iridium complex is believed to promote the formation of **2-H$_2$** where the hydride ligands occupy little space, instead of **2-olefin**. In contrast, the more "open" POCOP iridium complex is better able to bind the sterically demanding olefin ligand relative to PCP iridium.
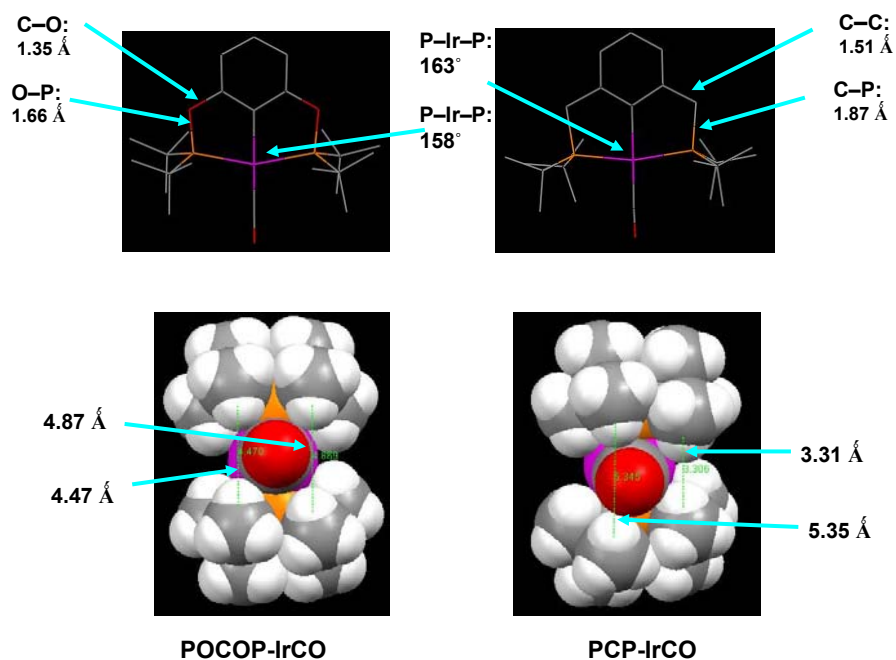
Fig. 2.2 The crystal structures of (^{t}Bu-POCOP)Ir-CO (left) and (^{t}Bu-PCP)Ir-CO (right).

The π-donation by two "O" atoms in the POCOP ligand raise the energy of the Ir d_{xz} orbital, resulting in increased backbonding from the Ir center to the π^* orbital of the ligand (see Fig. 2.3).[8] Therefore, the POCOP system is more favorable for olefin binding compared to the PCP system. The more electron-rich iridium center in the POCOP complex is also more reactive in oxidative addition of H_2 since it is the filled d_{xz} orbital which donate two electrons in forming the two new Ir-H bonds.[8]
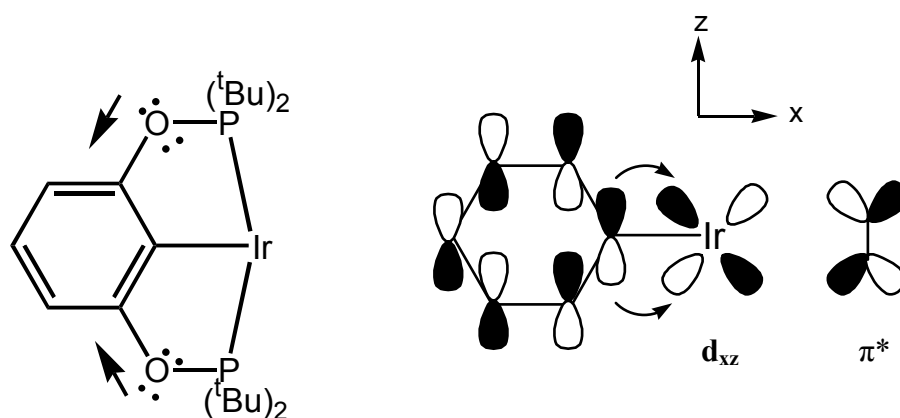
Fig. 2.3 Ir d_{xz} orbital raised by π-donation from two "O" atoms in the pincer ligand.

Indeed, the DFT calculations by the Goldman group show a remarkable energetic difference between (^{t}Bu-POCOP)Ir and (^{t}Bu-PCP)Ir for 1-butene binding and *n*-butane addition (both favorable for POCOP, $\Delta\Delta G$ = 12 kcal/mol). (^{t}Bu-POCOP)Ir also binds H_2 more strongly than (^{t}Bu-PCP)Ir, but the energetic difference is relatively small ($\Delta\Delta G$ = 3 kcal/mol, Table 2.2).
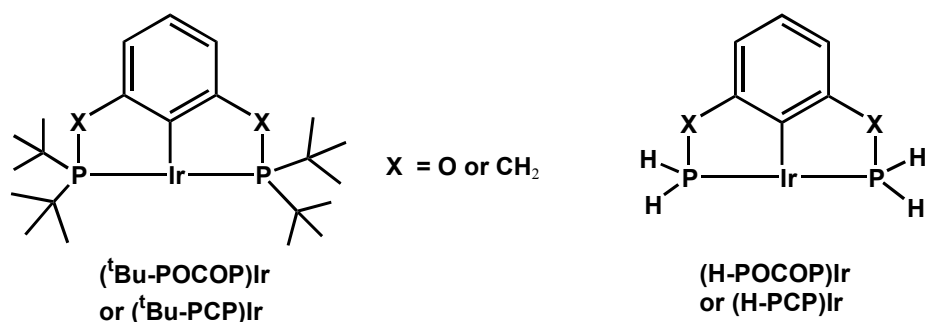
Fig. 2.4 Structures of ^{t}Bu and H-substituted pincer complexes used in DFT calculations.

Goldman *et al.* also conducted DFT calculations on the truncated pincer complexes (Fig. 2.4) in which steric effects have been greatly diminished by replacing the bulky *tert*-butyl groups with the small hydrogen atoms. The energetic differences between POCOP and PCP for olefin binding and alkane addition are decreased in the H-substituted system ($\Delta\Delta G =$ 5 kcal/mol, Table 2.2), suggesting that most of the difference between POCOP and PCP results from steric effects, but electronic differences also play a role.

Table 2.2 Binding free energies (kcal/mol) for 1-butene binding and ΔG for oxidative addition of butane and H_2 to the ^{t}Bu-substituted and truncated pincer complexes.

Reactions	^{t}Bu-substituted		H-substituted	
	ΔG	$\Delta\Delta G$	ΔG	$\Delta\Delta G$
(PCP)Ir + 1-butene → (PCP)Ir-(1-butene)	-5	12	-20	5
(POCOP)Ir + 1-butene → (POCOP)Ir-(1-butene)	-17		-25	
(PCP)Ir + *n*-butane → (PCP)Ir-(H)(butyl)	14	12	7	5
(POCOP)Ir + *n*-butane → (POCOP)Ir-(H)(butyl)	2		2	
(PCP)Ir + H_2 → (PCP)Ir-H_2	-18	3		
(POCOP)Ir + H_2 → (POCOP)Ir-H_2	-21			

4. Mechanism of olefin isomerization mediated by pincer iridium catalysts

Iridium catalysts have been known to dehydrogenate *n*-alkanes with high selectivity for α-olefin.[3] The formation of other alkanes besides ethane and *n*-decane from the metathesis of

n-hexane indicates isomerization of 1-hexene to internal hexenes prior to metathesis. The lower selectivity with the POCOP catalyst reflects a faster olefin isomerization compared to the PCP system. An olefin isomerization experiment carried out in the Goldman group showed that (^tBu-POCOP)Ir is apparently a faster isomerization catalyst than (^tBu-PCP)Ir when both complexes are present as Ir-(α-olefin) complexes, but the rate is only about 2 times greater at 125 °C, which is inadequate to account for the large difference of product selectivity in AM.
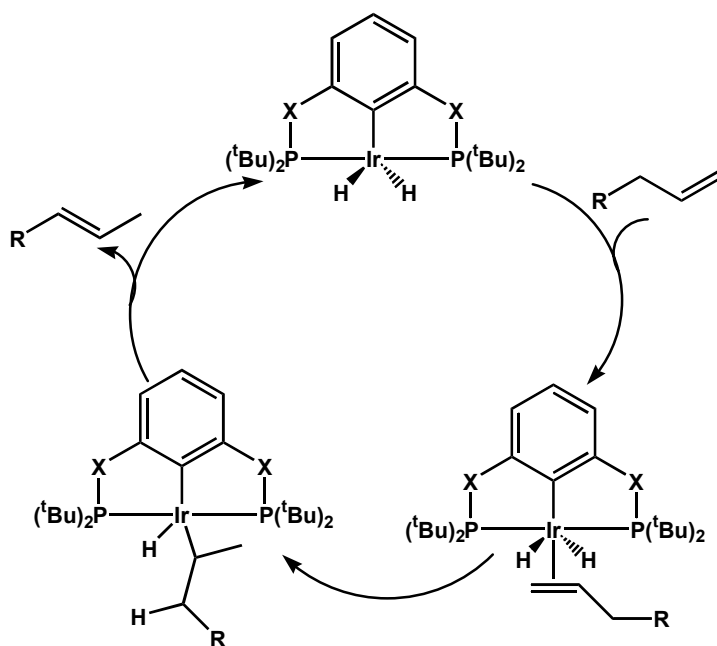
Fig. 2.5 A proposed "hydride insertion" olefin isomerization pathway by pincer iridium complex.

4.1 "Hydride insertion" *vs* "π–allyl" olefin isomerization mechanisms. Catalytic olefin isomerization by the pincer iridium complexes was initially assumed to proceed via 2,1 insertion of α-olefin into the Ir-H bond of a (pincer)IrH$_2$ complex, followed by β-H elimination to generate the isomerized 2-olefin ("hydride insertion" mechanism, Fig. 2.5).[3] If the **2-H$_2$** species was the major olefin isomerization catalyst, then increasing the alkane concentration should increase the isomerization rate. As shown in Eq 2, the concentration of

2-H₂ must be greater in *n*-alkane solvent than that in mesitylene solvent. However, a comparison of the 1-hexene isomerization with the PCP iridium catalyst in mixtures of *n*-hexane and mesitylene showed that the rate was even slightly slower with an increase in hexane, suggesting the iridium dihydride species is NOT the active catalyst for olefin isomerization.
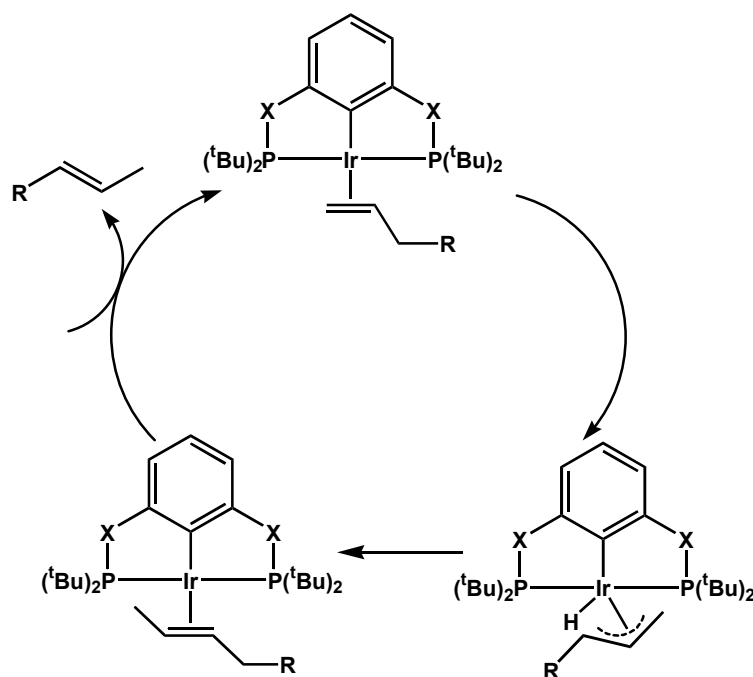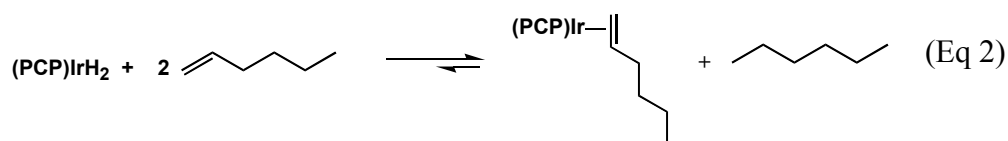
Fig. 2.6 A proposed "π–allyl" olefin isomerization pathway by pincer iridium.

An alternative pathway is a "π–allyl" olefin isomerization mechanism as shown in Fig. 2.6. DFT calculations on the PCP system gave a lower barrier to olefin isomerization via the "π–allyl" mechanism *vs* the "hydride insertion" mechanism (22 vs 29 kcal/mol) (Goldman). In this pathway, a Ir(III) η^3-allyl hydride species is formed from the Ir(I) olefin complex via

oxidative addition of an allylic C-H bond. Migration of the hydride to the terminal carbon leads to the formation of an Ir-(2-olefin) complex. Finally, the ligand substitution by an α-olefin releases the internal olefin product.

4.2 Intramolecular deuterium/hydrogen scrambling via the "π–allyl" mechanism.

To test the π–allyl olefin isomerization mechanism, complex **1a-propylene-d₃** containing a deuterium-labeled methyl group in the propylene ligand was prepared. Monitoring a mesitylene-d_{12} solution of **1a-propylene-d₃** by ¹H NMR indicated no hydrogen/deuterium (H/D) exchange at room temperature over a course of one day. However, heating the solution at 60 °C resulted in H/D scrambling between the methyl group and the terminal carbon of propylene (Fig. 2.7). The reaction reached equilibrium after ~20 hours with a rate of 0.08 h⁻¹. Increasing the temperature to 125 °C increased the rate and the reaction reached equilibrium in ~10 min.
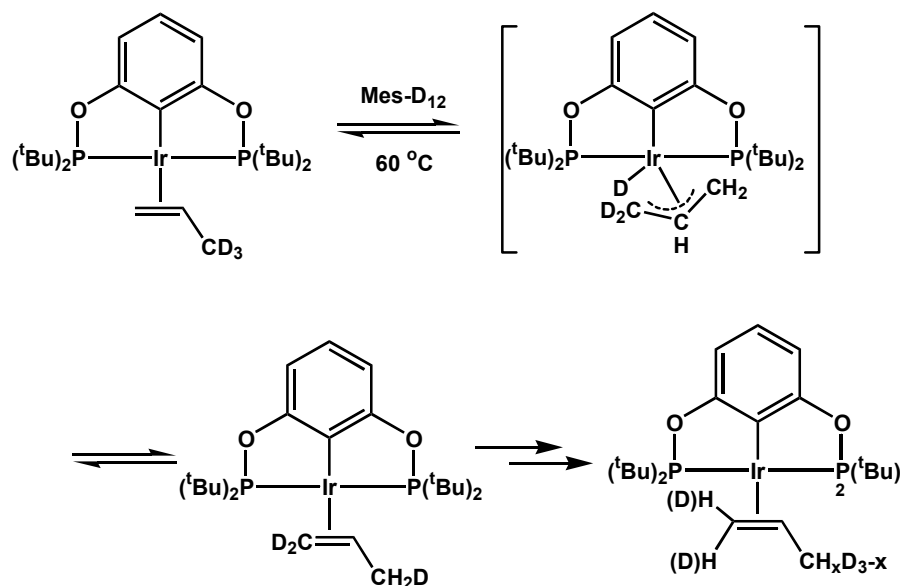
Fig. 2.7 Hydrogen/deuterium scrambling via a Ir(III) η³-allyl deuteride intermediate.

The H/D exchange must occur via the Ir(III) allyl hydride intermediate if no iridium hydride/deuteride species are formed during the reaction, which is presumed to be true in the system when using mesitylene as the solvent. To exclude the possibility of formation of an iridium hydride/deuteride species and isomerization via a "hydride insertion" mechanism (Fig. 2.5), a crossover experiment was carried out. Complex **1a-propylene-d$_6$** (perdeuterio propylene ligand) was treated with two equiv of free propylene (perhydrio) in mesitylene-d$_{12}$ at 60 °C (Fig. 2.8). If an iridium hydride/deuteride species was present in the system, a "hydride insertion" mechanism and intermolecular H/D scrambling would be expected. However, only ligand exchange was observed in this experiment. Complex **1a-propylene-d$_6$** (t$_{1/2}$ = 0.9 h) underwent ligand substitution with propylene, giving a mixture of 1/3 equiv **1a-propylene-d$_6$**, 2/3 equiv **1a-propylene**, 4/3 equiv propylene, and 2/3 equiv propylene-d$_6$. No crossover of H/D between the perdeuterio and perhydrio propylene occurred under the reaction conditions. These results indicate that no "iridium hydride" is involved in the H/D exchange reaction as discussed above. Thus, the "π–allyl" mechanism as shown in Fig. 2.7 fully accounts for the intramolecular H/D scrambling.
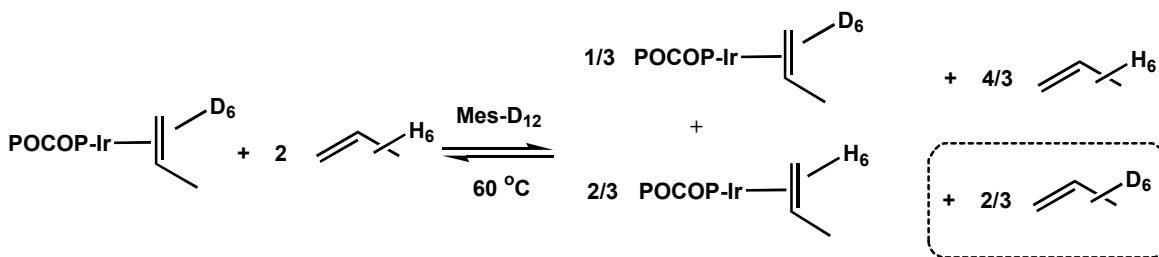
Fig. 2.8 Ligand exchanges reaction of **1a-propylene-d$_6$** and propylene.

Fig. 2.9 H/D scrambing at the central carbon of propylene involving a metallacyclobutane intermediate.
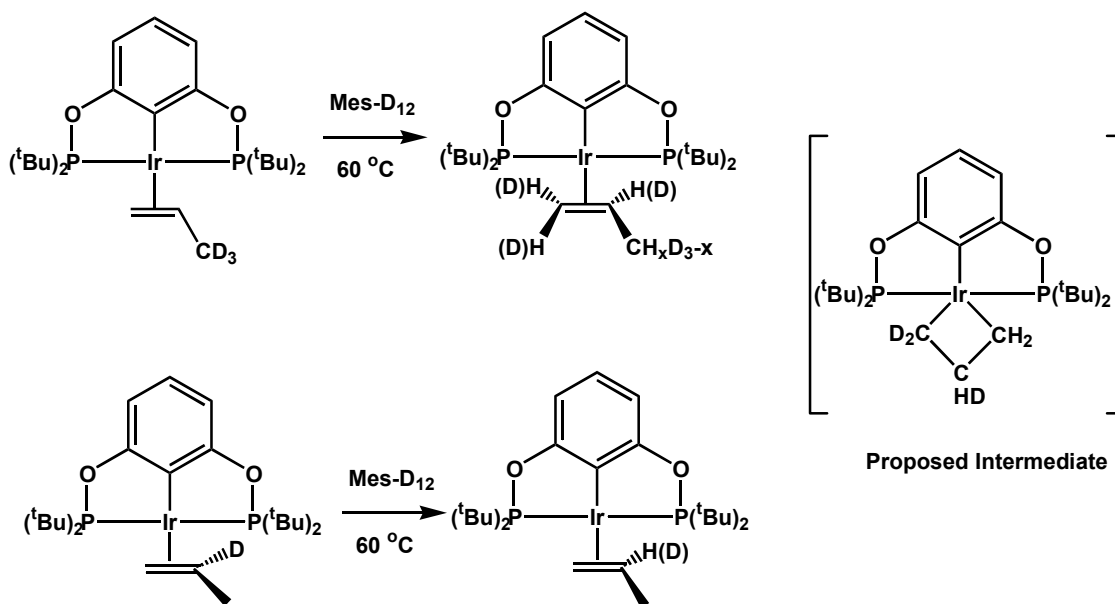
Interestingly, besides the H/D exchange between the terminal carbon and the methyl group, we also observed H/D scrambling at the central carbon of the propylene ligand in **1a-propylene-d$_3$** (Fig. 2.9), though the reaction rate (5×10^{-4} h^{-1} at 60 °C) is much slower compared to the H/D exchange involving the terminal carbon sites (0.08 h^{-1}). Complex **1a-propylene-d$_1$** (with deuterium at the central carbon, Fig. 2.9) was prepared and heated at 60 °C in mesitylene. The same H/D scrambling phenomenon was observed. The reaction presumably proceeds via a metallacyclobutane intermediate as depicted in Fig. 2.9. Similar iridium species have been reported by Ibers[9] and Stryker[10].

4.3 Observation of an Ir(III) η^3-allyl hydride intermediate. The intramolecular H/D exchange reactions, and the solvent effect on the olefin isomerization rate, as well as DFT calculations, support the "π–allyl" olefin isomerization mechanism. Furthermore, a key intermediate of this mechanism, the Ir(III) η^3-allyl hydride species has been formed and

characterized by low-temperature NMR techniques. Treatment of complex **1a-H₂** with allene (2 equiv) in methylcyclohexane-d$_{14}$ generated a mixture of **1a-H(allyl)** and **1a-propylene** (~1: 5 ratio) after 30 min at -83 °C (Scheme 2.2). The characteristic ^{1}H NMR data for complex **1a-H(allyl)** include a hydride resonance at -13.1 and five separate signals for the allyl unit: H$_{meso}$, 4.9; H$_{syn}$, 2.6, 2.8; H$_{anti}$, 2.0, 2.1 ppm. The ^{31}P NMR spectrum shows a pair of AB pattern doublets at 158.5 and 152.5 ppm for two non-equivalent phosphorus atoms. The observation of the **1a-H(allyl)** provides additional evidence for the "π–allyl" olefin isomerization mechanism.

Scheme 2.2 Formation of a Ir(III) hydride η^3-allyl and Ir(I) propylene complexes.
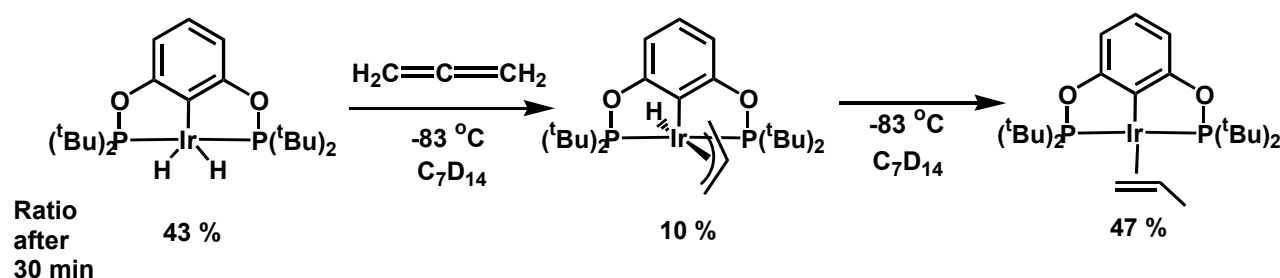
As discussed above, (^{t}Bu-POCOP)Ir is known to isomerize olefins 2 times faster than (^{t}Bu-PCP)Ir when both are present as Ir-(α-olefin) complexes. In AM, the (^{t}Bu-POCOP)Ir system has olefin complexes as the resting state with ~50% Ir-(α-olefin) complexes (see Fig. 2.1). In contrast, the (^{t}Bu-PCP)Ir system has the dihydride complex as the primary resting state. Therefore, under AM conditions, the (^{t}Bu-POCOP)Ir system isomerizes the α-olefins to form internal olefins much faster than the (^{t}Bu-PCP)Ir system via the π–allyl olefin isomerization mechanism, since very little of (^{t}Bu-PCP)Ir exists as an α-olefin complex, the precursor of the π–allyl hydride intermediate.

5. Transfer dehydrogenation and olefin isomerization by 1a-C₂H₄. Dehydrogenation of alkane by **1a-C₂H₄** is mainly inhibited by the binding of α-olefin. With *tert*-butyl ethylene as the hydrogen acceptor, the catalyst shows high activity for dehydrogenation of cyclooctane to form cyclooctene (~1600 TONs after 40 h)[11], but very poor activity for dehydrogenation of *n*-octane (~10 TONs after 40 h). The remarkably different activities arise from the dehydrogenation products — 1-octene binds more strongly to the Ir center than cyclooctene.

We carried out several transfer dehydrogenation and olefin isomerization reactions and monitored them by ^{1}H and ^{31}P NMR spectroscopy (Fig. 2.10). In the first run, complex **1a-C₂H₄** was completely converted to **1a-(1-hexene)** (87%) and **1a-(internal-hexene)** (13%) within 24 hours at 125 °C in the presence of excess *n*-hexane (solvent). Upon addition of ethylene (4 equiv), the rate of transfer dehydrogenation was significantly retarded and formed only 0.05 equiv of internal-hexene and 2% **1a-(1-hexene)** after 1 day at 125 °C. The major iridium species was **1a-C₂H₄** (98%). In run 3 with 1 equiv of 1-octene added, **1a-C₂H₄** (98%), **1a-(1-hexene)** (2%), and ca. 1 equiv of internal octenes were observed after 1 day. The amount of ethane were difficult to determine because of overlap with the alkane solvent in the ^{1}H NMR spectrum. However, based on the results of run 2, we reasoned that the amount of transfer dehydrogenation products must be very low. The internal octenes (~1 equiv) was most likely derived from 1-octene which displaced the ethylene to form **1a-(1-octene)**. Olefin isomerization of **1a-(1-octene)** generated **1a-(internal-octene)** and, following ligand exchange with ethylene, released the internal octenes and regenerated **1a-C₂H₄**. The iridium dihydide complex **1a-H₂** would be present in very low concentration due to the presence of excess ethylene. Thus, 1-octene was most likely isomerized via the π–allyl isomerization mechanism, instead of the "hydride insertion" mechanism.

31

(1)

87%   +   n=m=1 or n=0, m=2   13%   +

(2)

4 eq

125 °C, 1d

98%   +   2%

+   internal-hexene   +
    0.05 eqiv   trace

(3)

+ 1 eq 1-octene   4 eq

125 °C, 1d

98%   +   2%

+ ca. 1 eqiv internal-alkene

(4)

+ 8 eq 1-octene   0, 5, 30 eq

125 °C

+
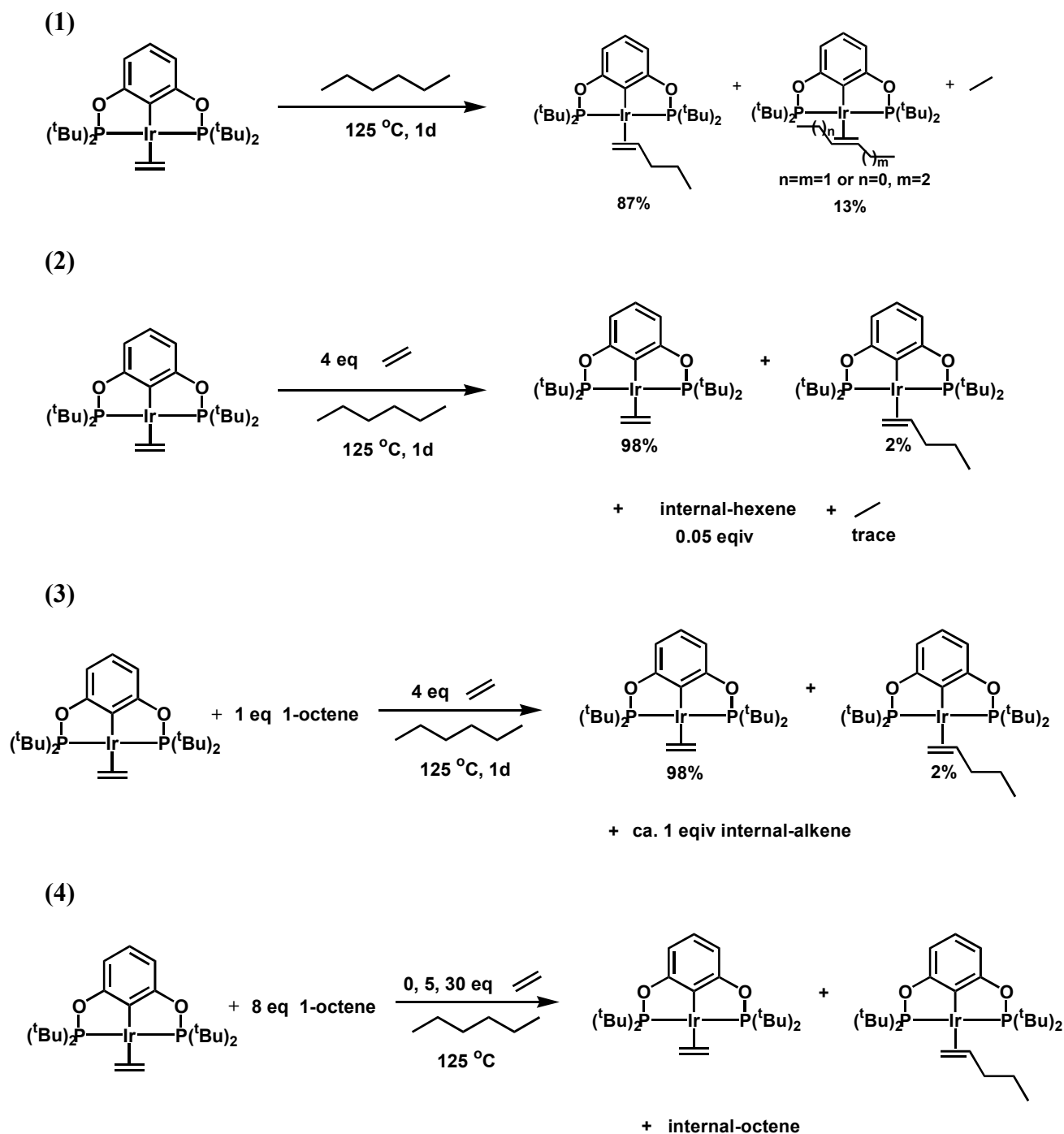
+ internal-octene

Fig. 2.10 Transfer dehydrogenation and olefin isomerization reactions by 1a-C_2H_4.

Upon addition of ethylene, the isomerzation of 1-octene to internal octenes was inhibited. In an isomerization reaction employing **1a-C_2H_4** and 1-octene (8 equiv) with *n*-octane as solvent, various quantities of ethylene (0, 5, and 30 equiv) were added. The

reaction without ethylene generated a mixture of **1a-(1-octene)** (26%), **1a-C₂H₄** (74%), free ethylene, as well as internal-octene (0.6 equiv) at 125 °C at an early stage (35 min). After 12 hours, more than 98% of 1-octene was converted to internal octenes. Due to the high binding affinity of ethylene relative to internal octenes, internal octenes were diplaced to generate **1a-C₂H₄** (96%). **1a-(1-octene)** was present as a minor iridium species (4%). The transfer dehydrogenation rate must be very slow because most of ethylene (96%) was still remaining. In a second reaction with 5 equiv of ethylene present, 1-octene isomerization was again complete in 12h (>98%); however, **1a-C₂H₄** was the only species observed at any stage of the reaction. Again, transfer dehydrogenation rate was slow.[12] When 30 equiv of ethylene were introduced, the olefin isomerization was significantly slower as only 50% of 1-octene had been isomerized after 12 hours. The iridium resting state was **1a-C₂H₄** and no transfer dehydrogenation occurred.

Conclusions

Through the mechanistic studies, a rationale has been put forward for the different product selectivities and resting states of the POCOP and PCP iridium catalysts in AM. Both steric and electronic effects favor the formation of (tBu-POCOP)Ir-olefin and (tBu-PCP)IrH₂ as the catalytic resting states in these systems. Olefin isomerization during AM occurs from a (pincer)Ir(I)-olefin complex via formation of a (pincer)Ir(III)(allyl)(H) intermediate, not via a (pincer)Ir(H)₂(olefin) intermediate. This conclusion was supported by DFT calculations, solvent effects on rate of olefin isomerization, and deuterium labeling experiments. The Ir(III) π–allyl hydride intermediate was independently generated; is was observed by low temperature NMR spectroscopy and shown to collapse to a (pincer)Ir-propylene complex.

Compared to the PCP system, the POCOP system, with iridium-olefin resting states, isomerizes olefins much faster during AM, resulting in low product selectivity. Finally, experiments show that olefin isomerization with the POCOP iridium complex can be prevented by addition of ethylene but dehydrogenation activity was inhibited as well.

Experimental Section

General Considerations. All manipulations were carried out using standard Schlenk, high-vacuum and glovebox techniques. Pentane and toluene were passed through columns of activated alumina. Mesitylene-d_{12} and methylcyclohexane-d_{12}, 1-pentene, 1-hexene, 1-octene, 1-decene, cis/trans 2-hexene and cis/trans 3-hexene were dried with 4 Å molecular sieves and degassed by freeze-pump-thaw cycles. *n*-hexane, *tert*-butylethylene and eicosane were purchased from Aldrich. Hexane and *tert*-butylethylene were dried with $LiAlH_4$ vacuum transferred into sealed flasks. Deuteride propylene gases, CD_3CHCH_2, CH_3CDCH_2, and CD_3CDCD_2 were purchased from CDN and used as received. Complex **Mo-F$_6$** was purchased from Strem and used as received. Complexes **1a-C$_2$H$_4$**,[1] **1a-H$_2$**,[7] **2-H$_2$**,[11] were synthesized as previously reported. Complex **1a-CO**[7] was synthesized as previously reported[7] and single crystal was obtained from a toluene solution.

NMR spectra were recorded on BRUKER DRX-400, AVANCE-400, and BRUKER DRX-500 MHz spectrometers. ^{1}H and ^{13}C NMR spectra were referenced to residual protio solvent peaks. [31]P chemical shifts were referenced to an external H_3PO_4 standard.

Synthesis of 1a-(alkene) (alkene = propene, 1-butene, 1-pentene, 1-hexene, 1-decene, and internal-hexene). To a solution of $\{C_6H_3$-2,6-[OP(*t*-Bu)$_2$]$_2\}$IrH$_2$ (**1a-H$_2$**) (5 mg, 8.4 μmol) and *n*-hexane (0.35 ml) in a medium-walled J. Young NMR tube was added excess of

respective olefins. After 30 min at room temperature, volatiles were evaporated under vacuum, and the resulting red solid was dried under vacuum overnight. $^{31}P\{^1H\}$ NMR (*n*-hexane): **1a-(propene)** δ 179.6 (s); **1a-(1-butene)** δ 179.5 (s); **1a-(1-pentene)** δ 179.4 (s); **1a-(1-hexene)** δ 179.4 (s); **1a-(1-decene)** δ 179.4 (s); **1a-(internal-hexene)** δ 176.3-176.5 (d).

Synthesis of 1a-(propylene-d_3), 1a-(propylene-d_1), and 1a-(propylene-d_6). To a solution of **1a-H$_2$** (5 mg, 8.4 μmol) and toluene (0.35 ml) in a medium-walled J. Young NMR tube was added 3-5 equiv of respective olefins. After 2 hours at room temperature, volatiles were evaporated under vacuum, and the resulting red solid was dried under vacuum overnight. **1a-(propylene-d_3):** ^1H NMR (162 MHz, 23 °C, Mes-d_{12}): δ 1.15 (virtual triplet, apparent J = 6.4 Hz, 18H, 2 × ^tBu), 1.33 (virtual triplet, apparent J = 6.4 Hz, 18H, 2 × ^tBu), 2.39 (d, $^3J_{H\text{-}H}$ = 8.0 Hz, 1H, CH_2), 3.74 (m, 1H, CH_2), 4.46 (m, 1H, CH), 6.67 (d, $^3J_{H\text{-}H}$ = 8.0 Hz, 2H), 6.84, (t, $^3J_{H\text{-}H}$ = 8.0 Hz, 1H). $^{31}P\{^1H\}$ NMR (400 MHz, 23 °C, Mes-d_{12}): δ 179.8 (s). **1a-(propylene-d_1):** ^1H NMR (400 MHz, 23 °C, Mes-d_{12}): δ 1.15 (virtual triplet, apparent J = 6.4 Hz, 18H, 2 × ^tBu), 1.33 (virtual triplet, apparent J = 6.4 Hz, 18H, 2 × ^tBu), 1.65 (s, 3H, CH$_3$ in propylene), 2.39, (s, 1H, CH_2), 3.74 (t, $^3J_{H\text{-}D}$ = 5.6 Hz, 1H, CH_2), 6.67 (d, $^3J_{H\text{-}H}$ = 8.0 Hz, 2H), 6.84, (t, $^3J_{H\text{-}H}$ = 8.0 Hz, 1H). $^{31}P\{^1H\}$ NMR (162 MHz, 23 °C, Mes-d_{12}): δ 179.8 (s). **1a-(propylene-d_6):** ^1H NMR (400 MHz, 23 °C, Mes-d_{12}): δ 1.15 (virtual triplet, apparent J = 6.4 Hz, 18H, 2 × ^tBu), 1.33 (virtual triplet, apparent J = 6.4 Hz, 18H, 2 × ^tBu), 6.67 (d, $^3J_{H\text{-}H}$ = 8.0 Hz, 2H), 6.84, (t, $^3J_{H\text{-}H}$ = 8.0 Hz, 1H). $^{31}P\{^1H\}$ NMR (162 MHz, 23 °C, Mes-d_{12}): δ 179.8 (s).

Formation of the Ir(III) η^3-allyl hydride complex. To a frozen methylcyclohexane-d_{14} (0.35 ml) solution of **1a-H$_2$** (5 mg, 8.4 μmol) in a medium-walled J. Young NMR tube was

added 2 equiv of allene. The J. Young NMR tube was shaken quickly when the solution was just beginning to melt and then the tube was inserted into the spectrometer at -83 °C. A mixture of **1a-(allyl)(H), 1a-H$_2$** and **1a-propylene** was observed by ^{1}H and ^{31}P NMR. **1a-(allyl)(H):** ^{1}H NMR (500 MHz, 23 °C, methylcyclohexane-d$_{14}$): δ −13.13 (s, 1H, Ir*H*), 2.00 (s, 1H, H$_{anti}$), 2.13 (s, 1H, H$_{anti}$), 2.64 (s, 1H, H$_{syn}$), 2.78 (s, 1H, H$_{syn}$), 4.94 (s, 1H, H$_{meso}$), 6.42 (s, 1H, H at the *meta*-position), 6.43 (s, 1H, H at the *meta*-position). The [t]Bu groups and one H at the *para*-position of the backbone were overlapping with thoses of **1a-H$_2$** and **1a-propylene**. ^{31}P{^{1}H} NMR (202 MHz, 23 °C, methylcyclohexane-d$_{14}$): δ 152.5 (d, $J_{P\text{-}P}$ = 341 Hz), 158.5 (d, $J_{P\text{-}P}$ = 341 Hz).

Procedures for resting state experiments: A medium-walled J. Young NMR tube was charged with 8 μmol of **1a-H$_2$**, 9.8 mg (13 μmol) of the hexafluorinated Schrock catalyst **3**, and 0.75 mL of *n*-hexane. The NMR tube was inserted into a 125 °C oil bath. Periodically, the tube was removed from the bath, cooled to room temperature, and analyzed by ^{31}P{^{1}H} NMR.

Procedures for alkane metathesis reactions: A flask was charged with 12.8 mg (21 μmol) of **1a-C$_2$H$_4$**, 6.5-26 mg (8.5-34 μmol) of **Mo-F$_6$**, 1.6 mL (12.07 mmol) of *n*-hexane, 0.852 g (3.02 mmol) of eicosane, and 10.2 mg (0.063 mmol) of hexamethylbenzene as internal standard. The flask was sealed tightly with a teflon plug under an argon atmosphere, and the solution stirred in a 125 °C oil bath. Periodically, the flask was removed from the bath and cooled in an ice bath. An aliquot was removed from the flask, and analyzed by GC. Product concentrations were calculated for each aliquot.

Intraligand deuterium/hydrogen exchange. A mesitylene-d$_{12}$ (0.35 ml) solution of **1a-(propylene-d$_3$)** or **1a-(propylene-d$_1$)** (8.4 μmol) in a medium-walled J. Young NMR was

heated at 60 or 125 °C. Peoriodically, the tube was cooled to room temperature and monitored by NMR.

Ligand exchanges reaction of 1a-(propylene-d$_6$). To a mesitylene-d$_{12}$ (0.35 ml) solution of **1a-(propylene-d$_6$)** (8.4 μmol) in a medium-walled J. Young NMR tube was added 2 equiv of propylene. The tube was heated at 60 °C. Peoriodically, the tube was cooled to room temperature and monitored by NMR.

Tansfer dehydrognenation and olefin isomerization by 1a-C$_2$H$_4$. To an *n*-hexane or *n*-octane (0.45 ml) solution of **1a-(C$_2$H$_4$)** (8-9 μmol) in a medium-walled J. Young NMR tube was added ethylene (0-30 equiv) and/or 1-octene (8 equiv). The tube was heated at 125 °C. Peoriodically, the tube was cooled to room temperature and monitored by NMR.

References and Note

(1) Goldman, A. S.; Roy, A. H.; Huang, Z.; Ahuja, R.; Schinski, W.; Brookhart, M. *Science* **2006**, *312*, 257.

(2) Bailey, B. C.; Schrock, R. R.; Kundu, S.; Goldman, A. S.; Huang, Z.; Brookhart, M. *Organometallic* **2009**, *28*, 355.

(3) Liu, F.; Pak, E. B.; Singh, B.; Jensen, C.; Goldman, A. S. *J. Am. Chem. Soc.* **1999**, *121*, 4086.

(4) Schrock, R. R.; Czekelius, C. C. *Adv. Synth. Catal.* **2007**, *349*, 55.

(5) Schrock, R. R. *Adv. Synth. Catal.* **2007**, *349*, 41.

(6) Schrock, R. R. *Chem. Rev.* **2002**, *102*, 145.

(7) Göttker-Schnetmann, I.; White, P. S.; Brookhart, M. *Organometallic* **2004**, *23*, 1766.

(8) Zhu, K.; Achord, P. D.; Zhang, X.; Krogh-Jespersen, K.; Goldman, A. S. *J. Am. Chem. Soc.* **2004**, *126*, 13044.

(9) Tulip, T. H.; Ibers, J. A. *J. Am. Chem. Soc.* **1979**, *101*, 42.

(10) Wakefield, J. B.; Stryker, J. M. *J. Am. Chem. Soc.* **1991**, *113*, 7057.

(11) Göttker-Schnetmann, I.; White, P. S.; Brookhart, M. *J. Am. Chem. Soc.* **2004**, *126*, 1804.

(12) No observable change of the amount of octenes and ethylene after 12 hours.

(13) Gupta, M.; Hagen, C; Flesher, R. J.; Kaska, W. C.; Jensen, C. M. *Chem. Commun.* **1996**, 2083.

CHAPTER THREE

Synthesis of New Iridium Pincer Complexes for Catalytic

Transfer Dehydrogenation and Alkane Metathesis

Introduction

Our initial homogeneous alkane metatheis (AM) systems were comprised of an iridium pincer dehydrogenation catalyst [(^{t}Bu-POCOP)IrC$_2$H$_4$ (**1a-C$_2$H$_4$**) or (^{t}Bu-PCP)IrH$_2$ (**2-H$_2$**), Fig. 3.1] and a Schrock olefin metathesis catalyst, Mo(NAr)(CHR)[OCMe(CF$_3$)$_2$]$_2$ (Ar = 2,6-diisopropylphenyl), (**Mo-F$_6$**).[1] More recently, over 40 molybdenum and tungsten imido alkylidene olefin metathesis catalysts were screened in combination with iridium catalysts for AM.[2] The results showed that W(NAr)(CHR)(OSiPh$_3$)$_2$ (**W-siloxyl**) was most active, performing about twice as well as the previously employed catalyst (**Mo-F$_6$**).

To date, only two iridium pincer catalysts, **1a** and **2**, have been examined for homogeneous AM. The POCOP catalyst, **1a**, gave higher yields than the PCP catalyst; the latter exhibited a higher selectivity for the formation of *n*-decane from the metathesis of *n*-hexane.[1,2] The lower selectivity with the POCOP system reflects a faster iridium-catalyzed olefin isomerization compared to the PCP system. Mechanistic studies (see Chapter 2) indicated that the product selectivity in AM was related to the resting state of the iridium species. Our experimental results and DFT calculations supported a "π–allyl" olefin

isomerization mechanism catalyzed by Ir complexes. The resting states of the POCOP-Ir catalysts are the Ir(I)(olefin) complexes. In contrast, the more sterically hindered PCP-Ir catalyst exhibits PCPIr-H_2 complex as the major resting state. Therefore, the POCOP system can isomerize the terminal-olefin to the internal-olefin(s) much faster than the PCP-Ir complex via the "π–allyl" mechanism. Through DFT calculations and crystal structure comparisons to assess steric effects, we found both steric and electronic consideration favor POCOP-Ir over PCP-Ir regarding olefin binding affinities. However, evidence suggested that the differences between POCOP and PCP mainly arise from the steric effect (see Chapter two).

1a-C$_2$H$_4$ L = C$_2$H$_4$
1a-H$_2$ L = H$_2$

2-H$_2$
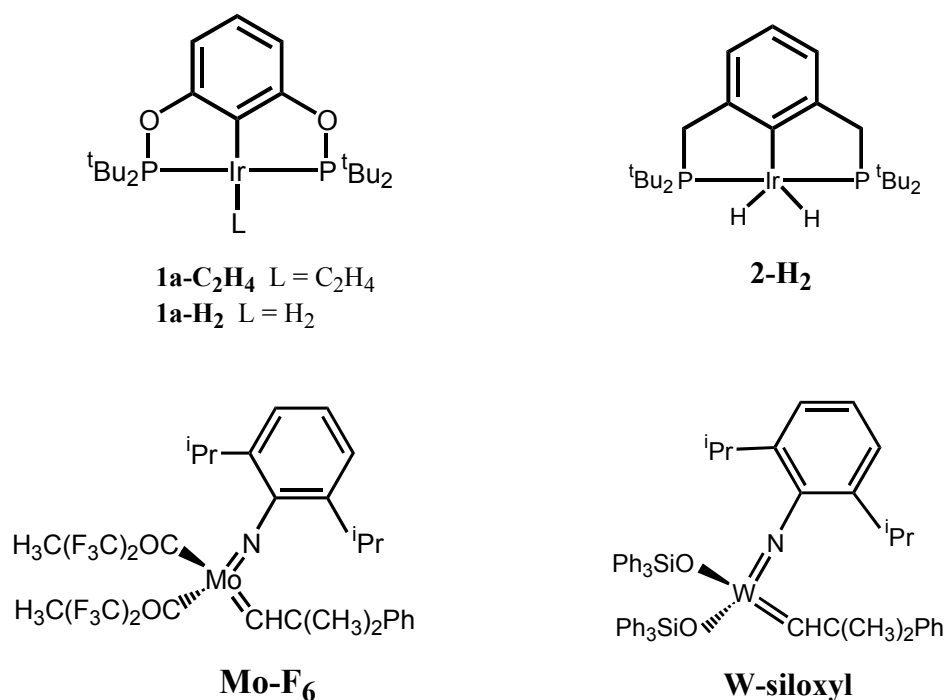
Mo-F$_6$

W-siloxyl

Fig. 3.1 Transfer dehydrogenation catalysts **1a** and **2** and Schrock olefin metathesis catalysts **Mo-F$_6$** and **W-siloxyl**.

1a	X = Y = O, R = R' = ^tBu	6	X = Y = O, R = R' = Ar
1b	X = Y = O, R = R' = ^iPr	7	X = Y = O, R = Ar, R' = Me
2	X = Y = CH$_2$, R = R' = ^tBu		
3a	X = S, Y = O, R = R' = ^tBu		
3b	X = S, Y = O, R = R' = ^iPr		
4	X = S, Y = NH, R = R' = ^tBu		
5	X = Y = S, R = R' = ^tBu		

L = C$_2$H$_4$, H$_2$
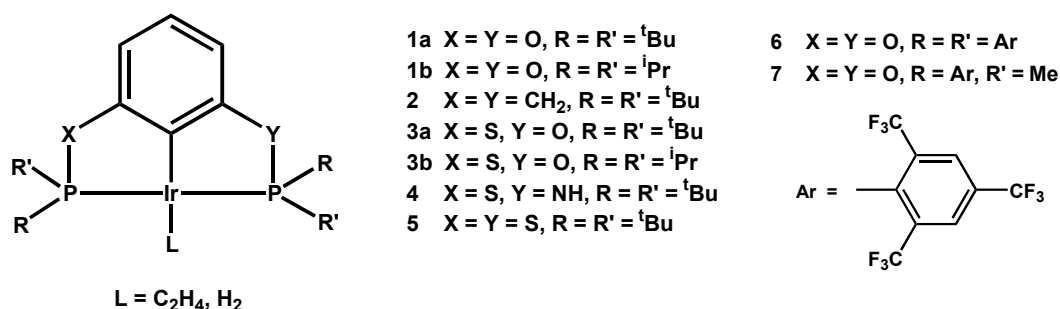
Fig. 3.2 Structures of iridium pincer complexes.

In this chapter, we report the syntheses of eight new iridium complexes with different substituents on the phosphorus atoms and various linkers between the backbone and phosphorus (see Fig. 3.2). These catalysts were screened for transfer dehydrogenation (TD), and AM in combination with the Schrock olefin metathesis catalyst. Interestingly, the least bulky complex **1b-C₂H₄**, (^{i}Pr-POCOP)IrC₂H₄, not only proved to be most efficient in both TD and AM, but also showed a higher product selectivity in AM than complex (^{t}Bu-POCOP)IrC₂H₄, **1a-C₂H₄**. A moderate productivity, but good selectivity, was obtained in AM using the bulky complex (^{t}Bu-PSCOP)IrC₂H₄, **3a-C₂H₄**. The most bulky complex **5-C₂H₄**, (^{t}Bu-PSCSP)IrC₂H₄, showed no and few TOs in TD and AM, respectively. Complexes **6-C₂H₄** and **7-C₂H₄** containing the sterically bulky and electron-withdrawing 2,4,6-tris(trifluoromethyl)phenyl substituents on the phosphorus atoms, exhibited low to moderate activities in TD and AM.

Results and Discussion

1. Syntheses of new pincer iridium complexes.

Complexes **1a-C₂H₄**, **1a-H₂** and **2-H₂** (Fig. 3.1) have been previously prepared and investigated for homogeneous alkane metathesis.[1] Complexes **1b-C₂H₄**, **3a-C₂H₄**, **3b-C₂H₄**, **4-C₂H₄**, **5-C₂H₄**, **6-C₂H₄** **7-C₂H₄** and **8-C₂H₄** (Fig. 3.2), previously unknown, were prepared in this study.

The chloro-bis[2,4,6-tris(trifluoromethyl)phenylphosphine[3] and chloro-methyl-2,4,6-tris(trifluoromethyl)phenylphosphine were prepared from 1,3,5- tris(trifluoromethyl)benzene as shown in Scheme 3.1. Deprotonation of resorcinol, 3-mercaptophenol, 3-aminothiophenol and benzene-1,3-dithiol with sodium hydride or *n*-butyllithium, followed by diphosphorylation with four different chlorophosphines formed the corresponding ligands (abbreviated as R-PXCYP or RR'-PXCYP if R is unequal to R', Scheme 3.2). The metalation conditions of these ligands are different and they are described below.

Scheme 3.1 Syntheses of tris(trifluoromethyl)phenyl-substituted phosphine compounds
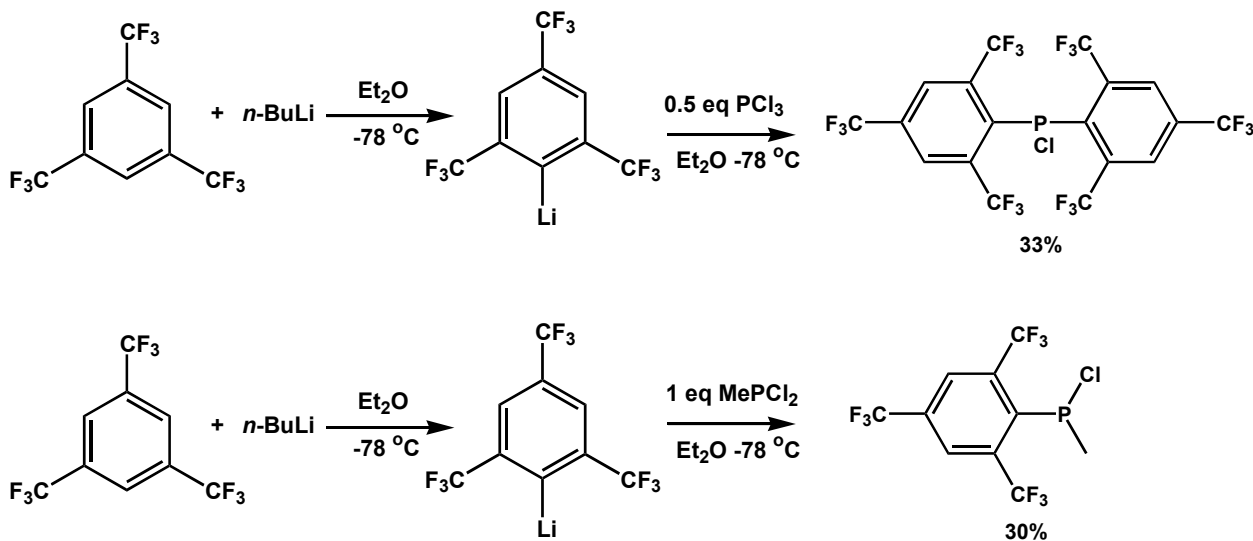
Scheme 3.2 Syntheses of the pincer ligands

X = Y = O, R = R' = ^{i}Pr 77% yield
X = S, Y = O, R = R' = ^{t}Bu 95%
X = S, Y = O, R = R' = ^{i}Pr 85%
X = S, Y = NH, R = R' = ^{t}Bu 24%
X = Y = S, R = R' = ^{t}Bu 46%
X = Y = O, R = R' = Ar 67%
X = Y = O, R= Ar, R' = Me 45%

R(R')-PXCYP or
R-PXCYP if R = R'
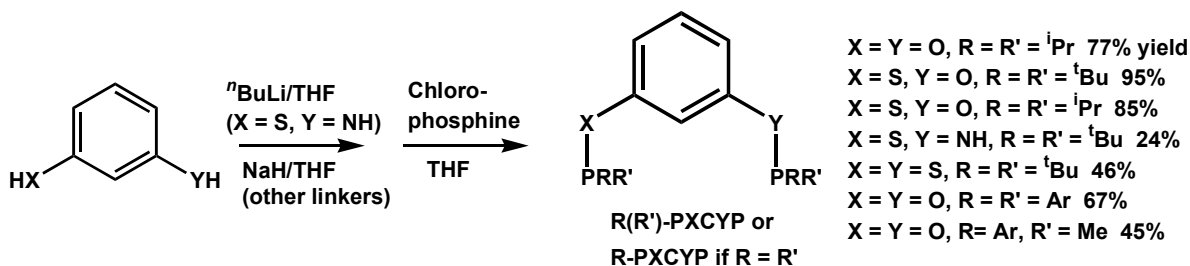
The *tert*-butyl substituted complexes **3a-C$_2$H$_4$**, **4-C$_2$H$_4$**, and **5-C$_2$H$_4$** were prepared in a similar way as outlined in Scheme 3.3. The reaction of the pincer ligand with [(COD)IrCl]$_2$ or [(COE)$_2$IrCl]$_2$ generated the monomeric hydrochloride (Note: complex **4-HCl** was prepared by Dr. Lalehzari). Treatment of the hydridochloride complexes with sodium *tert*-butyloxide in the presence of ethylene produced the corresponding ethylene iridium complexes.

Scheme 3.3 Formation of complexes **3a-C$_2$H$_4$**, **4-C$_2$H$_4$**, and **5-C$_2$H$_4$**

3a-HCl, X = S, Y = O, 71%
4-HCl, X = S, Y = NH, 55%
5-HCl, X = Y = S, 27%

3a-C$_2$H$_4$, X = S, Y = O, 89%
4-C$_2$H$_4$, X = S, Y = NH, 43%
5-C$_2$H$_4$, X = Y = S, 79%
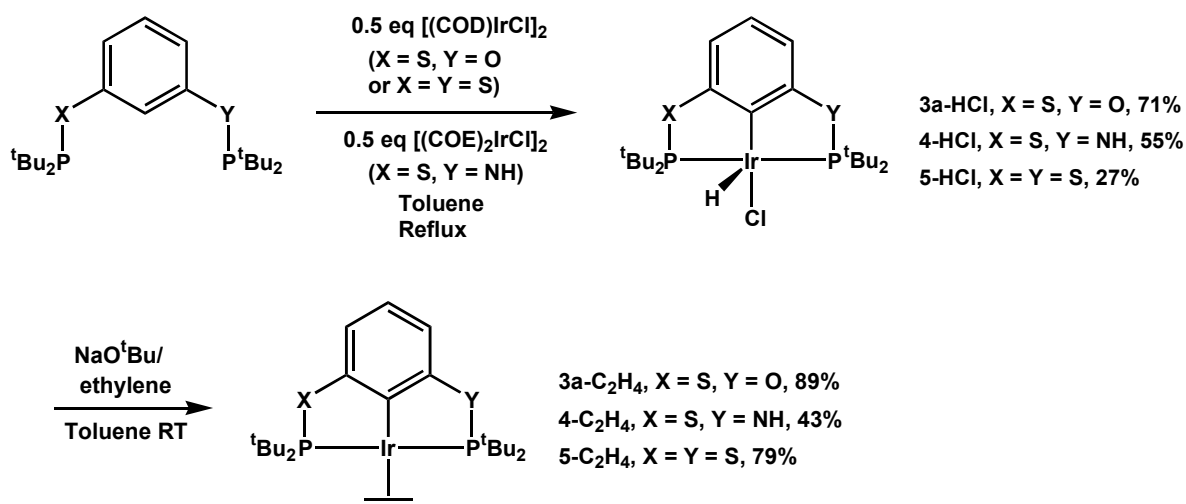
Syntheses of the *iso*-propyl substituted complexes **1b-C$_2$H$_4$** and **3b-C$_2$H$_4$** are outlined in Scheme 3.4. The monomeric iridium hydrochloride complex can be synthesized readily by

a reaction of the *tert*-butyl substituted pincer ligand with [(COD)IrCl]$_2$ or [(COE)$_2$IrCl]$_2$.

However, the less sterically bulky ligands, ^{i}Pr-POCOP and ^{i}Pr-PSCOP, react with an iridium

source to form the Cl-bridged dimeric complexes (**1b-dimer** and **3b-dimer**). It should be

noted that the iridium sources and reaction conditions are crucial to the formation of clean

products. Treatment of ^{i}Pr-POCOP with one equiv. of [(COE)$_2$IrCl]$_2$ *at room temperature*

generated a dimer, (^{i}Pr-POCOP)IrH(μ-Cl)$_2$Ir(COE)$_2$, in a low yield (20–30%); and the

reaction of ^{i}Pr-PSCOP with one equiv. of [(COD)IrCl]$_2$ and five equiv. of COD *at 130 °C*

formed (^{i}Pr-PSCOP)IrH(μ-Cl)$_2$Ir(COD) in 21% yield (addition of excess of COD prevents

the formation of Ir(0) metal). The dimeric complexes were then cleaved by NaO^{t}Bu to form

monomers **1b-C$_2$H$_4$** and **3b-C$_2$H$_4$** in the presence of ethylene.

Scheme 3.4 Formation of complexes **1b-C$_2$H$_4$** and **3b-C$_2$H$_4$**
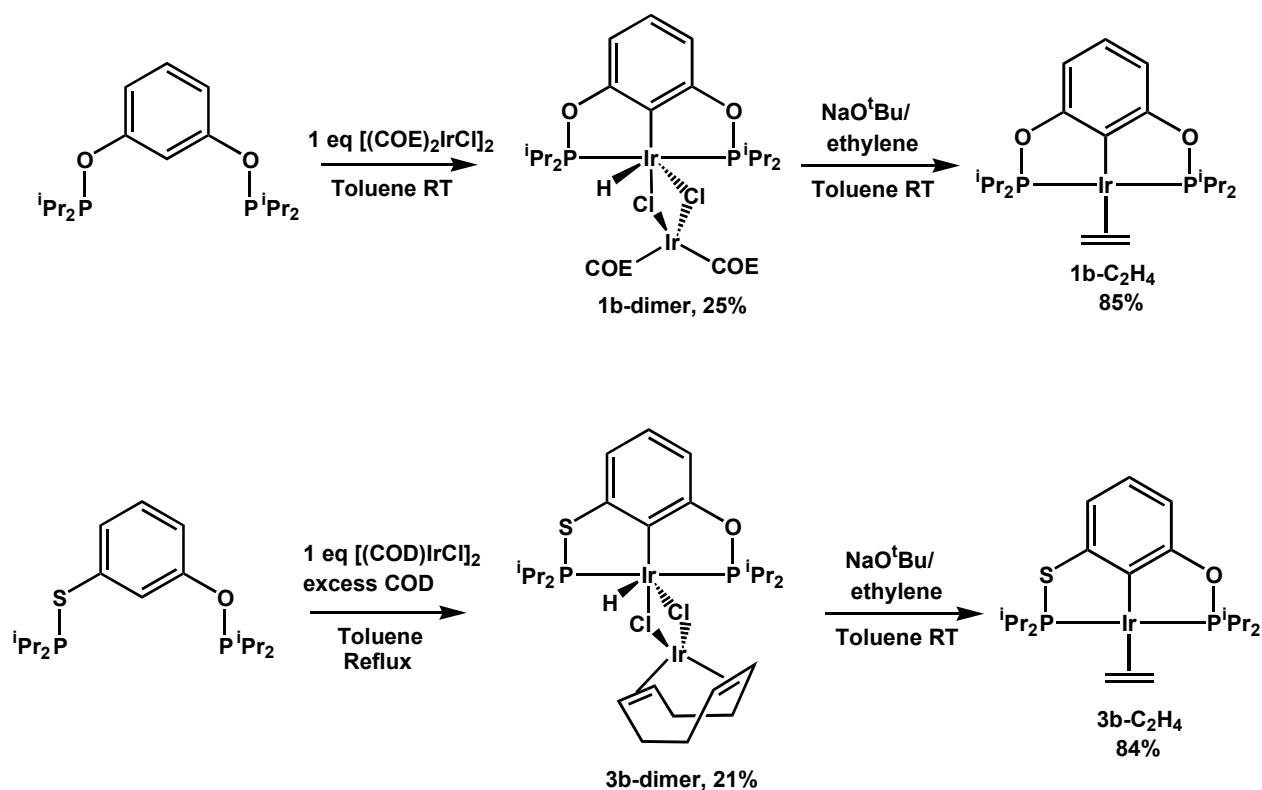
Scheme 3.5 Formation of complexes **6-C₂H₄** and **7-C₂H₄**
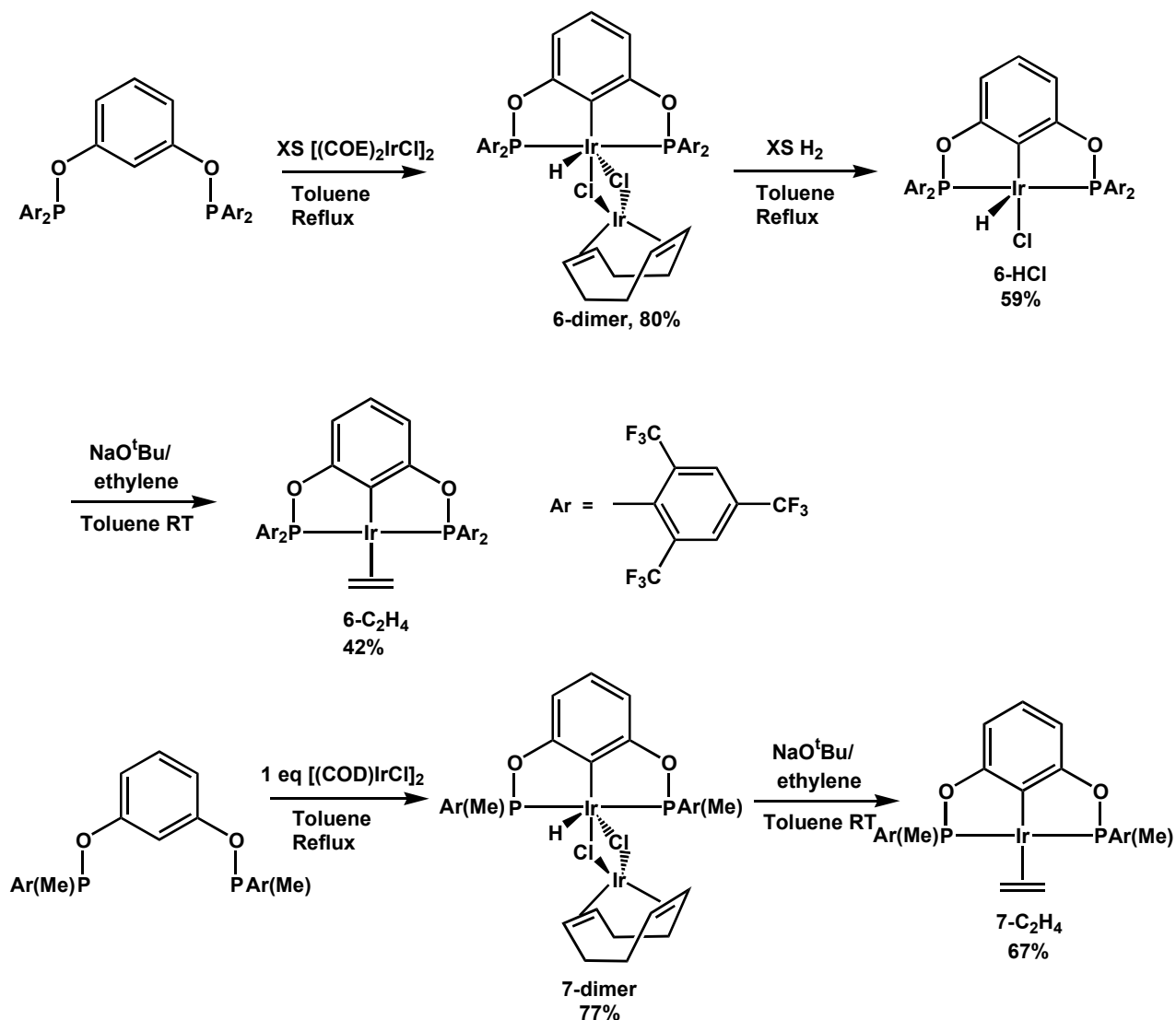
Syntheses of the 2,4,6-tris(trifluoromethyl)phenyl substituted complexes **6-C₂H₄** and **7-C₂H₄** are outlined in Scheme 3.5. The tetra-[2,4,6-tris(trifluoromethyl)phenyl] substituted pincer ligand, Ar-POCOP, reacts slowly with [(COE)₂IrCl]₂ to form a chloro-bridged dimer, **6-dimer**. Most of the [(COE)₂IrCl]₂ decomposed under the reaction conditions and thus excess [(COE)₂IrCl]₂ must be added. After 8 days with 16 periodic additions of [(COE)₂IrCl]₂ (one equiv. of Ir relative to ligand each time), the reaction

generated ca. 80% of product and [(COD)IrCl]$_2$ presumably through the dehydrogenation of COE. Heating a toluene solution of the dimer with excess of H$_2$ at 150 °C formed a monomeric iridium hydrochloride complex. The iridium ethylene complex, **6-C$_2$H$_4$,** was obtained from the reaction of **6-HCl** with NaO^{t}Bu in the presence of ethylene.

The less sterically bulky ligand, Ar(Me)-POCOP, reacted readily with one equiv. of [(COD)IrCl]$_2$ to form a chloro-bridged dimer, **7-dimer**, which was cleaved by NaO^{t}Bu to generate the iridium ethylene complex, **7-C$_2$H$_4$**.

Scheme 3.6 Formation of complexes **8-C$_2$H$_4$**
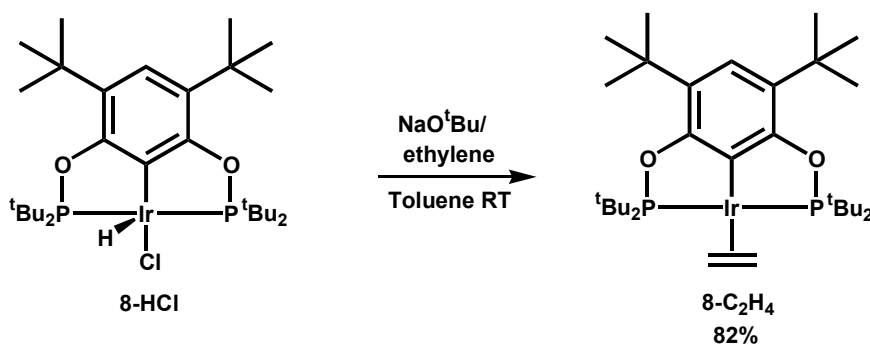
Syntheses of complex **8-C$_2$H$_4$** is outlined in Scheme 3.6. Complex **8-HCl** has been prepared by Dr. Göttker-Schnetmann. Treatment of the iridium hydrochloride complex with NaO^{t}Bu in the presence of ethylene generated **8-C$_2$H$_4$**.

2. Structural comparisons of iridium pincer complexes

Our previous studies indicated that steric effects in iridium complexes play an essential role in determining the selectivity and activity of AM. Thus, it is of interest to consider the structural features of the iridium pincer complexes, which provide information concerning the steric environment of the iridium center. The *tert*-butyl substituted complexes, **1a-C$_2$H$_4$** and **3a-C$_2$H$_4$**, will exhibit a more sterically hindered environment around the iridium center than the *iso*-propyl substituted analogues, **1b-C$_2$H$_4$** and **3b-C$_2$H$_4$**; Complex **6a-C$_2$H$_4$** with

two bulky tris(trifluoromethyl)phenyl substituents on one phosphorus is more crowded than **7a-C₂H₄** with one methyl and one tris(trifluoromethyl)phenyl substituent.

For the series of *tert*-butyl substituted complexes, the crystal structures provide insights into the extent of steric crowding at iridium. Here we compare the bond distances and angles of the hydridochloride complexes because they are easier to crystallize compared to the ethylene analogues. Fig. 3.3 shows the ORTEP diagrams of **1a-HCl**, **3a-HCl**, **4-HCl** and **6-HCl**. Tables 3.1 and 3.2 summarize the key bond distances and angles, and the crystallographic data. As the size of the linker atom (X) increases (S > N > O), the C-X and X-P bond distances and the P-Ir-P bond angle increase. For example, the P-Ir-P bond angles for complexes **1a-HCl**, **3a-HCl**, and **4-HCl** are 160.06(4)°, 168.32(3)° and 169.49(4)°, respectively. With the P-Ir-P bond angle increasing, the iridium center is more crowded as two *tert*-butyl groups on two phosphorus atoms become closer to each other. Thus, **3a-HCl** and **4-HCl** are similar to each other regarding steric crowding, but are much more crowded than **1a-HCl**. The solid-state structure of **5-HCl** is unavailable, but it must be the most hindered one as it has two large S atoms as the linkers. In short, the steric crowding of the series of *tert*-butyl substituted complexes increases as the atomic volume of the linker increases: **5-C₂H₄** (S,S linkers) > **4-C₂H₄** (S,N) > **3a-C₂H₄** (S,O) > **2-C₂H₄** (C,C) > **1a-C₂H₄** (O,O).

Due to the presence of the bulky tris(trifluoromethyl)phenyl substituents, **6-C₂H₄** is more sterically hindered than **1a-C₂H₄**, even though the P-Ir-P bond angle in **6-HCl** (158.61(13)°) is slightly smaller than that in **1a-HCl**. As shown in Fig. 3.3d, the four [(CF₃)₃C₆H₂] rings forms a deep pocket with two of trifluoromethyl groups very close to the Ir center (Ir···F = 3.074 and 3.187 Å).

Table 3.1 Selected bond distances (Å) and angles (deg) for single crystals **1a-HCl**, **3a-HCl**, **4-HCl** and **6-HCl**.

Crystals	bond distances (Å)	bond angles (deg)
1a-HCl	Ir1-C10 = 2.011(5), Ir1-P2 = 2.2928(12), Ir1-P1 = 2.2971(12), Ir1-Cl1 = 2.4041(12), P1-O9 = 1.662(3), P2-O16 = 1.662(3), O9-C11 = 1.399(5), C15-O16 = 1.394(5)	P2-Ir1-P1 = 160.06(4), C11-O9-P1 = 115.5(3), C15-O16-P2 = 115.5(3)
3a-HCl	Ir1-C17 = 2.019(3), Ir1-P1 = 2.2986(8), Ir1-P2 = 2.2980(8), Ir1-Cl1 = 2.4149(8), P1-S1 = 2.123(3), P2-O1 = 1.670(7), S1-C18 = 1.772(7), O1-C22 = 1.396(9)	P2-Ir1-P1 = 168.32(3), C18-S1-P1 = 99.1(3), C22-O1-P2 = 116.0(6)
4-HCl	Ir1-C9 = 2.031(4), Ir1-P2 = 2.3037(10), Ir1-P1 = 2.3055(10), Ir1-Cl1 = 2.4273(12), P1-S1 = 2.1069(15), P2-N15 = 1.696(4), S1-C10 = 1.777(4), C14-N15 = 1.392(6)	P2-Ir1-P1 = 169.49(4), C10-S1-P1 = 99.16(16), C14-N15-P2 = 118.7(3),
6-HCl	Ir1-C1 = 2.007(14), Ir1-P1 = 2.288(5), Ir1-P2 = 2.304(5), Ir1-Cl1 = 2.428(11), P1-O1 = 1.635(12), P2-O2 = 1.612(13), O1-C2 = 1.41(2), O2-C6 = 1.42(2)	P1-Ir1-P2 = 158.61(13), C2-O1-P1 = 115.9(10), C6-O2-P2 = 115.4(10)

Table 3.2 Crystal data and structure refinement summary of **1a-HCl**, **3a-HCl**, **4-HCl** and **6-HCl**.

	1a-HCl	**3a-HCl**	**4-HCl**	**6a-HCl**
Formula	$C_{22}H_{41}ClIrO_{2.5}P_2$	$C_{22}H_{39}ClIrOP_2S$	$C_{22}H_{41}ClIrNP_2S$	$C_{119}H_{62}Cl_2F_{72}Ir_2O_4P_4$
crystal system	Triclinic	Orthorhombic	Orthorhombic	Triclinic
Space group	P-1	Pbca	Pna2$_1$	P-1
a/Å	8.1459(2)	12.1021(4)	22.7124(6)	12.694(3)
b/Å	12.1660(2)	15.0014(5)	7.9189(2)	13.460(3)
c/Å	13.3405(3)	28.1281(9)	14.1470(5)	18.120(4)
α/deg	100.598(1)	90	90	81.197(16)
β/deg	95.618(1)	90	90	86.626(17)
γ/deg	103.830(1)	90	90	84.041(16)
V/(Å^3)	1247.84(5)	5106.6(3)	2544.44(13)	3040.1(12)
Z	2	8	4	1
T/K	100(2)	100(2)	100(2)	100(2)
$R1$ [$I>2\sigma(I)$]	0.0314	0.0226	0.0217	0.0818
$wR2$ (all data)	0.0746	0.0539	0.0528	0.2076
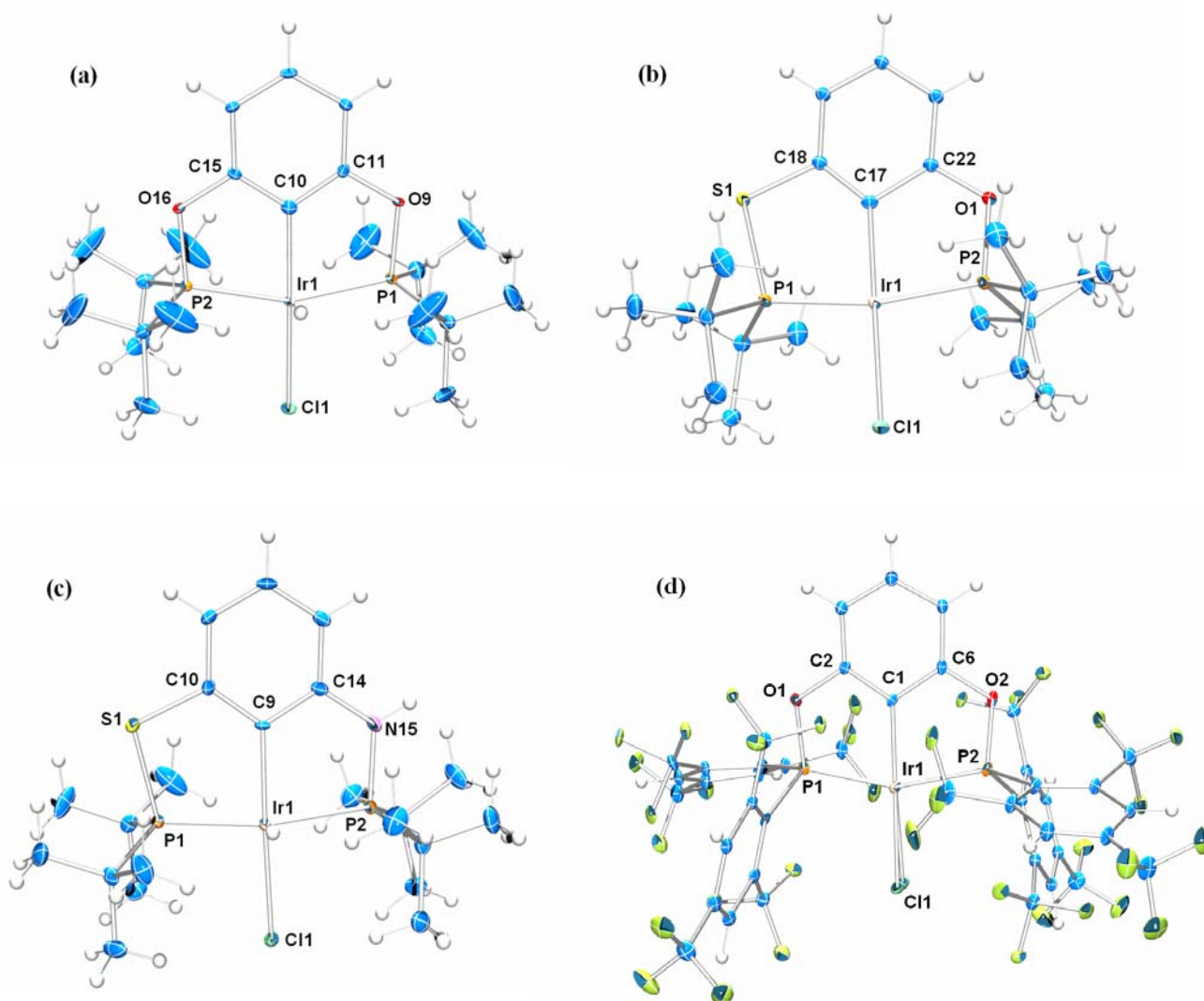
Fig. 3.3 Crystal structures of **1a-HCl** (a), **3a-HCl** (b), **4-HCl** (c) and **6-HCl** (d, chlorine atom is disordered). Hydrogen atom on the Ir center in **3a-HCl** and **6-HCl** can not be located.

3. Transfer dehydrogenation (TD) results with new iridium pincer complexes
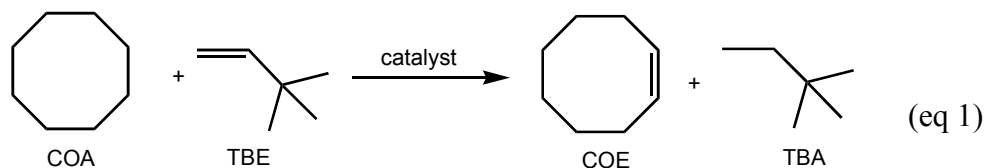
The newly synthesized iridium pincer complexes were examined for transfer dehydrogenation activity using the "benchmark" reaction (eq 1), the transfer of hydrogen

from cyclooctane (COA) to *tert*-butylethylene (TBE). In a typical reaction, a system containing 2.5 μmol of iridium catalyst, 7.5 mmol of COA (3000 equiv. relative to Ir) and 7.5 mmol of TBE, was heated to 200 °C under argon in a sealed vessel. The results are summarized in Table 3.3. The initial TD rate using the less bulky (^{i}Pr-POCOP)IrC$_2$H$_4$ complex, **1b-C$_2$H$_4$**, was lower than that using (^{t}Bu-POCOP)IrC$_2$H$_4$, **1a-C$_2$H$_4$** (310 vs 920 TONs at 30 min), but the ultimate conversion by **1b-C$_2$H$_4$** is greater (2680 vs 1580 TONs at 40 h). Compared to **1a-C$_2$H$_4$**, **1b-C$_2$H$_4$** appears to be less subject to inhibition by the dehydrogenation product, COE.[5,6] For the series of *tert*-butyl substituted catalysts, the TD activities decrease as the steric hindrance increases: **1a-C$_2$H$_4$** > **3a-C$_2$H$_4$** > **4-C$_2$H$_4$** > **5-C$_2$H$_4$**. As shown in Table 3.3, **1a-C$_2$H$_4$** gave 1580 TONs after 40 h compared to the run where no activity was observed using the most bulky (^{t}Bu-PSCSP)IrC$_2$H$_4$, **5-C$_2$H$_4$**.

The sterically bulky and electron-deficient **6-C$_2$H$_4$** showed very poor TD activity and short lifetime. The color of the solution changed from red to light yellow after 3 h and the catalyst lost activity completely as heating for longer time resulted no additional turnovers. By comparison, the less crowded and more electron-rich complex **7-C$_2$H$_4$** performed better, giving 310 TONs after 40 h.

Table 3.3 TONs in the transfer dehydrogenation of COA/TBE using **1a-C$_2$H$_4$**, **1b-C$_2$H$_4$**, **3a-C$_2$H$_4$**, **4-C$_2$H$_4$**, **5-C$_2$H$_4$**, **6-C$_2$H$_4$**, and **7-C$_2$H$_4$** at 200 °C.

Time (h)	1b-C$_2$H$_4$	1a-C$_2$H$_4$	3a-C$_2$H$_4$	4-C$_2$H$_4$	5-C$_2$H$_4$	6-C$_2$H$_4$	7-C$_2$H$_4$
0.5	310	920	120	17	0	--	230
3	1150	1190	140	--	0	30	280
15	2240	1510	170	--	0	--	--
40	2680	1580	170	17	0	30	310

4. Alkane metathesis (AM) results with new iridium pincer complexes

$$\text{Ir Pincer Catalyst} \quad + \quad n\text{-C}_6\text{H}_{14} \quad + \quad \text{Schrock cat.} \xrightarrow{\quad 125\ ^{\circ}\text{C}\quad} n\text{-alkanes} \quad \text{(eq 2)}$$

1 equiv   760 equiv   0.8 equiv
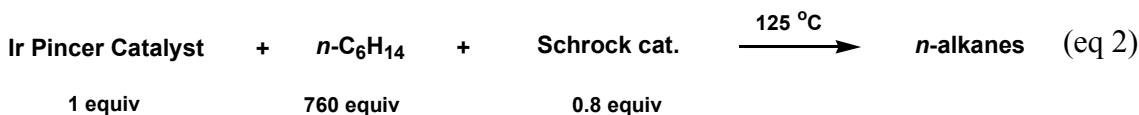
Finally, AM reactions were conducted with these new iridium catalysts. An n-hexane solution (760 equiv. relative to Ir) containing 10 mM iridium catalyst and 8 mM of Schrock catalyst (**Mo-F$_6$** unless otherwise specified) was heated at 125 °C (eq 2). The reactions were monitored by GC periodically using mesitylene as an internal standard. The product distributions are summarized in Table 3.4 and the activity and selectivity are described below.

Table 3.4 Distribution of C_2 to C_{15+} n-alkanes products from the metathesis of n-hexane (7.6 M) by various iridium catalysts (10 mM) and the Schrock catalyst **Mo-F$_6$** (8 mM) at 125 °C.

Entry	Ir cat.	Time	Product concentration (mM)												Total TONs
			C_2/C_3	C_4	C_5	C_7	C_8	C_9	C_{10}	C_{11}	C_{12}	C_{13}	C_{14}	C_{15+}	
1	1b-C$_2$H$_4$	1 h	79	38	94	62	25	37	39	3	1	1	---	---	38
		6 h	307	168	375	241	103	136	160	30	13	9	6	4	155
		24 h	307	175	392	261	114	150	169	34	15	11	7	5	164
		2 d	309	180	405	267	116	151	169 *24%^{a}*	34	15	11	7	5	167
		Added additional **Mo-F$_6$** (8 mM)													
		20 h	446	304	674	428	183	219	269	68	32	24	18	14	268
2	1a-C$_2$H$_4$	1 h	29	19	32	21	11	12	8	1	---	---	---	---	13
		6 h	89	67	115	82	46	45	29	53	2	1	---	---	48
		24 h	187	155	253	195	113	106	66	17	7	4	2	2	111
		2 d	238	194	323	240	134	128	80 *14%*	21	9	5	2	2	138
3	1a-H$_2$ w/o olefin	3 h	10	6	9	6	2	1	2	1	--	--	--	--	4
		24 h	123	89	175	130	59	50	37	3	1	--	--	--	67
		2 d	418	291	520	376	184	195	122 *14%*	27	12	7	3	2	216
		4 d	456	322	561	411	206	219	139	36	18	9	4	3	239
		7 d	495	366	643	459	220	221	134	34	17	9	4	3	261
4	2-H$_2$^{b}	23 h	307	127	306	155	37	49	232 *49%*	18	4	4	1	2	125

51

Entry	Cat.	Time													Total
5	3a-C$_2$H$_4$	1 h	21	4	11	6	1.7	3.4	8.7	1.7	--	--	--	--	6
		6 h	45	16	46	32	9	9	20	5	1	0.5	--	--	18
		24 h	110	41	124	89	22	25	60+6[c]	11	3	1	--	--	50
		2 d	170	65	190	129	35	39	110+4 *36%*	18	4	2	1	--	77

Entry	Cat.	Time													Total
6	3a-C$_2$H$_4$	**With 2.5 equiv. 5-decene**													
		1 h	26	13	30	22	8+1	4+7	4+9	2	1	--	--	--	11[d]
		6 h	74	39	112	88	30	20+6	29+11	11	4	1	0.7	--	41[d]
		24 h	201	101	275	196	61	52+4	100+6	24	7	3	1	--	101[d]
		2 d	217	106	283	206	67	62	108+1	27	9	4	2	1	107[d]

Entry	Cat.	Time													Total
7	3a-C$_2$H$_4$	**With 10 equiv. 5-decene**													
		1 h	33	21	55	48+4	22+3	10+17	7+26	6	5	2	1	--	16[e]
		6 h	99	61	155	116	46	29+12	35+24	14	6	2	1	--	50[e]
		24 h	95	61	154	128	52	40+6	52+8	18	8	3	1	1	52[e]

Entry	Cat.	Time													Total
8	3a-C$_2$H$_4$	**With W-siloxyl** as the olefin metathesis catalyst (8 mM)													
		2d	116	65	105	58	31	35	101 *45%*	10	5	3	2	--	47

Entry	Cat.	Time													Total
9	3b-C$_2$H$_4$	1 h	24	14	33	21	7	10	11	1	--	--	--	--	12
		6 h	49	32	76	43	13	16	29	3	1	--	--	--	26
		24 h	88	55	129	82	24	28	44	7	2	1	--	--	46
		2 d	84	54	126	84	27	33	49 *25%*	8	2	1	--	--	47

Entry	Cat.	Time													Total
10	4-C$_2$H$_4$	1 h	22	9	18	15	5	3+1	3+2	1	--	--	--	--	8
		6 h	30	15	33	28	12	7+1	5+1	3	2	1	--	--	14
		24 h	47	28	68	54	20	10+1	8+2	5	2	1	--	--	25
		2 d	47	29	79	70	28	15+1	12+1 *10%*	6	3	1	--	--	29

Entry	Cat.	Time													Total
11	5-C$_2$H$_4$	2d	12	4	6	3	1	--	--	--	--	--	--	--	2.6

Entry	Cat.	Time													Total
12	7-C$_2$H$_4$	1 h	16	12	31	23	7	6	3	2	1	--	--	--	10
		6 h	49	37	95	80	29	19	16	6	2	1	--	--	33
		24 h	88	67	164	140	53	35	28	6	2	1	--	--	59
		2 d	88	68	170	143	54	36	28 *11%*	10	4	2	1	--	60

Entry	Cat.	Time													Total
13	8-C$_2$H$_4$	6 h	134	84	156	110	56	64	57	8	3	1	--	--	67
		24 h	184	119	219	155	80	86	73	13	4	2	1	--	94
		2 d	211	139	254	181	94	102	87 *19%*	17	6	3	2	--	110

[a] Selectivity of formation of C$_{10}$: C$_{10}$/(C$_7$+C$_8$+C$_9$+C$_{10}$); [b] Using 16 mM of Mo-F$_6$ olefin metathesis catalyst; [c] [Olefin] observed in the reactions; [d] The total TONs was obtained after subtracting the amount of 5-decene (2.5 equiv.); [e] The total TONs was obtained after subtracting the amount of 5-decene (10 equiv.)

4.1. AM activities with various iridium catalysts. The AM activities of iridium complexes mirror somewhat the TD activities, which is consistent with our observation that the rate-determining step in AM is transfer dehydrogenation by the iridium catalyst (at least at the early stage). In general, the AM activity decreases as the steric hindrance of iridium complexes increases: **1b-C$_2$H$_4$** (169 TONs, 2 d) > **1a-C$_2$H$_4$** (138 TONs) > **3a-C$_2$H$_4$** (77 TONs) > **4-C$_2$H$_4$** (29 TONs) > **5-C$_2$H$_4$** (2.6 TONs). The least sterically hindered complex **1b-C$_2$H$_4$** was most efficient and three times faster than the **1a-C$_2$H$_4$** at the early stage (155 vs 48 TONs after 6 hours). The activity decayed after 6 h mainly due to the decomposition of Schrock catalyst (Table 3.4, entry 1) since addition of more **Mo-F$_6$** catalyst resulted in an additional 101 TONs after 20 h.

The most hindered complexes, **4-C$_2$H$_4$** and **5-C$_2$H$_4$**, gave very low TONs (entry 10 and 11). Complex **3a-C$_2$H$_4$** was moderately active in AM with 77 TONs after 2 days (entry 5). The less hindered complex (^{i}Pr-PSCOP)IrC$_2$H$_4$, **3b-C$_2$H$_4$** was initially faster (12 TONs by **3b-C$_2$H$_4$** vs 6 TONs by **3a-C$_2$H$_4$** after 1h), but the final conversion (47 TONs after 2 d) was less than that with **3a-C$_2$H$_4$**.

Complex **7-C$_2$H$_4$** exhibited a moderate activity with 60 TONs after 2 days (entry 12). Compared to the parent complex **1a-C$_2$H$_4$**, **7-C$_2$H$_4$** is more electron-deficient, but is presumably less sterically bulky with one methyl and one tris(trifluoromethyl)phenyl substituent on each phosphorus compared to two *tert*-butyl groups. Thus, the lower activity of **7-C$_2$H$_4$** seems to result from the reduced electron density at the Ir center. Complex **8-C$_2$H$_4$** is slightly less active than **1a-C$_2$H$_4$**, giving 111 TONs after 2 days (entry13). The *tert*-butyl substituents in the *meta*-positions of the backbone appear, as expected, to have a negligible effect in AM activity.

4.2. Product selectivity in AM. The product selectivity is as important as the activity in AM. The (ᵗBu-PCP)Ir complex **2-H₂** is known to be more selective than **1a-C₂H₄** for the formation of *n*-decane from the metathesis of *n*-hexane. For example, a reaction using **2-H₂** formed 49 mol% of *n*-C₁₀H₂₂ (entry 4) relative to the total production of the heavier alkanes (C₇H₁₆ − C₁₀H₂₂); the same reaction with **1a-C₂H₄** generated only 14% of *n*-C₁₀H₂₂ (entry 2). The initial product of dehydrogenation of *n*-hexane is presumed to be the 1-hexene. Thus, the formation of other alkane products besides ethane and *n*-decane reflects substantial olefin isomerization.[1] Experimental and computational results suggest that the selectivity in AM is closely related to the resting state and the steric crowding of iridium complexes. Because the (ᵗBu-PCP)Ir complex is more sterically crowded at iridium relative to (ᵗBu-POCOP)Ir, the Ir dihydride complex is the resting state, while for the (ᵗBu-POCOP)Ir system the olefin complexes are the resting states. It has been found that the pincer complexes isomerize olefins via a π–allyl hydride intermediate which forms from the olefin complexes. Thus the higher concentration of (pincer)Ir-olefin(s) in AM results in faster olefin isomerization, which consequently leads to a lower product selectivity. This feature accounts for the lower selectivity of the (ᵗBu-POCOP)Ir system relative to the (ᵗBu-PCP)Ir system

Complex **3a-C₂H₄** is more sterically hindered than **1a-C₂H₄**. As expected, the AM reaction with **3a-C₂H₄** formed *n*-decane with higher selectivity (36%, 2d) than **1a-C₂H₄** (14%). When another Schrock catalyst, **W-siloxyl**, was used, the reaction with **3a-C₂H₄** formed *n*-decane with 45% selectivity. However, the selectivity exhibited by **3a-C₂H₄** was still lower than that shown by **2-H₂** (49%), even though **3a** is more crowded than **2** as judged by crystal structures of each complex.

Monitoring the AM reaction with **3a-C$_2$H$_4$** and **Mo-F$_6$** by ^{31}P{^{1}H} NMR provided insight into the resting state(s) of the iridium species. As shown in Fig. 3.4, after 2 h at 125 °C, there was ca. 50% of **3a-H$_2$**, 30% of **3a-C$_2$H$_4$** and 20% of unidentified species. After 4 hours, **3a-H$_2$** became the major resting state (ca. 90%). The observation of an iridium dihydride resting state is consistent with our previous results: highly sterically hindered structures favor the formation of a dihydride resting state. As a result, the olefin isomerization by **3a** is relatively slow, resulting in a higher product selectivity.
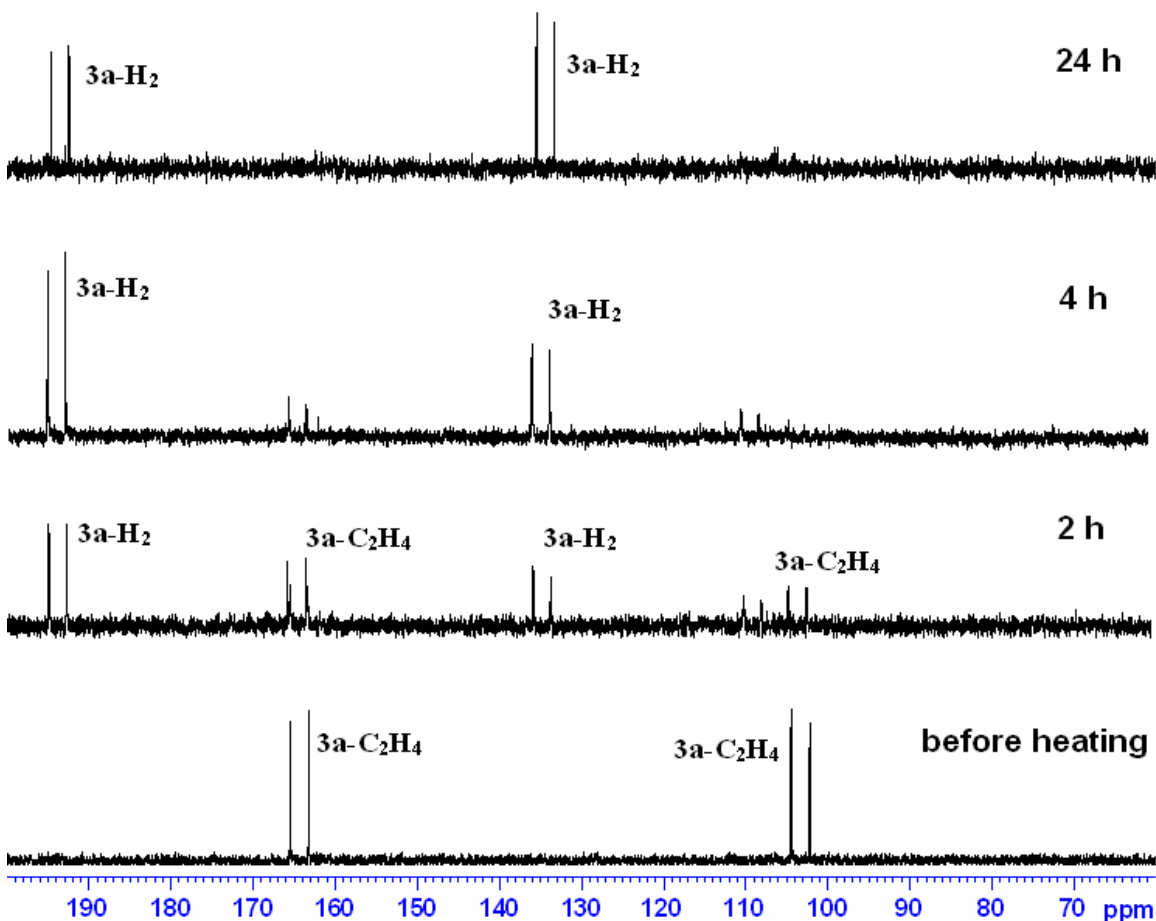
Fig. 3.4 Resting states of (^{t}Bu-PSCOP)Ir catalyst in AM.

It should be noted that the product selectivity of these iridium complexes is not always consistent with the relative bulk of the pincer ligands. For example, the most hindered complexes $4\text{-}C_2H_4$ and $5\text{-}C_2H_4$ exhibited very low product selectivity in AM (entry 10 and 11). The less sterically hindered complex $1b\text{-}C_2H_4$ surprisingly showed a better selectivity for *n*-decane (24%, entry 1) than $1a\text{-}C_2H_4$. A preliminary NMR study indicated iridium olefin complexes ($1b\text{-olefin}$) as the major resting states in AM. It is unclear which catalyst, $1a\text{-}C_2H_4$ or $1b\text{-}C_2H_4$, isomerizes olefins faster. Mechanistic studies of $1b\text{-}C_2H_4$ regarding transfer dehydrogenation and olefin isomerization are currently underway.

The electron-deficient complex $7\text{-}C_2H_4$ showed a low selectivity in AM, giving 11% of *n*-decane after 2 days (entry 12). Interestingly, complex $8\text{-}C_2H_4$ containing two bulky substituents in the *meta*-postions of the backbone is slightly more selective than $1a\text{-}C_2H_4$ (19% vs 14%).

4.3. Effect of added olefin on AM.

Some olefin products were observed in the AM reaction with $3a\text{-}C_2H_4$ (entry 5). Given the fact that the iridium catalyst has a dihydride resting state, the rate-determining step must be the olefin hydrogenation step. Indeed, when additional olefin (2.5 equiv. of 5-decene) was added, the initial reaction rate was more than doubled (entry 6). For instance, the reaction with 5-decene gave 41 TONs after 6 h, while the reaction without added olefin gave 18 TONs. The total conversion was also increased with olefin added (107 vs 77 TONs, 2 days). However, an addition of more olefin (10 equiv. of 5-decene, entry 7) led to an early decay of the catalytic system, even though the initial reaction rate was faster. After 6 h, essentially no further TOs were observed. It has been known that the Schrock catalyst decays in a bimolecular decomposition pathway involving coupling of methylidene units.[6-9] Thus,

the presence of excess olefin could accelerate the decomposition of Schrock catalyst by allowing it to more frequently sample the Mo methylidene structure and consequently decrease the final conversion.

In another experiment, we conducted a reaction of **1a-H₂** and **Mo-F₆** in hexane *without* any olefin to accept hydrogen (entry 3). Compared to the reaction with **1a-C₂H₄**, the initial rate was extremely slow with only 4 TONs after 3 h. However, the rate appeared to increase over time and gave 67 TONs after 1 day. It was possible that olefin had been generated from the **Mo-F₆** complex,[7-9] which could serve as the hydrogen acceptor. More importantly, the system was relatively long-lived as an additional 159 TONs was obtained from 1 day to 2 days. In contrast, the reaction employing **1a-C₂H₄** and **Mo-F₆** was nearly complete after 1 day (entry 2). As mentioned above, the early decomposition of Schrock catalyst in AM using **1a-C₂H₄** and **Mo-F₆** limits the conversion. The higher productivity in entry 3 presumably resulted from the longer lifetime of the Schrock catalyst with only very low concentration of olefin present which arised form the Schrock catalyst itself.[6-9]

Conclusions

By modifying the substituents and linkers in the pincer ligands, eight new iridium complexes were prepared with varying steric and electronic features. Compared to the parent **1a-C₂H₄**, the least bulky catalyst, **1b-C₂H₄**, displayed a higher activity in both TD and AM, as well as a better product selectivity. The sterically more hindered complex **3a-C₂H₄** showed low TD activity and moderate AM activity, but the product selectivity in AM was significantly improved which is presumably the result of a dihydride resting state (**3a-H₂**). The AM reaction rate and productivity could be increased upon addition of olefin in the

system using **3a-C$_2$H$_4$**. However, the lifetime of the Schrock olefin metathesis catalyst was controlled by the concentration of olefin, so using a large excess of olefin resulted a short lifetime for the Schrock catalyst. The other iridium catalysts we synthesized exhibited low to moderate activities in TD and AM and poor selectivity in AM.

Experimental Section

General Considerations. All manipulations were carried out using standard Schlenk, high-vacuum and glovebox techniques. Tetrahydrofuran (THF) was distilled under a nitrogen atmosphere from sodium benzophenone ketyl prior to use. Pentane and toluene were passed through columns of activated alumina. Benzene-d$_6$, THF-d$_8$, toluene-d$_8$, methylene chloride-d$_2$, chloroform-d$_1$, and cyclohexane-d$_{12}$ were dried with 4 Å molecular sieves and degassed by freeze-pump-thaw cycles. Cyclooctane (COA), 3,3'-dimethyl-1-butene (TBE), *n*-hexane and mesitylene were purchased from Aldrich, dried with LiAlH$_4$ or Na/K, and vacuum transferred into sealed flasks. Resorcinol, 3-mercaptophenol, 3-aminothiophenol, benzene-1,3-dithiol and tris(trifluromethyl)benzene were purchased from Aldrich and used as received. Schrock catalyst **Mo-F$_6$** was purchased from Strem and **W-siloxyl** was received as a gift from the Schrock group. Complexes **1a-C$_2$H$_4$,**[1] **1a-H$_2$,**[11] **2-H$_2$,**[10] [(COD)IrCl]$_2$, [(COE)$_2$IrCl]$_2$[12] were synthesized as previously reported.

NMR spectra were recorded on BRUKER DRX-400, AVANCE-400, and BRUKER DRX-500 MHz spectrometers. ^{1}H and ^{13}C NMR spectra were referenced to residual protio solvent peaks. ^{31}P chemical shifts were referenced to an external H$_3$PO$_4$ standard.

GC analyses (FID detection) was performed according to the following methods: Agilent 6850 Series GC System fitted with an Agilent HP-1 column (100%

dimethylpolysiloxane, 30m×0.32mm i.d., 0.25 µm film thickness). Typical temperature program: 5 min isothermal at 33 ºC, 20 ºC/ min heat up, 10 min isothermal at 300 ºC. Flow rate: 1 mL/min (He). Split ratio: 400. Inlet temperature: 250 °C. Detector temperature: 250 °C.
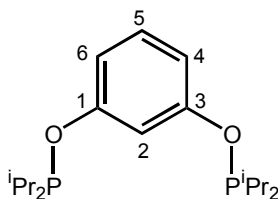
Synthesis of the pincer ligand ^{i}Pr-POCOP. A solution of 13.6 mmol of resorcinol (1.5 g) in 20 mL of THF was slowly added via syringe to a suspension of 30.3 mmol of NaH (725 mg) in 100 mL of THF under a flow of argon at room temperature (caution: hydrogen evolution). The mixture was then heated to reflux for 2 h, di-*iso*-propylchlorophosphine (27.2 mmol, 4.32 g) was then added via syringe, and the mixture was refluxed for additional 2 h. After evaporation of the solvent under high vacuum, the residue was extracted with 3 × 40 mL of pentane, and the extract was cannula transferred and filtered through a pad of Celite. After removal of pentane under high vacuum, the flask was heated to 50 °C for 2 h under high vacuum to remove residual amounts of di-*iso*-propylchlorophosphine. Product (> 95% purity) as a colorless oil was collected in 77% yield (10.5 mmol, 3.58 g). ^{1}H NMR (400 MHz, 23 °C, C$_6$D$_6$): δ 0.95 (dd, $^{3}J_{\text{H-H}}$ = 7.2 Hz, $^{3}J_{\text{H-P}}$ = 15.8 Hz, 12H, 4 × CH_3), 1.11 (dd, $^{3}J_{\text{H-H}}$ = 7.0 Hz, $^{3}J_{\text{H-P}}$ = 10.5 Hz, 12H, 4 × CH_3), 1.73 (m, 4 × CH(CH$_3$)$_2$), 7.00 (m, 3H, 4–6-H), 7.40 (m, 1H, 2-H). ^{31}P{^{1}H} NMR (162 MHz, 23 °C, C$_6$D$_6$): δ 149.8 (s).
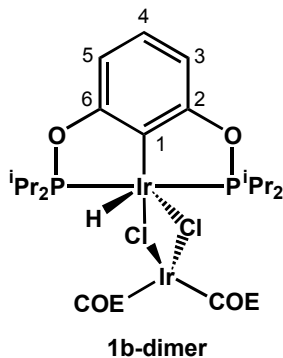
1b-dimer

Synthesis of the 1b-dimer. A Schlenk flask was charged with 0.26 mmol of ^{i}**Pr-POCOP** (90 mg) and 0.26 mmol of [(COE)$_2$IrCl]$_2$ (234 mg) and put under a flow of argon. Toluene (6 mL) was added via syringe, and the solution was stirred at room temperature for 20 min. Volatiles were removed under high vacuum and the residue was extracted with 3 × 8 mL of pentane. Removal of pentane solvent and other volatiles resulted in the isolation of **1b-dimer** as a yellow waxy solid. Yield, 66 mg, (65 μmol, 25%). ^{1}H NMR (400 MHz, 23 °C, CD$_2$Cl$_2$): δ -23.97 (t, $^2J_{P-H}$ = 14.8 Hz, 1H, Ir*H*), 0.98 (m, 2 × C*H*$_3$), 1.16 (m, 2 × C*H*$_3$), 1.36 (b, COE), 1.53 (m, 2 × C*H*$_3$), 1.88 (m, 2 × C*H*$_3$), 2.03 (m b, COE), 2.20 (m b, COE), 2.29 (m, 2 × C*H*(CH$_3$)$_2$), 3.29 (m, 2 × C*H*(CH$_3$)$_2$), 6.64 (d, $^3J_{H-H}$ = 7.8 Hz, 2H, 3, 5-H), 6.76 (t, $^3J_{H-H}$ = 7.8 Hz, 1H, 4-H). ^{31}P{^{1}H} NMR (162 MHz, 23 °C, CDCl$_3$): δ 153.4 (s).
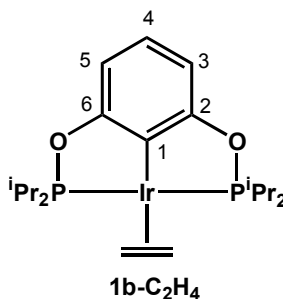
1b-C$_2$H$_4$

Synthesis of the ethylene complex 1b-C$_2$H$_4$. Complex **1b-dimer** (120 mg, 118 μmol) and NaO^{t}Bu (14 mg, 146 μmol) were weighed into a Schlenk flask and put under a flow of argon.

Toluene (8 mL) was added to the flask via syringe and ethylene was bubbled through the solution for 4 h. After evaporation of the solvent under high vacuum, the residue was extracted with 3 × 10 mL of pentane, and the extract was cannula transferred and filtered through a pad of Celite. Pentane was removed under high vacuum, and the red solid was dried under high vacuum overnight to give 56 mg (100 μmol, 85% yield) of pure product. ^{1}H NMR (400 MHz, 23 °C, C_6D_6): 1.00 (m, 12H, 4 × CH_3), 1.10 (m, 12H, 4 × CH_3), 2.27 (m, 4H, 4 × CH(CH$_3$)$_2$), 2.58 (t, $^3J_{H-H}$ = 2.2 Hz, 4H, C_2H_4), 6.97 (d, $^3J_{H-H}$ = 7.7 Hz, 2H, 3, 5-H), 7.04 (t, $^3J_{H-H}$ = 7.7 Hz, 1H, 4-H). ^{31}P{^{1}H} NMR (162 MHz, 23 °C, C_6D_6): δ 185.3 (s).
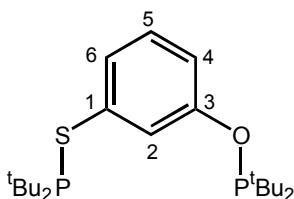
Synthesis of the pincer ligand ^{t}Bu-PSCOP. A solution of 39 mmol of 3-mercaptophenol (96% purity, 5.14 g) in 20 mL of THF was slowly added via syringe to a suspension of 82 mmol of NaH (1.96 g) in 100 mL of THF under a flow of argon at 0 °C (caution: hydrogen evolution). The mixture was then heated to reflux for 2 h, di-*tert*-butylchlorophosphine (81 mmol, 15.30 g) was then added via syringe, and the mixture was refluxed for additional 12 h. After evaporation of the solvent under high vacuum, the residue was extracted with 3 × 60 mL of pentane, and the extract was cannula transferred and filtered through a pad of Celite. After removal of pentane under high vacuum, the flask was heated to 55 °C for 3 h under high vacuum to remove residual amounts of di-*tert*-butylchlorophosphine. Pure product as a colorless oil was collected in 95% yield (36.9 mmol, 15.30 g). ^{1}H NMR (400 MHz, 23 °C, CD_2Cl_2): δ 1.15 (d, $^3J_{H-P}$ = 12.3 Hz, 18H, OP^{t}Bu$_2$), 1.27 (d, $^3J_{H-P}$ = 12.0 Hz, 18H, SP^{t}Bu$_2$), 6.94 (m, 1H, 5-H), 7.12 (m, 2H, 4 and 6-H), 7.38 (s, 1H, 2-H). ^{31}P{^{1}H} NMR (162 MHz, 23

°C, CD$_2$Cl$_2$): δ 155.9 (s, OP), 84.9 (s, SP). ^{13}C{^{1}H} NMR (100.5 MHz, 23 °C, CD$_2$Cl$_2$): δ

27.6 (CH$_3$, d, $^2J_{P\text{-}C}$ = 15.5 Hz, OP^tBu_2), 29.9 (CH$_3$, d, $^2J_{P\text{-}C}$ = 15.3 Hz, SP^tBu_2), 35.6 (C$_q$, d, $J_{P\text{-}C}$ = 30.6 Hz, OP^tBu_2), 36.0 (C$_q$, d, $J_{P\text{-}C}$ = 26.5 Hz, SP^tBu_2), 116.5 (CH, d, $^3J_{P\text{-}C}$ = 11.5 Hz, C4),

121.6 (CH, m, C2), 124.6 (CH, d, $^3J_{P\text{-}C}$ = 8.5 Hz, C6), 129.6 (CH, s, C5), 139.3 (C$_q$, d, $^2J_{P\text{-}C}$ =

15.1 Hz, C1), 160.4 (C$_q$, d, $^2J_{P\text{-}C}$ = 9.0 Hz, C3).
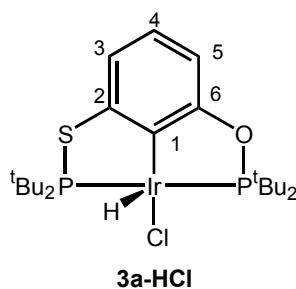
3a-HCl

Synthesis of the pincer iridium complex 3a-HCl. A Schlenk flask was charged with 1.6

mmol of ^{t}**Bu-PSCOP** (663 mg) and 0.8 mmol of [(COD)IrCl]$_2$ (537 mg) and put under a

flow of argon. Toluene (15 mL) was added via syringe, and the solution was stirred in an oil

bath for 16 h at 130 °C. The reaction mixture was cooled to room temperature. Volatiles were

removed under high vacuum and the resulting solid was washed with 4 × 7 mL of pentane

and dried under high vacuum overnight to yield 732 mg (1.14 mmol, 71%) of pure orange

product. ^{1}H NMR (400 MHz, 23 °C, CD$_2$Cl$_2$): δ -41.70 (t, $^2J_{P\text{-}H}$ = 12.4 Hz, 1H, IrH), 1.37 (t,

virtual triplet, apparent J = 14.0 Hz, 18H, 2 × ^{t}Bu), 1.47 (t, virtual triplet, apparent J = 14.0

Hz, 18H, 2 × ^{t}Bu), 6.56 (d, $^3J_{H\text{-}H}$ = 6.4 Hz, 1H, 5-H), 6.72 (m, 1H, 4-H), 6.97 (d, $^3J_{H\text{-}H}$ = 6.4

Hz, 1H, 3-H). ^{31}P{^{1}H} NMR (162 MHz, 23 °C, CD$_2$Cl$_2$): δ 106.8 (d, $J_{P\text{-}P}$ = 353 Hz, SP^tBu$_2$),

163.7 (d, $J_{P\text{-}P}$ = 353 Hz, OP^tBu$_2$). ^{13}C{^{1}H} NMR (100.5 MHz, 23 °C, CD$_2$Cl$_2$): δ 27.2 (CH$_3$,

d, $^2J_{P\text{-}C}$ = 4.2 Hz, OP^tBu_2), 27.5 (CH$_3$, d, $^2J_{P\text{-}C}$ = 4.5 Hz, OP^tBu_2), 29.0 (CH$_3$, d, $^2J_{P\text{-}C}$ = 4.2 Hz,

SP^tBu_2), 29.3 (CH$_3$, d, $^2J_{P\text{-}C}$ = 4.5 Hz, SP^tBu_2), 39.4 (C$_q$, m, OP^tBu_2), 39.5 (C$_q$, m, SP^tBu_2),

42.5 (C_q, m, SP^tBu_2), 43.1 (C_q, m, OP^tBu_2), 107.3 (CH, d, $^3J_{\text{P-C}}$ = 11.8 Hz, C5), 115.8 (CH, d,

$^3J_{\text{P-C}}$ = 10.3 Hz, C3), 124.7 (CH, s, C4), 132.1 (C_q, m br, C1), 153.4 (C_q, m, C2), 167.3 (C_q,

m, C6).
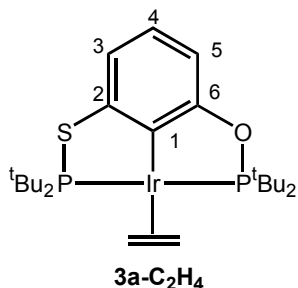
3a-C$_2$H$_4$

Synthesis of the ethylene complex 3a-C$_2$H$_4$. Complex **3a-HCl** (225 mg, 0.35 mmol) and

NaO^{t}Bu (37 mg, 0.39 mmol) were weighed into a Schlenk flask and put under a flow of

argon. Toluene (15 mL) was added to the flask via syringe and ethylene was bubbled through

the solution for 3 h. After evaporation of the solvent under high vacuum, the residue was

extracted with 3 × 20 mL of pentane, and the extract was cannula transferred and filtered

through a pad of Celite. Pentane was removed under high vacuum, and the brown solid was

dried under high vacuum overnight to give 198 mg (0.31 mmol, 89% yield) of pure product.

^{1}H NMR (400 MHz, 23 °C, CD$_2$Cl$_2$): δ 1.31 (d, $^3J_{\text{P-H}}$ = 13.2 Hz, 18H, OP^{t}Bu$_2$), 1.42 (d, $^3J_{\text{P-H}}$

= 13.2 Hz, 18H, SP^{t}Bu$_2$), 3.17 (m, 4H, C$_2$$H_4$), 6.66 (d, $^3J_{\text{H-H}}$ = 7.6 Hz, 1H, 5-H), 6.87 (m, 1H,

4-H), 7.09 (d, $^3J_{\text{H-H}}$ = 7.6 Hz, 1H, 3-H). ^{31}P{^{1}H} NMR (162 MHz, 23 °C, CD$_2$Cl$_2$): δ 106.8 (d,

$J_{\text{P-P}}$ = 353 Hz, SP^tBu$_2$), 166.6 (d, $J_{\text{P-P}}$ = 353 Hz, OP^tBu$_2$). ^{13}C{^{1}H} NMR (125.8 MHz, 23 °C,

CD$_2$Cl$_2$): δ 29.0 (CH$_3$, d, $^2J_{\text{P-C}}$ = 5.0 Hz, OP^{t}Bu$_2$), δ 30.3 (CH$_3$, d, $^2J_{\text{P-C}}$ = 4.9 Hz, SP^{t}Bu$_2$),

39.3 (CH$_2$, s, C_2H$_4$), 41.5 (C_q, m, OP^{t}Bu$_2$), 41.6 (C_q, m, SP^{t}Bu$_2$), 106.3 (CH, d, $^3J_{\text{P-C}}$ = 12.6

Hz, C5), 113.6 (CH, d, $^3J_{\text{P-C}}$ = 10.8 Hz, C3), 127.3 (CH, s, C4), 156.4 (C_q, m, C1), 164.8 (C_q,

m, C2), 168.4 (C_q, m, C6).
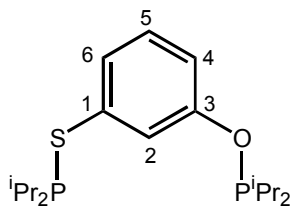
Synthesis of the pincer ligand ^{i}Pr-PSCOP. A solution of 11.4 mmol of 3-mercaptophenol (96% purity, 1.5 g) in 20 mL of THF was slowly added via syringe to a suspension of 23.3 mmol of NaH (0.56 g) in 80 mL of THF under a flow of argon at 0 °C (caution: hydrogen evolution). The mixture was then heated to reflux for 2 h, di-*iso*-propylchlorophosphine (23 mmol, 3.65 g) was then added via syringe, and the mixture was refluxed for additional 2 h. After evaporation of the solvent under high vacuum, the residue was extracted with 3 × 30 mL of pentane, and the extract was cannula transferred and filtered through a pad of Celite. After removal of pentane under high vacuum, the flask was heated to 50 °C for 2 hours under high vacuum to remove residual amounts of di-*sio*-propylchlorophosphine. Pure product as a colorless oil was collected in 85% yield (9.69 mmol, 3.47 g). ^{1}H NMR (400 MHz, 23 °C, CDCl$_3$): δ 1.04-1.21 (m, 24H, 4 × ^{i}Pr), 1.89 (m, 2H, OP^{i}Pr$_2$), 2.00 (m, 2H, SP^{i}Pr$_2$), 6.87 (m, 1H, 5-H), 7.08 (m, 2H, 4 and 6-H), 7.27 (s, 1H, 2-H). ^{31}P{^{1}H} NMR (162 MHz, 23 °C, CDCl$_3$): δ 149.2 (s, O*P*), 66.1 (s, S*P*). ^{13}C{^{1}H} NMR (125.8 MHz, 23 °C, CDCl$_3$): δ 16.9 (CH$_3$, d, $^2J_{P-C}$ = 8.6 Hz, 2 × *CH$_3$*), 17.6 (CH$_3$, d, $^2J_{P-C}$ = 20.3 Hz, 2 × *CH$_3$*), 18.5 (CH$_3$, d, $^2J_{P-C}$ = 8.1 Hz, 2 × *CH$_3$*), 19.4 (CH$_3$, d, $^2J_{P-C}$ = 19.0 Hz, 2 × *CH$_3$*), 25.6 (C$_q$, d, J_{P-C} = 20.9 Hz, 2 × *CH*), 38.2 (C$_q$, d, J_{P-C} = 17.9 Hz, 2 × *CH*), 116.2 (CH, d, $^3J_{P-C}$ = 11.3 Hz, C4), 121.4 (CH, m, C2), 124.5 (CH, d, $^3J_{P-C}$ = 7.5 Hz, C6), 129.1 (CH, s, C5), 137.5 (C$_q$, d, $^2J_{P-C}$ = 13.8 Hz, C1), 159.2 (C$_q$, d, $^2J_{P-C}$ = 7.5 Hz, C3).
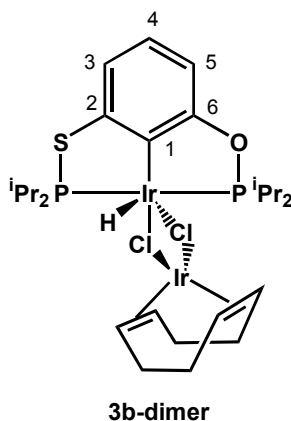
3b-dimer

Synthesis of the 3b-dimer. A Schlenk flask was charged with 0.42 mmol of ⁱ**Pr-PSCOP** (150 mg), 0.42 mmol of [(COD)IrCl]$_2$ (281 mg) and 2.1 mmol COD (400 mg) and put under a flow of argon. Toluene (6 mL) was added via syringe, and the solution was stirred in an oil bath for 2 days at 130 °C. The reaction mixture was cooled to room temperature. Volatiles were removed under high vacuum and the residue was extracted with 3 × 15 mL of pentane. Removal of pentane solvent and other volatiles resulted in the isolation of **3b-dimer** as a yellow-brown waxy solid. Yield, 81 mg, (88 μmol, 21%). ^{1}H NMR (400 MHz, 23 °C, C$_6$D$_6$): δ -24.75 (t, $^2J_{\text{P-H}}$ = 15.0 Hz, 1H, Ir*H*), 1.0-1.8 (m, 24H, 8 × C*H$_3$*), 2.04 (m, 8H, CH$_2$ in COD), 2.35 (m, 1H, C*H*), 2.66 (m, 1H, C*H*), 3.50 (m, 1H, C*H*), 3.64 (m, 1H, C*H*), 3.95 (m, 4H, CH in COD), 6.61 (m, 2H, 3- and 5-H), 6.61 (m, 1H, 4-H). ^{31}P{^{1}H} NMR (162 MHz, 23 °C, C$_6$D$_6$): δ 77.1 (d, $J_{\text{P-P}}$ = 381 Hz, S*P*), 145.9 (d, $J_{\text{P-P}}$ = 381 Hz, O*P*).

3b-C$_2$H$_4$

65
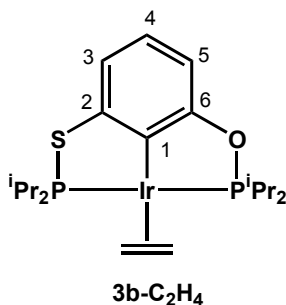
**Synthesis of the ethylene complex 3b-C₂H₄.** Complex **3b-dimer** (50 mg, 54 μmol) and NaOᵗBu (10 mg, 104 μmol) were weighed into a Kontes flask. Toluene (6 mL) was added to the flask via syringe and the solution was degassed by three freeze-pump-thaw cycles. The flask was refilled with ethylene at -78 °C and then sealed tightly with a Teflon plug. The mixture was stirred at room temperature for 3 d. Volatiles were removed under high vacuum and the residue was extracted with 3×10 mL of pentane. The extract was cannula transferred and filtered through a 0.2μm pore size syringe filter. Pentane was removed under high vacuum to give 26 mg (45 μmol, 84% yield) of product as a dark-red waxy solid. ^{1}H NMR (400 MHz, 23 °C, C_6D_6): δ 1.08 (m, 24H, $8 \times CH_3$), 2.29 (m, 2H, $2 \times CH(CH_3)_2$), 2.31 (m, 2H, $2 \times CH(CH_3)_2$), 2.91 (s, 4H, C_2H_4), 6.92 (m, 2H, 4 and 5-H), 7.39 (d, $^3J_{H-H}$ = 7.2 Hz, 1H, 3-H). ^{31}P{^{1}H} NMR (162 MHz, 23 °C, C_6D_6): δ 95.1 (d, J_{P-P} = 355 Hz, SP), 165.9 (d, J_{P-P} = 355 Hz, OP).
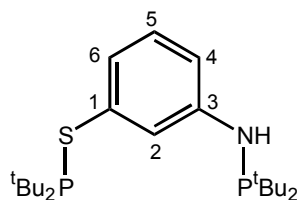
Synthesis of the pincer ligand ᵗBu-PSCNP. A solution of 12 mmol of ^{n}BuLi (7.5 mL, 1.6 M in hexane) was slowly added via syringe to a mixture of 4.0 mmol of 3-aminothiophenol (0.5 g) and 12 mmol of di-*tert*-butylchlorophosphine (2.27 g) in 5 mL of THF under a flow of argon at -78 °C. The mixture was then warmed to room temperature and stirred overnight. After evaporation of the solvent under high vacuum, the residue was extracted with 3×5 mL of pentane, and the extract was cannula transferred and filtered through a pad of Celite. After removal of pentane under high vacuum, the flask was heated to 55 °C for 3 h under high vacuum to remove residual amounts of di-*tert*-butylchlorophosphine. Product as a while-

yellow solid was collected in 24% yield (0.96 mmol, 0.4 g, ca. 71% purity by NMR). ^{1}H NMR (400 MHz, 23 °C, C$_7$D$_8$ & DMSO-d$_6$): δ 1.06 (d, $^3J_{\text{H-P}}$ = 11.6 Hz, 18H, ^{t}Bu$_2$), 1.15 (d, $^3J_{\text{H-P}}$ = 11.6 Hz, 18H, ^{t}Bu$_2$), 3.61 (s, NH), 5.59 (d, $^3J_{\text{H-H}}$ = 11.6 Hz, 4-H), 6.91 (m, 1H, 5-H), 7.08 (m, 1H, 6-H), 7.58 (s, 1H, 2-H). ^{31}P{^{1}H} NMR (162 MHz, 23 °C, C$_7$D$_8$ & DMSO-d$_6$): δ 80.1 (s, SP), 60.9 (s, NP).
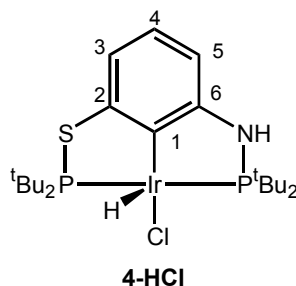

4-HCl

Synthesis of the pincer iridium complex 4-HCl. A Schlenk flask was charged with 1.37 mmol of ^{t}**Bu-PSCNP** (565 mg) and 0.68 mmol of [(COD)IrCl]$_2$ (385 mg) and put under a flow of argon. Toluene (10 mL) was added via syringe, and the solution was stirred in an oil bath for 2 days at 130 °C. The reaction mixture was cooled to room temperature. Red crystals precipitated which were collected through filtration. Yield: 400 g (0.62 mmol, 55%). ^{1}H NMR (400 MHz, 23 °C, CDCl$_3$): δ -42.49 (t, virtual triplet, $^2J_{\text{P-H}}$ = 12.7 Hz, 1H, IrH), 1.36 (m, 18H, 2 × ^{t}Bu), 1.47 (m, 18H, 2 × ^{t}Bu), 4.6 (s, 1H, NH), 6.31 (d, $^3J_{\text{H-H}}$ = 7.0 Hz, 1H, 5-H), 6.64 (m, 1H, 4-H), 6.83 (d, $^3J_{\text{H-H}}$ = 7.5 Hz, 1H, 3-H). ^{31}P{^{1}H} NMR (202 MHz, 23 °C, CDCl$_3$): δ 99.3 (d, $J_{\text{P-P}}$ = 349 Hz, NP^tBu$_2$), 105.8 (d, $J_{\text{P-P}}$ = 349 Hz, SP^tBu$_2$). ^{13}C{^{1}H} NMR (125.8 MHz, 23 °C, CD$_2$Cl$_2$): δ 28.2 (CH$_3$, m, NP^{t}Bu$_2$), 28.3 (CH$_3$, m, NP^{t}Bu$_2$), 29.3 (CH$_3$, m, SP^{t}Bu$_2$), 29.6 (CH$_3$, m, SP^{t}Bu$_2$), 38.3 (C$_q$, m, NP^{t}Bu$_2$), 39.5 (C$_q$, m, SP^{t}Bu$_2$), 41.7 (C$_q$, m, NP^{t}Bu$_2$), 42.5 (C$_q$, m, SP^{t}Bu$_2$), 105.2 (CH, d, $^3J_{\text{P-C}}$ = 12.1 Hz, C5), 113.3 (CH, d, $^3J_{\text{P-C}}$ = 10.6 Hz, C3), 124.2 (CH, s, C4), 128.5 (C$_q$, m br, C1), 154.2 (C$_q$, m, C2), 158.1 (C$_q$, m, C6).
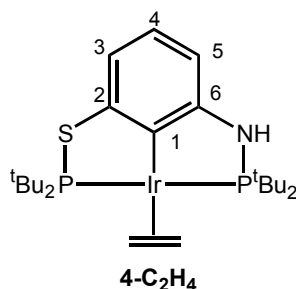
4-C₂H₄

Synthesis of the ethylene complex 4-C$_2$H$_4$. Complex **4-HCl** (300 mg, 0.46 mmol) and NaO^{t}Bu (48 mg, 0.50 mmol) were weighed into a Schlenk flask and put under a flow of argon. Toluene (10 mL) was added to the flask via syringe and ethylene was bubbled through the solution for 3 h. After evaporation of the solvent under high vacuum, the residue was extracted with 3 × 15 mL of pentane, and the extract was cannula transferred and filtered through a pad of Celite. Pentane was removed under high vacuum, and the brown solid was dried under high vacuum overnight to give 128 mg (0.20 mmol, 43% yield) of pure product. ^{1}H NMR (400 MHz, 23 °C, C$_6$D$_6$): δ 1.10 (d, $^3J_{P-H}$ = 12.4 Hz, 18H, OP^{t}Bu$_2$), 1.41 (d, $^3J_{P-H}$ = 12.8 Hz, 18H, SP^{t}Bu$_2$), 3.24 (s, 4H, C$_2$H$_4$), 4.30 (s, 1H, NH), 6.40 (d, $^3J_{H-H}$ = 7.2 Hz, 1H, 5-H), 6.92 (m, 1H, 4-H), 7.35 (d, $^3J_{H-H}$ = 7.2 Hz, 1H, 3-H). ^{31}P{^{1}H} NMR (161.9 MHz, 23 °C, C$_6$D$_6$): δ 95.1 (d, J_{P-P} = 370 Hz, NP^{t}Bu$_2$), 103.0 (d, J_{P-P} = 370 Hz, OP^{t}Bu$_2$). ^{13}C{^{1}H} NMR (125.8 MHz, 23 °C, C$_6$D$_6$): δ 29.4 (CH$_3$, d, $^2J_{P-C}$ = 5.2 Hz, NP^{t}Bu$_2$), 30.6 (CH$_3$, d, $^2J_{P-C}$ = 5.0 Hz, SP^{t}Bu$_2$), 36.8 (CH$_2$, m, C$_2$H$_4$), 39.2 (C$_q$, d, J_{P-C} = 4.0 Hz, OP^{t}Bu$_2$), 39.3 (C$_q$, d, J_{P-C} = 3.9 Hz, OP^{t}Bu$_2$), 41.3 (C$_q$, d, J_{P-C} = 3.1 Hz, SP^{t}Bu$_2$), 41.3 (C$_q$, d, J_{P-C} = 3.3 Hz, SP^{t}Bu$_2$), 104.7 (CH, d, $^3J_{P-C}$ = 13.7 Hz, C5), 111.6 (CH, d, $^3J_{P-C}$ = 11.1 Hz, C3), 130.6 (CH, s, C4), 158.1 (C$_q$, m, C1), 160.2 (C$_q$, m, C2), 163.3 (C$_q$, m, C6).
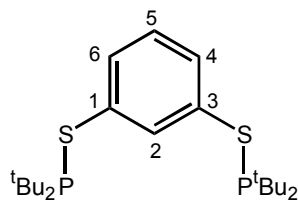
Synthesis of the pincer ligand ^tBu-PSCSP. A solution of 17.3 mmol of benzene-1,3-dithiol (2.46 g) in 20 mL of THF was slowly added via syringe to a suspension of 35 mmol of NaH (0.84 g) in 80 mL of THF under a flow of argon at 0 °C (caution: hydrogen evolution). The mixture was then heated to reflux for 2 h, di-*tert*-butylchlorophosphine (34.5 mmol, 6.5 g) was then added via syringe, and the mixture was refluxed for additional 20 h. After evaporation of the solvent under high vacuum, the residue was extracted with 3 × 50 mL of pentane, and the extract was cannula transferred and filtered through a pad of Celite. Volatiles were removed under high vacuum. The residue was washed with 3 × 10 mL of pentane at -78 °C and the resulting white solid was dried under high vacuum to give 3.42 g (7.96 mmol, 46% yield) of white solid product (92% purity). ^{1}H NMR (400 MHz, 23 °C, CD$_2$Cl$_2$): δ 1.20 (d, $^3J_{\text{H-P}}$ = 12.0 Hz, 36H, 4 × ^{t}Bu), 6.91 (t, $^3J_{\text{H-H}}$ = 7.6 Hz, 1H, 5-H), 7.42 (d, $^3J_{\text{H-H}}$ = 7.6 Hz, 2H, 4 and 6-H), 8.16 (m, 1H, 2-H). ^{31}P{^{1}H} NMR (162 MHz, 23 °C, C$_7$D$_8$): δ 82.8 (s b).
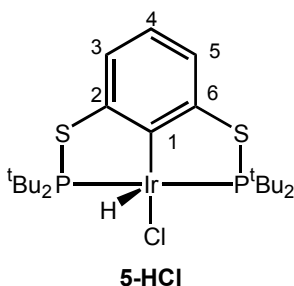
5-HCl

Synthesis of the pincer iridium complex 5-HCl. A Schlenk flask was charged with 1.47 mmol of ^tBu-PSCSP (633 mg) and 0.88 mmol of [(COD)IrCl]$_2$ (795 mg) and put under a

flow of argon. Toluene (10 mL) was added via syringe, and the solution was stirred in an oil

bath for 15 h at 130 °C. The reaction mixture was cooled to room temperature. Volatiles were

removed under high vacuum and the resulting solid was washed with 3 × 10 mL of pentane

and dried under high vacuum overnight. The residue was extracted with 3 × 5 mL of toluene

and the solvent was removed under vacuum to yield 260 mg (0.40 mmol, 27%) of pure red

product. ^{1}H NMR (400 MHz, 23 °C, C_6D_6): δ -42.02 (t, $^2J_{P-H}$ = 12.6 Hz, 1H, IrH), 1.37 (t,

virtual triplet, apparent J = 7.6 Hz, 18H, 2 × ^tBu), 1.45 (t, virtual triplet, apparent J = 7.8 Hz,

18H, 2 × ^tBu), 6.53 (t, $^3J_{H-H}$ = 7.6 Hz, 1H, 4-H), 7.00 (d, $^3J_{H-H}$ = 7.6 Hz, 2H, 3 and 5-H).

$^{31}P\{^1H\}$ NMR (162 MHz, 23 °C, C_6D_6): δ 94.2 (s).
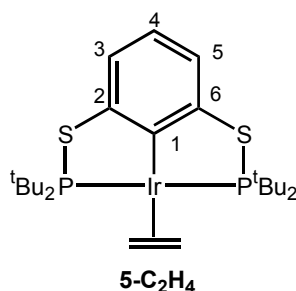
5-C_2H_4

Synthesis of the ethylene complex 5-C_2H_4. Complex **5-HCl** (80 mg, 0.12 mmol) and

NaO^tBu (14 mg, 0.15 mmol) were weighed into a Schlenk flask and put under a flow of

argon. Toluene (5 mL) was added to the flask via syringe and ethylene was bubbled through

the solution for 3 h. After evaporation of the solvent under high vacuum, the residue was

extracted with 3 × 10 mL of pentane, and the extract was cannula transferred and filtered

through a pad of Celite. Pentane was removed under high vacuum, and the red solid was

dried under high vacuum overnight to give 62 mg (95 µmol, 79% yield) of pure product. ^{1}H

NMR (400 MHz, 23 °C, C_6D_6): δ 1.35 (t, virtual triplet, apparent J = 6.8 Hz, 36H, 4 × ^tBu),

3.23 (t, $^3J_{\text{P-H}}$ = 3.2 Hz, 4H, C$_2$H$_4$), 6.70 (t, $^3J_{\text{H-H}}$ = 7.6 Hz, 1H, 5-H), 7.41 (d, $^3J_{\text{H-H}}$ = 7.6 Hz, 2H, 3 and 5-H). ^{31}P{^{1}H} NMR (162 MHz, 23 °C, C$_6$D$_6$): δ 93.0 (s).
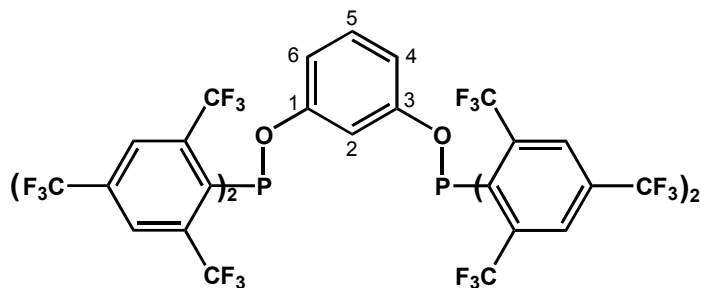
Synthesis of the pincer ligand {η^3-C$_6$H$_3$[OP-(C$_6$H$_2$(CF$_3$)$_3$-2,4,6)$_2$]$_2$-1,3}, (Ar-POCOP)

A solution of 1.2 mmol of resorcinol (132 mg) in 20 mL of THF was slowly added via syringe to a suspension of 2.5 mmol of NaH (60 mg) in 10 mL of THF under a flow of argon (caution: hydrogen evolution). The mixture was heated to reflux for 1 h, then a solution of 2.4 mmol of di-2,4,6-tris(trifluoromethyl)phenylchlorophosphine (1.508 g) in 10 ml of THF was added via syringe. The white solution turned to blue upon addition of phosphine. The mixture was then refluxed for additional 2 h. After evaporation of the solvent under high vacuum, the residue was extracted with 3 × 40 mL of pentane at room temperature, and the extract was cannula transferred and filtered through a pad of Celite. Volatiles were removed under high vacuum. The residue was washed with 3 × 5 mL of pentane at -34 °C and the resulting white solid was dried under high vacuum to give 1.035 g (0.8 mmol, 67% yield) of pure product. ^{1}H NMR (400 MHz, 23 °C, CDCl$_3$): δ 6.81 (m, 3H, 2-, 4-H, and 6-H), 7.11 (t, $^3J_{\text{H-H}}$= 8.2 Hz, 1H, 5-H), 8.14 (s, 8H, Ar(CF$_3$)$_3$-H). ^{31}P{^{1}H} NMR (162 MHz, 23 °C, CDCl$_3$): δ 109.35 (septep, $^4J_{\text{P-F}}$ = 35.3). ^{19}F NMR (376 MHz, 23 °C, CDCl$_3$): δ -56.2 (d, $^4J_{\text{P-F}}$ = 35.3, 24F, o-CF$_3$), -64.7 (s, 12F, p-CF$_3$). ^{13}C{^{1}H} NMR (126 MHz, 23 °C, CDCl$_3$): δ 108.5 (CH, t, $^3J_{\text{C-P}}$ = 11.3 Hz, C2), 113.0 (CH, d, $^3J_{\text{C-P}}$ = 12.1 Hz, C4 and C6), 122.2 (C$_q$, q, $^1J_{\text{C-F}}$ = 272.9 Hz, p-CF$_3$), 122.7 (C$_q$, q, $^1J_{\text{C-F}}$ = 276.7 Hz, o-CF$_3$), 127.9, (CH, s, C$_m$), 129.9 (CH, s, C5),

133.2 (C_q, q, $^2J_{C\text{-}F}$ = 34.8 Hz, C_o), 135.8 (C_q, q, $^2J_{C\text{-}F}$ = 34.8 Hz, C_p), 143.3 (C_q, d, $^1J_{P\text{-}C}$ = 70.4 Hz, C_i), 154.8 (C_q, d, $^2J_{P\text{-}C}$ = 16.4 Hz, C1 and C3).
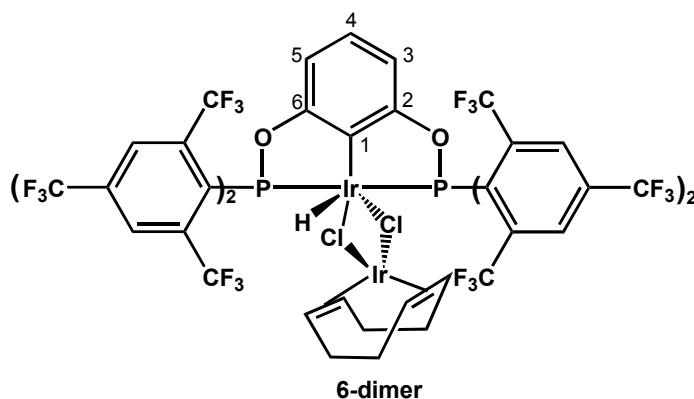
6-dimer

Synthesis of the dimer {C$_6$H$_3$-2,6-[OP-(C$_6$H$_2$(CF$_3$)$_3$-2,4,6)$_2$]$_2$}IrH(μ-Cl)$_2$Ir(COD), 6-dimer

The pincer ligand reacts slowly with [(COE)$_2$IrCl]$_2$ to form a chloro-bridged dimer, Most of [(COE)$_2$IrCl]$_2$ decomposes under the reaction conditions and thus excess [(COE)$_2$IrCl]$_2$ must be added. In a typical reaction, a Schlenk flask was charged with 0.3 mmol of ligand (388 mg) and 0.15 mmol of [(COE)$_2$IrCl]$_2$ (135 mg) and put under a flow of argon. Toluene (5 mL) was added via syringe, and the solution was stirred in an oil bath for 12 h at 150 °C. Black solid precipitated during the process and ca. 10% of product was observed by ^{31}P{^{1}H} NMR. Additional [(COE)$_2$IrCl]$_2$ (0.15 mmol, 135 mg) was then added and the mixture was heated for another 12 h at 150 °C. After 8 days with 16 periodic addition of [(COE)$_2$IrCl]$_2$ (0.15 mmol each), the reaction generated ca. 90% of product and [(COD)IrCl]$_2$ presumably through the dehydrogenation of COE ([(COD)IrCl]$_2$ does not react with the pincer ligand). Volatiles were removed under high vacuum overnight and the residue was extracted with 3 × 30 mL of pentane. Removal of the pentane solvent resulted in the isolation of both [(COD)IrCl]$_2$ and the dimer {C$_6$H$_3$-2,6-[OP-(C$_6$H$_2$(CF$_3$)$_3$-2,4,6)$_2$]$_2$}IrH(μ-Cl)$_2$Ir(COD). The

dimer is more soluble than [(COD)IrCl]$_2$ in pentane, thus part of [(COD)IrCl]$_2$ was isolated through recrystallization from pentane at -34 °C. After filtration, the pentane solvent was removed and the resulting solid was dried under high vacuum overnight to yield 1.25 g of red solid [(COD)IrCl]$_2$ and yellow solid {C$_6$H$_3$-2,6-[OP-(C$_6$H$_2$(CF$_3$)$_3$-2,4,6)$_2$]$_2$}IrH(μ-Cl)$_2$Ir(COD), (ca. 0.24 mmol, 80% yield) in *ca.* a 5:1 ratio (determined by ^{1}H NMR). ^{1}H NMR of **A** (400 MHz, 23 °C, C$_6$D$_6$): δ -22.85 (t, $^2J_{P-H}$ = 13.0 Hz, 1H, Ir*H*), 6.76 (m, 3H, 3-, 4-H, and 5-H), 7.80 (s, 2H, Ar(CF$_3$)$_3$-H), 7.85 (s, 2H, Ar(CF$_3$)$_3$-H), 8.16 (s, 2H, Ar(CF$_3$)$_3$-H), 8.20 (s, 2H, Ar(CF$_3$)$_3$-H) (the signals for COD in the dimer are overlapping with those of [(COD)IrCl]$_2$). ^{31}P{^{1}H} NMR (162 MHz, 23 °C, C$_6$D$_6$): δ 111.3 (m, b). ^{19}F NMR (376 MHz, 23 °C, C$_6$D$_6$): δ -49.0 (m, 6F, *o*-CF$_3$), -50.3 (m, 6F, *o*-CF$_3$), -52.1 (m, 6F, *o*-CF$_3$), -54.3 (m, 6F, *o*-CF$_3$), -64.1 (s, 6F, *p*-CF$_3$), -64.2 (s, 6F, *p*-CF$_3$). Yellow single crystals of {C$_6$H$_3$-2,6-[OP-(C$_6$H$_2$(CF$_3$)$_3$-2,4,6)$_2$]$_2$}IrH(μ-Cl)$_2$Ir(COD) suitable for X-ray analysis were obained from toluene solution. The stucture is shown in Fig. 3.5 and X-ray crystallographic data are summarized in Table 3.5.

Fig. 3.5 ORTEP diagram of **6-dimer**. Hydrogen atom on the iridium center can not be located.
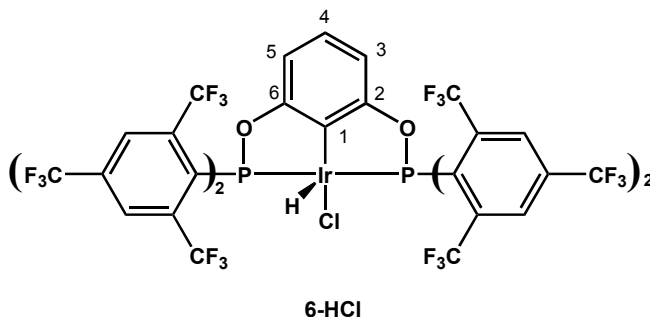
6-HCl

Synthesis of 6-HCl

The mixture of {C$_6$H$_3$-2,6-[OP-(C$_6$H$_2$(CF$_3$)$_3$-2,4,6)$_2$]$_2$}IrH(µ-Cl)$_2$Ir(COD), **6-dimer**, and [(COD)IrCl]$_2$ (625 mg total, containing *ca.* 0.12 mmol of **6-dimer**), and toluene (10 mL) were added to a Kontes flask. The toluene solution was degassed by three freeze-pump-thaw cycles. The flask was refilled with hydrogen gas at -190 °C and then sealed tightly with a Teflon plug. The mixture was heated at 120 °C for 15 h. Volatiles were removed under high vacuum overnight and the residue was extracted with 3 × 20 mL of pentane. Pentane was removed under high vacuum, and the red solid was dried under high vacuum overnight to give 108 mg (0.071 mmol, 59% yield) of pure product. ^{1}H NMR (400 MHz, 23 °C, C$_6$D$_{12}$): δ -34.60 (m, 1H, Ir*H*), 6.63 (d, $^3J_{H-H}$ = 8.0 Hz, 2H, 3- and 5-H), 6.85 (t, $^3J_{H-H}$ = 8.0 Hz, 1H, 4-H), 8.12 (s, 4H, Ar(CF$_3$)$_3$-H), 8.18 (s, 4H, Ar(CF$_3$)$_3$-H). ^{31}P{^{1}H} NMR (162 MHz, 23 °C, C$_6$D$_{12}$): δ 119.5 (m). ^{19}F NMR (376 MHz, 23 °C, C$_6$D$_{12}$): δ -54.5 (b, 24F, *o*-CF$_3$), -65.7 (s, 6F, *p*-CF$_3$), -65.8 (s, 6F, *p*-CF$_3$). Red single crystals of **6-HCl** suitable for X-ray analysis were obained from toluene solution. The stucture is shown in Fig. 3.3d. and X-ray crystallographic data are summarized in Table 3.2.
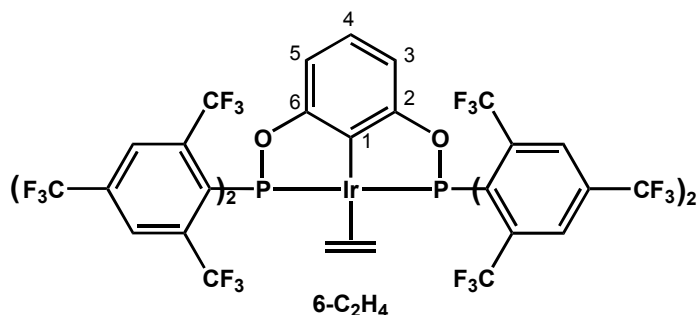
6-C₂H₄

Synthesis of 6-C₂H₄

A solution of 0.12 mmol of complex **6-HCl** (183 mg) in 5 mL of toluene and NaO^{t}Bu (20 mg, 0.21 mmol) were added to a Kontes flask. The mixture was degassed by three freeze-pump-thaw cycles. The flask was refilled with ethylene at -78 °C and then sealed tightly with a Teflon plug. The mixture was stirred at room temperature for 2 h. Volatiles were removed under high vacuum and the residue was extracted with 3 × 10 mL of pentane. The extract was cannula transferred and filtered through a 0.2μm pore size syringe filter. Pentane was removed under high vacuum to give 75 mg (20 μmol, 42% yield) of product as a deep-red waxy solid. ^{1}H NMR (400 MHz, 23 °C, C$_6$D$_6$): δ 3.35 (s, b, 4H, Ir-C$_2$H$_4$), 7.04 (s, 3H, 3-, 4- and 5-H), 7.81 (s, 8H, Ar(CF$_3$)$_3$-H). ^{31}P{^{1}H} NMR (162 MHz, 23 °C, C$_6$D$_6$): δ 111.3 (s). ^{19}F NMR (471 MHz, 23 °C, C$_6$D$_6$): δ -53.1 (b, 24F, o-CF$_3$), -64.1 (s, 12F, p-CF$_3$).
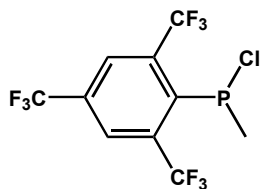
Synthesis of chloro-methyl-2,4,6-tris(trifluoromethyl)phenylphosphine. A solution of 16.5 mmol of n-butyllithium (2.5 M, 6.6 mL) in hexanes was slowly added via syringe to a

solution of 16.4 mmol of 1,3,5-tristrifluromethylbenzene (4.77 g) in 25 mL of Et$_2$O under a flow of argon at -78 °C. Then the mixture was warmed to room temperature and stirred for additional 4 h to form a brown mixture. The mixture was slowly cannula transferred into a solution of 16.4 mmol of dichloromethylphosphine (2.0 g) in 15 mL of Et$_2$O at -78 °C. The mixture was warmed to room temperature and stirred for additional 2 h. After evaporation of the solvent under high vacuum at -30 °C, the residue was extracted with 3 × 30 mL of pentane, and the extract was cannula transferred and filtered through a pad of Celite. Volatiles were removed under high vacuum at -30 °C to give 1.81 g (5.0 mmol, 30% yield) of product (> 95% purity). ^{1}H NMR (400 MHz, 23 °C, C$_6$D$_6$): δ 1.52 (d, $^2J_{P-H}$ = 15.2 Hz, 3H, CH$_3$), 7.72 (s, 2H, Ar(CF$_3$)$_3$-H). ^{31}P{^{1}H} NMR (162 MHz, 23 °C, C$_6$D$_{12}$): δ 83.3 (septep, $^4J_{P-F}$ = 51.8).
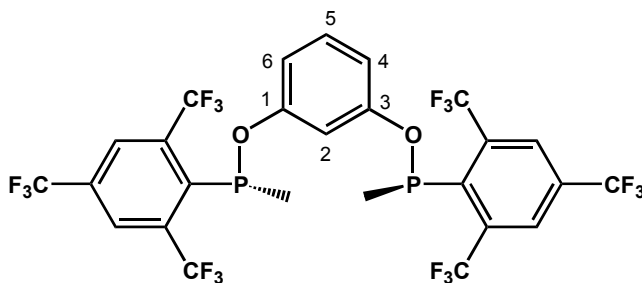
Synthesis of the pincer ligand {η^3-C$_6$H$_3$[OP-Me(C$_6$H$_2$(CF$_3$)$_3$-2,4,6)]$_2$-1,3} (ArMe-POCOP)

Note: excess NaH and resorcinol were required to prepare the pincer ligand in good yield. A solution of 5.7 mmol of resorcinol (630 mg) in 20 mL of THF was slowly added via syringe to a suspension of 20 mmol of NaH (480 mg) in 15 mL of THF under a flow of argon (caution: hydrogen evolution). The mixture was heated to reflux for 1.5 h, then a solution of 5.0 mmol of chloro-methyl-2,4,6-tris(trifluoromethyl)phenylphosphine (5.0 g) in 10 ml of THF was added via syringe. The mixture was then refluxed for additional 4 d. After evaporation of the solvent under high vacuum, the residue was extracted with 3 × 40 mL of

pentane at room temperature, and the extract was cannula transferred and filtered through a pad of Celite. Volatiles were removed under high vacuum. The residue was washed with 4 × 5 mL of pentane at -78 °C and the resulting white solid was dried under high vacuum to give 850 g (1.1 mmol, 45% yield) of pure product. ^{1}H NMR (400 MHz, 23 °C, C_6D_6): δ 1.47 (d, $^2J_{P-H}$ = 9.6 Hz, 6H, CH_3), 6.76 (d, $^3J_{H-H}$ = 8.4 Hz, 2H, 4 and 6-H), 6.84 (t, $^3J_{H-H}$ = 8.4 Hz, 1H, 5-H), 6.94 (s, 1H, 2-H), 7.81 (s, 4H, $Ar(CF_3)_3$-H). ^{31}P{^{1}H} NMR (162 MHz, 23 °C, C_6D_6): δ 115.3 (septep, $^4J_{P-F}$ = 46.5). ^{19}F NMR (471 MHz, 23 °C, C_6D_6): δ -55.3 (d, $^4J_{P-F}$ = 47.1, 12F, o-CF_3), -63.2 (s, 6F, p-CF_3).
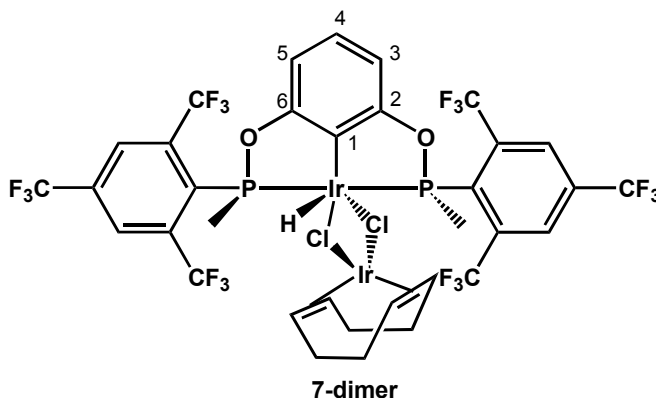
7-dimer

Synthesis of the dimer {C_6H_3-2,6-[OP-Me($C_6H_2(CF_3)_3$-2,4,6)]$_2$}IrH(µ-Cl)$_2$Ir(COD), 7-dimer

A Schlenk flask was charged with 0.41 mmol of ligand (311 mg) and 0.46 mmol of [(COD)IrCl]$_2$ (310 mg) and put under a flow of argon. Toluene (5 mL) was added via syringe, and the solution was stirred in an oil bath for 30 h at 130 °C. The toluene solution was degassed by three freeze-pump-thaw cycles. The flask was refilled with hydrogen gas at -190 °C and then sealed tightly with a Teflon plug. The mixture was heated at 120 °C for 15 h. Volatiles were removed under high vacuum and the residue was extracted with 3 × 15 mL of pentane. Removal of pentane solvent and other volatiles resulted in the isolation of **7-dimer**

77

as a yellow solid. Yield, 0.42 g, (0.32 μmol, 77%). ^{1}H NMR (400 MHz, 23 °C, C$_6$D$_6$): δ -24.59 (t, $^{2}J_{P-H}$ = 19.2 Hz, 1H, IrH), 1.26 (m, 2H, CH$_2$ in COD), 1.59 (m, 2H, CH$_2$ in COD), 1.93 (m, 2H, CH$_2$ in COD), 2.03 (m, 2H, CH$_2$ in COD), 2.07 (s b, 3H, PCH_3), 2.59 (s b, 3H, PCH_3), 3.46 (m, 1H, CH in COD), 3.75 (m, 1H, CH in COD), 3.85 (m, 1H, CH in COD), 4.12 (m, 1H, CH in COD), 6.72 (m, 2H, 3- and 5-H), 6.85 (t, $^{3}J_{H-H}$ = 8.0 Hz, 1H, 4-H), 7.73 (s, 2H, Ar(CF$_3$)$_3$-H), 7.98 (s, 1H, Ar(CF$_3$)$_3$-H), 8.11 (s, 1H, Ar(CF$_3$)$_3$-H). ^{31}P{^{1}H} NMR (162 MHz, 23 °C, C$_6$D$_6$) δ 123.2 (s), 123.5 (s). Yellow single crystals of **7-dimer** suitable for X-ray analysis were obained from toluene solution. The stucture is shown in Fig. 3.6 and X-ray crystallographic data are summarized in Table 3.5.
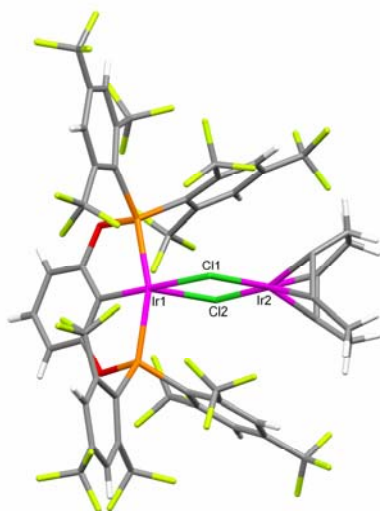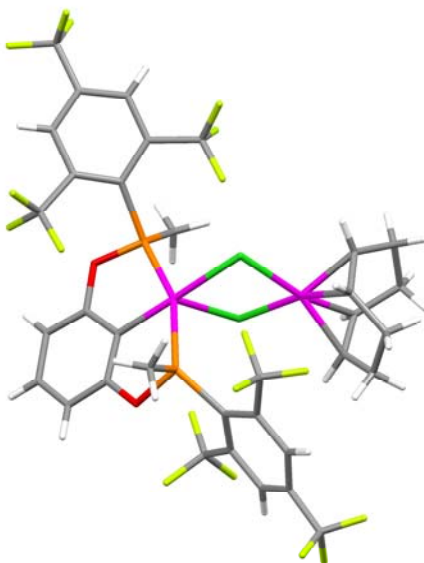

Fig. 3.6 ORTEP diagram of the **7-dimer**. Hydrogen atom on the iridium center can not be located.

Table 3.5 Crystal data and structure refinement summary of **6-dimer** and **7-dimer**

	6-dimer	7-dimer
Formula	$C_{71}H_{41.50}Cl_2F_{36}Ir_2O_2P_2$	$C_{34}H_{25}Cl_2F_{18}Ir_2O_2P_2$
crystal system	monoclinic	monoclinic
Space group	P 1 21/m 1	P 1 21/c 1
a/Å	13.1594(5)	13.3274(7)
b/Å	19.9987(10)	11.9056(8)
c/Å	13.3599(5)	24.8018(14)
α/deg	90	90
β/deg	95.880(2)	98.669(2)
γ/deg	90	90
V/(Å^3)	3497.4(3)	3890.4(4)
Z	2	4
T/K	100(2)	100(2)
$R1$ [$I>2\sigma(I)$]	0.0413	0.0257
$wR2$ (all data)	0.1033	0.0620
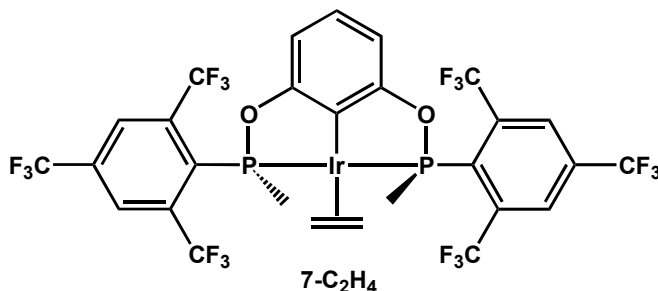
7-C$_2$H$_4$

Synthesis of the ethylene complex, 7-C$_2$H$_4$. Complex **7-dimer** (200 mg, 0.18 mmol) and NaO^{t}Bu (29 mg, 0.30 mmol) were weighed into a Schlenk flask and put under a flow of ethylene. Toluene (5 mL) was added to the flask via syringe and ethylene was bubbled through the solution for 3 h. After evaporation of the solvent under high vacuum, the residue was extracted with 3 × 10 mL of pentane, and the extract was cannula transferred and filtered through a 0.2μm pore size syringe filter. Pentane was removed under high vacuum to give 120 mg (0.12 mmol, 67% yield) of product as a red solid. ^{1}H NMR (400 MHz, 23 °C, C$_6$D$_6$):

δ 1.76 (s, 6H, CH$_3$), 3.23 (m, 4H, C$_2$H$_4$), 7.00 (d, $^3J_{H-H}$ = 6 Hz, 3H, 3 and 5-H), 7.18 (t, $^3J_{H-H}$ = 8 Hz, 1H, 4-H), 7.78 (s, 4H, Ar(CF$_3$)$_3$-H). ^{31}P{^{1}H} NMR (162 MHz, 23 °C, C$_6$D$_6$): δ 143.8 (s). ^{19}F NMR (376 MHz, 23 °C, C$_6$D$_6$): δ -54.8 (s, 12F, o-CF$_3$), -63.3 (s, 6F, p-CF$_3$).
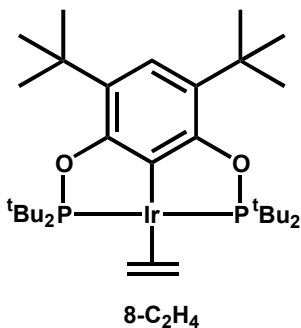
8-C$_2$H$_4$

Synthesis of 8-C$_2$H$_4$: Complex **8-HCl** (210 mg, 0.28 mmol) and NaO^{t}Bu (29 mg, 0.30 mmol) were weighed into a Schlenk flask and put under a flow of argon. Toluene (10 mL) was added to the flask via syringe and ethylene was bubbled through the solution for 3 h. After evaporation of the solvent under high vacuum, the residue was extracted with 3 × 20 mL of pentane, and the extract was cannula transferred and filtered through a pad of Celite. Pentane was removed under high vacuum, and the brown solid was dried under high vacuum overnight to give 168 mg (0.23 mmol, 82% yield) of pure product. ^{1}H NMR (400 MHz, 23 °C, CDCl$_3$): δ 1.30 (virtual triplet, apparent J = 6.4 Hz, 36H, 2 × P^{t}Bu$_2$), 1.61 (s, 16H, 2 × ^{t}Bu), 3.17 (s, 4H, C$_2$H$_4$), 7.38 (s, 1H, 4-H). ^{31}P{^{1}H} NMR (162 MHz, 23 °C, CDCl$_3$): δ 180.9 (s). ^{13}C{^{1}H} NMR (100.6 MHz, 23 °C, CDCl$_3$): δ 29.2 (CH$_3$, virtual triplet, apparent J = 3.0 Hz, 2 × P^{t}Bu$_2$), δ 31.1 (CH$_3$, S, 2 × ^{t}Bu), 34.8 (C$_q$, s, 2 × ^{t}Bu), 36.8 (CH$_2$, s, C$_2$H$_4$), 42.0 (C$_q$, t, J_{P-C} = 11.1 Hz, 2 × P^{t}Bu$_2$), 123.3 (C$_q$, s, C3 and C5), 125.0 (C$_q$, m, C1), 150.5 (C$_q$, s, C4), 163.6 (C$_q$, virtual triplet, apparent J = 8.0 Hz, C2 and C6).

Hydrogen transfer from COA to TBE catalyzed by iridium pincer complexes: A flask was charged with iridium pincer complex (2.5 μmol), COA (7.5 mmol), and TBE (7.5 mmol). The flask was sealed tightly with a Teflon plug under an argon atmosphere, and the solution was stirred in an oil bath at 200 °C. Periodically, the flask was removed from the bath and cooled in an ice bath. An aliquot was removed from the flask, and analyzed by GC.

Procedures for alkane metathesis reactions: A flask was charged with 0.021 mmol of iridium pincer complex, 0.017 mmol of the Schrock catalyst **Mo-F$_6$** or **W-siloxyl**, 2 mL (15.1 mmol) of *n*-hexane, and 8.8 μL (0.063 mmol) of mesitylene as internal standard. The flask was sealed tightly with a teflon plug under an argon atmosphere, and the solution stirred in a 125 °C oil bath. Periodically, the flask was removed from the bath and cooled in an ice bath. An aliquot was removed from the flask, and analyzed by GC. Product concentrations were calculated for each aliquot.

References

(1) Goldman, A. S.; Roy, A. H.; Huang, Z.; Ahuja, R.; Schinski, W.; Brookhart, M. *Science* **2006**, *312*, 257.

(2) Bailey, B. C.; Schrock, R. R.; Kundu, S.; Goldman, A. S.; Huang, Z.; Brookhart, M. *Organometallic* **2009**, *28*, 355.

(3) Batsanov, A. S.; Cornet, S. M.; Dillon, K. B.; Goeta, A. E.; Hazendonk, P.; Thompson, A. L. *Dalton Transactions* **2002**, 4622.

(4) Göttker-Schnetmann, I.; White, P. S.; Brookhart, M. *J. Am. Chem. Soc.* **2004**, *126*, 1804.

(5) Göttker-Schnetmann, I.; Brookhart, M. *J. Am. Chem. Soc.* **2004**, *126*, 9330.

(6)   Robbins, J.; Bazan, G. C.; Murdzek, J. S.; O'Regan, M. B.; Schrock, R. R. *Organometallic* **1991**, *10*, 2902.

(7)   Schrock, R. R.; Czekelius, C. C. *Adv. Synth. Catal.* **2007**, *349*, 55.

(8)   Schrock, R. R. *Adv. Synth. Catal.* **2007**, *349*, 41.

(9)   Schrock, R. R. *Chem. Rev.* **2002**, *102*, 145.

(10) Gupta, M.; Hagen, C.; Flesher, R. J.; Kaska, W. C.; Jensen, C. M. *Chem. Commun.* **1996**, 2083.

(11) Göttker-Schnetmann, I.; White, P. S.; Brookhart, M. *Organometallic* **2004**, *23*, 1766.

(12) Herde, J. L.; Lambert, J. C.; Senoff, C. V. *Inorganic Syntheses* **1974**, *15*, 18.

CHAPTER FOUR

Highly Active and Recyclable Heterogeneous Iridium Pincer Catalysts for Transfer Dehydrogenation of Alkanes

Introduction

Catalytic alkane dehydrogenation is carried out industrially on an enormous scale for the conversion of inexpensive saturated hydrocarbon feedstocks to higher-value olefins and arenes. Heterogeneous catalysts are used in these cracking and reforming processes which typically operate at high temperatures (400–600 °C), resulting in low product selectivities and poor energy efficiency.[1]

While numerous homogeneous catalytic alkane dehydrogenation systems have been reported,[2] iridium pincer complexes have been shown to be the most productive. Two examples of such systems are shown in Fig. 4.1. The iridium bis(phosphine) (^{t}Bu-PCP) complex, **1a**,[3] has been investigated by Jensen, Kaska and Goldman,[3] while the

bis(phosphinite) (^{t}Bu-POCOP) complexes, **2a–e**, have been studied by Brookhart.[4,5] Other related iridium pincer systems have also shown good activity in alkane dehydrogenation.[6] Operating under relatively mild conditions (100–200 °C), these iridium pincer complexes can effect the transfer-dehydrogenation of alkanes, using sacrificial olefins as hydrogen acceptors (as in eq 1), or dehydrogenation in the absence of sacrificial acceptors under conditions where H_2 is allowed to escape from the system.

By comparison with conventional heterogeneous dehydrogenation systems, the iridium pincer catalysts (like other homogeneous dehydrogenation catalysts) show excellent chemoselectivity: "cracking" (C-C bond cleavage side-reactions) has never been reported. Even more notably, these complexes have been reported to catalyze dehydrogenation with high regioselectivity for the terminal positions of *n*-alkanes or *n*-alkyl groups. Moreover, in addition to simple alkanes, iridium pincer complexes have been reported to catalyze dehydrogenation of numerous other substrates including amines,[7] alcohols,[8] and polyolefins.[9] Mechanistic details of the dehydrogenations by both iridium PCP and POCOP pincer catalysts have been disclosed.[10]
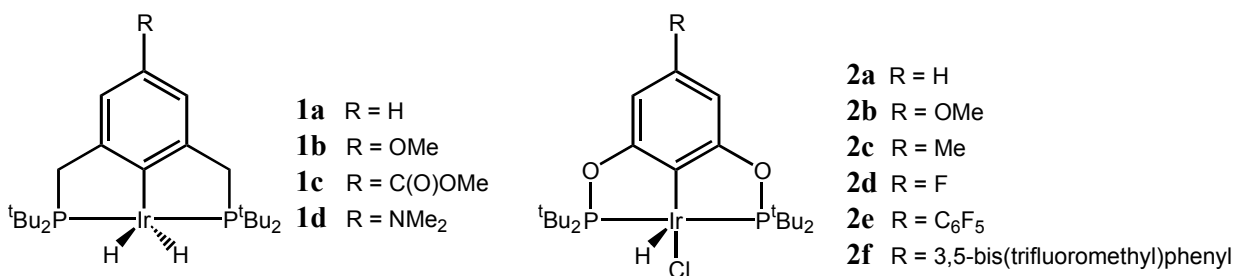
Fig. 4.1 Structures of Ir–PCP and Ir–POCOP complexes.
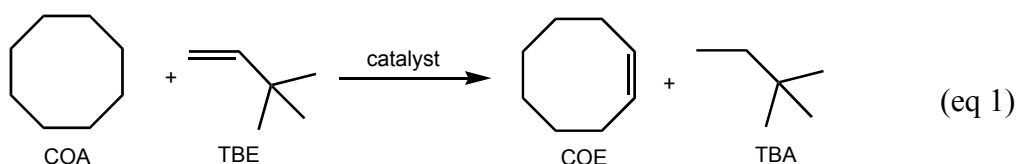
While the iridium pincer systems are quite robust, the utility of these homogeneous catalysts is limited due to problems of catalyst recyclability and product separation. Heterogeneous iridium pincer systems therefore hold promise for a broad range of applications. In particular, our groups desired such catalysts to combine with heterogeneous olefin metathesis catalysts to generate a fully heterogeneous catalyst system for alkane metathesis.[11]

In this paper we report the results of three strategies for preparing supported iridium pincer complexes: (i) Covalent attachment of an iridium complex containing a phenoxide functionality to a Merrifield resin through an S_N2 reaction with the chlorobenzyl moieties. (ii) Covalent bonding to silica of iridium pincer complexes containing a pendant alkoxy silane group. (iii) Adsorption of Ir pincer complexes (particularly those containing basic functional groups) on γ-Al_2O_3 through a Lewis acid/Lewis base interaction. The Merrifield resin–supported iridium POCOP catalyst was found to have low transfer-dehydrogenation activity. The silica-supported iridium POCOP catalyst showed good transfer dehydrogenation activity at early stages but poor lifetimes. Notably, the γ-Al_2O_3–supported iridium complexes were recyclable and highly active, and in some cases even more productive than the analogous homogeneous system for transfer dehydrogenation.

Results and Discussion

1. Alumina-supported iridium pincer catalyst systems.

The iridium PCP dihydride complexes (**1a-d**) and POCOP ethylene complexes (**3–5**) shown in Fig. 4.1 and 4.2 were used in the alumina adsorption studies. Complexes **1a, 1b, 1c**

and **3** have been previously prepared. Complexes **1d**, **4** and **5**, previously unknown, contain polar groups in the para position and were thought to be good candidates for adsorption.
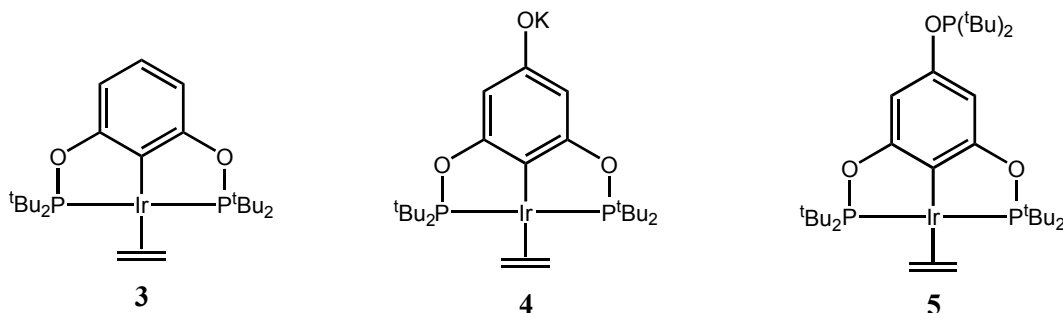
Fig. 4.2 Structures of iridium POCOP complexes used for absorption on γ-alumina.

1.1. Syntheses of complexes 1d, 4 and 5. Synthesis of the bis(phosphine) PCP complex **1d** is outlined in Scheme 4.1.[12] Dimethylation of the commercially available dimethyl-5-aminoisophthalate (**6**) was achieved by adaptation of a method developed by Borch and Hassid.[13] The diester **7** was then reduced to 5-dimethylamino-1,3-benzenedimethanol (**8**) by lithium aluminum hydride in THF.[14] Diol **8** was then treated with PBr$_3$ in acetonitrile and the resulting dibromide **9** was recrystallized in 77% yield from acetonitrile/water[15] before conversion to Me$_2$N-PCP-H (**10**) by an adaptation of the method of Moulton and Shaw.[16] Metalation of the free ligand could only be achieved under H$_2$; the resulting iridium hydrido chloride was reduced to the iridium dihydride (**1d**) and tetrahydride in analogy with the synthesis of **1a** and the corresponding tetrahydride. Although we were not successful in obtaining crystals of either (Me$_2$N-PCP)IrH$_2$ or (Me$_2$N-PCP)IrH$_4$, the reaction of this mixture with CO, in analogy with the reaction of the unsubstituted PCP hydrides, gave clean conversion to (Me$_2$N-PCP)Ir(CO) which was crystallographically characterized (see Supporting Information). For catalytic runs, **1d** was generally used as a mixture of (Me$_2$N-

PCP)IrH$_2$ and (Me$_2$N-PCP)IrH$_4$ (the iridium PCP and POCOP tetrahydrides readily convert to the dihydrides under catalytic conditions).

Scheme 4.1 Synthesis of (p-Me$_2$N-PCP)IrH$_2$ complex
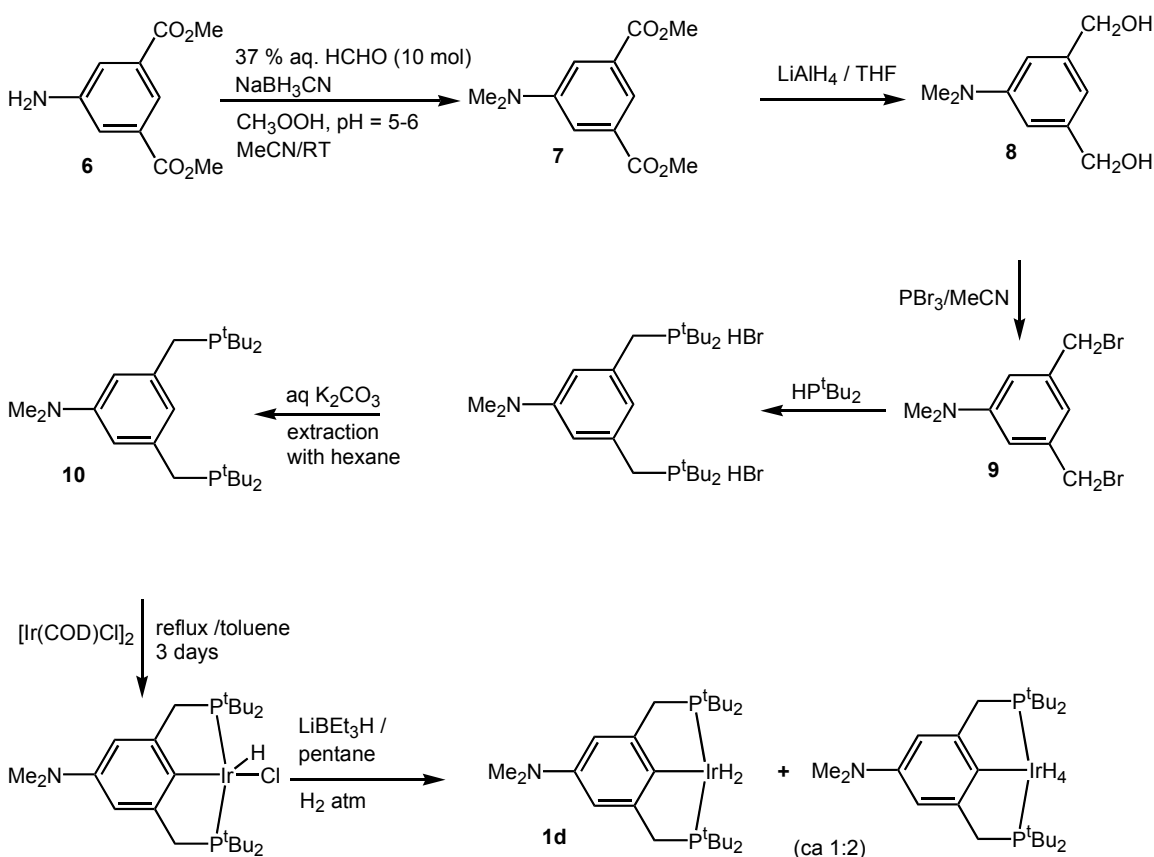
The synthesis of complex **4** is outlined in Scheme 4.2. Deprotection of the methoxy group of previously reported[4] {p-OMe-C$_6$H$_2$-2,6-[OP(t-Bu$_2$)]$_2$}IrHCl, **2b**, with 9-I-BBN (9-I-BBN = 9-iodo-9-borabicyclo[3.3.1]nonane, 1M in hexanes), followed by hydrolysis with water lead to the formation of {4-HO-C$_6$H$_2$-2,6-[OP(t-Bu$_2$)]$_2$}IrHI, **11**, in 86% yield. Treatment of **11** with 2 equivalents of KH in THF produces Ir dihydride complex, {p-KO-C$_6$H$_2$-2,6-[OP(t-Bu$_2$)]$_2$}Ir(H)$_2$, **12**, which then reacts with ethylene to form {p-KO-C$_6$H$_2$-2,6-[OP(t-Bu$_2$)]$_2$}Ir(C$_2$H$_4$), **4**, in 70% yield.

Scheme 4.2 Synthesis of (*p*-KO-POCOP)IrC₂H₄ complex
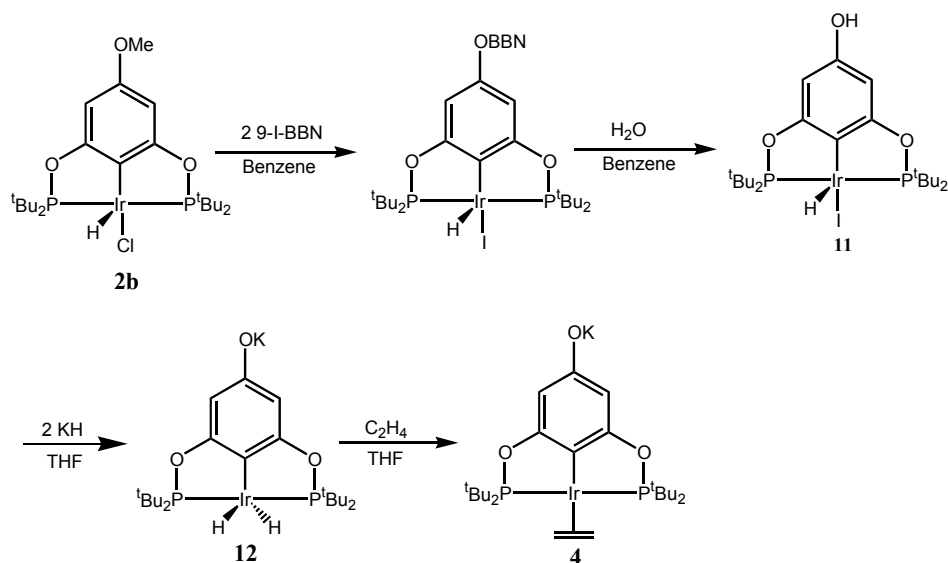
Preparation of tris(phosphinite) Ir pincer complex, **5**, is outlined in Scheme 4.3. The tris(phosphinite) POCOP ligand, **13**, was synthesized in 89% yield by reaction of 1,3,5-benzenetriol with di-*tert*-butylchlorophosphine and sodium hydride. Ir hydrido chloride complex, **14**, was obtained from the reaction of 0.5 equivalent of [Ir(COD)Cl]₂ with the tris(phosphinite) ligand in toluene for 12 h at 130 °C (82% yield). Treatment of the hydridochloride complex with sodium *tert*-butyloxide in the presence of ethylene produced **5** (75% yield).

Scheme 4.3 Synthesis of (*p*-ᵗBu₂PO-POCOP)IrC₂H₄ complex
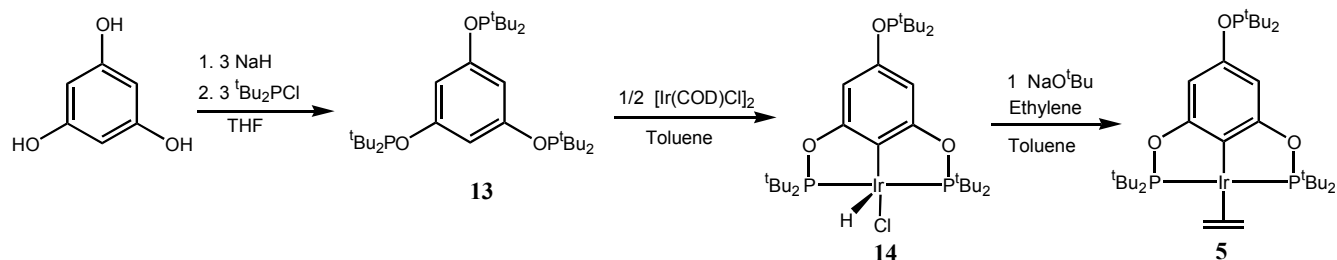
1.2 Support of bisphosphinite (POCOP) complexes 3 and 4 on γ-alumina; transfer-dehydrogenation activity. γ-Al_2O_3 has been widely used to support metals or metal oxides for heterogeneous catalysis, with most applications being in the petroleum industry.[17] For example, a γ-Al_2O_3–supported cobalt catalyst has been used in the Fisher-Tropsch process for decades. However, γ-Al_2O_3 is rarely used to support organometallic catalysts. Since alumina contains Lewis acidic sites we considered that iridium pincer complexes containing basic and/or polar functional groups could be strongly adsorbed on this support. We visually examined the effects of adding alumina to cyclooctane solutions of the pincer catalysts, which are orange in color. When 50 mg of γ-Al_2O_3 is added to 1.0 mL of a COA solution containing 2.5 μmol of phenoxide complex **4**, the solution is completely decolorized and the alumina acquires the orange color of the pincer complex. In contrast, a similarly treated solution of **3** retains an orange color. Addition of a further 50 mg alumina results in a nearly colorless solution, suggesting that the parent complex, **3**, can be adsorbed but that the interaction is weaker than with **4**.
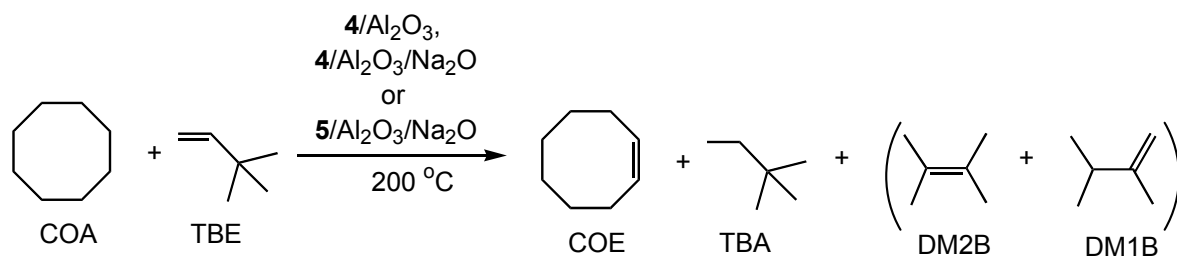
Fig. 4.3 Transfer dehydrogenation of COA and TBE with alumina-supported Ir catalysts.

The transfer of hydrogen from COA to *tert*-butylethylene (TBE) as acceptor to yield cyclooctene (COE) and 2,2-dimethylbutane (TBA) (eq 1) is a commonly used "benchmark" reaction;[18] this reaction is thermodynamically favorable by 6 kcal/mol.[19] Using the iridium PCP complex **1a**, TONs up to 1000 can be achieved at 200 °C but require portionwise

addition of TBE which is a strong inhibitor. The iridium POCOP systems, **2a-2f**, are much less subject to inhibition by TBE; TONs up to 2200 have been observed at 200 °C with substrate : catalyst ratios of 3300 : 1.[4]

The γ-Al$_2$O$_3$–supported complex **4** was examined for transfer-dehydrogenation activity using the COA/TBE couple. Results are summarized in Table 4.1. A system containing 2.5 μmol of the iridium catalyst **4** supported on 280 mg of γ-Al$_2$O$_3$, 7.5 mmol of COA (3000 equivalents relative to Ir), and 7.5 mmol of TBE, was heated at 200 °C under argon in a sealed glass vessel for 40 h. This process converted 1990 equivalents (relative to Ir) of TBE to TBA, and COA to COE and 1,3-cyclooctadiene (COE/COD ~ 5/1).[20] The activity is similar to the homogeneous system under identical conditions (1970 TONs, 40 h, Table 4.1). In the heterogeneous system, part of the TBE was isomerized to form 2,3-dimethyl-2-butene (DM2B, 810 equivalents, 40 h) and 2,3-dimethyl-1-butene (DM1B, 70 equivalents, 40 h). These isomerized olefins were shown to be poor acceptors. For the homogeneous system, no TBE isomerization products were observed.

The homogenous catalyst **4** gradually decomposed and unidentified black solids precipitated during the transfer dehydrogenation reaction. The catalytic activity was completely lost after evaporation of volatiles and addition of fresh COA and TBE solutions (Table 4.1). However, when supported on γ-Al$_2$O$_3$, **4** can be recycled with only modest loss of activity. Surprisingly, the extent of isomerization of TBE increased after each recycle. After the first run (showing 1990 TONs), the catalyst was isolated and recharged with COA and TBE (3000 equivalents respectively). After 40 h at 200 °C, 1420 equivalents of TBE were converted to TBA, with the formation of 1150 equivalents of DM2B and 200

equivalents of DM1B. A second recycle exhibited 1200 turnovers (TONs) with 1200 equivalents of DM2B and 580 equivalents of DM1B formed as isomerization products.

The isomerization of TBE decreases the transfer dehydrogenation efficiency since DM2B and DM1B are inefficient hydrogen acceptors. (No 2,3-dimethylbutane, the hydrogenation product of DM2B or DM1B, was observed in the transfer dehydrogenation reaction catalyzed by $4/\gamma$-Al_2O_3). In control experiments with 280 mg of γ-Al_2O_3 (no Ir), 7.5 mmol of COA, and 7.5 mmol of TBE, 98 % of TBE was isomerized at 200 °C to form DM2B (78 %) and DM1B (22 %) after 6 h. No transfer dehydrogenation products TBA or COE were observed. This result indicates that the isomerization of TBE is catalyzed by the γ-Al_2O_3, presumably by acidic sites on the alumina surface. DM1B and DM2B are well known products of acid-catalyzed rearrangement of TBE.[21]

The supported parent complex **3** (**3**/γ-Al_2O_3; 2.5 μmol of **3** on 280 mg of γ-Al_2O_3) was also investigated for transfer dehydrogenation under similar conditions. Compared to **4**/γ-Al_2O_3, the transfer reaction catalyzed by **3**/γ-Al_2O_3 shows a higher TBE isomerization rate and poorer dehydrogenation activity. After 15 h at 200 °C, 2300 and 480 equivalents of DM2B and DM1B were produced with the **3**/γ-Al_2O_3, and only 190 equivalents of TBA were produced as the transfer dehydrogenation product. The reaction with **4**/γ-Al_2O_3 under the same reaction conditions produced 690 equivalents of DM2B, 40 equivalents of DM1B, and 1600 equivalents of TBA (See Table 4.1). In contrast to the neutral complex **3**, the basic phenoxide complex **4** must, to a certain extent, "neutralize" the acidity of γ-Al_2O_3, thus decreasing the TBE isomerization rate. Since most of the TBE was isomerized to form DM2B and DM1B with **3**/γ-Al_2O_3, the transfer dehydrogenation efficiency is very low.

Table 4.1 Transfer dehydrogenation of COA/TBE using **4** (solution phase) or **4**/γ-Al$_2$O$_3$ at 200 °C[a]

time	**4**/solution (homogeneous) Equivs.	**4**/γ-Al$_2$O$_3$ (heterogeneous) Equivs.			
	TBA	TBA	DM2B	DM1B	TBE
0.5 h	450	800	280	0	1920
3 h	1450	1290	530	0	1180
15 h	1800	1600	690	40	670
40 h	1970	1990	810	70	130
1st recycle					
40 h	No activity	1420	1150	200	230
2nd recycle					
40 h	No activity	1200	1200	580	20

a) 1.23 mM iridium catalyst in solution or equivalent amount in the case of supported systems; $[COA]_o = [TBE]_o = 3.7$ M; 280 mg γ-Al$_2$O$_3$.

Solid-state ^{31}P MAS NMR analysis of the γ-Al$_2$O$_3$–supported **4** (5.0 μmol of **4** on 150 mg of γ-Al$_2$O$_3$) shows a single species with a ^{31}P shift at 177 ppm which is close to that of complex **4** in solution (170 ppm). After 1090 turnovers in the hydrogen transfer reaction, a new minor (ca. 10 %) species with a ^{31}P shift of 66 ppm appears (See Fig. 4.4). This shift corresponds to one for the species generated when the supported catalyst is exposed to oxygen and suggests that catalyst decay occurs through oxidation, probably at phosphorus.
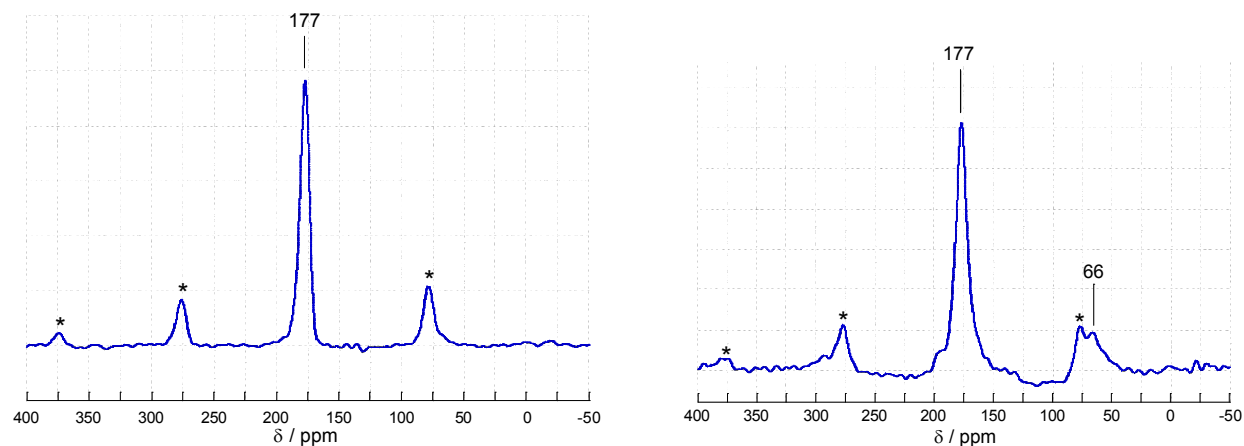
Fig. 4.4 Left: Solid-state ^{31}P MAS NMR of fresh **4**/γ-Al$_2$O$_3$. Right: Solid-state ^{31}P MAS NMR of **4**/γ-Al$_2$O$_3$ after use for catalytic transfer-dehydrogenation (1090 TOs). 12 kHz MAS, 20 °C, referenced to 85% H$_3$PO$_4$. Starred signals represent spinning sidebands.

1.3. Preparation of basic alumina and transfer dehydrogenation activity of basic alumina–supported 4 and 5. As discussed above, the acid-catalyzed isomerization of TBE by γ-Al$_2$O$_3$ results in decreased efficiency of COA/TBE transfer dehydrogenation. A variety of commercially available aluminas, including acidic, neutral, and basic were screened as the supports for the iridium catalyst. However, all of these aluminas were found to isomerize TBE rapidly. To decrease the acidity of alumina, a Na$_2$O-modified γ-Al$_2$O$_3$ (2.7 wt% of Na$_2$O) solid support was synthesized by adding an aqueous solution of NaOH or Na$_2$CO$_3$ to γ-Al$_2$O$_3$. The solid was calcined at 550 °C for 18 h under a flow of O$_2$. A control experiment with 310 mg of the Na$_2$O-modified alumina (Al$_2$O$_3$/Na$_2$O)**,** 7.5 mmol of COA, and 7.5 mmol of TBE, resulted in isomerization of only 1 % of the TBE to form DM2B after 48 h at 200 °C.

The Al$_2$O$_3$/Na$_2$O solid (310 mg) was used to support catalyst **4** (1.3 μmol) and was screened for transfer dehydrogenation activity (Table 4.2). Transfer dehydrogenation of COA and TBE (7500 equivalents relative to Ir) catalyzed by **4**/Al$_2$O$_3$/Na$_2$O results in 4140 turnovers and only 2.4 % isomerization of TBE after 40 h at 200 °C. Recycle showed only 660 TONs were obtained after 15 h (Table 4.2). It should be noted that **the transfer**

dehydrogenation activity with the heterogeneous system 4/Al₂O₃/Na₂O is much higher

than the activity with the homogenous catalyst 4 which exhibited only 1860 TONs after 40

h under the same reaction conditions (Table 4.2). The homogenous catalyst **4** decays faster

than the heterogeneous system, and no catalytic activity was observed after evaporation of

volatiles and addition of fresh COA and TBE solutions (Table 4.2). Heating at a higher

temperature, 240 °C, with the heterogeneous system **B** and 11000 equivalents of COA and

TBE gave 7010 turnovers after 40 h, and only 1.6 % of TBE was isomerized to form DM2B

(Table 2).

Table 4.2 Transfer dehydrogenation of COA/TBE with solution-phase or supported **4** and **5**.

	Homogeneous		Heterogeneous					
	4[a] (200 ˚C)	**5**[a] (200 ˚C)	**4/Al₂O₃/Na₂O**[a] (200 ˚C)		**5/Al₂O₃/Na₂O**[a] (200 ˚C)		**4/Al₂O₃/Na₂O**[b] (240 ˚C)	
time	TBA	TBA	TBA	DM2B	TBA	DM2B	TBA	DM2B
0.5 h	270	1260	1220	30	980	0	2170	0
3 h	1380	2110	2220	80	2520	0	3620	40
15 h	1830	2540	3490	160	3730	30	6240	130
40 h	1860	2660	4140	180	4310	40	7010	180
	recycle, 200 ˚C	recycle, 200 ˚C	recycle, 200 ˚C		recycle, 200 ˚C		recycle, 240 ˚C	
15 h	No activity	No activity	660	60	1520	0	940	50

a) 0.49 mM iridium catalyst in solution or equivalent amount in the case of supported systems (1.34 μmol supported iridium catalyst); 10.05 mmol COA and TBE, $[COA]_o$ = $[TBE]_o$ = 3.7 M; 310 mg γ-Al₂O₃/Na₂O. b) 1.34 μmol supported iridium catalyst; 14.74 mmol COA and TBE, $[COA]_o$ = $[TBE]_o$ = 3.7 M; 310 mg γ-Al₂O₃/Na₂O.

One major disadvantage of catalyst **4** is its lengthy and involved synthesis. Complex **5**,

readily prepared from 1,3,5-benzenetriol, was found to adsorb strongly on alumina. Analysis

of the Al₂O₃/Na₂O–supported **5** (7.6 μmol of **5** on 150 mg of Al₂O₃/Na₂O) by solid-state [31]P

MAS NMR shows two major phosphorus environments (see Fig. 4.5). The peak at 176.5 ppm is assigned to the intact, coordinated phosphinite group with a spinning sideband at 275 ppm (the spinning sideband expected at 78 ppm is obscured by the second peak in the spectrum). This constitutes a slight upfield shift from the solution-state chemical shift of 181.1 ppm and is a result of complex-support interactions. The peak at 78.0 ppm is attributed to the phosphinite group not coordinated to Ir, which is shifted far upfield from its solution state chemical shift of 150.8 ppm. The significant upfield shift indicates an intensive interaction between the uncoordinated phosphinite and the alumina. There is a third, minor ^{31}P NMR signal observed at 151.2 ppm. This signal position is close to the uncoordinated phosphine in solution (150.8 ppm) and is ascribed to some of **5** in which the free phosphinite group is not interacting with alumina.
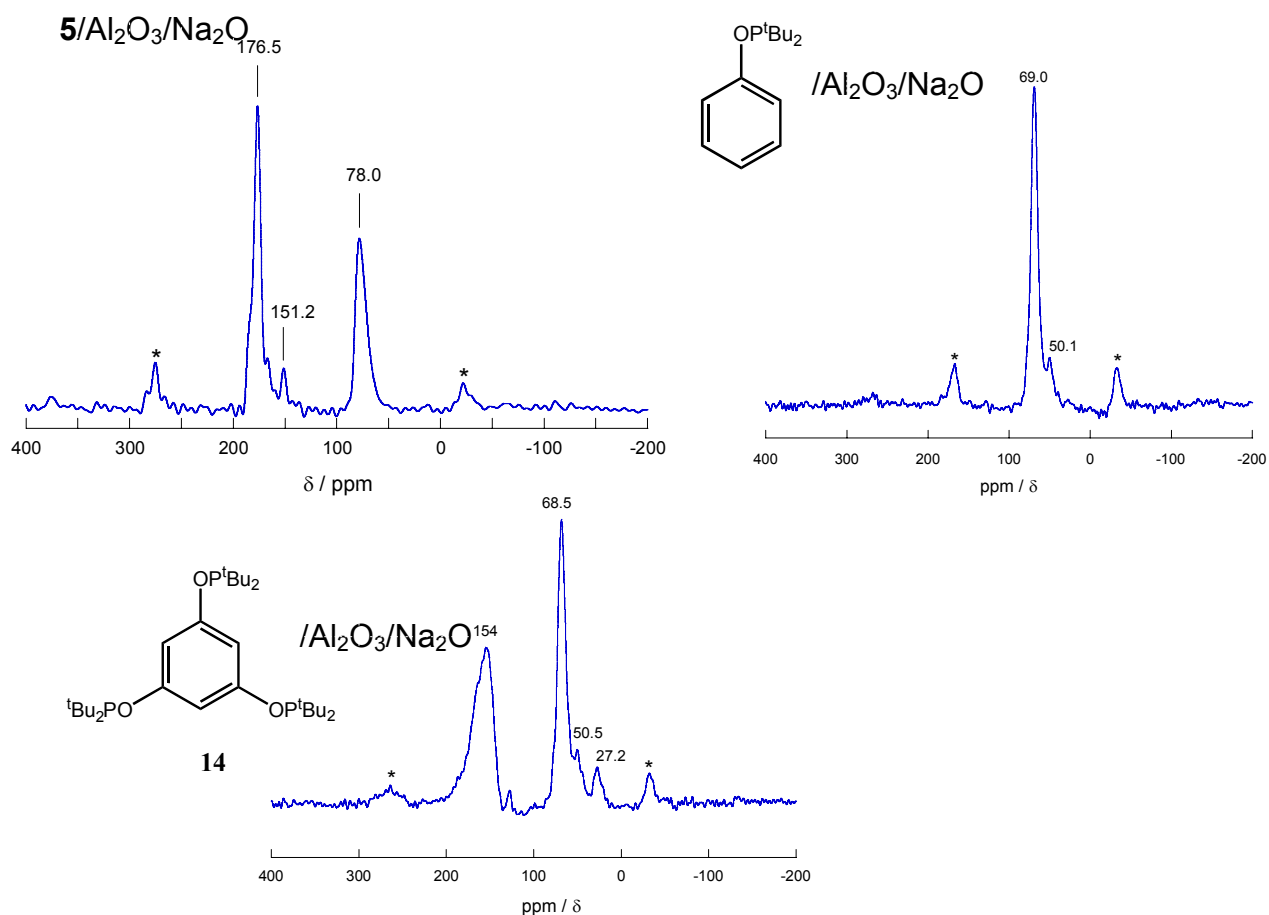
Fig. 4.5 Solid-state ^{31}P MAS NMR of the **5**/Al$_2$O$_3$/Na$_2$O (top left), phenyl di-*tert*-butylphosphinite /Al$_2$O$_3$/Na$_2$O (top right), and triphosphinte-benzene/Al$_2$O$_3$/Na$_2$O (bottom), 12 kHz MAS, 20 °C, referenced to 85% H$_3$PO$_4$. Starred signals represent spinning sidebands.

To investigate the interaction of uncoordinated phosphinite with alumina, the free 1,3,5-tri(di-*tert*-butylphosphinite)benzene ligand and the model compound phenyl di-*tert*-butylphosphinite were supported on Al$_2$O$_3$/Na$_2$O. Analysis of the Al$_2$O$_3$/Na$_2$O-supported phenyl di-*tert*-butylphosphinite by solid-state ^{31}P MAS NMR shows a large upfield shift from the solution-state chemical shift of 153 ppm to 69 ppm (see Fig. 4.5). Supporting the 1,3,5-tri(di-*tert*-butylphosphinite)benzene results in two major phosphorus environments. The sharp peak at 68.5 ppm is consistent with a phosphinite interacting with the alumina

surface as in the phenyl di-*tert*-butylphosphinite sample. The broad peak at 154 ppm is assigned to the phosphinite groups not directly interacting with the surface. The results indicate the uncoordinated phosphinite in complex **5** can indeed interact with the alumina surface and this results in a ^{31}P upfield shift by about 70–80 ppm in the ^{31}P MAS NMR spectrum. The nature of this interaction is currently under study.

The Al_2O_3/Na_2O-supported **5** (1.3 μmol **5** on 310 mg Al_2O_3/Na_2O) mirrors the activity of Al_2O_3/Na_2O-supported **4** but recycle of **5**/Al_2O_3/Na_2O is much more efficient. For example, transfer dehydrogenation of COA and TBE (7500 equivalents each relative to Ir) catalyzed by **5**/Al_2O_3/Na_2O results in 4310 turnovers and less than 1 % isomerization of TBE after 40 h at 200 °C. The first recycle exhibited 1520 turnovers after 15 h (Table 2). For the homogenous system, the conversion at early time (30 min., 1260 TONs) is greater than the heterogeneous system (30 min., 980 TONs), however; after 40 h, the homogeneous system exhibited only 2660 TONs relative to 4310 TONs for the supported system**.** Attempted recycle of the solution-phase catalyst **5** by evaporation of volatiles and addition of fresh COA and TBE resulted in no additional turnovers, indicating the complete decomposition of **5** under transfer dehydrogenation condition. Thus the alumina–supported **5** has a much longer lifetime than catalyst **5** in solution.

1.4. Leaching experiments. COA suspensions of **4**/Al_2O_3/Na_2O and **5**/Al_2O_3/Na_2O were filtered at 200 °C. The solid material was extracted twice more with COA at 200 °C and the colorless filtrates were combined and analyzed for iridium content by ICP-MS. The analysis of solutions indicated that only 0.02 % of Ir had leached into the solution from the Al_2O_3/Na_2O-supported **4** and only 0.007 % from the Al_2O_3/Na_2O-supported **5**. The solutions showed no activity for COA/TBE transfer dehydrogenation. These results, in combination

with the activity of the supported systems being comparable to or even greater than that of the catalysts in solution phase, clearly indicate that the active catalytic species remains bound to the alumina surface during the transfer dehydrogenation reaction.

1.5. Catalytic activity of bisphosphine (PCP) complexes supported on γ-alumina. Unlike the bisphosphinite analogues, (PCP)IrH$_2$ (**1a**) and derivatives react with TBE, if present in high concentration, to give an unidentified, catalytically inactive, decomposition product. Thus we conducted our study of alumina-supported PCP complexes under conditions somewhat different than those applied in studies of the alumina-supported POCOP complexes.

Complexes (MeO-PCP)IrH$_2$ (**1b**) and (MeOC(O)-PCP)IrH$_2$ (**1c**) have been previously synthesized.[22] The methoxy-substituted complex **1b** was previously reported to be a more robust alkane dehydrogenation catalyst than the parent complex **1a**,[23] while giving slightly higher rates of acceptorless dehydrogenation (of cyclodecane) but slightly lower rates of *n*-octane/NBE transfer-dehydrogenation. As seen in Table 4.3 (solution phase), turnover frequencies (TOFs) for COA/TBE transfer-dehydrogenation by **1b** are also somewhat lower than are found for **1a**. The ester-substituted complex **1c** is found to afford slightly greater initial rates for catalytic COA/TBE transfer dehydrogenation than either **1b** or **1a** (Table 4.3). However **1c** apparently undergoes significant decomposition under the catalytic conditions as indicated by a decrease in catalytic activity. Accordingly, ^{31}P and ^{1}H NMR spectroscopy independently reveal that in the presence of TBE **1c** reacts to give six-coordinate iridium hydride complexes. This decomposition is attributable to intermolecular addition of a C-H bond ortho to the ester functionality, in accord with the previously reported reaction of (PCP)Ir with acetophenone.[24]

Table 4.3 COA/TBE transfer-dehydrogenation catalyzed by solution-phase and γ–alumina-supported (PCP)Ir-based complexes at 125 °C.[a]

Catalyst (5 mM)	time (min)	homogeneous (solution phase) [COE] (mM)	heterogeneous (γ-alumina) [COE] (mM)
(PCP)IrH$_2$ (**1a**)	15	61	3
	60	164	3
	240	368	4
(MeO-PCP)IrH$_2$ (**1b**)	15	36	28
	60	115	60
	240	352	84
(MeO$_2$C-PCP)IrH$_2$ (**1c**)	15	73	49
	60	155	119
	240	258	354
(Me$_2$N-PCP)IrH$_2$ (**1d**)	15	20	42
	60	68	111
	240	200	283

a) 5 mM iridium catalyst in solution or equivalent amount in the case of supported systems; [TBE]$_o$ = 0.4 M, 1 mL COA and 100mg γ-Al$_2$O$_3$.

Upon addition of γ-alumina to a COA (100mg γ-Al$_2$O$_3$ + 1 mL COA) solution of unsubstituted PCP iridium complex **1a** (5 mM) the red solution turned clear and the solid acquired the characteristic red color of the complex. Upon heating to 125 °C the red solid rapidly turned orange, suggesting that decomposition had occurred. Accordingly, very little COA/TBE transfer-hydrogenation occurred in the presence of alumina at 125 °C (less than 5 mM COE formed; Table 4.3).

Attempts to support (PCP)Ir-based catalysts on alumina were more promising with MeO-PCP complex **1b** than with **1a**, but were still not satisfactory. As in the case of **1a**, upon addition of alumina the solution lost its red color which was acquired by the alumina, but, in contrast to alumina-supported **1a**, no color change was observed even upon heating. After 15 min at 125 °C, **1b** (5 mM) afforded product yields in the presence of alumina only slightly

less than in the absence of alumina (28 mM vs. 36 mM). But after 240 min the total yield was substantially less than was obtained in the absence of alumina (84 vs. 352 mM).

In contrast to results with **1a** and **1b**, the catalyst lifetime and total turnovers effected by ester-substituted complex **1c** were *increased* in the presence of alumina. As with all the bound iridium PCP catalysts, adsorbtion of **1c** visually appeared to be complete. Although initial rates of COA/TBE transfer-dehydrogenation were slightly lowered by the presence of alumina (49 mM vs. 73 mM after 15 min), the yield of COE was appreciably greater after 240 min than was obtained with the solution-phase catalyst (354 mM vs. 258 mM). This effect can be rationalized by assuming that adsorbtion of the catalyst to alumina inhibits the intermolecular catalyst de-activation reaction noted above. However, attempts to recycle the **1c**/γ-alumina catalyst system met with only partial success. The solution was removed from the solid, which was then washed two times with COA (2 x 2 mL) and a fresh TBE/COA solution was then added. The subsequent catalytic runs showed significantly decreased reactivity (Table 4.4).

Table 4.4 COA/TBE transfer dehydrogenation: recycling catalysts **1c** and **1d**.[a]

catalyst (5 mM equivalent)	Time (h)	1st cycle	2nd cycle	3rd cycle	4th cycle	5th cycle	6th cycle	7th cycle	8th cycle
(MeO$_2$C-PCP)IrH$_2$ **(1c)** **heterogeneous** (γ-alumina-supported)	1	117	101	27					
	4	331	188	41					
	8	440	259	49					
(Me$_2$N-PCP)IrH$_2$ **(1d)** **homogeneous** (solution-phase)	1	75	67	56	47	30	15	9	4
	4	281	222	154	116	70	41	20	11
	8	465	339	246	161	114	65	30	14
(Me$_2$N-PCP)IrH$_2$ **(1d)** **heterogeneous** (γ-alumina-supported)	1	115	91	66	61	46	16	10	6
	4	314	173	135	119	74	43	23	12
	8	464	315	216	197	117	65	31	15

a) 5 mM iridium catalyst in solution or equivalent amount in the case of supported systems. [TBE]$_o$ = 0.6 M, 1 mL COA and 100mg γ-Al$_2$O$_3$.

Very promising results were obtained with the new catalyst (Me$_2$N-PCP)IrH$_2$ (**1d**). Of the four X-PCP iridium catalysts used in this study, **1d** gave the lowest TOFs for COA/TBE transfer-dehydrogenation in solution (Table 4.3). Thus it is found that initial COA/TBE solution-phase transfer-dehydrogenation rates increase with decreasing electron-donating ability of the group X: Me$_2$N < MeO < H < CO$_2$Me. However, when **1d** was adsorbed on γ-alumina, initial rates of COA/TBE transfer-dehydrogenation were greater than obtained by solution-phase **1d**. This is consistent with the correlation with electron-withdrawing ability of X; binding of the Me$_2$N group to a Lewis acidic surface site would indeed be expected, based on this correlation, to increased catalytic activity.

In addition to the increased TOFs observed upon binding **1d** to alumina, the total TONs effected by the **1d**/γ-alumina system after 4 h were significantly greater than achieved with the homogeneous system (283 vs. 200 mM; Table 4.3). The system proved to be robust and recyclable (Table 4.4). The solution was removed after 8 h of catalysis at 125 °C and the remaining solid was washed two times with COA; upon addition of fresh TBE/COA solution to the solid, each subsequent run showed only a relatively small decrease in catalytic activity. This process involves extensive exposure of the catalyst (which is sensitive to O$_2$, H$_2$O and even N$_2$) to an imperfect glove-box atmosphere; thus the observed decrease in TOF for each cycle represents only an upper limit of the degree of decomposition that occurred during the actual catalytic run. Recycling of the solution-phase catalyst necessarily involves a different protocol, namely, removal of solvent in vacuo before adding fresh solution. While this presumably involves less exposure to impurities, the loss of activity with each cycle is approximately the same as that observed in the case of the alumina-supported system (Table 4.4).

The **1d**/γ-alumina system was also effective for the transfer dehydrogenation of *n*-octane, and as was found with COA, more active than solution-phase **1d** (Table 4.5).

Table 4.5 *n*-Octane/TBE transfer-dehydrogenation by (Me$_2$N-PCP)IrH$_2$ (**1d**) at 125 °C.[a]

time (min)	homogeneous (solution-phase)		heterogeneous (γ-alumina-supported)	
	1-octene (mM)	total octene (mM)	1-octene (mM)	total octene (mM)
15	4	7	2	15
30	9	22	3	30
60	15	43	3	59
120	16	73	4	99
240	16	98	4	130

a) 5 mM iridium catalyst in solution or equivalent amount in the case of supported systems. [TBE]$_o$ = 0.4 M, 1 mL *n*-octane and 100mg γ-Al$_2$O$_3$.

Table 4.6 Control experiment: isomerization of 1-octene by γ–alumina (no iridium present, 100mg γ-Al$_2$O$_3$ + 1 mL *n*-octane).

initial [1-octene]	time (min)	1-octene (mM)	trans-2-octene (mM)	2-cis-octene (mM)
29 mM	5	27	1	1
	10	26	2	1
	15	24	3	2
	30	20	6	3
	60	14	8	5
427 mM	5	413	8	6
	10	404	14	12
	15	393	22	15
	30	366	46	24
	60	307	88	40

The yield of 1-octene from *n*-octane with this system is much lower than with solution-phase **1d**. We initially assumed that this lower apparent selectivity was due to the isomerization of 1-octene by γ-alumina. Control experiments with γ-alumina, with no iridium present, do indeed show that 1-octene is isomerized under these conditions (Table 4.6). For example, after ca. 60 min, with an initial 1-octene concentration of 29 mM, isomerization is ca. 50% complete with cis- and trans-2-octene being the only major products. However, it

does not seem that this level of isomerization activity (half-life of ca. 60 min), by itself, could account for the much lower yields of 1-octene obtained from **1d**/γ-alumina vs. solution phase **1d** (e.g. 3 mM 1-octene out of 30 mM total octene product vs. 9 mM 1-octene out of 22 mM total octene, after only 30 min of catalysis). Further work is ongoing to elucidate the reason for the relatively low yield of terminal alkene, but possible explanations include formation of a minor decomposition product on alumina that acts as a highly active catalyst for isomerization, or perhaps simply increased isomerization activity from **1d** upon binding to alumina (possibly due to decreased electron-density at Ir). It should be noted, however, that even the small yields of 1-octene observed at early reaction times indicate that at least partial selectivity for dehydrogenation at the terminal position is retained upon binding to alumina (even the low 1-octene concentrations observed at early reaction times are much greater than equilibrium values). Furthermore, the predominant internal octenes observed are cis- and trans-2-octene, with much lower concentrations of 3- and 4-octene (e.g. >80% 2-octene after 60 min); this is indicative of selectivity for the terminal position followed by rapid α−β isomerization and slower further internal isomerization.

To summarize the results in this section, (PCP)IrH$_2$ (**1a**) shows very rapid loss of catalytic activity in the presence of γ-alumina. All three para-substituted complexes investigated in this study underwent decomposition in the presence of γ-alumina far more slowly than **1a**, if at all. Thus para-substituent binding appears to inhibit a decomposition reaction of the iridium center with alumina. In the case of complex **1c** the presence of alumina also appears to inhibit the intermolecular decomposition reaction that is observed in the solution phase; this effect is similar to that observed for complexes **4** and **5** as discussed in the preceding section. In the case of catalyst **1b**, deactivation by alumina still occurs, albeit

slowly, suggesting that the methoxy group does not bind as strongly as the ester or dimethyl amino groups of **1c** or **1d**, respectively. Electron-withdrawing ability of the para-substituent is correlated with catalytic TOFs in solution; consistent with the presumed binding of the Me_2N group to a Lewis acidic surface site, the Me_2N-PCP catalyst **1d** affords increased TOFs when bound to γ-alumina. The **1d**/γ-alumina system is also found to be quite stable under catalytic conditions, and even tolerates multiple cycles of solvent removal, washing, and reuse. In the case of *n*-alkane, the product distribution from the **1d**/γ-alumina system is predominantly 2-octene, but this is likely due to increased rates of $\alpha-\beta$ isomerization rather than selectivity for dehydrogenation the 2-position of the alkane chain.

1.6. Quantifying the strength of binding of the Me_2N-PCP unit to alumina. $(Me_2N$-PCP)IrH_2 (30 mg) was dissolved in 10 mL COA in the presence of 1g γ-alumina. The mixture was stirred for 15 min and then filtered; the filtrate was then evaporated in vacuo. The residue was analyzed by X-ray fluorescence and the iridium content was found to be below the detection limit of this method, which is estimated as $<1 \times 10^{-6}$ g, or 0.003% of the initial amount of iridium.

The iridium carbonyl complexes are much more robust than the catalytically active hydrides. For this reason, $(Me_2N$-PCP)Ir(CO) (**1d-CO**) was used to help quantify, by UV-visible spectroscopy, the strength of binding of the $(Me_2N$-PCP)Ir unit to alumina. A *n*-hexane solution of **1d-CO** (2.5 mM; 3mg in 2.0 mL) has an absorbance of 1.58 at $\lambda = 493$ nm (1.0 cm pathlength). When 2.0 mL of the same solution was stirred in the presence of 50 mg γ-alumina for 15 minutes and then filtered, the absorbance at $\lambda = 493$ nm was found to be $<1 \times 10^{-4}$. The concentration of **1d-CO** in solution under these conditions is therefore $<0.006\%$ of that present prior to the addition of alumina.

1.7. Infrared spectroscopic characterization of the iridium complexes supported on γ-alumina. C-O stretching frequencies act as a valuable[25] indicator of small changes in electron density at the metal center of transition metal carbonyl complexes. In order to probe the nature of the binding of the X-PCP complexes to γ-alumina, we prepared the corresponding (X-PCP)Ir(CO) complexes. All complexes appeared, visually, to be fully adsorbed by γ-alumina. After removal of solvent, nujol mulls of the material were prepared for IR analysis.

Table 4.7 C-O stretching frequencies of complexes (X-PCP)Ir(CO) in solution and adsorbed on γ-alumina.

compound	ν_{CO} (cm^{-1}) (Nujol)	ν_{CO} (cm^{-1}) (γ-alumina, Nujol)
(PCP)Ir(CO)	1925.3	1925.9
(MeO-PCP)Ir(CO)	1922.6	1927.5
(Me$_2$N-PCP)Ir(CO)	1918.4	1928.9
(MeO$_2$C-PCP)Ir(CO)	1931.0	1930.5
(KO-POCOP)Ir(CO)	1945	1945
(^{t}Bu$_2$PO-POCOP)Ir(CO)	1934	1945

Adsorbtion of (PCP)Ir(CO) (**1a-CO**) on alumina results in a negligible change in C-O stretching frequency as compared with **1a-CO** dissolved in Nujol hydrocarbon (1925.9 cm^{-1} vs. 1925.3 cm^{-1}; Table 4.7). The value of ν_{CO} of (MeO-PCP)Ir(CO) in Nujol is ca. 3 cm^{-1} red-shifted versus solution-phase **1a-CO**, consistent with the electron-donating properties of the *p*-methoxy group. When bound to alumina however, ν_{CO} of **1b-CO** is 5 cm^{-1} greater than solution-phase **1b-CO** and ca. 2 cm^{-1} greater than either solution phase **1a-CO** or **1a-CO**/γ–alumina. These data indicate that **1b-CO** binds to γ-alumina with the *p*-methoxy group acting as a Lewis base toward a Lewis acid surface site; the bound methoxy group is then electron-withdrawing, as might be expected. Likewise, the ν_{CO} value of complex **1d-CO** in solution is 7 cm^{-1} less than that of **1a-CO**; but upon binding to alumina, ν_{CO} is blue-shifted

by 10.5 cm^{-1} and is then 3 cm^{-1} higher than that of **1a-CO**/γ-alumina. Thus, as indicated by the relative binding-induced blue-shifts, the Me$_2$N group of **1d-CO** apparently donates significantly more electron-density to the alumina than does the MeO group of **1b-CO**; this is in accord with results of the catalytic runs which indicated that **1d** binds more strongly to γ-alumina than does **1b**.

Ester substituted complex **1c-CO** shows no significant change in ν$_{CO}$ upon binding to alumina. This may be attributable to a weak interaction with alumina; alternatively, the binding may proceed via a trans-esterification type reaction that does not result in a large change in electron density at the iridium center. Likewise, the binding of (KO-POCOP)Ir(CO) to alumina yields no significant change in ν$_{CO}$; this suggests that the alumina surface exerts an electronic effect similar to that of the K$^+$ counterion in solution. Finally, (^{t}Bu$_2$PO-POCOP)Ir(CO) shows a significant blue shift upon binding to alumina (1934 cm^{-1} to 1945 cm^{-1}). While this large shift is consistent with a strong Lewis acid-base interaction, it may also be noted that the resulting ν$_{CO}$ value is equal to that of alumina-bound (KO-POCOP)Ir(CO). This may suggest that the binding involves cleavage of the ^{t}Bu$_2$P-O bond to give a species very similar to that obtained from the binding of (KO-POCOP)Ir; this is currently under further investigation.

2. Synthesis of a Merrifield resin–supported iridium pincer complex and transfer dehydrogenation activity.

Complex **4**, which contains a phenoxide functionality, was attached to a Merrifield resin through an S$_N$2 reaction with the chlorobenzyl moieties (Scheme 4.4). The Merrifield resin (2% cross-linked, 200-400 mesh, 2.25 mmol Cl/g) was swollen in THF-d$_8$ for 1 h

before the coupling reaction. To prevent the possible dissociation of the ethylene ligand, reactions were conducted under *ca* 1.5 atmosphere of ethylene. Protonation of the phenoxide group of **4** occurred during the reaction though the THF solvent and Merrifield resin were dried before use. With the addition of KH (2–3 equivalents relative to Ir), the conversion to phenol was avoided. When a red THF-d_8 solution of **4** (18 mg, 27 μmol) was treated with a stoichiometric amount of Merrifield resin (12 mg, 27 μmol) (Ir:chlorobenzyl moiety = 1:1) for 15 days at 65 °C, the THF solution was still red indicating incomplete reaction. Analysis of the THF-d_8 solution by ^{1}H NMR spectroscopy indicated that only about 45% of **4** was immobilized on the resin. When **4** was treated with a 7 molar excess of Merrifield resin (Ir:chlorobenzyl moiety = 1:7) in THF, after 7 days at 65 °C the original red solution of complex **4** faded to colorless and the original white resin was now red. Analysis of the THF-d_8 solution by NMR indicated that no **4** remained in solution. The solids were filtered and washed with 3 times of THF. To remove the excess KH in the solid mixture, excess ^{t}BuOH was added to the solid mixture in THF-d_8 under an ethylene atmosphere (^{t}BuOH has proven to be compatible with the parent complex **3**). Reaction of ^{t}BuOH with KH produced KO^{t}Bu and H_2 which then hydrogenated ethylene to form ethane (ethane was observed by ^{1}H NMR spectroscopy). The red resin was filtered, washed 3 times with THF and H_2O (to remove KCl and KO^{t}Bu) under argon and then dried under high vacuum overnight.

Scheme 4.4 Synthesis of a Merrifield resin-supported Ir pincer catalyst
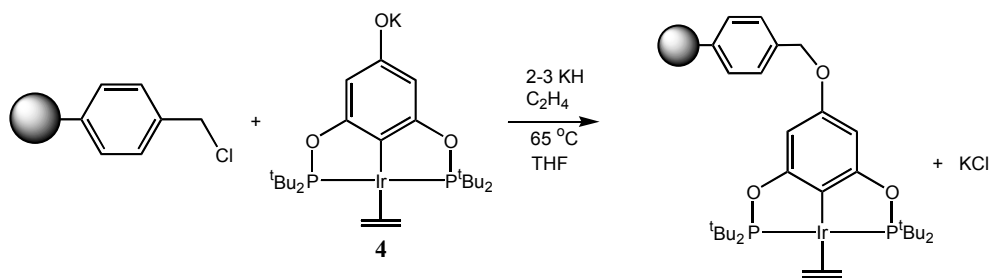
The polymer–supported iridium catalyst shows poor activity and short lifetimes for transfer dehydrogenation of COA by TBE. A system containing 5.4 μmol of the polymer–supported iridium catalyst, 240 μmol of COA (44 equivalents relative to Ir), 240 μmol of TBE, and 0.3 ml of mesitylene-d$_{12}$ was heated at 175 °C under argon in a J-Young NMR tube. After 2 days, 85% conversion of TBE to TBA (37 TONs) was observed by ^{1}H NMR. The supported catalyst was recovered and recharged with same amount of COA, TBE, and mesitylene. Heating the sample for 2 days at 175 °C resulted in 20 % conversion (9 TONs). After the second cycle, the catalyst lost activity completely and the support changed in color from red to black. The decomposition product is unidentified. One possible decomposition pathway could result from reaction of the remaining chlorobenzyl moieties of the Merrifield resin with the Ir center. In light of the low activity of this system, further experiments were not pursued.

3. Covalent attachment of iridium pincer complexes containing pendant alkoxy silane groups to silica and transfer dehydrogenation activity.

Iridium pincer complexes containing either a pendant -Si(OMe)$_3$ group, **15**, or -Si(Me)$_2$OMe group, **16**, were prepared by treating **4** with either

3-iodopropyldimethylmethoxy silane or 3-iodopropyltrimethoxy silane, respectively, in THF under an ethylene atmosphere (Scheme 4.5).

Attachment of **15** to silica was achieved by heating 300 mg silica (Grace XPO 2402) with 16 mg (20 μmol) **15** in toluene-d_8 at 120 °C under an atmosphere of ethylene to prevent ethylene loss from the Ir center.[26] Periodic analysis of the solution by ^{1}H NMR showed that as the concentration of **15** decreased, methanol and ethane formed and increased in concentration. After 2 days, the original red solution became colorless and the silica acquired a pink color. No detectable **15** remained in solution and ca. two equivalents of methanol were produced (relative to Ir) which indicated that on average two methoxy groups of **15** reacted with the silanol groups on silica surface to produce a siloxane linkage and methanol. Excess trimethylsilyldimethylamine was added to cap the remaining silanol groups.[27] This supported catalyst, which contained 63 μmol Ir/g, was isolated, washed with pentane, toluene, and THF three times respectively, and dried under high vacuum.

Scheme 4.5 Syntheses of silica-supported Ir pincer catalysts
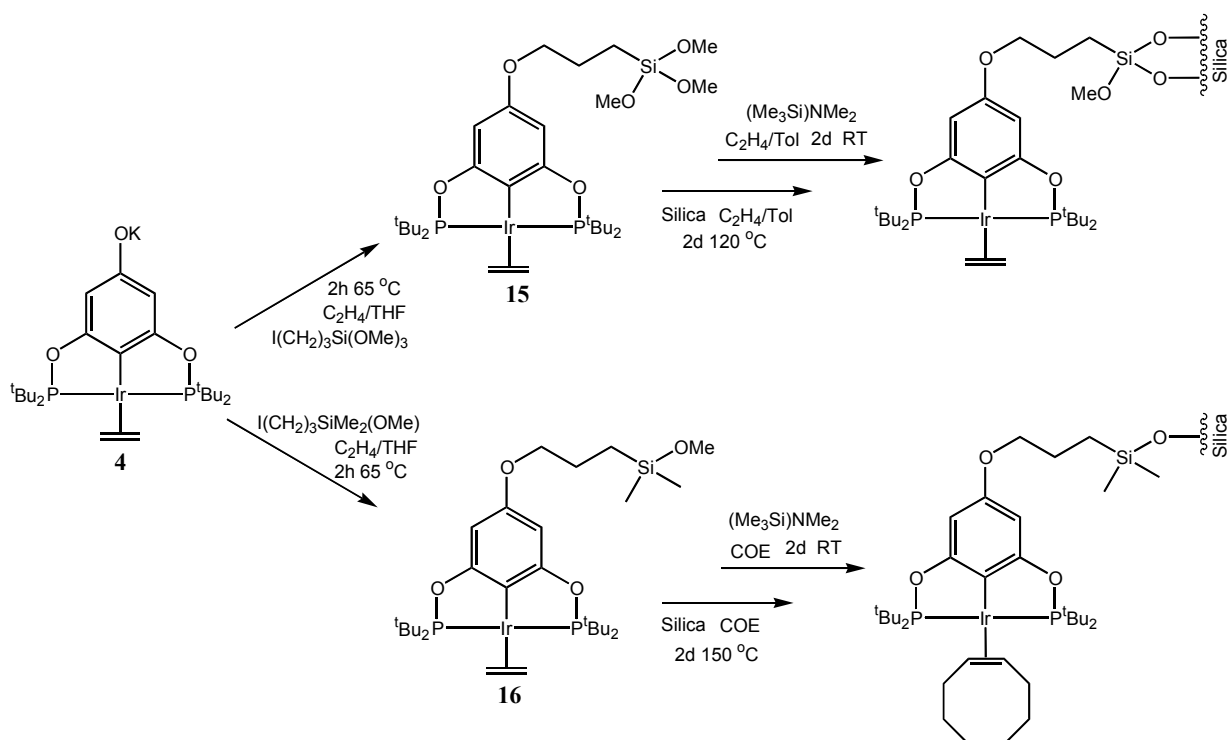
Transfer dehydrogenation of COA/TBE with this silica–supported catalyst (50 mg, 3.15 μmol Ir) showed low activity. Reaction with 750 equivalents of COA and TBE at 200 °C gave only 135 turnovers after 24 h. Heating for longer times resulted in no additional turnovers, indicating the decomposition of the catalyst.

The formation of ethane during the immobilization process indicates that hydrogenation of ethylene occurred. A control experiment was conducted by heating homogeneous complex **3** with 3 equivalents of methanol under ethylene atmosphere in toluene at 120 °C. Iridium carbonyl complex **17** and ethane were formed as observed by NMR spectroscopy. Production of CO from methanol will produce hydrogen necessary for hydrogenation of ethylene (see Scheme 4.6). The formation of ethane during the immobilization process implies conversion of a significant fraction of the Ir ethylene complex to an Ir carbonyl complex which we have shown is inactive for dehydrogenation.

Scheme 4.6 Proposed pathway for formation of Ir carbonyl complex
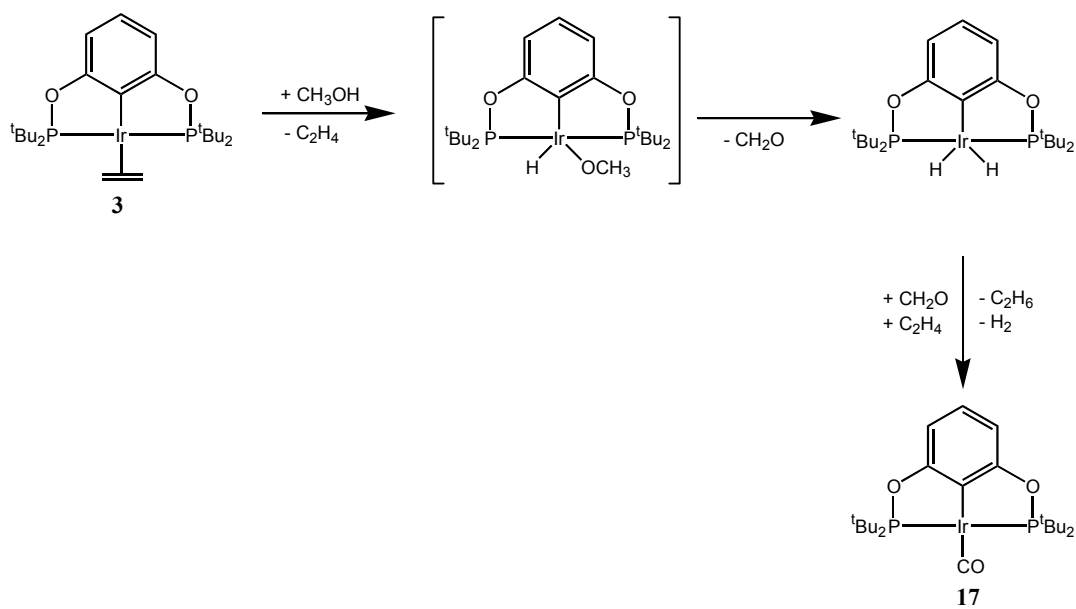
In order to avoid extensive production of an iridium carbonyl complex, reaction conditions and starting material were modified (Scheme 4.5). The monomethoxy complex **16** was employed to reduce the production of methanol to one equivalent and cyclooctene (COE) was used as the reaction solvent to provide a high concentration of alkene to "protect" the Ir center (we assume under these conditions the ethylene complex will be converted to the COE complex). After reaction of **16** with silica for 2 days at 150 °C in COE, the original red solution became colorless and the silica particles were now red. Excess dimethyl(trimethylsilyl)amine was then added to cap the remaining silanol groups on silica. The solid material was collected and washed with pentane, toluene, and THF three times respectively, and was dried under high vacuum. The catalyst made by this modified procedure showed improved activity for transfer dehydrogenation. After 15 h, transfer dehydrogenation of COA/TBE (3000 equivalents of COA and TBE) at 200 °C yielded 790 turnovers. However, heating for longer times did not increase the TON (790 after 39 h), which indicates that this silica–supported catalyst is not stable and loses activity at a relatively fast rate.

Conclusions

Three approaches are reported here for constructing iridium pincer-based transfer dehydrogenation catalysts. POCOP iridium catalysts were covalently attached to a Merrifield resin and to silica. These systems showed low to moderate transfer dehydrogenation activity. A third method was developed in which iridium pincer complexes bearing basic functional groups in the *para*-position bind to γ-alumina through a Lewis acid/Lewis base interaction. These alumina-supported complexes have been characterized by solid state ^{31}P NMR and IR

spectroscopies which yield information concerning the nature of surface binding. The catalysts are thermally robust and recyclable and display high activities with turnover numbers up to 7000 for transfer of hydrogen from cyclooctane to t-butylethylene. ICP-MS experiments with *para*-phosphinite- and *para*-oxide-supported systems show negligible leaching from alumina under reaction conditions. A number of applications can be envisioned for these catalysts including use in alkane metathesis.[11]

Experimental Section

General Considerations. All manipulations were carried out using standard Schlenk, high-vacuum and glovebox techniques. Tetrahydrofuran (THF) was distilled under a nitrogen atmosphere from sodium benzophenone ketyl prior to use. Pentane and toluene were passed through columns of activated alumina. Water was degassed by purging with argon. Benzene, THF-d_8, and toluene-d_8 were dried with 4 Å molecular sieves and degassed by freeze-pump-thaw cycles. Acetone was dried with 3 Å molecular sieves for 7 hours and degassed by freeze-pump-thaw methods. Cyclooctane (COA), 3,3'-dimethyl-1-butene (TBE), *p*-xylene and mesitylene were purchased from Aldrich, dried with $LiAlH_4$ or Na/K, and vacuum transferred into sealed flasks. Complexes **1a**, **1b**, **1c**, **3,**[4] and $[Ir(COD)Cl]_2$[28] were synthesized as previously reported. KH was purchased from Aldrich as 30 wt% in oil and washed with hexanes five times prior to use. $I(CH_2)_3Si(OMe)_3$ and $Cl(CH_2)_3Si(Me)_2(OMe)$ were purchased from Gelest and used as received. $I(CH_2)_3Si(Me)_2(OMe)$ was prepared through the Finkelstein reaction by stirring the mixture of NaI and $Cl(CH_2)_3Si(Me)_2(OMe)$ in dried acetone overnight at 60 ºC. γ-Al_2O_3, acidic γ-Al_2O_3, neutral γ-Al_2O_3, and basic γ-Al_2O_3 were purchased from Strem and calcined as noted below. Merrifield resin (2% cross-linked, 200-

400 mesh, 2.25 mmol Cl/g) was purchased from Aldrich and dried under high vacuum at 40 °C for 20 hours. Silica (Grace XPO 2402) was supplied by DuPont and used as received. All other reagents were purchased from Sigma-Aldrich or Strem and used as received.

NMR spectra were recorded on DRX-400, VANCE-400, Varian-400 and Varian-500 spectrometers. ^{1}H and ^{13}C NMR spectra were referenced to residual protio solvent peaks. [31]P chemical shifts were referenced to an external H_3PO_4 standard. The samples for solid-state ^{31}P MAS NMR spectra were packed into 4 mm zirconia solid-state NMR rotors under an argon atmosphere and sealed with tight-fitting rotor caps. Solid-state ^{31}P MAS NMR spectra were recorded on a Bruker Avance DSX300 spectrometer operating at 121.49 MHz with magic angle spinning (MAS) of 12 kHz. The rotors were spun with N_2 in order to keep the samples air-free. All spectra were recorded at room temperature and are referenced to an aqueous 85% H_3PO_4 solution.

UV-visible spectra were recorded on a Varian Cary-50 spectrophotometer. Infrared spectra were recorded on a Thermo Nicolet 360-FT-IR instrument. Elemental analyses were carried out by Robertson Microlit Laboratories, NJ.

GC analyses (FID detection) were performed according to the following methods:

Method A. Agilent 6850 Series GC System fitted with an Agilent HP-1 column (100% dimethylpolysiloxane, 30m×0.32mm i.d., 0.25 μm film thickness). Typical temperature program: 5 min isothermal at 33 ºC, 20 ºC/ min heat up, 10 min isothermal at 300 ºC. Flow rate: 1 mL/min (He). Split ratio: 400. Inlet temperature: 250 °C. Detector temperature: 250 °C.

Method B. Thermo Electron Corporation Focus GC instrument fitted with an Agilent HP-1 column (100% methyl silicone gum: 100m x 0.25mm ID x 0.5 μm film thickness). Typical

temperature program: Starting temperature 100 ℃, 5 ℃/min up to 230 °C with hold time 10 min, then 5 ℃/min up to ending temperature 250 °C. Flow rate: 1 mL/min (He). Split ratio: 25. Inlet temperature: 230 °C. Detector temperature: 250 °C.

Method C. As in Method B but with typical temperature program: Starting temperature 60 ℃ with hold time 70 min, 10 °C/min up to 200 °C with hold time 10 min, then 10 °C/min up to ending temperature 250 °C.

ICP-MS Analysis was performed on a Varian 820-MS. Sample preparation for ICP-MS: The COA (2 mL × 3) suspension of alumina-supported iridium complex (2.50 μmol Ir on 310 mg of alumina) was filtered through a frit separated double-cell glassware. The COA solution was combined and dried under high vacuum and the residue was digested by a 69.5 % HNO_3 solution at 100 ° C for 2 hours. Finally, the sample was diluted with HNO_3 at 2%. The quantification was carried out using external calibration curves from dilution of a certified ICP-MS Ir standard (Varian). The calibration curves were made as follows: ^{191}Ir and ^{193}Ir: 1000, 500, 250, 50, and 5 ppb. The certified standard was diluted with 2% HNO_3 solution. The quadratic correlation coefficient obtained in the regression line was 0.99997. ^{115}In was used as the internal standard for correcting possible instrumental drifts. Both of ^{191}Ir and ^{193}Ir were analyzed. Five replicates were carried out for each isotope analyzed. The RSD mean obtained was 3.0%.

11
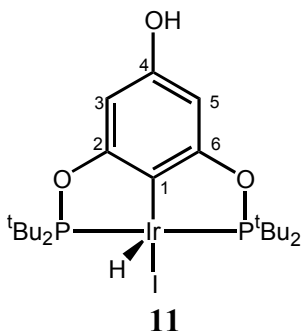
Synthesis of iridium complex {p-OH-C₆H₂-2,6-[OP(t-Bu₂)]₂}IrHI, 11. {p-OMe-C$_6$H$_2$-2,6-[OP(t-Bu$_2$)]$_2$}IrHCl, **2b,** (200 mg, 0.305 mmol) was dissolved in benzene (6 mL) in a flame-dried Schlenk flask and put under a flow of argon. 9-I-BBN (1M in hexanes, 0.63 mL) was added, and the solution was stirred for 2 hours at room temperature. The solvent was removed at room temperature under high vacuum and then the by-product 9-Cl-BBN and the extra 9-I-BBN were removed at 80 °C under high vacuum. A mixture of benzene (3 mL) and degassed water (7 mL) was added into the residue, and the solution was stirred at room temperature overnight. Volatiles were removed under high vacuum. The residue was washed with pentane (3 × 6 mL) and the resulting red solid was dried under high vacuum overnight to give 192 mg (0.262 mmol, 86% yield) of pure product. ^{1}H NMR (400 MHz, 23 °C, CDCl$_3$): δ -42.11 (t, $^2J_{\text{P-H}}$ = 13.0 Hz, 1H, IrH), 1.36 (virtual triplet, apparent J = 7.2 Hz, 36H, 4 × tBu), 4.49 (s, 1H, OH), 6.19 (s, 2H, 3- and 5-H). ^{31}P{^{1}H} NMR (162 MHz, 23 °C, CDCl$_3$): δ 181.3. ^{13}C{^{1}H} NMR (100.6 MHz, 23 °C, CDCl$_3$): δ 28.0 (CH$_3$, virtual triplet, apparent J = 2.8 Hz, P(tBu)$_2$), 28.1 (CH$_3$, virtual triplet, apparent J = 2.6 Hz, P(tBu)$_2$), 40.1 (C$_q$, virtual triplet, apparent J = 12.6 Hz, P(tBu)$_2$), 43.4 (C$_q$, virtual triplet, apparent J = 11.5 Hz, 2 × P(tBu)$_2$), 93.3 (CH, virtual triplet, apparent J = 6.0 Hz, C3 and C5), 111.7 (C$_q$, m br, C1), 155.3 (C$_q$, s, C4), 166.9 (C$_q$, virtual triplet, apparent J = 6.0 Hz, C2 and C6). Elemental analysis calculated for C$_{22}$H$_{40}$IO$_3$P$_2$Ir (734.11): C, 36.02; H, 5.50. Found: C, 36.87; H, 5.31.

4
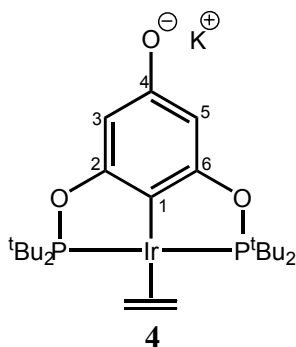
Synthesis of iridium complex {*p*-OK-C$_6$H$_2$-2,6-[OP(*t*-Bu$_2$)]$_2$}Ir(C$_2$H$_4$), 4. Complex **11** (160 mg, 0.218 mmol) and KH (22 mg, 0.548 mmol) were weighed into a flame-dried Kontes flask under an argon atmosphere. THF (5 mL) was added to the flask via syringe and the resulting suspension was stirred for 2 hours at room temperature. The solution was filtered into a Schlenk flask through a 0.2 μm pore size syringe filter (Nalgene 199-2020). Ethylene was bubbled through the solution for 2 hours. Volatiles were removed under high vacuum, and the red solid was dried under high vacuum for 4 hours to give 105 mg (0.156 mmol, 72% yield) of pure product. ^{1}H NMR (400 MHz, 23 °C, THF-d$_8$): δ 1.26 (virtual triplet, apparent J = 6.2 Hz, 36H, 4 × *t*Bu), 2.64 (s, 4H, C$_2$*H*$_4$), 5.67 (s, 2H, 3- and 5-H). ^{31}P{^{1}H} NMR (162 MHz, 23 °C, THF-d8): δ 170.3 (s). ^{13}C{^{1}H} NMR (100.6 MHz, 23 °C, THF-d$_8$): δ 26.5 (CH$_3$, m, 2 × P(*t*Bu)$_2$), 28.6 (s, C$_2$H$_4$), 38.5 (C$_q$, apparent J = 11.1 Hz, 2 × P(*t*Bu)$_2$), 91.1 (CH, virtual triplet, apparent J = 5.5 Hz, C3 and C5), 134.5 (C$_q$, m, C1), 168.8 (C$_q$, virtual triplet, apparent J = 7.0 Hz, C2 and C6), 174.4 (C$_q$, s, C4). Elemental analysis calculated for C$_{24}$H$_{42}$O$_3$P$_2$IrK (672.19): C, 42.90; H, 6.30. Found: C, 42.66; H, 6.31.

Synthesis of phenyl di-*tert*-butylphosphinite. A solution of 10.63 mmol of phenol (1.0 g) in 25 mL of THF was slowly added via syringe to a suspension of 10.8 mmol of NaH (259 mg) in 25 mL of THF under a flow of argon (caution: hydrogen evolution). The mixture was heated to reflux for 2 hours, di-*tert*-butylchlorophosphine (10.63 mmol, 2.0 g) was then added via syringe, and the mixture was refluxed for an additional 8 hours. After evaporation of the solvent under high vacuum, the residue was extracted with 3 × 40 mL of pentane, and the extract was cannula transferred and filtered through a pad of Celite. After removal of pentane under high vacuum, the flask was heated to 55 °C for 3 hours under high vacuum to

remove residual amounts of di-*tert*-butylchlorophosphine. Pure product as clear oil was collected in 92 % yield (9.8 mmol, 2.334 g). ^{1}H NMR (400 MHz, 23 °C, CDCl$_3$): δ 1.13 (d, $^3J_{\text{P-H}}$ = 11.6 Hz, 18H, 2 × *t*Bu), 6.90 (t, $^3J_{\text{H-H}}$ = 7.2 Hz, 1H, 4-H), 7.11 (d, $^3J_{\text{H-H}}$ = 7.6 Hz, 2H, 2- and 6-H), 7.20 (m, 2H, 3- and 5-H). ^{31}P{^{1}H} NMR (162 MHz, 23 °C, CDCl$_3$): δ 153.12 (s). ^{13}C{^{1}H} NMR (100.6 MHz, 23 °C, CDCl$_3$): δ 27.4 (CH$_3$, d, $^2J_{\text{P-C}}$ = 15.1 Hz, P(*t*Bu)$_2$), 35.6 (C$_q$, d, $J_{\text{P-C}}$ = 25.1 Hz, P(*t*Bu)$_2$), 118.4 (CH, d, $^3J_{\text{P-C}}$ = 10.1 Hz, C2 and C6), 121.3 (CH, s, C4), 129.3 (CH, s, C3 and C5), 159.9 (C$_q$, d, $^2J_{\text{P-C}}$ = 9.0 Hz, C1).

Synthesis of pincer ligand 1,3,5-tri(di-*tert*-butylphosphinite)benzene, **13**. A solution of 10 mmol of 1,3,5-trihydroxybenzene (1.261 g) in 25 mL of THF was slowly added via syringe to a suspension of 31 mmol of NaH (782 mg) in 25 mL of THF under a flow of argon (caution: hydrogen evolution). The mixture was heated to reflux for 2 hours, di-*tert*-butylchlorophosphine (31.0 mmol, 5.834 g) was then added via syringe, and the mixture was refluxed for additional 2 hours. After evaporation of the solvent under high vacuum, the residue was extracted with 3 × 40 mL of pentane, and the extract was cannula transferred and filtered through a pad of Celite. After removal of pentane under high vacuum, the flask was heated to 55 °C for 3 hours under high vacuum to remove residual amounts of di-*tert*-butylchlorophosphine. Pure product as clear waxy solid was collected in 89 % yield (8.9 mmol, 4.972 g). ^{1}H NMR (400 MHz, 23 °C, CDCl$_3$): δ 1.13 (d, $^3J_{\text{P-H}}$ = 11.6 Hz, 54H, 6 × *t*Bu), 6.58 (m, 3H, 2-, 4-, and 6-H). ^{31}P{^{1}H} NMR (162 MHz, 23 °C, CDCl$_3$): δ 151.22 (s). ^{13}C{^{1}H} NMR (100.6 MHz, 23 °C, CDCl$_3$): δ 27.4 (CH$_3$, d, $^2J_{\text{P-C}}$ = 16.1 Hz, 3 × P(*t*Bu)$_2$), 35.6 (C$_q$, d, $J_{\text{P-C}}$ = 26.1 Hz, 3 × P(*t*Bu)$_2$), 100.0 (CH, t, $^3J_{\text{P-C}}$ = 10.6 Hz, C2, C4, and C6), 161.0 (C$_q$, d, $^2J_{\text{P-C}}$ = 9.0 Hz, C1, C3, and C5).

14
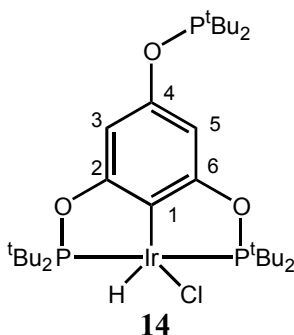
Synthesis of iridium complex {p-OP(t-Bu$_2$)-C$_6$H$_2$-2,6-[OP(t-Bu$_2$)]$_2$}IrHCl, 14. A Schlenk flask was charged with 1.1 mmol of **13** and 0.5 mmol of [(COD)IrCl]$_2$ and put under a flow of argon. Toluene (5 mL) was added via syringe, and the solution was stirred in an oil bath for 15 hours at 150 °C. The reaction mixture was cooled to room temperature. Volatiles were removed under high vacuum and the residue was extracted with 10 mL of pentane under ultrasound (10 min). After filtration (no inert gas required), the solid was washed with 3 × 10 mL of pentane and dried under high vacuum overnight to yield 645 mg (0.82 mmol, 82%) of pure red purple product. ^{1}H NMR (400 MHz, 23 °C, CDCl$_3$): δ -41.91 (t, $^2J_{P-H}$ = 13.2 Hz, 1H, IrH), 1.16 (d, $^3J_{P-H}$ = 12 Hz, 18H, 2 × tBu), 1.33 (m, 36H, 4 × tBu), 6.43 (s, 2H, 3- and 5-H). ^{31}P{^{1}H} NMR (162 MHz, 23 °C, CDCl$_3$): δ 154.2 (s, uncoordinated P(tBu)$_2$), 175.8 (s, coordinated 2 × P(tBu)$_2$). ^{13}C{^{1}H} NMR (100.6 MHz, 23 °C, CDCl$_3$): δ 27.5 (CH$_3$, d, $^2J_{P-C}$ = 16.1 Hz, uncoordinated P(tBu)$_2$), 27.6 (CH$_3$, br, coordinated P(tBu)$_2$), 27.8 (CH$_3$, br, coordinated P(tBu)$_2$), 35.6 (C$_q$, d, J_{P-C} = 25.1 Hz, uncoordinated P(tBu)$_2$), 39.5 (C$_q$, virtual triplet, apparent J = 12.6 Hz, coordinated P(tBu)$_2$), 43.1 (C$_q$, virtual triplet, apparent J = 11.1 Hz, coordinated P(tBu)$_2$), 96.2 (CH, dvt, apparent J = 4.0 and 9.0 Hz, C3 and C5), 109.3 (C$_q$, m br, C1), 159.4 (C$_q$, m br, C4), 166.9 (C$_q$, virtual triplet, apparent J = 5.5, C2 and C6).

Elemental analysis calculated for $C_{30}H_{57}O_3P_3ClIr$ (786.28): C, 45.82; H, 7.31. Found: C, 45.58; H, 7.04.

5
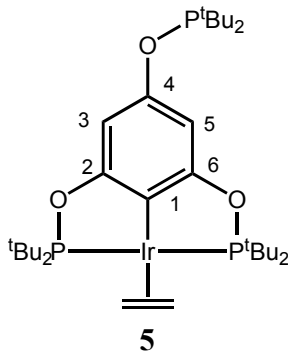
Synthesis of iridium complex {*p*-OP(*t*-Bu₂)-C₆H₂-2,6-[OP(*t*-Bu₂)]₂}Ir(C₂H₄), 5. Complex **14** (500 mg, 0.636 mmol) and NaO*t*Bu (64 mg, 0.666 mmol) were weighed into a Schlenk flask and put under a flow of argon. Toluene (20 mL) was added to the flask via syringe and ethylene was bubbled through the solution for 2 hours. After evaporation of the solvent under high vacuum, the residue was extracted with 3 × 20 mL of pentane, and the extract was cannula transferred and filtered through a pad of Celite. Pentane was removed under high vacuum, and the red brown solid was dried under high vacuum overnight to give 371 mg (0.477 mmol, 75% yield) of pure product. ^{1}H NMR (400 MHz, 23 °C, C_6D_6): δ 1.10 (d, $^{3}J_{P-H}$ = 8.0 Hz, 18H, 2 × *t*Bu), 1.23 (virtual triplet, apparent J = 6.8 Hz, 36H, 4 × *t*Bu), 3.11 (s, 4H, C_2H_4), 7.06 (s, 2H, 3- and 5-H). ^{31}P{^{1}H} NMR (162 MHz, 23 °C, C_6D_6): δ 150.8 (s, uncoordinated P(*t*Bu)₂), 181.1 (s, coordinated 2 × P(*t*Bu)₂). ^{13}C{^{1}H} NMR (100.6 MHz, 23 °C, C_6D_6): δ 27.6 (CH₃, d, $^{2}J_{P-C}$ = 15.8 Hz, uncoordinated P(*t*Bu)₂), 28.7 (CH₃, virtual triplet, apparent J = 3.0 Hz, coordinated 2 × P(*t*Bu)₂), 35.6 (C_q, d, J_{P-C} = 26.8 Hz, uncoordinated P(*t*Bu)₂), 35.8 (s, C_2H_4), 41.5 (C_q, virtual triplet, apparent J = 11.0 Hz, coordinated 2 × P(*t*Bu)₂), 94.7 (CH, dvt, apparent J = 5.5 and 11.1 Hz, C3 and C5), 139.7 (C_q, m, C1), 161.5

(C_q, d, J_{P-C} = 10.1 Hz, C4) 168.8 (C_q, virtual triplet, apparent J = 8.0, C2 and C6). Elemental analysis calculated for $C_{32}H_{60}O_3P_3Ir$ (778.34): C, 49.40; H, 7.77. Found: C, 49.60; H, 7.60.

Calcination of alumina. γ-Al_2O_3, acidic γ-Al_2O_3, neutral γ-Al_2O_3, and basic γ-Al_2O_3 were calcined at 550 °C for 2 hours under a flow of O_2 and cooled to 135 °C under O_2, then cooled to room temperature under high vacuum. The solid were brought into the drybox under high vacuum and stored under argon.

Synthesis of Na₂O-modified alumina. In a vial, 235 mg (2.22 mmol) of Na_2CO_3 or 178 mg (4.45 mmol) of NaOH was dissolved in 10 mL of distilled water. The solution was added to 5 g of γ-Al_2O_3. The suspension was stirred at room temperature until all of the water was absorbed by the alumina. The solid was dried in a 120 °C oven overnight, then calcined at 550 °C for 17 hours under a flow of O_2 and cooled to 135 °C under O_2, and then cooled to room temperature under high vacuum. The solid was brought into the drybox under high vacuum and stored under argon.

Synthesis of alumina-supported iridium pincer complexes.

The alumina-supported pincer Ir ethylene complexes can be prepared either in situ or by using pentane as solvent.

Method A (In situ): Ir complex (1.34 – 2.50 μmol) was dissolved in alkane (1 – 3 mL) (cyclooctane or linear alkanes). The solution was added to 280 – 310 mg (2.74 – 3.04 mmol) of γ-Al_2O_3. The suspension was stirred at room temperature. After 10 – 20 min, the original red solution turned colorless and the alumina acquired a rust-red color. The suspension continued to stir for 2 – 4 hours.

Method B (Pentane): Ir complex (1.34 – 2.50 μmol) was dissolved in pentane (1.5 mL). The solution was added to 280 – 310 mg (2.74 – 3.04 mmol) of γ-Al_2O_3. The suspension was

stirred at room temperature for 2 – 4 hours. The original red solution turned colorless and the alimina acquired a rust-red color. The solvent was removed by syringe in the glovebox. The solid was washed with pentane three times. Pentane was evaporated in the glovebox (no vacuum applied) and the rust-red solid was collected.

Synthesis of alumina-supported 13 and phenyl di-*tert*-butylphosphinite. Compound **13** (26 μmol), or phenyl di-*tert*-butylphosphinite, was dissolved in pentane (1.5 mL). The solution was added to 200 mg (1.96 mmol) of γ-Al$_2$O$_3$. The suspension was stirred at room temperature for 2 – 4 hours. The solvent was removed by syringe in the glovebox. The solid was washed with pentane three times. Volatile was evaporated in the glovebox and the white solid was collected.

Hydrogen transfer from cyclooctane (COA) to 3,3-dimethyl-1-butene (TBE) catalyzed by γ-Al$_2$O$_3$-supported iridium pincer complexes. Complexes **1a-d**: the iridium complex (5 μmol) was dissolved in COA (1mL) in a Kontes flask. γ-Al$_2$O$_3$ (100 mg, 0.98 mmol) was added to the solution and the suspension was stirred at room temperature for 20 min. TBE (95%, 70 μL, 0.54 mmol) was added to the suspension. The flask was sealed tightly with a Teflon plug under an argon atmosphere, and the suspension was stirred in an oil bath at 125 °C. Periodically, the flask was removed from the bath and cooled in an ice bath. An aliquot was removed from the flask, and analyzed by GC (method **B**). Turnover numbers were calculated for each aliquot using mesitylene as a GC standard. Complexes **3-5**: the iridium complex (1.34 – 2.50 μmol) was dissolved in COA (0.842 – 1.655 g, 7.50 – 14.74 mmol) in a Kontes flask. γ-Al$_2$O$_3$ (280 – 310 mg, 2.74 – 3.04 mmol) was added to the solution and the suspension was stirred at room temperature for 2 – 4 hours. TBE (95%, 0.664 – 1.306 g, 7.50 – 14.74 mmol) was added to the suspension. The procedure was otherwise as described

above for complexes 1a-d but reactions were conducted at 200 or 240 °C and the solution was analyzed by GC using method **A**. Turnover numbers were calculated for each aliquot. Results are summarized in the text.

The heterogeneous catalysts can be recycled. After each cycle, the solution was syringed out and the solid was washed 2-3 times with COA. Fresh COA and TBE were then added.

Hydrogen transfer from COA or *n*-octane to TBE catalyzed by solution-phase iridium pincer complexes. A flask was charged with iridium pincer complex **1a**, **1b**, **1c** or **1d** (5 µmol), COA or *n*-octane (1mL), and TBE (95%, 70 µL, 0.54 mmol). Respective values in the case of complex **4** or **5**: iridium complex, 1.34 – 2.50 *µ*mol; COA, 0.842 – 1.655 g, 7.50 – 14.74 mmol; TBE (95%), 0.664 – 1.306 g, 7.50 – 14.74 mmol. The flask was sealed tightly with a Teflon plug under an argon atmosphere, and the solution was stirred in an oil bath at 125 °C (complexes **1a-d**) or 200 °C (complexes **4** and **5**). Periodically, the flask was removed from the bath and cooled in an ice bath. An aliquot was removed from the flask, and analyzed by GC (method **A**, complexes **1a-d**; method **B**, complexes **1a-d**). Turnover numbers were calculated for each aliquot. Recycle of the homogeneous catalysts was obtained by evaporation of under high vacuum and addition of fresh COA and TBE. Results are summarized in the text.

Isomerization of TBE or 1-octene by alumina (control experiments). A flask was charged with 280–310 mg of γ-Al$_2$O$_3$ or Al$_2$O$_3$/Na$_2$O, 0.842 g of COA (7.50 mmol), and 0.664 g of TBE (7.50 mmol). In the case of 1-octene, a flask was charged with 100 mg of γ-Al$_2$O$_3$, COA (1mL), and 1-octene (4.55 µL, 29 mmol or 67 µL, 427 mmol). The flask was sealed tightly with a Teflon plug under an argon atmosphere, and the solution was stirred in an oil bath at

125 °C (1-octene) or 200 ° (TBE). Periodically, the flask was removed from the bath and cooled in an ice bath. An aliquot was removed from the flask, and analyzed by GC.

Synthesis of a Merrifield-resin-supported iridium pincer complex. The Merrifield resin (12 mg, 27 μmol chlorobenzyl moiety; or 84 mg, 189 μmol chlorobenzyl moiety when Merrifield resin was used in excess) was swollen in THF-d$_8$ (0.5 mL) for 1 to 2 hours in a thick walled J. Young tube in the glovebox. Complex **4** (18 mg, 26.8 μmol) and KH (3 mg, 75 μmol) were added to the tube. The THF-d$_8$ solution was degassed by freeze-pump-thaw cycles. The tube was refilled with ethylene gas at -78 °C. The suspension was heated at 65˚C. The solution was monitored by ^{1}H and ^{31}P{^{1}H} NMR spectroscopy periodically. For the sample with Ir:chlorobenzyl moiety ratios of 1:1, after 15 days, about 45% of **4** was immobilized on the resin (determined by NMR). For the sample with a 7 molar excess of Merrifield resin, after 7 days, no **4** was observed in the solution. The solid was collected by filtration and washed with 3 times of THF (0.5 mL each) in the golvebox. The solid was reloaded into a thick walled J. Young tube and THF-d$_8$ (0.5 mL) was added to the tube. Degassed ^{t}BuOH (ca 0.2 mL) was added into the J. Young tube by vacuum transfer method (caution, hydrogen evolution). The red resin was filtered, washed with 3 times of THF and H$_2$O (0.5 mL each) under an argon atmosphere, and then dried under high vacuum overnight.

Hydrogen transfer from COA to TBE catalyzed by Merrifield-resin-supported iridium pincer complex. A J. Young tube was charged with 8 mg of the Merrifield resin supported iridium catalyst (5.4 μmol of Ir), 32 μL of COA (240 μmol), 33 μL of TBE (240 μmol), and 0.3 ml of mesitylene-d$_{12}$. The tube was sealed tightly under an argon atmosphere, and then heated in an oil bath at 175 °C. The sample was analyzed by NMR spectroscopy periodically.

After each cycle, the catalyst was filtered, washed with pentane and dried under high vacuum. Fresh COA, TBE and mesitylene-d_{12} were then added. Results are summarized in the text.

Synthesis of dimethyl 5-dimethylaminoisophthalate (7). The compound was prepared via the literature procedure for reductive alkylation of aromatic amines. Sodium cyanoborohydride (5 g, 75.6 mmol) was added to a stirred solution of 5 g (23.4 mmol) of dimethyl 5-aminoisophthalate (**6**) (98%) and 20 mL (269 mmol) of 37% aqueous formaldehyde in 150 mL acetonitrile. This was followed by slow addition (over a period of 20 min) of 3 mL of glacial acetic acid to adjust the pH at 5-6. The resulting solution was stirred at room temperature for 8 hr and the solvent was removed under reduced pressure. The wet-solid obtained thereby was washed thoroughly with distilled water and air-dried to give 5.39 g of **7** as a light yellowish-white solid in near quantitative yield (97%). ^{1}H NMR (CDCl$_3$): δ 8.01 (s, 1H, *Ar*), 7.56 (s, 2H, *Ar*), 3.94 (s, 6H, CO$_2$C*H$_3$*), 3.05 (s, 6H, (C*H$_3$*)$_2$N).

Synthesis of 5-dimethylamino-1,3-benzenedimethanol (8). To a stirred suspension of 2.69 g (67.4 mmol) of lithium aluminum hydride (95%) in THF (50 mL) at 0 °C under argon atmosphere was slowly added a THF (100 mL) solution of **7** (5 g, 21.1 mmol). After the addition was complete, the resultant suspension was refluxed for 18 h, diluted with 100 mL tetrahydrofuran and cooled to 0 °C. Excess LiAlH$_4$ was quenched by slow addition of a saturated sodium sulfate solution followed by distilled water and the suspension was stirred at 0 °C - 5 °C for 1 h (until the gray color of LiAlH$_4$ disappeared completely). The suspension was filtered through a pad of anhydrous magnesium sulfate and subsequently washed with ethyl acetate (3 × 50 mL). The combined filtrates were concentrated under reduced pressure to give a clear colorless oil that crystallized upon standing. The product **8** was recrystallized from THF/heptane system as a white powder (3.49 g, 91% yield). ^{1}H

NMR (DMSO-d$_6$): δ 6.58 (s, 1H, *Ar*), 6.56 (s, 2H, *Ar*), 5.03 (t, 2H, O*H*), 4.41 (d, 4H, C*H$_2$*), 2.87 (s, 6H, (C*H$_3$*)$_2$N).

Synthesis of 1,3-bis(bromomethyl)-5-dimethylaminobenzene (9). PBr$_3$ (10.4 mL, 110 mmol) was added dropwise over a 30-minute period to a stirred solution of **8** (5.0 g, 27.6 mmol) in 140 mL of anhydrous acetonitrile at 0 °C under argon atmosphere. The solution was stirred at room temperature for 2 h and then heated to 70 °C for an additional 4 h. The reaction was quenched by pouring the solution over ice followed by slow addition of a saturated NaHCO$_3$ solution to adjust pH to ~ 7. The solution was filtered and the precipitate product was dissolved in acetonitrile. Pure **9** was recrystallized out from acetonitrile/water system to give 6.52 g of white powder in 77% yield. ^{1}H NMR (CDCl3): δ 6.78 (s, 1H, *Ar*), 6.66 (s, 2H, *Ar*), 4.45 (s, 4H, C*H$_2$*), 2.99 (s, 6H, (C*H$_3$*)$_2$N).

Synthesis of 1,3-bis[di(t-butyl)phosphinomethyl]-5-dimethylaminobenzene (Me$_2$N-PCP-H) (10). Synthesis of this ligand and its corresponding iridium hydrido chloride were based on reported syntheses by Shaw for the parent ligand.[16] To 1.0 g of **9** (3.25 mmol) in 20 mL of degassed acetone was added 1.36 mL (7.2 mmol) of di-tert-butylphosphine (98%) (Strem) at room temperature. The mixture was heated under reflux with stirring for 24 h under an argon atmosphere, and the solvent was removed *in vacuo*. The solid was dissolved in degassed deionized water (15 mL) and treated with a solution of potassium carbonate (2.7 g, 19.5 mmol) in degassed deionized water (10 mL). The diphosphine ligand was extracted with degassed *n*-hexane (3 x 20 mL) and the solvent was evaporated under vacuum, giving 1.03 g (72%) of the ligand **10** as a white solid. ^{31}P{^{1}H} NMR (C$_6$D$_6$): δ 31.03 (s). ^{1}H NMR (C$_6$D$_6$): δ 6.98 (s, 1H, *Ar*), 6.79 (s, 2H, *Ar*), 2.87 (d, $^2J_{H-P}$ = 2.4 Hz, 4H, C*H$_2$*), 2.78 (s, 6H, (C*H$_3$*)$_2$N), 1.18 (d, $^3J_{H-P}$ = 10.8 Hz, 36H, C(C*H$_3$*)$_3$).

Synthesis of (Me₂N-PCP)IrHCl. To 0.51 g of **10** (1.16 mmol) in 30 mL of toluene was added 0.38 g of [Ir(COD)Cl]₂ (0.57 mmol) at room temperature and stirred for 30 min under a hydrogen atmosphere. (*note*: the solution changes color from yellow to deep red under the hydrogen atmosphere at room temperature). This mixture was refluxed for three days under the hydrogen with stirring, and the solvent was removed in vacuo giving 0.78 g of **(Me₂N-PCP)IrHCl** as dark-red solid in 94% yield. $^{31}P\{^1H\}$ NMR (C₆D₆): δ 67.03 (s). ^1H NMR (C₆D₆): δ 6.65 (s, 2H, *Ar*), 3.16 (dvt, the left part of ABX₂, $^2J_{H-H}$ = 17.7 Hz, J_{H-P} = 3.9 Hz, 2H, C*H₂*), 3.06 (dvt, the right part of ABX₂, $^2J_{H-H}$ = 17.7 Hz, apparent J = 3.9 Hz, 2H, C*H₂*), 2.77 (s, 6H, (C*H₃*)₂N), 1.34 (virtual triplet, apparent J = 6.9 Hz, 18H, C(C*H₃*)₃), 1.29 (virtual triplet, apparent J = 6.9 Hz, 18H, C(C*H₃*)₃), - 43.11 (t, $^2J_{H-P}$ = 12.8 Hz, 1H, Ir-*H*).

Synthesis of (Me₂N-PCP)IrH₄ and (Me₂N-PCP)IrH₂ (1d). A stream of hydrogen was passed through a solution of 0.73 g of **(Me₂N-PCP)IrHCl** (1.1 mmol) in 300 mL anhydrous pentane for about 30 min. This was followed by a slow dropwise addition of 1.1 mL of 1 M LiBEt₃H in THF (1.1 mmol) to this solution with continuous stirring under hydrogen atmosphere. The solution turned nearly colorless and some white precipitate was formed at the bottom of the flask. After the addition of LiBEt₃H was complete, stirring was continued for 1 h and finally the solution was filtered under argon atmosphere. (*note*: on changing from H₂ to argon atmosphere the solution rapidly turned deep red). The solvent was removed *in vacuo,* giving 0.55 g (79%) of **1d** as reddish brown crystals containing ca. 10% of (Me₂N-PCP)IrH₄. (All the PCP-Ir tetrahydrides are quickly converted to the corresponding dihydrides under catalytic conditions; accordingly, for catalytic runs, the dihydrides are frequently used containing varying amounts of tetrahydride.) NMR data for (Me₂N-PCP)IrH₄: $^{31}P\{^1H\}$ NMR (C₆D₆): δ 72.42 (s). 1H NMR (C₆D₆): δ 6.73 (s, 2H, *Ar*), 3.32 (virtual triplet,

126

apparent J = 3.9 Hz, 4H, CH_2), 2.79 (s, 6H, (CH_3)$_2$N), 1.24 (virtual triplet, apparent J = 6.9

Hz, 36H, C(CH_3)$_3$), -9.09 (t, $^2J_{\text{H-P}}$ = 9.9 Hz, 4H, IrH_4). NMR data for **1d**: ^{31}P{^{1}H} NMR

(C$_6$D$_6$): δ 85.48 (s). 1H NMR (C$_6$D$_6$): δ 6.84 (s, 2H, *Ar*), 3.62 (virtual triplet, apparent J = 3.6

Hz, 4H, CH_2), 2.76 (s, 6H, (CH_3)$_2$N), 1.33 (virtual triplet, apparent J = 6.9 Hz, 36H,

C(CH_3)$_3$), -19.99 (t, $^2J_{\text{H-P}}$ = 8.7 Hz, 2H, IrH_2).

15
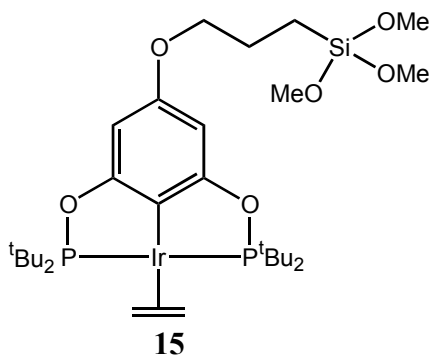
Synthesis of {*p*-O(CH$_2$)$_3$Si(OMe)$_3$-C$_6$H$_2$-2,6-[OP(*t*-Bu$_2$)]$_2$}Ir(C$_2$H$_4$) (15). Complex **4** (80

mg, 0.119 mmol), I(CH$_2$)$_3$Si(OMe)$_3$ (138 mg, 0.476 mmol), and THF (10 mL) were added to

a Kontes flask. The THF solution was degassed by freeze-pump-thaw cycles. The flask was

refilled with ethylene gas at -78 °C. The mixture was heated at 65 °C for 2 hours. NaOMe

(22 mg, 0.407 mmol) was then added to the Kontes flask in the glovebox and the flask was

refilled with ethylene gas at -78 °C. The mixture was stirred at RT for 2 days. NaOMe

reacted with the excess of I(CH$_2$)$_3$Si(OMe)$_3$ (80 °C/2 mm) to produce NaI and

CH$_2$=CHCH$_2$Si(OMe)$_3$ which is relatively more volatile (bp, 146 °C/760 mm) and easier to

remove. Volatiles were then removed under high vacuum. The residue was extracted with 3

× 10 mL of pentane, and the extract was filtered through a 0.2 μm pore size syringe filter

(Nalgene 199-2020) into a Schlenk flask. Removal of the solvent under high vacuum yielded

69 mg (0.086 mmol, 73% yield) of red waxy solid which contained ca. 95% of **11** by NMR

and was used without further purification in the next step. ^{1}H NMR (400 MHz, 23 °C, C$_6$D$_6$): δ 0.75 (m, 2H, CH_2Si), 1.27 (virtual triplet, apparent J = 6.6 Hz, 36H, 4 × tBu), 1.88 (m, 2H, OCH$_2$CH_2), 3.14 (t, $^3J_{P\text{-}H}$ = 2.7 Hz, 4H, C$_2$H$_4$), 3.40, (s, 9H, 3 × OMe), 3.71 (t, $^2J_{H\text{-}H}$ = 6.5 Hz, 2H, OCH_2CH$_2$), 6.65 (s, 2H, 3- and 5-H). ^{31}P{^{1}H} NMR (162 MHz, 23 °C, C$_6$D$_6$): δ 181.4.

16
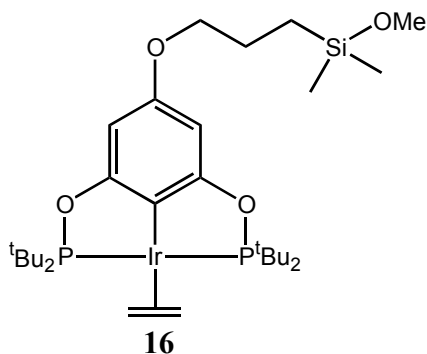
Synthesis of {p-O(CH$_2$)$_3$Si(Me)$_2$(OMe)-C$_6$H$_2$-2,6-[OP(t-Bu$_2$)]$_2$}Ir(C$_2$H$_4$) (16). The same synthetic procedure used for **15** was used except that I(CH$_2$)$_3$Si(OMe)$_3$ was replaced by I(CH$_2$)$_3$Si(Me)$_2$(OMe) (123 mg, 0.476 mmol), giving 63 mg (0.082 mmol, 69% yield) of red waxy solid which contained ca. 95% of **12** by NMR and was used without further purification in the next step. ^{1}H NMR (400 MHz, 23 °C, C$_6$D$_6$): δ 0.09 (s, 6H, Si(CH_3)$_2$), 0.56 (m, 2H, CH_2Si), 1.27 (virtual triplet, apparent J = 6.4 Hz, 36H, 4 × tBu), 1.69 (m, 2H, OCH$_2$CH_2), 3.14 (t, $^3J_{P\text{-}H}$ = 2.7 Hz, 4H, C$_2$H$_4$), 3.17, (s, 3H, OMe), 3.71 (t, $^2J_{H\text{-}H}$ = 6.4 Hz, 2H, OCH_2CH$_2$), 6.68 (s, 2H, 3- and 5-H). ^{31}P{^{1}H} NMR (162 MHz, 23 °C, C$_6$D$_6$): δ 181.5.

Synthesis of silica supported-iridium pincer complex 15. Complex **15** (50 mg, 0.062 mmol), silica (1.5 g), and toluene (10 mL) were added to a Kontes flask. The toluene suspension was degassed by freeze-pump-thaw cycles. The flask was refilled with ethylene gas at -78 °C and the suspension was stirred at 120 °C for 2 days. The flask was cooled to

room temperature and ethylene gas was removed by freeze-pump-thaw cycles. Excess trimethylsilyldimethylamine (3 mL, 18.7 mmol) was added in the glovebox and the flask was degassed and refilled with ethylene gas at -78 °C. The suspension was stirred at room temperature for 2 days. This supported catalyst was filtered under argon, and washed with pentane, toluene and THF three times (5 ml each), respectively. The orange solid was dried under high vacuum overnight to give 1.46 g of product.

Synthesis of silica supported-iridium pincer complex 16. Complex **16** (48 mg, 0.062 mmol), silica (1.05 g), and COE (5 mL) were added to a Kontes flask. The COE suspension was stirred at 150 °C for 2 days. The flask was cooled to room temperature and excess trimethylsilyldimethylamine (3 mL, 18.7 mmol) was added in the glovebox. The suspension was stirred at room temperature for 2 days. This supported catalyst was filtered under argon, and washed with pentane, toluene and THF three times (5 ml each), respectively. The light orange solid was dried under high vacuum overnight to give 0.86 g of product.

Hydrogen transfer from COA to TBE, catalyzed by silica-supported iridium pincer complexes. The silica-supported complex **11** or **12** (2.0 – 3.15 μmol), COA (0.265 – 0.674 g, 2.36 – 6.0 mmol), and TBE (95%, 0.209 – 0.532 g, 2.36 – 6.0 mmol) were added to a Kontes flask. The flask was sealed tightly with a Teflon plug under an argon atmosphere and the suspension stirred in an oil bath at 200 °C. Periodically, the flask was removed from the bath and cooled in an ice bath. An aliquot was removed from the flask, and analyzed by GC (method **A**). Turnover numbers were calculated for each aliquot. Details are summarized in the text.

References

(1) a) Wieseman, P. *Petrochemicals*; Ellis Horwood: Chichester, England 1986; pp 90. b) Weissermel, K.; Arpel, H.-J. *Industrial Organic Chemistry*, Wiley-VCH: Weinheim, Germany, 2003; pp 59.

(2) For recent reviews on this topic, see: a) Kakiuchi, F.; Chatani, N. *Adv. Synth. Catal.* **2003**, *345*, 1077. b) Labinger, J. A.; Bercaw, J. E. *Nature* **2002**, *417*, 507. c) Crabtree, R. H. *J. Chem. Soc., Dalton Trans.* **2001**, 2437-2450. d) Jensen, C. M. *Chem. Commun.* **1999**, 2443. e) Begman, R. G. *Nature* **2007**, *446*, 391.

(3) a) Gupta, M.; Hagen, C.; Flesher, R. J.; Kaska, W. C.; Jensen, C. M. *Chem. Commun.* **1996**, 2083. b) Gupta, M.; Hagen, C.; Kaska, C. W.; Cramer, R. E.; Jensen, C. M. *J. Am. Chem. Soc.* **1997**, *119*, 840. c) Xu, W.-W.; Rosini, G. P.; Gupta, M.; Jensen, C. M.; Kaska, W. C.; Krogh-Jespersen, K.; Goldman, A. S. *Chem. Commun.* **1997**, 2273.

(4) Göttker-Schnetmann, I.; White, P. S.; Brookhart, M. *J. Am. Chem. Soc.* **2004**, *126*, 1804.

(5) Jensen *et al.* prepared the analogous ^iPr-POCOP iridium complexes and studied its alkane dehydrogenation activity. Morales-Morales, D.; Redón, R.; Yung, C.; Jensen, C. M. *Inorg Chim. Acta* **2004**, *357*, 2953.

(6) a) M. W. Haenel, S. Oevers, K. Angermund, W. C. Kaska, H.-J. Fan, M. B. Hall, *Angew. Chem., Int. Ed.* **2001**, *40*, 3596. b) S. A. Kuklin, A. M. Sheloumov, F. M. Dolgushin, M. G. Ezernitskaya, A. S. Peregudov, P. V. Petrovskii, A. A. Koridze *Organometallics* **2006,** *25,* 5466.

(7) a) Zhang, X.; Fried, A.; Knapp, S.; Goldman, A. S. *Chem. Comm.* **2003**, 2060. b) Bernskoetter, W. H.; Brookhart, M. *Organometallics* **2008,** *27,* 2036.

(8) Morales-Morales, D.; Redon, R.; Wang, Z.; Lee, D. W.; Yung, C.; Magnuson, K.; Jensen, C. M. *Can. J. Chem.* **2001**, *79*, 823.

(9) Ray, A.; Zhu, K.; Kissin, Y. V.; Cherian, A. E.; Coates, G. W.; Goldman, A. S. *Chem. Commun.* **2005**, 3388.

(10) a) Göttker-Schnetmann, I.; Brookhart, M. *J. Am. Chem. Soc.* **2004**, 126, 9330. b) Renkema, K. B.; Kissin, Y. V.; Goldman, A. S. *J. Am. Chem. Soc.* **2003**, *125*, 7770. c) Krogh-Jespersen, K.; Czerw, M.; Summa, N.; Renkema, K. B.; Achord, P. D.; Goldman, A. S. *J. Am. Chem. Soc.* **2002**, *124*, 11404. d) Li, S.; Hall, M. B. *Organometallics* **2001**, *20*, 2153. e) Morales-Morales, D.; Lee, D. W.; Wang, Z.; Jensen, C. M. *Organometallics* **2001**, *20*, 1144. f) Kanzelberger, M.; Singh, B.; Czerw, M.; Krogh-Jespersen, K.; Goldman, A. S. *J. Am. Chem. Soc.* **2000**, *122*, 11017. g) Liu, F.; Pak, E. B.;

Singh, B.; Jensen, C. M.; Goldman, A. S. *J. Am. Chem. Soc.* **1999**, *121*, 4086. h) Niu, S.; Hall, M. B. *J. Am. Chem. Soc.* **1999**, *121*, 3992. i) Liu, F.; Goldman, A. S. *Chem. Commun.* **1999**, 655. j) Lee, D. W.; Kaska, W. C.; Jensen, C. M. *Organometallics* **1998**, *17*, 1.

(11) Goldman, A. S.; Roy, A. H.; Huang, Z.; Ahuja, R.; Schinski, W.; Brookhart, M. *Science* **2006**, *312*, 257.

(12) Ray, A. **2007**, PhD thesis, Rutgers University.

(13) Borch, R. F.; Hassid, A. I. *J. Org. Chem.* **1972**, *37*, 1673.

(14) Stang, S. L.; Meier, R.; Rocaboy, C.; Gladysz, J. A. *J. Fluorine Chem.* **2003**, *119*, 141.

(15) Mao, Y.; Boekelheide, V. *J. Org. Chem.* **1980**, *45*, 2746.

(16) Moulton, C. J.; Shaw, B. L. *J. Chem. Soc., Dalton Trans.* **1976**, 1020.

(17) Trueba, M.; Trasatti, S. P. *Eur. J. Inorg. Chem.* **2005**, 3393-3403.

(18) Crabtree, R. H.; Mihelcic, J. M.; Quirk, J. M. *J. Am. Chem. Soc.* **1979**, *101*, 7738.

(19) NIST Standard Reference Database Number 69 - March, 2003 Release, http://webbook.nist.gov/chemistry/.

(20) TONs were extracted from the ratio of TBE, TBA, DM1B, and DM2B analyzed by GC. The ratio of COE and 1,3-COD was extracted from the olefinic signals of COE and COD in $^{13}C[^{1}H]$ NMR (COE and COD have identical retention times in GC). Determined by NMR, the sum of COE and COD double bonds equals TON of TBE within 5% difference.

(21) Haag, W. O.; Pines, H. *J. Am. Chem. Soc.* **1960**, *82*, 2488.

(22) Krogh-Jespersen, K.; Czerw, M.; Zhu, K.; Singh, B.; Kanzelberger, M.; Darji, N.; Achord, P. D.; Renkema, K. B.; Goldman, A. S. *J. Am. Chem. Soc.* **2002**, *124*, 10797.

(23) Zhu, K.; Achord, P. D.; Zhang, X.; Krogh-Jespersen, K.; Goldman, A. S. *J. Am. Chem. Soc.* **2004**, *126*, 13044.

(24) Zhang, X.; Kanzelberger, M.; Emge, T. J.; Goldman, A. S. *J. Am. Chem. Soc.* **2004**, *126*, 13192.

(25) Goldman, A. S.; Krogh-Jespersen, K. *J. Am. Chem. Soc.* **1996**, *118*, 12159.

(26) Covalent attachment of palladium pincer complexes to silica has been reported by Weck and Jones, and van Koten: a) Yu, K.; Sommer, W. J.; Richardson, J. M.; Weck, M.; Jones, C. W. *Adv. Synth. Catal.* **2005**, *347*, 161. b) Sommer, W. J.; Yu, K.; Sears, J. S.; Ji, Y.; Zhang, X.; Davis, R. J.; Sherrill, C. D.; Jones, C. W.; Weck, M. *Organometallics* **2005**, *24*, 4351. c) Mehendale, N. C.; Sietsma, J. R. A.; Jong, K. P. de; van Walree, C. A.; Klein Gebbink, R. J. M.; van Koten, G. *Adv. Synth. Catal.* **2007**, *349*, 2619.

(27) Yu, K.; Sommer, W. J.; Weck, M.; Jones, C. W. *J. Catal.* **2004**, *226*, 101.

(28) Herde, J. L.; Lambert, J. C. ; Senoff, C. V. *Inorg. Synth.* **1974**, *15*, 18.

CHAPTER FIVE

An Efficient Heterogeneous Dual Catalyst System

for Alkane Metathesis

(Experiments carried out with (POCOP)IrC$_2$H$_4$ in collaborations with Dr. Amy H. R. MarArthur; (*p*-Meo-POCOP)IrC$_2$H$_4$ and (*p*-NMe$_2$-PCP)IrH$_2$ in collaborations with Dr. Emily Carson; pyrimidine-derived Ir catalyst **6** in collaborations with Eleanor Rolfe).

Introduction

We have reported both homogeneous and heterogeneous tandem catalytic systems (Scheme 5.1) in which alkane metathesis was achieved at moderate temperatures (125 – 175 °C) with complete selectivity for linear alkanes.[1] The iridium-based pincer complexes (Fig. 5.1), reported by Jensen, Kaska, Goldman[2,3] and our own group[4], serve as the alkane-dehydrogenation/olefin-hydrogenation catalysts. The combination of a Mo olefin metathesis catalysts, [Mo(C$_{10}$H$_{12}$)(C$_{12}$H$_{17}$N)[OC(CH$_3$)(CF$_3$)$_2$]$_2$ (**Mo-F$_6$**),[1] or other Schrock-type olefin metathesis catalysts[5] and an iridium catalyst provided efficient homogeneous AM systems. For instance, a reaction conducted at 125 °C converted *ca.* 125 – 200 equivalents of *n*-hexane to a range of C$_2$ to C$_{15}$ *n*-alkanes after one day.[1] The Schrock catalyst was found to decay much faster than the Ir catalyst and its early decomposition limited conversion.[1,5]

Scheme 5.1 Alkane metathesis via tandem transfer dehydrogenation/olefin metathesis
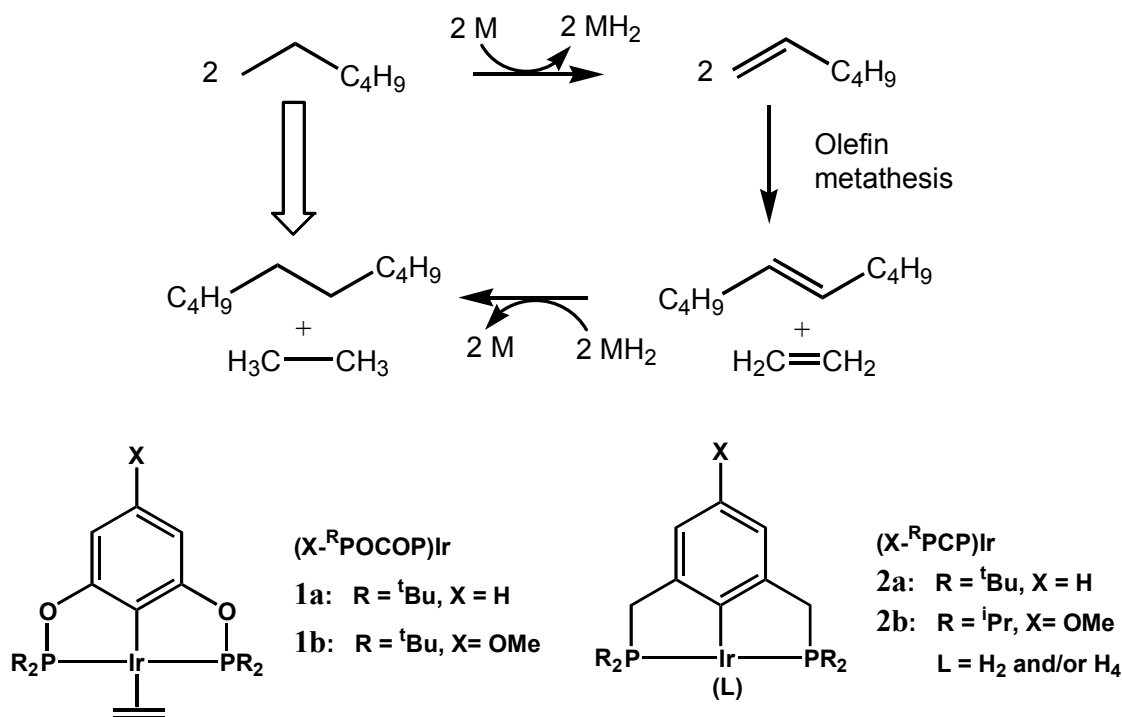
Fig. 5.1 Structures of (POCOP)Ir and (PCP)Ir complexes

Alumina-supported Re_2O_7 can be used as a heterogeneous metathesis catalyst, and when used in combination with iridium pincer catalysts, provides a more stable and longer lived AM dual catalyst system. For example, heating an *n*-decane solution of **1b** and *t*-butylethylene at 175 °C over Re_2O_7/Al_2O_3 gave linear alkane products in the C_2-C_{34} range with 485 turnovers after 9 days.[1] We showed in these systems that iridium complexes were partially or completely adsorbed on the Re_2O_7 alumina support. These observations led us to study alumina-supported-iridium pincer complexes for catalytic transfer dehydrogenation. We showed that iridium pincer complexes, especially those bearing basic functional groups in the *para*-position of the pincer ligands (Fig. 5.2), bind to γ-alumina through a Lewis acid/Lewis base interaction.[6] These alumina-supported catalysts are thermally robust and recyclable, and display high activities for transfer of hydrogen from cyclooctane to *tert*-

butylethylene (see Chapter four).[6] The goal of the work reported here is to combine such catalysts with heterogeneous olefin metathesis catalysts to generate a fully heterogeneous catalyst system for AM.
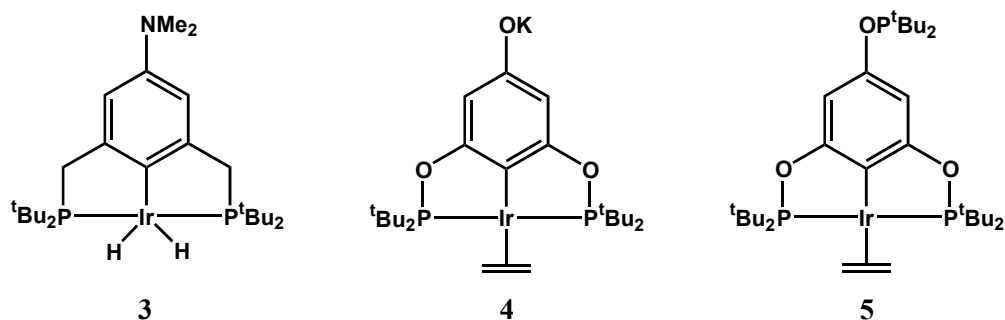
Fig. 5.2 Structure of iridium pincer complexes with basic functional groups in the *para-*position

In this chapter, an investigation of heterogenous AM using six γ-alumina-supported iridium pincer catalysts in combination with the heterogeneous olefin metathesis catalyst Re_2O_7/Al_2O_3 is reported. These heterogeneous catalyst systems show significantly higher activity for alkane metathesis than homogeneous systems examined earlier. Since the Re_2O_7/Al_2O_3 catalyst is longer-lived and operates more efficiently at temperatures substantially below optimum temperatures for the Ir pincer catalysts, a device has been constructed in which the catalysts can be isolated from one another and run at different temperatures. The system with separated catalysts is long-lived, recyclable and quite efficient for AM, exhibiting total turnover numbers (TONs) up to 7000. When this device is used the product distribution favors heavy alkanes and shows few or no secondary AM products. A readily available heterogeneous olefin metathesis catalyst, $MoO_3/CoO/Al_2O_3$, has also been investigated for AM. High activity is achieved with alumina-supported iridium and MoO_3 catalysts isolated and operated at different temperatures.

Result and Discussion

1. Iridium pincer catalysts used in AM with Re₂O₇/Al₂O₃.

Iridium pincer complexes used as hydrogen transfer catalysts in this study include unsubstituted complex **1a** and pincer complexes bearing basic functionality in the *para* position of the arene ring **1b**, **3**, **4** and **5**. The syntheses of these catalysts have been previously reported.[1,6] In addition, a new catalyst, **6**, derived from 4,6-dihydroxypyrimidine has also been examined. Its synthesis is outline in Scheme 5.2.

Scheme 5.2 Formation of complex **6**
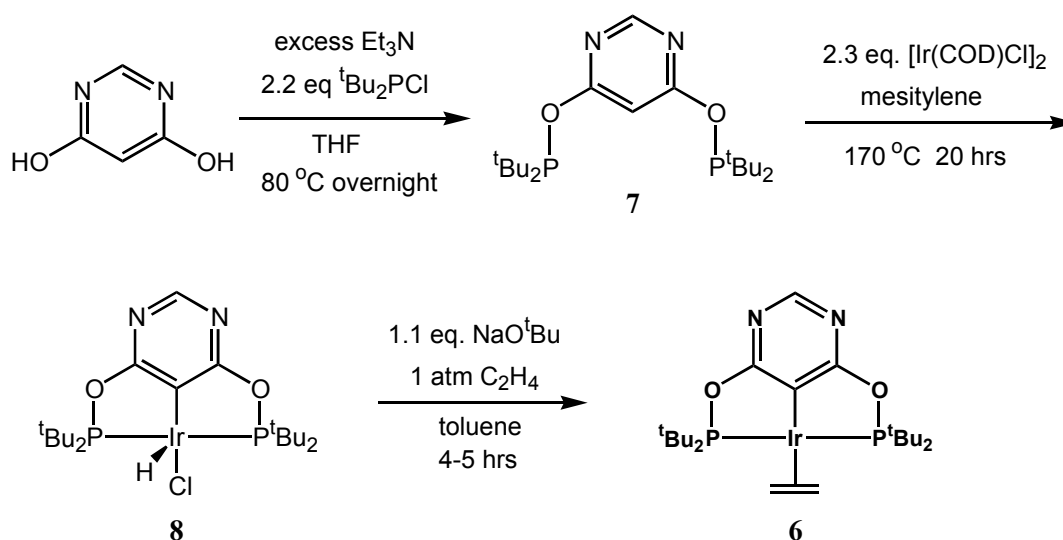
The POCOP ligand, **7**, was synthesized in 79% crude yield by reaction of 4,6-dihydroxypyrimidine with di-*tert*-butylchlorophosphine and excess triethylamine. NMR analysis shows a 15% impurity presumed to be the monophosphinite. Iridium hydridochloride complex, **8**, was obtained from the reaction of excess [Ir(COD)Cl]₂ with the ligand in mesitylene for 12 h at 170°C (60% yield). The impurity observed in the ligand does not undergo metallation, and thus does not interfere with the isolation of pure **8**. The square pyramidal geometry at the metal center, in which hydrogen occupies the apical position, was confirmed by single crystal X-ray diffraction analysis. An ORTEP diagram of **8** is shown in

Fig. 5.3. Treatment of the hydridochloride complex with sodium *tert*-butyloxide in the presence of ethylene produced **6** (53% yield).
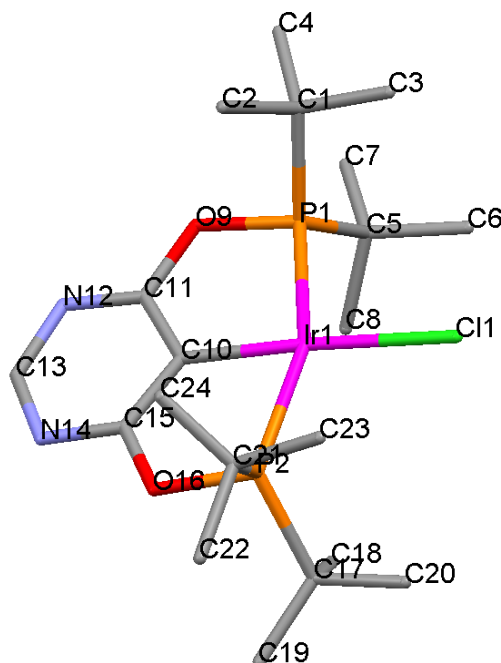
Fig. 5.3 ORTEP diagram of **8**. The bond distances around the metal center are 1.988(7) Å (Ir1-C10), 2.3031(19)Å (Ir1-P1), 2.2968 (Ir1-P2), and 2.392(2) Å (Ir1-Cl1). Selected bond angles (deg): 158.77(7) (P1-Ir1-P2), 79.6(2) (C10-Ir1-P1), 79.1(2) (C10-Ir1-P2), 175.3(2) (C10-Ir1-Cl). Hydrogen on the Ir center can not be located.

2. Alkane metathesis with 1a and Re_2O_7/Al_2O_3.

1a + Re_2O_7/Al_2O_3 + *n*-decane + C_6Me_6 $\xrightarrow{175\,^oC}$ **linear alkanes**   Eq 1

8.4-10.0 mM   5-13 wt % Re_2O_7 5.12 M
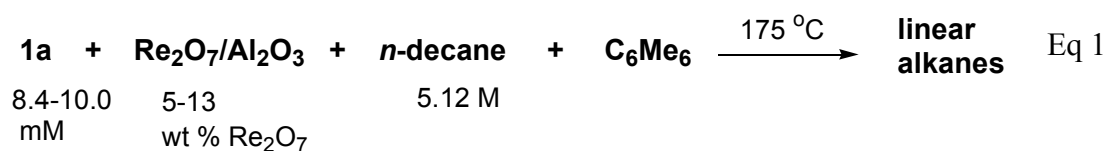
Catalytic alkane metathesis reactions were run using *n*-decane as the solvent in combination with unsubstituted iridium catalyst **1a** and heterogeneous olefin metathesis catalyst Re_2O_7 on alumina. Reactions were carried out under argon and monitored by GC

with hexamethylbenzene or mesitylene used as an internal standard (See Eq 1). Results are summarized in Table 5.1. Initial runs at 125 and 175 °C (entries 1 and 2) employed 22.8 μmol **1a** with a 1:2.5 molar ratio of **1a** : Re_2O_7, supported on 540 mg of γ-alumina. At 125 °C very low productivity was observed (14 TO after 4 days) compared to the 175 °C run where 140 TOs were observed after 5 days. All subsequent runs were thus carried out at 175 °C. In runs 1 and 2 we noted *n*-decane solutions of **1a** were orange prior to addition of Re_2O_7/Al_2O_3. When Re_2O_7/Al_2O_3 was added, these solutions lightened and became nearly colorless, suggesting that a significant fraction of **1a** was adsorbed on the alumina.

Entries 3-7, all run with similar concentrations of **1a** in *n*-decane, show that a critical feature in determining the productivity of these reactions is the amount of alumina present. For example, when a 1:4.2 molar ratio of **1a** : Re_2O_7 on 1020 mg Al_2O_3 (5 wt% of Re_2O_7) was used (entry 3) TONs are more than doubled relative to entry 2; however, when conditions of entry 2 are used and 506 mg of pure alumina added (entry 4, bringing total alumina to 1048mg), a *similar* increase in TONs is observed. In entry 6, a **1a** : Re_2O_7 molar ratio of 1:3 was used (similar to entry 2) except a 13 wt% loading of Re_2O_7 on Al_2O_3 was employed[7-9], so only 225 mg of Al_2O_3 was required. Very poor productivity was observed. Finally compare entries 5 and 7. A low 1: 1.5 molar ratio of **1a** : Re_2O_7 was used in each case, but in entry 7 additional Al_2O_3 (415 mg) had been added. With no added alumina (entry 5), productivity was poor but with added alumina (entry 7) productivity was *equal* to that of entry 2 even though a significantly lower molar quantity of Re_2O_7 was used.

These results argue strongly that as the fraction of **1a** which is supported on alumina increases, the AM productivity of the system increases. Furthermore, it seems plausible that

the system is deactivated by the interaction of **1a** with Re_2O_7 since the thermal stability of **1a**

in alkane solution at 175 °C is very long.

Table 5.1. Total turnover numbers (TONs)[a] and concentration of products from the metathesis of *n*-decane (2.5 mL, 5.12 M) by **1a** (21 to 25 µmol) and varied loading of Re_2O_7 with or without additional Al_2O_3.

Entry	Temp (˚C)	wt % Re_2O_7	[1a]/ 1a:Re_2O_7	Re_2O_7/ Al_2O_3	Added Al_2O_3	[Product] (M)/TONs		
						3 hrs	5 days	End of RXN[b]
1	125	5	22.8 µmol/ 1 : 2.5	540 mg	0 mg	trace	---	0.13 (4d)/ 14.2
2	175	5	22.8 µmol/ 1 : 2.5	540 mg	0 mg	0.153/ 17	1.28/ 140	1.59 (9d) 177
3	175	5	25.0 µmol/ 1 : 4.2	1020 mg	0 mg	0.295/ 30	3.63/ 363	4.51 (11d)/ 451
4	175	5	22.8 µmol/ 1 : 2.5	542 mg	*506* mg	0.281/ 31	2.65/ 291	2.92 (8d)/ 321
5	175	13	21.0 µmol/ 1: 1.5	128 mg	0 mg	trace	---	0.04 (2d)/ 4.8
6	175	13	22.3 µmol/ 1 : 3	255 mg	0 mg	trace	---	0.436 (3d)/ 49
7	175	13	21.0 µmol/ 1: 1.5	130 mg	*415* mg	0.196/ 23	1.29/ 154	1.70 (9d)/ 202

[a] TONs relative to Ir; [b] When the system has lost activity completely.

3. AM with γ-alumina-supported iridium complexes 1b, 3 and 4.

Our previous studies indicated that iridium pincer complexes containing basic functional groups in the *para*-position are adsorbed strongly on **γ**-alumina through a Lewis acid/Lewis base interaction[6]. ICP-MS experiments with *para*-oxide- and *para*-phosphinite-supported systems (2.5 µmol of complexes **4** and **5** on 310 mg of alumina) show negligible leaching from alumina when heated in cyclooctane for several hours at 200 °C. These alumina-supported catalysts are highly active for transfer dehydrogenation of alkanes and can be efficiently recycled. The strong adsorption of these iridium complexes by alumina should retard the interaction between the iridium catalyst and the olefin metathesis catalyst as was seen for weakly adsorbed unsubstituted **1a**.

Table 5.2. Total TONs and concentration of products from the metathesis of *n*-decane (2.5 or 10 mL, 5.12 M) by Re_2O_7/Al_2O_3 (ca. 540 mg, 5 wt % of Re_2O_7) and iridium catalyst **1b**, **3**, or **4** (23.5 to 27 µmol) with or without additional Al_2O_3 at 175 °C.

Entry	Ir	[Ir] (µmol)	Re_2O_7/Al_2O_3	Added Al_2O_3	[Product] (M)/TONs		
					3 h	1 d	7 d
1	**1b**	23.5	570 mg	0 mg	2.49/ 265	3.06/ 326	3.24/ 345
2	**1b**	23.8	550 mg	*502* mg	2.15/ 226	3.10/ 326	4.12/ 434
3	**3**	24.0	547 mg	0 mg	---	3.07/ 320	3.88/ 406
4	**3**	24.0	538 mg	*503* mg	2.22/ 231	4.30/ 448	4.75/ 495
5	**3**	25.0*	540 mg	*503* mg	0.687/ 277	2.05/ 827	2.67/ 1077
6	**4**	24.3	538 mg	0 mg	2.02/ 208	---	3.85/ 402
7	**4**	27.0	530 mg	*506* mg	3.36/ 311	3.92/ 363	4.55/ 421

*With 10 mL of *n*-decane as starting material.

In combination with Re_2O_7/Al_2O_3 (5 wt% of Re_2O_7), catalysts **1b**, **3** and **4** were screened for AM using *n*-decane. In most runs ca. 23.8 µmol Ir was used together with ca. 550 mg of Re_2O_7/Al_2O_3 which corresponds to a 1:2.5 molar ratio or Ir : Re_2O_7. Reactions were carried out at 175 °C and monitored by GC at 3 h, 1 d and 7 d. Table 5.2 summarizes the total concentration of alkane products (C_2-C_9 plus C_{11}-C_{34}) and TONs. In runs 1, 3, and 6 the iridium complex was added to *n*-decane and was adsorbed on Re_2O_7/Al_2O_3. In these runs the reaction rates and productivities were significantly increased by using **1b**, **3** or **4** relative to **1a**. For example, after 3 h at 175 °C, AM with **1b** and **4** gave 265 and 208 TONs, respectively. Under identical conditions, only 17 TONs were obtained in the reaction using **1a** (Table 5.1, entry 2). The reactions with **3** and **4** formed alkane products in 79% yield (406 and 402 TONs respectively) after 7 days. When the reaction with **1a** was terminated at 9 days, the total conversion was only 31% (177 TONs).

The effect of added alumina was also investigated in these systems by using *ca.* 500 mg of alumina to support iridium complexes **1b**, **3** and **4** *prior* to the addition of the Re_2O_7/Al_2O_3 catalyst. Using the *para*-methoxy-supported system **1b** supported on the Re_2O_7/Al_2O_3 particles, catalysis was finished after *ca.* one day, as heating an additional 6 days resulted in only 19 additional TOs (Table 5.2, entry 1). Supporting **1b** on 502 mg Al_2O_3 prior to exposure to Re_2O_7/Al_2O_3 resulted in a significant increase in catalyst lifetime with TONs reaching 434 at 7 days (entry 2). The effect on productivity of supporting the iridium catalyst on alumina is more significant for the *para*-dimethylamino-supported **3/Al$_2$O$_3$** and *para*-oxide-supported systems **4/Al$_2$O$_3$**. For example, the productivity using catalyst **4** was significantly increased by the presence of additional alumina (208 TONs *vs* 311 TONs after 30 mins). Among these systems, the *para*-dimethylamino catalyst **3** supported by additional alumina was most productive and gave 495 TONs after 7 days (entry 4). Remarkably, the *n*-decane starting alkane was present in lower molar quantities than *n*-nonane and *n*-octane, with measured C_8 : C_9 : C_{10} : C_{11} molar ratios of 1.46 : 1.06 : 1.0 : 0.66 (Fig. 5.4). Encouraged by these high productivities, the substrate *n*-decane was increased from 2.5 mL to 10 mL using the same quantities of **3**, alumina and Re_2O_7/Al_2O_3. After 7 days at 175 °C, the product concentration reached 2.67 M with a total of 1077 TOs (entry 5).

These results show that iridium complexes bearing polar groups in the *para*-position adsorb strongly on alumina and perform much better than the weakly adsorbed parent complex **1a** in AM. Though the complexes bind strongly to the Re_2O_7/Al_2O_3 particles, the reaction rates and productivities are improved by independently adsorbing Ir complexes on additional alumina prior to exposure to Re_2O_7/Al_2O_3.
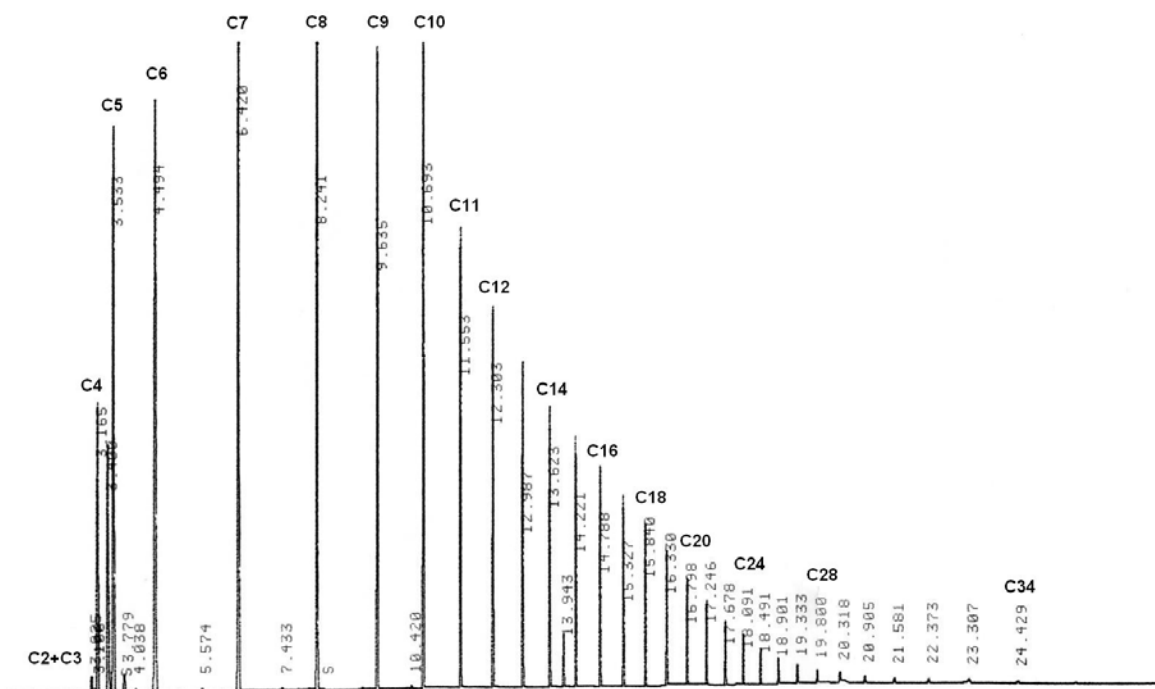
Fig. 5.4 GC trace of product mixture resulting from the metathesis of *n*-decane (solvent) by **3**/Al$_2$O$_3$ and Re$_2$O$_7$/Al$_2$O$_3$ after 7days at 175 °C (see Table 5.2).

4. AM with low loading of iridium catalysts 4, 5 and 6.

As demonstrated above, using additional alumina to support iridium catalysts prevents the interaction between the iridium catalysts and Re$_2$O$_3$/Al$_2$O$_3$. An alternative method of minimizing these presumed interactions is to decrease the loading of iridium catalyst on Re$_2$O$_7$/Al$_2$O$_3$. Complex **4** together with iridium complexes **5**, bearing a phosphinite group in the *para*-position, and **6** possessing a pyrimidine backbone in the pincer ligand, were tested under these low-load conditions. Complexes **4** and **5** have been previously shown to adsorb strongly on alumina through a Lewis acid/Lewis base interaction[6]. A similar phenomenon occurs with **6**, which most likely binds to acidic sites on the alumina through the basic nitrogen atoms in the pincer backbone. In these AM reactions, 4.2 *μ*mol of either **4**, **5** or **6** were combined with Re$_2$O$_7$/Al$_2$O$_3$ (*ca.* 540 mg) in *n*-decane (2.5 mL) *without* additional alumina and heated at 175 °C. Results are summarized in Table 5.3

142

and Fig. 5.5. Catalysis with **4** gave 291 TONs after 3 hours and 1672 TONs after 2 days (Table 5.3, entry 1). Among the three systems, the initial rate using **6** was fastest with 1914 TONs after 1 day (64% conversion); however, activity ceased after ca. 1 day as heating for 6 more days resulted in only 143 additional TONs (see Table 5.3 and Fig. 5.5). The system employing phosphinite catalyst **5** appears to be the most stable and long-lived. After 7 days, the catalyst was still active for AM and TONs up to 2521 (84% conversion) were obtained after 14 days.

The plot of turnovers *vs* time for all three catalysts (Fig 5.5) is instructive. All show an initial burst of activity in the first hour. Catalyst **6** shows highest initial productivity but quickly loses activity. The para-phosphinite catalyst **5** shows a steady increase after this burst and at long times clearly outperforms both **4** and **6**. We don't fully understand the reaction profiles, but we note that previous ICP-MS experiments[6] suggest the phosphinite system is most strongly adsorbed on alumina relative to **4**.

Table 5.3. Total TONs and concentration of products from the metathesis of *n*-decane (2.5 mL, 5.12 M) by Re_2O_7/Al_2O_3 (ca. 540 mg, 5 wt % of Re_2O_7) and iridium catalysts **4**, **5** and **6** (4.2 μmol) *without additional Al$_2$O$_3$* at 175 °C.

Entry	**Ir**	**[Ir]** Ir:Re$_2$O$_7$	Re$_2$O$_7$/Al$_2$O$_3$	[Product] (M)/TONs			
				3 h	1 d	7 d	14 d
1	**4**	4.2 μmol 1 : 14.4	544 mg	0.489/ 291	1.20/ 715	2.38/ 1419	2.81/ 1672
2	**5**	4.2 μmol 1 : 14.4	546 mg	0.366/ 218	2.32/ 1382	3.26/ 1942	4.24/ 2521
3	**6**	4.2 μmol 1 : 14.4	544 mg	0.687/ 609	3.22/ 1914	3.46/ 2057	--
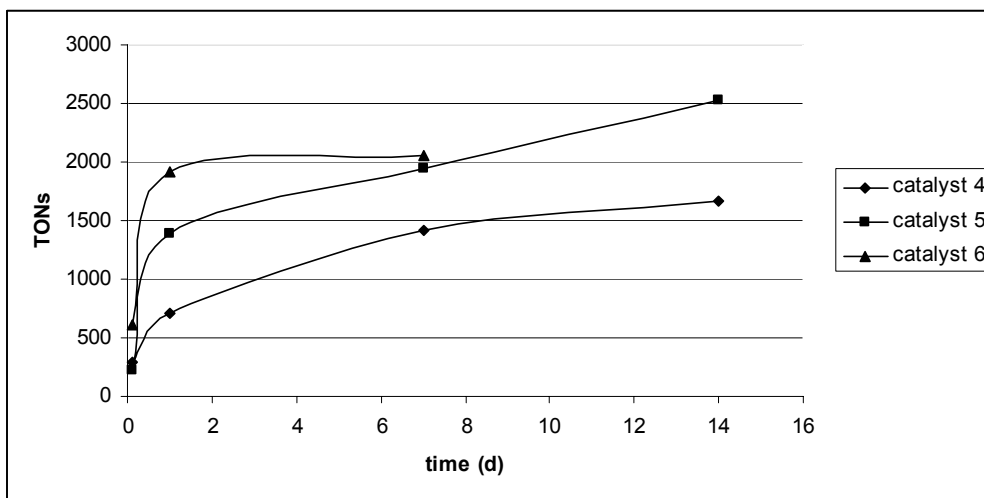
Fig. 5.5 Plot of total AM TONs employing **4**, **5**, and **6** with Re_2O_7/Al_2O_3.

Table 5.4 Distribution of C_2 to C_{34} *n*-alkane products (equivalents relative to **Ir**) from the metathesis of *n*-decane (2.5 mL, 5.12 M) by **4**, **5** and **6** (4.2 μmol) and Re_2O_7/Al_2O_3 (ca. 540 mg, 5 wt % of Re_2O_7) *without additional Al_2O_3* at 175 °C after 7 days.

Entry	**Ir**	C_2-C_5	C_6-C_9	C_{11}-C_{14}	C_{15}-C_{18}	$C_{>18}$	Total TON
1	**4**	160	727	376	121	35	1419
2	**5**	357	833	489	201	62	1942
3	**6**	366	834	553	235	69	2057

Heterogeneous AM reactions with *n*-decane as substrate form products in the C_2-C_{34} range. Table 5.4 summarizes the alkane product distributions formed using catalysts **4**, **5** and **6** after 7 days (Entries 1, 2, and 3, Table 5.4). Selectivity for the desirable products, ethane and *n*-$C_{18}H_{38}$, is low and is attributed to olefin isomerization, which is known to be catalyzed by the iridium complexes and may also be catalyzed by Re_2O_7/Al_2O_3 and even Al_2O_3 itself. Alkanes heavier than *n*-$C_{18}H_{38}$ must be produced via secondary alkane metathesis since they are derived from metathesis of at least one olefin of $C_{n>10}$, which is necessarily a product of primary alkane metathesis.

5. AM using physically separated 4/Al$_2$O$_3$ and Re$_2$O$_7$/Al$_2$O$_3$

A disadvantage of using Al$_2$O$_3$-supported iridium catalysts together with Re$_2$O$_7$/Al$_2$O$_3$ in the same pot is that the Ir catalysts function at viable rates only above 175 °C while the rhenium metathesis catalysts function most effectively at 20-100 °C[8-11] and degrade moderately rapidly at temperatures above 80 °C.[9] Thus, carrying out reactions at 175 °C results in decay of the rhenium catalyst while 175 °C is actually lower than optimum for the highly stable iridium catalysts. Furthermore, there is a potential interaction between Ir and Re$_2$O$_3$ catalyst in the one-pot system which accelerates the decomposition rate of both catalysts and decrease the activity. These circumstances limit overall conversion and prevent efficient catalyst recycling, the normal advantage of easily reisolated heterogeneous catalysts. To circumvent these problems we have designed a simple apparatus shown in Fig. 5.6 which allows physical separation and operation of the two catalysts at two different temperatures. The device contains two "pots" connected by two tubes as shown. The upper, larger diameter tube is heavily insulated. The lower pot is loaded with the Ir catalyst and the upper pot is loaded with Re$_2$O$_7$/Al$_2$O$_3$. The lower tube contains a frit at the mouth of the upper pot to prevent the rhenium catalyst from being washed into the lower pot. When the lower pot is heated, hydrocarbons distill through the upper insulated tube and condense in the upper pot which is stirred and held at a lower temperature (50 °C). Olefin metathesis occurs readily at these temperatures and product returns to the lower pot through the lower tube. Table 5.5 summarizes the results of an experiment using *n*-octane (6594 equiv relative to Ir) and Re$_2$O$_7$/Al$_2$O$_3$ (540 mg, 5 wt % of Re$_2$O$_7$) in the upper pot (50 °C) and the alumina-supported Ir catalyst **4** (2.8 μmol of Ir on 280 mg Al$_2$O$_3$) in the lower pot (220 °C). After 52 h 3907 TOs were observed (entry 1). After solutions were removed from each pot and the device

recharged, the first recycle produced 1370 TOs after 52 h (entry 2). The second recycle gave 670 TOs after 18 h (entry 3). The decay of activity of the system may be due to the loss of olefins upon removal of product (at lease 1 equiv of olefin is required to support the catalytic cycle). Therefore, twenty equiv of 1-octene were added to the *n*-octane charge in the third recycle. This third recycle produced 1620 TOs after 28 h and was an improvement over even the first recycle. The result suggests that the loss of olefin is clearly a factor affecting recyclability but may not be the only one.
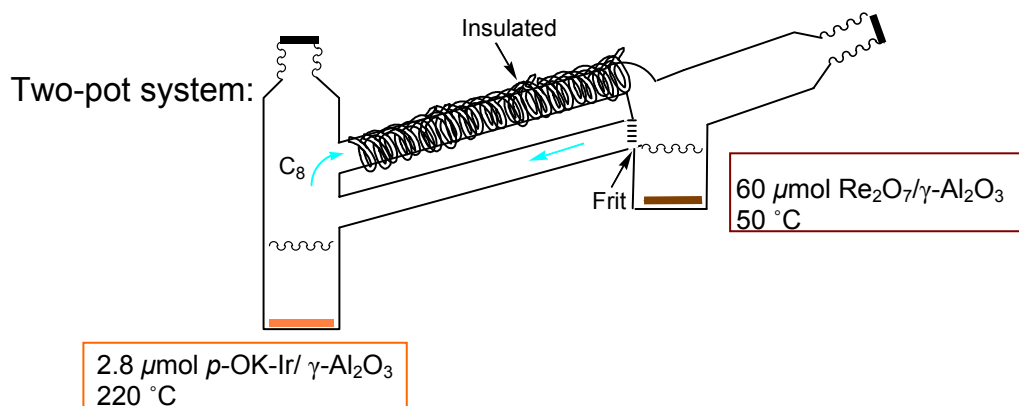
Fig. 5.6 A two-pot device for alkane metathesis.

Table 5.5. Distribution of C_2 to C_{16} *n*-alkane products (equivalents relative to **Ir**) from the metathesis of *n*-octane (3 ml, 6.15 M) by alumina-supported **4** (2.8 μmol) and Re_2O_7/Al_2O_3 (540 mg, 5 wt % of Re_2O_7) at 175 °C using a two-pot reactor.

	C_2-C_4	C_5-C_7	C_9-C_{11}	C_{12}-C_{14}	C_{15},C_{16}	Total TON
18 h	88	642	717	114	1	1562
52 h	300	1421	1775	392	19	3907
1st recycle						
18 h	48	284	357	58	1	748
52 h	109	479	653	122	3	1370
2nd recycle						
18 h	33	205	375	61	0	674
add 20 equiv of 1-octene						
28 h	139	506	817	162	0	1624

146

Alkane Product Distributions Using the Two-pot Device. Using the two-pot system avoids the build up of heavy alkanes via secondary alkane metathesis. Alkanes n-$C_{15}H_{32}$ and n-$C_{16}H_{34}$ are the only two observable products of secondary alkane metathesis and are present in very small amounts (19 equiv total after 52 h in the first cycle). The yield of alkanes above C_{14} is low because olefins heavier than octenes are difficult to distill and therefore they are less likely to reach the upper pot containing the olefin metathesis catalyst. Consequently, the heavier olefins ($C_{>8}$) seldom undergo metathesis and serve primarily as hydrogen acceptors in the lower pot. Moreover, the alkane product distribution is concentrated in the C_9-C_{14} range relative to the distributions in the "one pot" reaction. Such a skew in the distribution is favorable for diesel production. The molar ratio of C_9-C_{14} n-alkanes to C_2-C_7 n-alkanes obtained from octane in the two pot reactor is 1.3 : 1. In contrast, alkane metathesis by the mixed catalysts favors the formation of alkanes lighter than the starting alkane. For example, metathesis of n-decane by **4** and Re_2O_3/Al_2O_3 in the one pot system (Table 5.4, entry 1) forms heavier alkanes C_{11}-C_{18} and lighter alkanes C_2-C_9 n-alkanes in a 0.56 : 1 molar ratio. This favorable change in hydrocarbon distribution arises from the fact that the lower molecular weight olefins are more volatile and can be repeatedly distilled into the upper pot for secondary metathesis, while the heavy olefins tend to remain in the lower pot and serve as hydrogen acceptors.

6. AM with $MoO_3/CoO/Al_2O_3$ as the olefin metathesis catalyst

While Re_2O_7/Al_2O_3 is an efficient heterogeneous catalyst when operated at 20-100 °C, heterogeneous molybdenum and tungsten catalysts are known to operate above these temperatures.[8,10,11] $Mo_2O_3/CoO/Al_2O_3$ was particularly attractive in that it is commercially available at low cost and so this catalyst was screened in AM. $Mo_2O_3/CoO/Al_2O_3$ pellets

(Strem) were calcined at 550 °C under air prior to use. Following calcining these pellets showed excellent activity in olefin metathesis at 175 °C. Initial AM experiments were carried out by mixing the $MoO_3/CoO/Al_2O_3$ (240 mg, 243 μmol of Mo) catalyst with alumina-supported **4** (2.5 μmol of Ir on 310 mg of alumina) in *n*-decane (5130 equiv relative to Ir) and heating at 175 °C. AM activity was low with only 120 TOs seen after 4 days (Table 5.6, entry 1). Remarkably, when the metathesis catalyst was isolated from the iridium catalyst by using the two-pot device, the productivity was very significantly increased. In a typical experiment, *n*-octane (7385 equiv relative to Ir) was heated with alumina-supported **4** (2.5 μmol of Ir on 310 mg of alumina) at 220 °C in the lower pot and the Mo catalyst (240 mg) was heated in the upper pot at 100 °C. After 9 days, TONs up to 3127 were obtained (Table 5.6). These results indicate that in the one pot system there must be interaction between the Ir and Mo catalysts which significant decreases catalyst activity and stability and that this can be circumvented by physically separating the catalysts. The mode and nature of this deleterious interaction is unknown.

Table 5.6. Total TONs of products from the metathesis of *n*-decane (2.5 mL) or *n*-octane (3 mL) by alumina–supported **4** (2.5 μmol Ir, 310 mg Al_2O_3) and $MoO_3/CoO/Al_2O_3$ (240 mg, 243 μmol Mo).

Entry	System	Temp (°C)	[Product] (M)/TONs			
			1 day	2 day	4 days	9 days
1	Mixed	175	---	---	120	---
2	Separated	220/100	1026	1753	2450	3127

Conclusions

In summary, several **γ**-alumina-supported iridium systems were investigated for alkane metathesis. The Ir catalysts, which adsorb strongly on alumina through a Lewis acid/Lewis base interaction, exhibit unprecedented high activity for alkane metathesis in

combination with Re_2O_7/Al_2O_3. Addition of alumina was found to improve the productivity and catalyst stability by minimizing the potential interaction between the iridium species and Re_2O_7/Al_2O_3. Using a "two-pot" device, the supported Ir catalysts, and the metathesis catalysts, including Re_2O_7/Al_2O_3 and the commercial available $MoO_3/CoO/Al_2O_3$, can be isolated and run at different temperatures. The system with separated Ir and Re_2O_7 catalysts is recyclable, highly efficient, and shows selectivity for heavy alkanes products. The AM process holds promise for selective conversion of the less useful n-alkanes in the C_3-C_8 range to heavier alkanes in the diesel range.

Experimental Section

General Considerations. All manipulations were carried out using standard Schlenk, high-vacuum and glovebox techniques. Argon was purified by passage through columns of BASF R3-11 (Chemalog) and 4 Å molecular sieves. Tetrahydrofuran (THF) was distilled under a nitrogen atmosphere from sodium benzophenone ketyl prior to use. Pentane and toluene were passed through columns of activated alumina. Triethylamine, THF-d_8, and toluene-d_8 were dried with 4 Å molecular sieves and degassed by freeze-pump-thaw cycles. Anhydrous decane was purchased from Aldrich, dried with 4 Å molecular sieves and degassed by freeze-pump-thaw cycles. Mesitylene and n-octane were purchased from Aldrich, dried with Na or LiAlH$_4$, and vacuum transferred into sealed flasks. Ammonium perrhenate was purchased from Aldrich and used as received. γ-Al$_2$O$_3$ (97.7%) and $MoO_3/CoO/Al_2O_3$ were purchased from Strem and calcined as noted below. Complexes **1a**,[4] **1b**,[4] **3**,[6] **4**,[6] **5**[6] and [(COD)IrCl]$_2$[15] were synthesized as previously reported. All other reagents were purchased from Sigma-Aldrich or Strem and used as received.

NMR spectra were recorded on BRUKER DRX-400, AVANCE-400, and BRUKER DRX-500 MHz spectrometers. ^{1}H and ^{13}C NMR spectra were referenced to residual protio solvent peaks. ^{31}P chemical shifts were referenced to an external H_3PO_4 standard. Elemental analyses were carried out by Robertson Microlit Laboratories, NJ.

GC analyses (FID detection) was performed according to the following methods: Agilent 6850 Series GC System fitted with an Agilent HP-1 column (100% dimethylpolysiloxane, 30m×0.32mm i.d., 0.25 μm film thickness). Typical temperature program: 5 min isothermal at 33 ºC, 20 ºC/ min heat up, 10 min isothermal at 300 ºC. Flow rate: 1 mL/min (He). Split ratio: 400. Inlet temperature: 250 °C. Detector temperature: 250 °C.

Synthesis of pyrimidine-based POCOP pincer ligand {$C_4H_1N_2$-[OP(t-Bu)$_2$]$_2$-4,6}, 7. To a cloudy, pale yellow suspension of 400 mg (3.57 mmol) 4,6-dihydroxypyrimidine in 40 mL THF was added 3.6 mL (25.90 mmol) Et$_3$N and 1.5 mL (7.85 mmol) di-*tert*-butyl-chlorophosphine, both via syringe. The reaction mixture was heated to 80 °C and was allowed to reflux overnight. The solvent was removed under high vacuum, yielding the crude product as a pale yellow solid. The product was extracted in 40 mL toluene and filtered through a pad of celite. Toluene was removed under vacuum; 1.13 g (2.81 mmol, 79%) product was obtained as pale yellow powders (ca. 85% purity by NMR). ^{1}H NMR (400 MHz, 23°C, toluene-d$_8$): δ 7.10 (s, 1H, H2), 6.98 (s, 1H, H5), 1.11 [d, $^3J_{P-H}$ = 11.6 Hz, 36H, 4 × ^{t}Bu]. ^{31}P{^{1}H} NMR (162 MHz, 23 °C, toluene-d$_8$): δ 158.4 (15%, monophosphorylated impurity), 157.5 (85%). ^{13}C{^{1}H} NMR (101 MHz, 23 °C, CDCl$_3$): δ 172.6 (d, J_{P-C} = 8.1 Hz, C4 and C6), 158.2 (s, C2), 94.2 (t, J_{C-C} = 5.1 Hz), 35.5 [C$_q$, m, C(CH$_3$)$_3$], 27.2 (CH$_3$, m, 4 × ^{t}Bu).

Synthesis of hydridochloride complex (POCOP)IrHCl, 8. The ligand (530 mg, 1.32 mmol) and [(COD)IrCl$_2$] (387 mg, 0.58 mmol) were suspended in 25 mL mesitylene; this mixture was heated at 170 °C for 20 hours. Solvent was removed under vacuum. The pure product was extracted by washing with toluene (methylene chloride could also be used). Solvent was removed under vaccum; 493.7 mg (0.86 mmol, 60%) was obtained as a mixture of red-orange powder and burgundy crystals. ^{1}H NMR (400 MHz, 23°C, toluene-d_8): δ 8.29 (s, 1H, H2), 1.16 (m, 36H, 4 × ^{t}Bu), -40.14 (t, $^2J_{\text{P-H}}$ = 12.8 Hz, 1H, IrH). ^{31}P{^{1}H} NMR (162 MHz, 23 °C, CDCl$_3$): δ 172.4. Elemental analysis calcd for C$_{20}$H$_{38}$N$_2$O$_2$P$_2$ClIr (628.15): C, 38.24; N, 4.46; H, 6.10. Found: C, 37.63; N, 4.47; H, 5.67.

Synthesis of (POCOP)IrC$_2$H$_4$, 6. A flask containing 200 mg (0.318 mmol) **8** and 33.9 mg (0.352 mmol) sodium *tert*-butoxide was placed under positive argon pressure. Next, the flask was placed under positive ethylene pressure via a needle connected to the ethylene hose; after several minutes, 25 mL toluene was added via syringe, producing a cloudy, red-orange liquid. The needle connected to the ethylene hose was submerged in the suspension, and the liquid was allowed to stir for 5 h. After three hours, the reaction mixture was a deep burgundy color. The solution was cannula transferred and filtered through a pad of celite. The solvent was removed under vacuum; the pure product was isolated as a red-orange powder. ^{1}H NMR (400 MHz, 23°C, toluene-d$_8$): δ 8.61 (s, 1H, H2), 2.95 (t, $J_{\text{H-H}}$ = 2 Hz, 4H, C$_2$H$_4$), 1.15 [m, 36H, 4 × ^{t}Bu]. ^{31}P{^{1}H} NMR (162 MHz, 23 °C, toluene-d$_8$): δ 177.1. ^{13}C{^{1}H} NMR (101 MHz, 23 °C, CDCl$_3$): δ 179.7 (C$_q$, vt, C4 and C6), 153.7 (CH, s, C2), 127.0 (C$_q$, m, C5), 42.2 (C$_q$, vt, 4 × ^{t}Bu$_2$), 38.1 (CH$_2$, s, C$_2$H$_4$), 28.6 [CH$_3$, vt, 2 × ^{t}Bu$_2$]. Elemental analysis calcd for C$_{22}$H$_{41}$N$_2$O$_2$P$_2$Ir (619.74): C, 42.64; N, 4.52; H, 6.67. Found: C, 42.85; N, 4.38; H, 6.43.

Procedures for alkane metathesis reactions:

Table 5.1 and **5.2**: A flask was charged with the Ir catalyst (21-27 μmol), varied loading of Re$_2$O$_7$ on alumina (5 wt% or 13 wt%), 2.5 mL (12.8 mmol) of *n*-decane, and hexamethylbenzene (ca. 60 μmol) as internal standard. In the entries of Table 5.1 where additional alumina was introduced, the alumina was added together with solid starting material prior to the addition of decane. In the entries of Table 5.2, the alumina was added to the decane solution of Ir catalyst. After the solution turned to colorless, Re$_2$O$_7$/Al$_2$O$_3$ was added. The flask was sealed tightly with a teflon plug under an argon atmosphere, and the solution stirred in a 175 °C oil bath. Periodically, the flask was removed from the bath and cooled in an ice bath. An aliquot was removed from the flask, and analyzed by GC. Turnover numbers were calculated for each aliquot.

Table 5.3 and **5.4**: A flask was charged with the Ir catalyst (4.2 μmol), ~540 mg Re$_2$O$_7$/Al$_2$O$_3$, 2.5 mL (12.8 mmol) of *n*-decane, and mesitylene (ca. 70 μmol) as internal standard. The flask was sealed tightly with a teflon plug under an argon atmosphere, and the solution stirred in a 175 °C oil bath. Periodically, the flask was removed from the bath and cooled in an ice bath. An aliquot was removed from the flask, and analyzed by GC. Turnover numbers were calculated for each aliquot.

Table 5.5: The lower pot of the two-pot apparatus was charged with γ-alumina-supported iridium catalyst **4** (2.8 μmol), hexamethylbenzene (60 μmol) and 3 mL of *n*-octane. And the upper pot was charged with 540 mg of Re$_2$O$_7$/Al$_2$O$_3$ (5 wt%). The device was sealed tightly with two teflon plugs under an argon atmosphere. The lower pot was heated at 220 °C and the upper pot was heated at 50 °C. Periodically, the flask was removed from the bath and cooled in an ice bath. An aliquot was removed from the flask, and analyzed by GC. Turnover numbers were calculated for each aliquot.

The heterogeneous catalysts can be recycled. After each cycle, the solution was syringed out and the solid was washed 3 times with penane and *n*-octane, respectively. Fresh *n*-octane and internal standard were then added.

Table 5.6: For the one-pot system, the procedure was similar to than in Table 5.3 except 240 mg of $MoO_3/CoO/Al_2O_3$ was used as the olefin metathesis catalyst. For the two-pot system, the procedure was similar to that in Table 5.5 except 240 mg of $MoO_3/CoO/Al_2O_3$ was charged in the upper pot of the device.

References and Note

(1) Goldman, A. S.; Roy, A. H.; Huang, Z.; Ahuja, R.; Schinski, W.; Brookhart, M. *Science* **2006**, *312*, 257.

(2) a) Gupta, M.; Hagen, C.; Flesher, R. J.; Kaska, W. C.; Jensen, C. M. *Chem. Commun.*, **1996**, 2083. b) Gupta, M.; Hagen, C.; Kaska, W. C.; Cramer, R. E.; Jensen, C. M. *J. Am. Chem. Soc .***1997**, *119*, 840.

(3) Xu, W.-W.; Rosini, G. P.; Gupta, M.; Jensen, C. M.; Kaska, W. C.; Krogh-Jespersen, K.; Goldman, A. S. *Chem. Commun.* **1997**, 2273.

(4) Göttker-Schnetmann, I.; White, P.; Brookhart, M. *J. Am. Chem. Soc.* **2004**, *126*, 1804.

(5) Bailey, B. C.; Schrock, R. R.; Kundu, S.; Goldman, A. S.; Huang, Z.; Brookhart, M. *Organometallic* **2009**, *28*, 355.

(6) Huang, Z.; Brookhart, M.; Goldman, A. S.; Kundu, S.; Scott, S. L.; Vicente, B. C. *Adv. Synth. Catal.* **2009**, *351*, 188.

(7) In olefin metathesis reaction, this catalyst with 13 wt % of Re_2O_7 loading on Al_2O_3 performs better than that with 5 wt % of Re_2O_7.

(8) Ivin, K. J. *Olefin Metathesis*, Academic Press. London, **1983**.

(9) Spronk, R.; Andreini, A.; Mol. J. *J. Mol. Catal.* **1991**, *65*, 219.

(10) Ivin, K. J.; Mol. J. C. *Olefin Metathesis and Metathesis Polymerization*, Academic Press. London, **1997**.

(11) Mol. J. C. *J. Mol. Catal. A: Chem.* **2004**, *213*, 39.

(12) Herde, J. L.; Lambert, J. C.; Senoff, C. V. *Inorg. Synth.* **1974**, *15*, 18-19.

CHAPTER SIX

Ligand Exchange Reactions and Selective Catalytic Hydrogenation in Nonporous Single Crystals

Introduction

In analogy with enzymatic transformations, reactions within the interior of single crystals are likely to be highly selective and are thus of considerable interest due to potential applications in selective catalytic transformations and chemical sensor technology. Examples of single-crystal-to-single-crystal (SC–SC) transformations are uncommon since crystallinity is difficult to retain following the rearrangement of atoms in the solid-state.[1–13] The most widely studied SC–SC transformations involve guest (solvent) exchange in porous coordination polymers or metal-organic frameworks (MOFs) which take advantage of the robust polymeric framework of the hosts.[6-9] Examples of SC–SC transformations in molecular organic crystals have been reported and generally involve photo-induced coupling of alkenes or alkynes contained within the crystal.[2,10-13] A remarkable exception is the report by Atwood and Barbour of a calix[4]arene which upon uptake of vinyl bromide undergoes a SC–SC phase transformation with significant rearrangement of the host molecule.[14] For nonporous molecular inorganic and organometallic crystals, SC–SC transformations involving cleavage and formation of metal-ligand bonds are quite rare[15,16] and normally

involve ligand loss from the single crystal and reversible religation. Ligand loss is often accompanied by conversion of the single crystal to a microcrystalline powder as in the case of loss of SO_2 from a Pt(II) NCN pincer complex reported by Albrecht and van Koten[17] and loss of pyridine from bis(benzoylacetonato)pyridine copper(II) reported by Lennartson.[18] Brammer has described loss of ethanol from a single crystal silver coordination polymer with retention of single crystal character.[15] Uptake of ethanol was shown to occur in microcrystalline powders of the ethanol-free product. Reversible exchange of ethanol and water at an iron center in a single crystal of a triiron cluster is reported by Das to occur *without* loss of single crystal character.[16]

We report here a series of unprecedented SC–SC transformations involving exchange of multiple small gaseous ligands (L = N_2, CO, NH_3, C_2H_4, H_2, O_2) at an iridium center in single crystals of a pincer iridium complex **[Ir]-L**, **[Ir]** = {C_6H_3-[OP-($C_6H_2(CF_3)_3$–2,4,6)$_2$]$_2$–2,6}–Ir. The single crystal remains intact during these ligand exchanges[19] which, remarkably, occur within the crystal and do not require prior ligand extrusion. The single crystals **[Ir]-N₂**, **[Ir]-(H)₂(H₂)** and **[Ir]-C₂H₄** serve as catalysts for hydrogenation of ethylene. When the surface sites are passified by CO, high selectively for hydrogenation of ethylene relative to propylene is observed.

Scheme 6.1 Formation of **[Ir]-N₂**

[Ir]-N₂
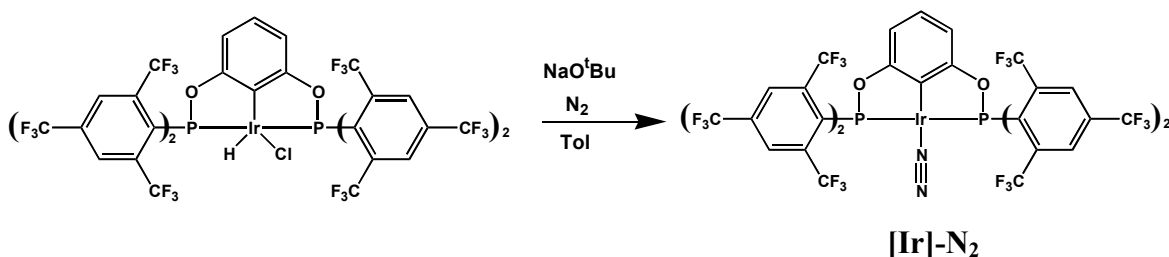
Results and Discussion

The iridium complexes reported here are supported by a highly sterically hindered and electron-deficient pincer ligand {$C_6H_3[OP(C_6H_2(CF_3)_3-2,4,6)_2]_2-1,3$}. Light red single crystals of the nitrogen iridium pincer complex **[Ir]-N₂** form upon reaction of **[Ir]HCl** (see Scheme 6.1) and NaO^{t}Bu in the presence of N_2 in toluene. As shown by the ORTEP diagram of **[Ir]-N₂** in Fig. 6.1, the coordination geometry around the Ir(I) center is square planar. Tables 6.1 and 6.2 summarize the crystal data as well as selected bond distances and angles. The Ir(1)–C(1) and Ir(1)–N(1) bond distances are 2.010(3) and 1.977(3) Å, respectively. Nitrogen coordinates to the Ir(I) center in an end-on mode with an N(2)–N(1)–Ir(1) bond angle of 176.5(5)° and an N(1)–N(2) bond distance of 1.106(5) Å, which is close to the reported value in free N_2 (1.098 Å).[20] In contrast, analogous complexes bearing less hindered pincer ligands form the dinitrogen-bridged dinuclear complex (PCP)Ir–N≡N–Ir(PCP).[21,22] In **[Ir]-N₂**, the four tris-trifluoromethylphenyl [$2,4,6-(CF_3)_3C_6H_2$] rings form a deep pocket around the Ir center (see Fig. 6.1) and prevent dimer formation.

The crystals of **[Ir]-N₂** have a non-merohedral twinned structure with a rotation of ~180° about the reciprocal axis [0,0,1]. (All the other derived structures mirror this twinning behaviour.) Each unit cell contains two independent **[Ir]-N₂** molecules related by a crystallographic center of symmetry and five toluene molecules (Fig. 6.2a). One of the toluene molecules is disordered and is located at the corner of the unit cell. As depicted in Fig. 6.2c, the **[Ir]-N₂** molecules are stacked along the *a* axis to form channels which are filled with the (disordered) toluene molecules. Along the *b* axis, there is a second channel which is filled with four toluene molecules per unit cell (Fig. 6.2b).
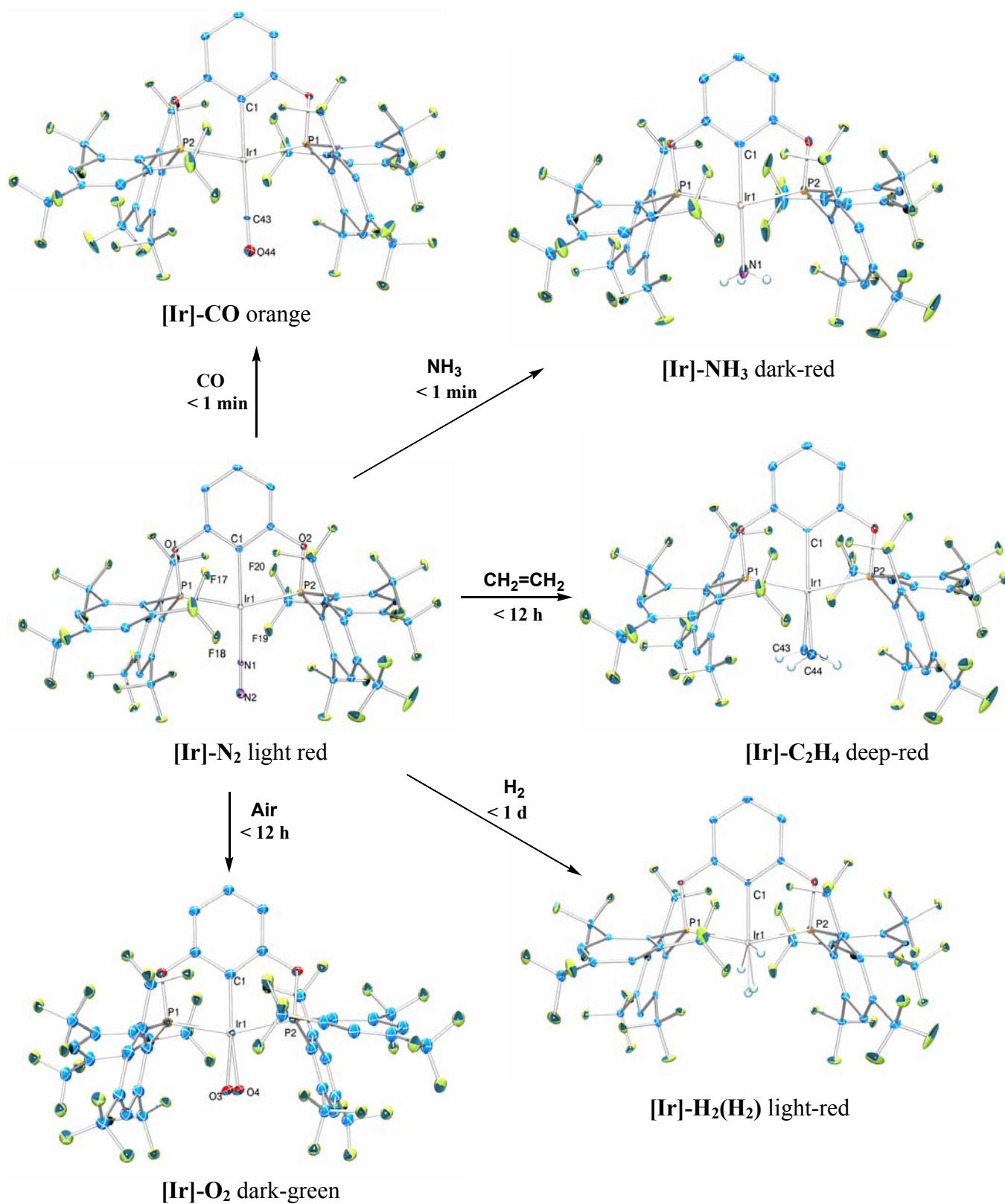
Fig. 6.1 ORTEP structures of single crystals **[Ir]-N₂**, **[Ir]-CO**, **[Ir]-NH₃**, **[Ir]-C₂H₄**, **[Ir]-H₂(H₂)**, and **[Ir]-O₂**. Iridium, flesh; Phosphorus, orange; Fluorine, yellowgreen; Oxygen, red;

Nitrogen, purple; Carbon, stateblue; Hydrogen, cyan. Hydrogen atoms are omitted for clarity except for those in C_2H_4, NH_3 and H_2 ligands. All single-crystal-single-crystal transformations occur at ambient temperature in the presence of one atm pressure of gas except for the transformation from **[Ir]-N₂** to **[Ir]-H₂(H₂)** (1.5 atm of H_2 was employed).

(a)   (b)

(c)
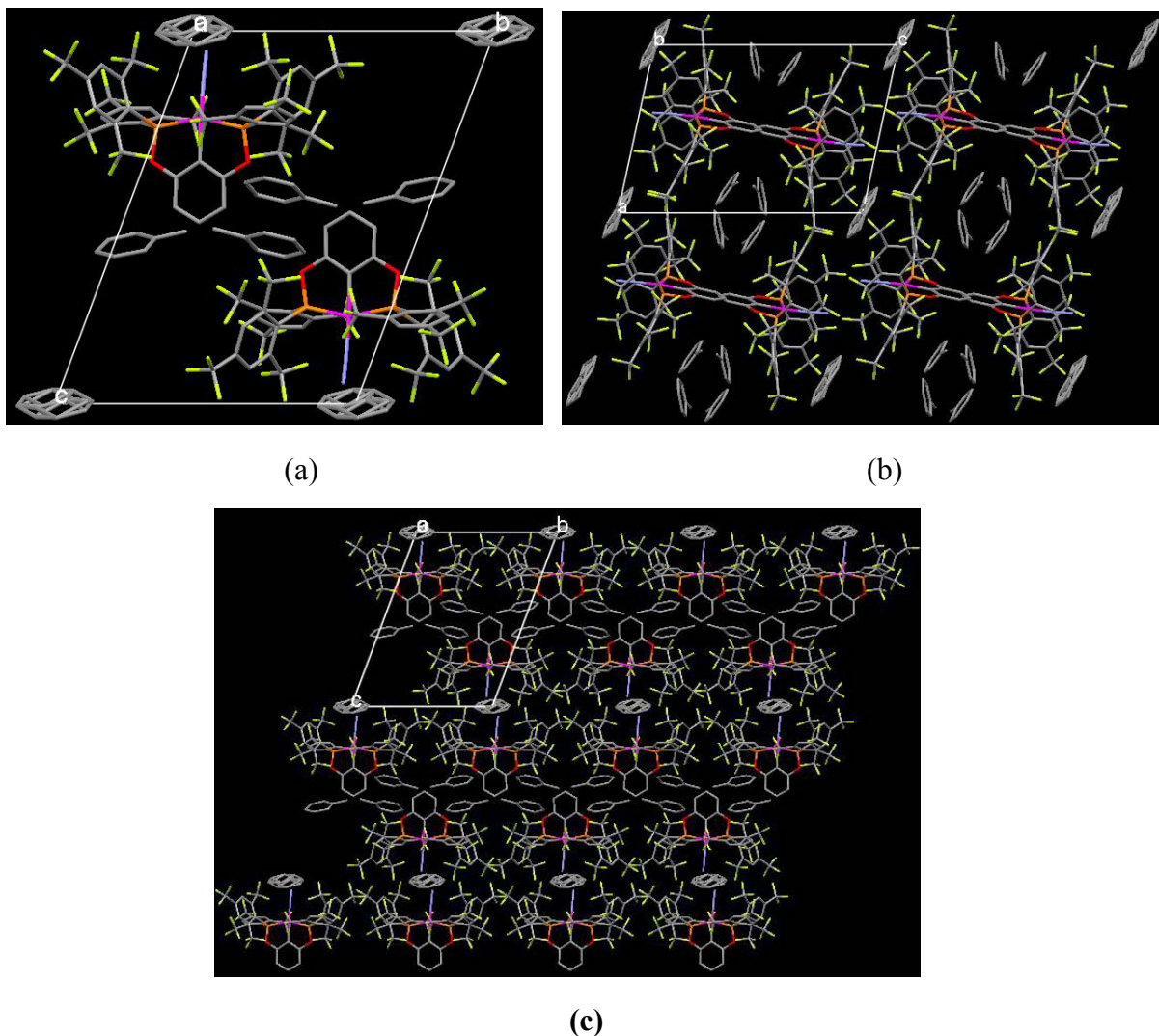
Fig. 6.2 (a) Unit cell of single crystal **[Ir]-N₂** along *a* direction; (b) stacking diagram of single crystal **[Ir]-N₂** along *b* direction; (c) along *a* direction showing the disordered toluene (hydrogen atoms are omitted for clarity).

Exposure of single crystals of **[Ir]-N₂** to one atmosphere (atm) of CO results in a rapid (< 1 min) color change from light red to orange with retention of the single crystal morphology. Examination of this crystal by X-ray diffraction revealed that a carbonyl

complex, **[Ir]-CO**, had been formed. The ORTEP diagram is shown in Fig. 6.1 with crystal data and selected bond lengths and angles summarized in Tables 6.1 and 6.2. The Ir(1)–C(43) and C(43)–O(44) bond distances are 1.937(5) and 1.101(7) Å, respectively and are consistent with analogous bond lengths in a similar pincer Ir(I) CO complex, [C$_6$H$_3$(OPtBu$_2$)$_2$-2,6]Ir-CO, [Ir–C$_{carbonyl}$ = 1.890(3), C–O = 1.130(3) Å]. **[Ir]-CO** exhibits the same space group, and essentially identical lattice parameters as **[Ir]-N$_2$**. The ligand sets of the two systems are superimposable as are the positions of the toluene molecules in the crystal. In short, N$_2$ has been rapidly displaced by CO in crystals of **[Ir]-N$_2$** with complete retention of the atomic positions of all other atoms in the crystal.

Similar ligand substitution reactions in the single crystal occur when **[Ir]-N$_2$** is exposed to ammonia, ethylene or hydrogen. Exposure of single crystals of **[Ir]-N$_2$** to NH$_3$ results in a color change from pale red to dark red in less than 1 min and formation of **[Ir]-NH$_3$**. The ORTEP diagram for **[Ir]-NH$_3$** is shown in Fig. 6.1 and crystal data as well as key bond lengths and angles are contained in Tables 6.1 and 6.2. The Ir(1)–N(1) distance of 2.163(8) Å is close to a similar distance in a square planar pincer Ir(I) ammonia complex.[23] As with the CO complex, identical lattice parameters are observed and all atoms including those of the solvent molecules occupy superimposable positions in the crystal.

Treatment of single crystals of **[Ir]-N$_2$** with one atm of ethylene results in nitrogen displacement to form deep red single crystals of **[Ir]-C$_2$H$_4$** over the course of a few hours. The structure of **[Ir]-C$_2$H$_4$** shows ethylene to be bound perpendicular to the square plane with Ir(1)–C(43) and Ir(1)–C(44) distances of 2.182(8) and 2.168(8) Å (see Table 6.2). The lattice parameters of **[Ir]-C$_2$H$_4$** are identical to those of **[Ir]-N$_2$**, **[Ir]-CO** and **[Ir]-NH$_3$** and

the pincer ligand and solvent molecules are again superimposable with the positions of these groups in the other crystals.

Fig. 6.3 A superposition of crystal structures of **[Ir]-N₂** (violet), **[Ir]-CO** (blue), **[Ir]-NH₃** (cyan), **[Ir]-C₂H₄** (green) and **[Ir]-(H)₂(H₂)** (red).

Exposure of single crystals of **[Ir]-N₂** to H_2 (~1.5 atm) does not lead to any significant color change after several days. However, examination of the single crystal by X-ray diffraction revealed complete loss of nitrogen and formation of an apparent tetrahydride. Since the precise location of metal-bound hydrogen atoms by X-ray diffraction is problematic, the formation of a tetrahydride was confirmed by solution ^{1}H NMR spectroscopy. Dissolution in toluene-d_8 of crystals exposed to H_2 reveal a broad signal at -9.21 ppm (23 °C) in ^{1}H nuclear magnetic resonance spectroscopy (NMR) which integrates for four hydrogens. The chemical shift of -9.21 ppm is consistent with similar pincer iridium tetrahydrides.[22] The structure of this tetrahydride is very likely an Ir(III) dihydride η^2-dihydrogen complex **[Ir]-(H)₂(H₂)** but this cannot be confirmed based on the X-ray data reported here. Again, **[Ir]-(H)₂(H₂)** exhibits the same lattice parameters as **[Ir]-N₂**, **[Ir]-CO**,

[Ir]-NH₃ and **[Ir]-C₂H₄** and identical positions of all ligand and solvent molecules. Fig. 6.3 shows a superposition of **[Ir]-N₂**, **[Ir]-CO**, **[Ir]-NH₃**, **[Ir]-C₂H₄** and **[Ir]-(H)₂(H₂)** which clearly demonstrates the fidelity of ligand and solvent positions in each of these structures.

Under air**,** pale red single crystals of **[Ir]-N₂** acquire a dark green color in less than 12 h and (visually) retain single crystal morphology. X-ray diffraction analysis revealed loss of N₂ and formation of a mono peroxo Ir(III) complex **[Ir]-O₂**. The ORTEP diagram of **[Ir]-O₂** is shown in Fig. 6.1 and bond lengths and angles and crystal data are summarized in Tables 6.2 and 6.1. Oxygen binds to the Ir center in a side-on mode with an O(3)–Ir(1)–O(4) bond angle of 39.3(5)°. The pentacoordinate Ir(III) center has a distorted trigonal bipyrimidal geometry with the two P atoms occupying axial positions. The Ir(1)–O(3) and Ir(1)–O(4) bond distances are 2.052(10) and 2.024(10) Å, respectively. The O(3)–O(4) bond distance of 1.372(15) Å is typical of peroxo complexes[24]. Interestingly, **[Ir]-O₂** is somewhat more distorted from **[Ir]-N₂** compared to the other four systems (Table 6.1) and is composed of at least three (and possible some minor unidentifiable) components as a result of a twin/split structure. The structure was thus refined using a non-standard unit cell so as to be consistent with the other compounds. To date, **[Ir]-O₂** is the first unsaturated iridium peroxo complex characterized by single crystal X-ray diffraction.[24]

The transformations described above all involved displacement of the nitrogen ligand from **[Ir]-N₂**. Other SC–SC interconversions are possible depending on the relative binding strengths of the ligands (Fig. 6.4). For example, we have observed conversion of **[Ir]-C₂H₄** to **[Ir]-CO** (~30 min under one atm of CO) and conversion of **[Ir]-(H)₂(H₂)** to **[Ir]-CO** (less than 1 min under one atm of CO). CO exhibits the strongest binding constant in this series as none of the other ligands studied here displace CO from **[Ir]-CO.** Size selectivity is exhibited

in exchange reactions. Exposure of single crystals of **[Ir]-N₂** to one atm pressure of propylene leads to no displacement of nitrogen over the course of five days. However, exposure of toluene-d₈ solutions of **[Ir]-N₂** to one atm of propylene results in complete displacement of nitrogen in 10 min, establishing that propylene exhibits a higher binding affinity to Ir relative to nitrogen.

Table 6.1. Crystal data and structure refinement summary of **[Ir]-N₂**, **[Ir]-CO**, **[Ir]-NH₃**, **[Ir]-C₂H₄**, **[Ir]-(H)₂(H₂)** and **[Ir]-O₂**.

	[Ir]-N₂	**[Ir]-CO**	**[Ir]-NH₃**	**[Ir]-C₂H₄**	**[Ir]-(H)₂(H₂)**	**[Ir]-O₂**
Formula	$C_{59.5}H_{31}F_{36}Ir$ $N_2O_2P_2$	$C_{60.5}H_{31}F_{36}Ir$ O_3P_2	$C_{59.5}H_{34}F_{36}Ir$ NO_2P_2	$C_{61.5}H_{35}F_{36}Ir$ O_2P_2	$C_{59.5}H_{35}F_{36}Ir$ O_2P_2	$C_{59.5}H_{31}F_{36}Ir$ O_4P_2
crystal system	Triclinic	Triclinic	Triclinic	Triclinic	Triclinic	Triclinic
Space group	P-1	P-1	P-1	P-1	P-1	P-1
a/Å	12.4720(3)	12.4680(5)	12.4758(5)	12.4844(6)	12.4334(11)	12.769(3)
b/Å	14.0891(4)	14.1099(6)	14.0658(5)	14.2365(6)	14.0615(12)	13.637(3)
c/Å	18.6382(5)	18.6021(7)	18.5976(6)	18.5497(9)	18.6354(14)	17.835(3)
α/deg	108.865(2)	108.852(3)	108.155(2)	108.791(3)	108.879(5)	99.088(13)
β/deg	99.010(2)	98.939(3)	99.291(3	98.572(3)	98.956(6)	87.194(15)
γ/deg	97.567(2)	97.635(3)	97.445(3)	98.284(3)	97.594(6)	96.357(17)
V/(Å³)	3002.11(14)	3000.1(2)	3003.56(19)	3020.6(2)	2986.6(4)	3046.3(10)
Z	2	2	2	2	2	2
T/K	100(2)	100(2)	100(2)	100(2)	100(2)	100(2)
$R1$ [$I>2\sigma(I)$]	0.0389	0.0415	0.0556	0.0531	0.0445	0.1090
$wR2$ (all data)	0.0866	0.0916	0.1305	0.1313	0.1001	0.2925

Table 6.2. Selected bond distances (Å) and angles (deg) for single crystals **[Ir]-N₂**, **[Ir]-CO**, **[Ir]-NH₃**, **[Ir]-C₂H₄**, **[Ir]-(H)₂(H₂)** and **[Ir]-O₂**.

Crystals	Ir1–C1	Ir1–P1	Ir1–P2	P1–Ir1–P2	Other
[Ir]-N₂	2.010(3)	2.2660(10)	2.2706(11)	157.85(3)	Ir1-N1=1.977(3), N1-N2=1.106(5), C1-Ir1-N1=174.64(18), N2-N1-Ir1=176.5(5)
[Ir]-CO	2.030(5)	2.2665(17)	2.2729(17)	157.36(4)	Ir1-C43=1.937(5), C43-O44=1.101(7), C1-Ir1-C43=174.9(3), O44-C43-Ir1=174.5(7)
[Ir]-NH₃	2.009(6)	2.2423(16)	2.2465(17)	157.17(6)	Ir1-N1 = 2.163(8), C1-Ir1-N1=174.7(4)
[Ir]-C₂H₄	2.039(5)	2.2733(17)	2.2764(18)	156.87(5)	Ir1-C43=2.182(8), Ir1-C44=2.168(8), C43-C44=1.311(10), C1-Ir1-C44=162.1(3), C1-Ir1-C43=162.9(3), C43-Ir1-C44=35.1(3)
[Ir]-(H)₂(H₂)	2.005(5)	2.2506(18)	2.2511(19)	158.44(5)	
[Ir]-O₂	1.963(13)	2.311(4)	2.293(4)	159.53(12)	Ir1-O3=2.052(10), Ir1-O4=2.024(10), O3-O4=1.372(15), C1-Ir1-O3=161.0(6), C1-Ir1-O4=159.7(6), O3-Ir1-O4=39.3(5)
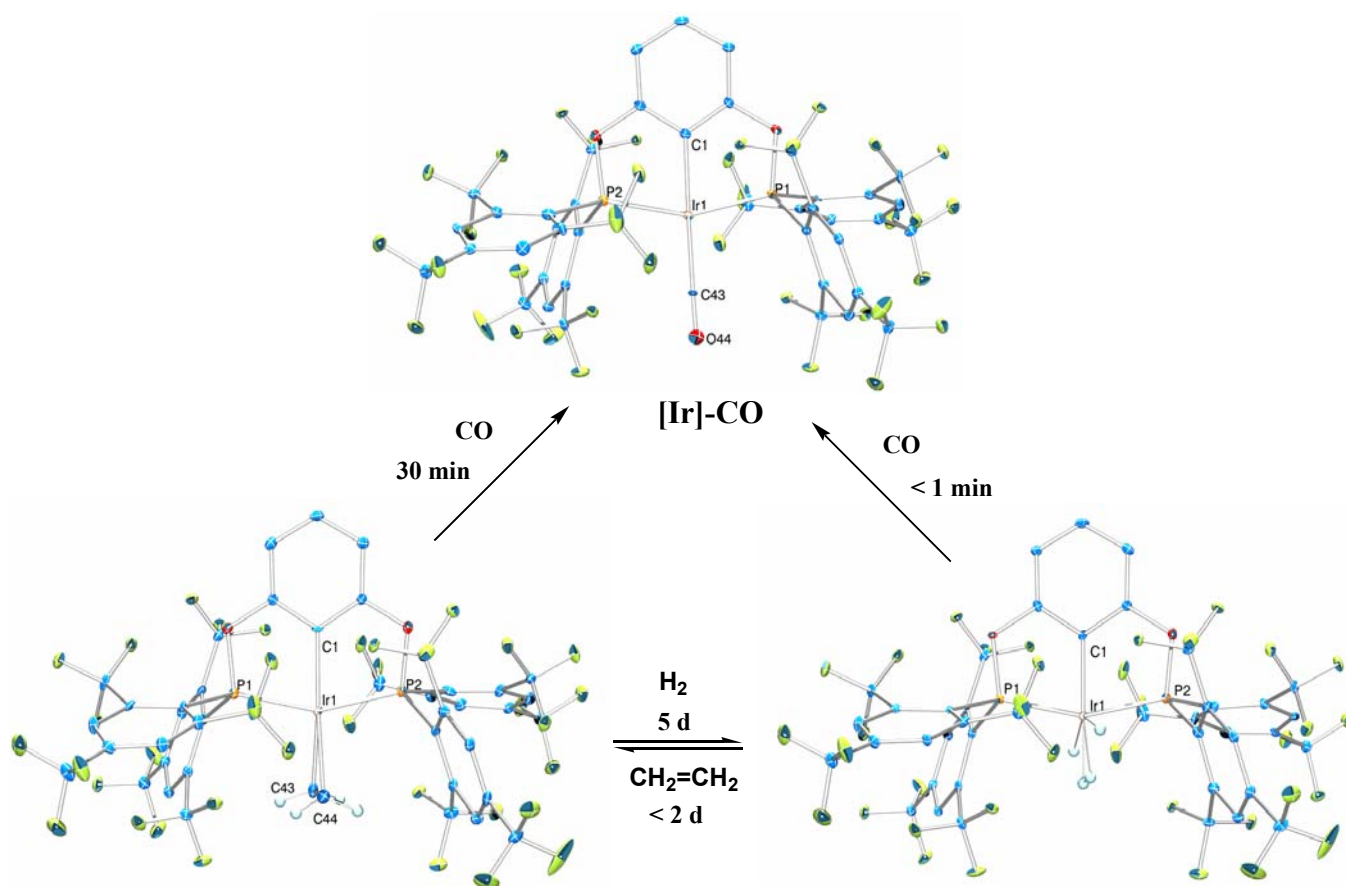
Fig. 6.4 Single-crystal-single-crystal transformation between **[Ir]-CO**, **[Ir]-C₂H₄**, and **[Ir]-(H)₂(H₂)**

Reversible transformations between single crystals of **[Ir]-C₂H₄** and single crystals of **[Ir]-(H)₂(H₂)** have been observed. Exposure of single crystals of **[Ir]-(H)₂(H₂)** to one atm of ethylene results in formation of deep red single crystals of **[Ir]-C₂H₄** and ethane in less than two days, while exposure of **[Ir]-C₂H₄** to one atm of hydrogen generates light red single crystals of **[Ir]-(H)₂(H₂)** and ethane after about five days. Single crystals of **[Ir]-N₂**, **[Ir]-C₂H₄** and **[Ir]-(H)₂(H₂)** are hydrogenation catalysts for mixtures of hydrogen and ethylene. For example, treatment of single crystals of **[Ir]-N₂** containing 0.6 μmol Ir with ~120 equiv of ethylene and 200 equiv of hydrogen (relative to Ir, total pressure ~2.3 atm) at room

164

temperature produced ethane (95% conversion after 5 h). Heating the system at 75 °C increased the hydrogenation rate and led to greater than 99% conversion in 30 min. The solid-state catalysts maintain single crystal morphology throughout the hydrogenation process. The deep-red color of the crystals suggests **[Ir]-C₂H₄** as the dominant catalyst resting state. The single crystals can be reused and show no loss of catalytic activity after three recycles. Hydrogenation of olefins with well-characterized organometallic single crystals appears to be unprecedented.

High selectivity for catalytic hydrogenation of ethylene versus propylene can be achieved using these Ir single crystals. As a comparison experiment, an equimolar mixture of ethylene and propylene was hydrogenated with 10% palladium on carbon. Ethane and propane were formed in an initial ratio of 1:1 indicating no selectivity for hydrogenation using this heterogeneous catalyst. In initial experiments, single crystals of **[Ir]-N₂** or **[Ir]-C₂H₄** (0.6 μmol) were treated with ~200 equiv of hydrogen and 120 equiv each of ethylene and propylene (total pressure ~3.2 atm). Hydrogenation at 25 °C occurs with a turnover frequency of 5/min with formation of ethane and propane in an initial ratio of 1.8:1. Given the fact that propylene cannot penetrate the channels of these crystals, this moderate selectivity was surprising and suggested that hydrogenation may occur unselectively at surface or near-surface sites. We reasoned these sites could be passivated by CO since CO cannot be displaced in the crystals by either ethylene or hydrogen. Thus, crystals of **[Ir]-N₂** were exposed to a CO/N₂ mixture (0.6 vol.% CO, 0.5 equiv relative to Ir) for four days. Using these poisoned crystals, as expected, the rate of hydrogenation is significantly reduced with negligible turnover at 25 °C. However, hydrogenation of a mix of 200 equiv. hydrogen/120 equiv. propylene/12 equiv. ethylene at 75 °C (total pressure ~2.4 atm, 1:10

molar ratio ethylene: propylene) occurs with a turnover frequency of 0.3/min and produces an initial ratio (ca. 15% consumption of ethylene) of ethane : propane of 2.5:1, indicating a dramatic increase in selectivity for ethylene hydrogenation of 25:1. It seems likely that the small fraction of propylene that undergoes hydrogenation may be occurring at surface or near-surface sites that were not poisoned by CO.

Exposure of single crystals of **[Ir]-N$_2$** to high vacuum results in no loss of nitrogen or toluene over one week; yet exposure to CO or NH$_3$ results in conversion of **[Ir]-N$_2$** to **[Ir]-CO** or **[Ir]-NH$_3$**, respectively, within minutes. Furthermore, exposure of single crystals of **[Ir]-N$_2$** to toluene-d$_8$ vapor did not lead to any toluene-h$_8$/toluene-d$_8$ exchange. These observations point to ligand exchange occurring within the crystal rather than nitrogen or solvent loss from the crystal followed by diffusion of CO or NH$_3$ into the nitrogen or solvent-depleted crystal. As noted above, examination of the packing diagram (Fig. 6.2b and Fig. 6.2c) reveals solvent-filled channels along the *a* and *b* axes. The channel along the *a* axis containing disordered toluene molecules appears to offer the best access to the Ir center so it is likely ligands enter this channel. Remarkably, the free volume of the crystal as estimated by the PLATON program[25] using a modified method (see Experimental Section) is only ca. 0.2% (~6 Å^3) per unit cell vol. of 3002 Å^3. It may be that these channels have the ability to temporarily expand in some manner to allow facile ligand diffusion in and out.

Conclusions

In summary, we have observed an unprecedented series of single-crystal-to-single-crystal transformations in which small gaseous ligands CO, NH$_3$, C$_2$H$_4$, H$_2$ and O$_2$ displace N$_2$ from nonporous, molecular single crystals of an iridium(I) pincer complex with retention of the

single crystal morphology. In contrast to the few reports of ligand exchanges in crystals,[15-18] the substitutions reported here occur associatively within the crystal and not by ligand loss followed by uptake of the incoming ligand by the "unsaturated" crystal. Furthermore, although these crystals contain 2.5 equiv of toluene solvent, exchange of bound toluene with toluene vapor does not occur, showing solvent loss is not a requirement for ligand exchange. Size selectivity is exhibited in these exchange reactions. While ethylene displaces nitrogen from single crystals of **[Ir]-N$_2$**, propylene will not. Yet the displacement of nitrogen by propylene occurs readily in solutions of **[Ir]-N$_2$**. Most remarkable is that single crystals of **[Ir]-N$_2$**, **[Ir]-(H)$_2$(H$_2$)** or **[Ir]-C$_2$H$_4$** function as olefin hydrogenation catalysts. When surface and near-surface sites are passivated by treatment with CO, a 25:1 selectivity is observed for hydrogenating ethylene vs propylene, suggesting hydrogenation occurs within the crystal. This is the first demonstration of a catalytic reaction occurring within the interior of a nonporous organometallic crystal, and as expected, this catalytic hydrogenation exhibits high substrate selectivity. These results demonstrate the potential for using nonporous crystals to carry out selective catalytic reactions.

Experimental Section

1. General Experimental Section

General Considerations. All manipulations were carried out using standard Schlenk, high-vacuum and glovebox techniques. Tetrahydrofuran (THF) was distilled under a nitrogen atmosphere from sodium benzophenone ketyl prior to use. Pentane and toluene were passed through columns of activated alumina. Cyclohexane-d$_{12}$, and toluene-d$_8$ were dried with 4 Å molecular sieves and degassed by three freeze-pump-thaw cycles. Di-2,4,6-tris(trifluoromethyl)phenylchlorophosphine[26] and [(COE)$_2$IrCl]$_2$[27] were synthesized as

previously reported. The syntheses of the pincer ligand and complex **[Ir]HCl** have been reported in Chapter three. CO and ethylene gases were purchased from Matheson, H_2 and N_2 gases from National Welders, and NH_3 and propylene gases from Aldrich. All these gases were used as received. Palladium (10 wt %) on activated carbon was purchased from Sigma-Aldrich and used as received. All other reagents were used as purchased from Sigma-Aldrich. NMR spectra were recorded on BRUKER DRX-400, AVANCE-400, and BRUKER DRX-500 MHz spectrometers. ^{1}H and ^{13}C NMR spectra were referenced to residual protio solvent peaks. ^{31}P chemical shifts were referenced to an external aqueous 85% H_3PO_4 standard. ^{19}F chemical shifts have not been referenced.

X-ray data collection and structure determinations. X-ray single-crystal diffraction data for all complexes were collected on a Bruker Smart APEX-2 diffractometer at 100(2) K with Cu Kα radiation (λ= 1.54175 Å) or Mo Kα radiation (λ= 0.71073 Å). The program SAINT was used for integration of the diffraction profiles. All the iridium positions were located by Patterson methods and other non-hydrogen atoms by different syntheses, and refined by full-matrix leastsquares methods with SHELXL (absorption corrections were applied using TWINABS or SADABS program). The hydrogen atoms of the ligand were generated theoretically onto the specific atoms and refined isotropically with fixed thermal factors. Further details for structural analysis are summarized in Table 6.1.

2. Synthesis and experimental section

2.1 Synthesis of single crystals of {C_6H_3-2,6-[OP-($C_6H_2(CF_3)_3$-2,4,6)$_2$]$_2$}Ir-N_2 [Ir]-N_2

A J. Young tube was charged with complex **[Ir]HCl** (5 mg, 3.3 μmol), NaO^{t}Bu (2.5 mg, 26 μmol) and tol-d_8 or tol-h_8 (0.3 mL) in the glovebox. The toluene solution was degassed by three freeze-pump-thaw cycles. The tube was refilled with N_2 gas at -78 °C and then sealed

tightly with a Teflon plug. The tube was slowly rotated with a mechanical stirrer. Block red single crystals suitable for X-ray analysis were obtained over 5–12 h. After filtration, the crystals were washed with 3 × 0.2 mL of cold toluene and dried under high vacuum. Yield: 45% (2.6 mg). ^{1}H NMR (500 MHz, 23 °C, C$_7$D$_8$): 6.85 (s, 3H, 3-H, 4-H and 5-H), 7.86 (s, 8H, Ar(CF$_3$)$_3$-H). ^{31}P{^{1}H} NMR (202 MHz, 23 °C, C$_7$D$_8$): 119.0 (m,b). ^{19}F NMR (471 MHz, 23 °C, C$_7$D$_8$): -52.5 (s, 24F, o-CF$_3$), -64.5 (s, 12F, p-CF$_3$).

2.2 Synthesis of single crystals of [Ir]-CO, [Ir]-NH$_3$, [Ir]-C$_2$H$_4$, [Ir]-(H)$_2$(H$_2$) and [Ir]-O$_2$ ([Ir] = {C$_6$H$_3$-2,6-[OP-(C$_6$H$_2$(CF$_3$)$_3$-2,4,6)$_2$]$_2$}Ir) through single-crystal-to-single-crystal transformations

All the single crystals of **[Ir]-CO**, **[Ir]-NH$_3$**, **[Ir]-C$_2$H$_4$**, **[Ir]-(H)$_2$(H$_2$)** and **[Ir]-O$_2$** were obtained in a quantitative yield by a similar method as described below.

[Ir]-CO. Single crystals of **[Ir]-N$_2$** were added to a 30 mL Schlenk flask in the glovebox. The flask was evacuated and CO gas (1 atm) was then introduced. The flask was sealed and kept at room temperature. In less than 1 min, the red single crystals turned to orange. ^{1}H NMR (500 MHz, 23 °C, C$_6$D$_{12}$): 2.27 (s, 7.5 H, 2.5 × tol.) 6.73 (d, $^{3}J_{H-H}$ = 8.0 Hz, 2H, 3- and 5-H), 6.94 (t, $^{3}J_{H-H}$ = 8.0 Hz, 1H, 4-H), 6.99-7.13 (m, 12.5 H, 2.5 × tol.), 8.13 (s, 8H, Ar(CF$_3$)$_3$-H). ^{31}P{^{1}H} NMR (202 MHz, 23 °C, C$_6$D$_{12}$): 124.2 (s). ^{19}F NMR (471 MHz, 23 °C, C$_6$D$_{12}$): -52.4 (s, 24F, o-CF$_3$), -65.4 (s, 12F, p-CF$_3$).

[Ir]-NH$_3$. Obtained by exposure of single crystals of **[Ir]-N$_2$** to 1 atm of NH$_3$ gas. Visually complete in less than 1 min. ^{1}H NMR (500 MHz, 23 °C, C$_7$D$_8$): -4.46 (s, 3H, NH_3), 6.73 (d, $^{3}J_{H-H}$ = 8.0 Hz, 2H, 3-, and 5-H), 6.80 (t, $^{3}J_{H-H}$ = 8.0 Hz, 1H, 4-H), 7.94 (s, 8H, Ar(CF$_3$)$_3$-H). ^{31}P{^{1}H} NMR (202 MHz, 23 °C, C$_7$D$_8$): 116.9 (m, b). ^{9}F NMR (471 MHz, 23 °C, C$_7$D$_8$): -53.4 (s, 24F, o-CF$_3$), -63.7 (s, 12F, p-CF$_3$).

[Ir]-C₂H₄. Obtained by exposure of single crystals of **[Ir]-N₂** to 1 atm of ethylene gas over 12 h. ^{1}H NMR (500 MHz, 23 °C, C_7D_8): 3.35 (s, b, 4H, Ir-C_2H_4), 7.04 (s, 3H, 3-, 4- and 5-H), 7.81 (s, 8H, Ar(CF$_3$)$_3$-H). ^{31}P{^{1}H} NMR (202 MHz, 23 °C, C_7D_8): 111.3 (s). ^{19}F NMR (471 MHz, 23 °C, C_7D_8): -53.1 (b, 24F, o-CF$_3$), -64.1 (s, 12F, p-CF$_3$).

[Ir]-(H)₂(H₂). Obtained by exposure of single crystals of **[Ir]-N₂** to ca. 1.5 atm of H$_2$ gas in 1 day. ^{1}H NMR (500 MHz, 23 °C, C_7D_8): -9.21 (s, b, 4H, Ir-H_4), 7.06 (s, 3H, 3-, 4- and 5-H), 7.76 (s, 8H, Ar(CF$_3$)$_3$-H). ^{31}P{^{1}H} NMR (202 MHz, 23 °C, C_7D_8): 121.3 (s). ^{19}F NMR (471 MHz, 23 °C, C_7D_8): -52.2 (s, 24F, o-CF$_3$), -64.6 (s, 12F, p-CF$_3$).

[Ir]-O₂. Obtained by exposure of single crystals of **[Ir]-N₂** to air. Visually complete in less than in 12 h. ^{1}H NMR (500 MHz, 23 °C, C_6D_{12}): 2.27 (s, 7.5 H, 2.5 × tol.), 6.78 (d, $^3J_{H-H}$ = 8.0 Hz, 2H, 3- and 5-H), 6.96 (t, $^3J_{H-H}$ = 8.0 Hz, 1H, 4-H), 6.99-7.13 (m, 12.5 H, 2.5 × tol.), 8.11 (s, 8H, Ar(CF$_3$)$_3$-H). ^{31}P{^{1}H} NMR (202 MHz, 23 °C, C_6D_{12}): 106.3 (m, b). ^{19}F (471 MHz, 23 °C, C_6D_{12}): -53.6 (b, 24F, o-CF$_3$), -63.4 (s, 12F, p-CF$_3$).

3. General procedure for hydrogenation of olefins by single crystals

3.1 Preparation of the gaseous mixture

H$_2$/C$_2$H$_4$: In an evacuated 60 mL Kontes flask, ethylene gas (1 atm) was added at room temperature. The flask was then cooled to -130 °C which liquified ethylene. Then 1 atm of H$_2$ gas was added. The flask was sealed tightly with a Teflon plug and warmed to room temperature. The gaseous mixture was added to a 2 mL evacuated J. Young tube through an 8 ml "T"-shape tube at room temperature. Since the total volume of the gaseous mixture was increased from 60 mL to 70 mL, the ethylene pressure decreased from 1 atm to ~0.86 atm. The amount of ethylene in the J. Young tube was calculated using the ideal gas law. The molar ratio of ethylene : H$_2$ was determined by the gas-phase ^{1}H NMR.

H$_2$/C$_2$H$_4$/C$_3$H$_6$: The same procedure as for H$_2$/C$_2$H$_4$ was used except that 1 atm of propylene was added at room temperature, ethylene gas was added at -78 °C, and H$_2$ gas was added at -130 °C.

3.2 Hydrogenation of olefins by single crystals

Single crystals of **[Ir]-N$_2$**, **[Ir]-C$_2$H$_4$** or **[Ir]-(H)$_2$(H$_2$)** (0.6–1.2 μmol) were added to a 2 mL J. Young tube. The tube was evacuated and the H$_2$/C$_2$H$_4$ or H$_2$/C$_2$H$_4$/C$_3$H$_6$ gaseous mixture was then introduced. The NMR tube was sealed tightly with a Teflon plug and kept at room temperature or heated at 75 °C. Periodically, the hydrogenation reaction was monitored by the gas-phase ^{1}H NMR.

3.3 Hydrogenation of ethylene vs propylene by palladium (10 wt%) on activated carbon

Palladium (10 wt %) on activated carbon **(**0.9 μmol**)** was added to a 2 mL J. Young tube. The tube was evacuated and the H$_2$/C$_2$H$_4$/C$_3$H$_6$ gaseous mixture was then introduced (A 1.0:1.0 mol ratio of C$_2$H$_4$:C$_3$H$_6$ was used). The NMR tube was sealed tightly with a Teflon plug and kept at room temperature. Periodically, the hydrogenation reaction was monitored by the gas-phase ^{1}H NMR.

3.4 Treatment of single crystals with CO

To a 500 mL Schlenk flask filled with 1 atm of N$_2$, CO (3 mL) was added via a syringe. The CO/N$_2$ gaseous mixture (2 mL, 1 atm) was then introduced into a J. Young tube of single crystals containing 0.6 μmol of **[Ir]-N$_2$**. The J. Young tube was sealed tightly with a Teflon plug and kept at room temperature for 4 days.

4. Calculation of void volume by PLATON

The calculation of **[Ir]-N$_2$** by PLATON software indicates 0% void volume. However, the calculation of the disordered toluene was incorrect because PLATON recognized it as C$_9$H$_{10}$

instead of C_7H_8. Thus, a modified method was used by replacing the disordered toluene with an ordered toluene. The *disordered* toluene (one equiv. per unit cell) was deleted from the structure and 6.3% of void volume was observed; while the removal of *ordered* toluene (two equiv. per unit cell) formed 12.2% of void volume. Thus, the real void volume should be $(6.3\% - 12.2\%/2) * 3002 \ \text{Å}^3$ / unit cell = 6 Å^3 / unit cell.

References and Note

(1) Foxman, B. M.; Ward M. D. *Molecules in the solid state*, MRS, Warrendale, Pa, **2007**.

(2) Vittal, J. J. *Coord. Chem. Rev.* **2007**, *251*, 1781-1795 and references cited therein.

(3) Cotton, F. A.; Li, Z.; Murillo, C. A.; Wang X.; Yu, R.; Zhao, Q. *Inorg. Chem.* **2007**, *46*, 3245.

(4) Hu, C.-H.; Englert, U. *Angew. Chem., Int. Ed.* **2006**, 45, 3457.

(5) Iordanidis, L. ; Kanatzidis, M. G. *Angew. Chem., Int. Ed.* **2000**, *39*, 1928.

(6) Ghosh, S. K.; Kaneko, W.; Kiriya, D.; Ohba, M. and Kitagawa, S. *Angew. Chem., Int. Ed.* **2008**, *47*, 8843.

(7) Haneda, T.; Kawano, M.; Kawamichi, T.; Fujita, M. *J. Am. Chem. Soc.* **2008**, *130*, 1578.

(8) Ghosh, S. K.; Zhang, J.; Kitagawa, S. *Angew. Chem., Int. Ed.* **2007**, *46*, 7965.

(9) Kawano, M.; Fujita, M. *Coord. Chem. Rev.* **2007**, *251*, 2592 and references cited therein.

(10) Garcia-Garibay, M. A. *Angew. Chem., Int. Ed.* **2007**, *46*, 8945.

(12) Kobatake, S.; Takami, S.; Muto, H.; Ishikawa, T.; Irie, M. *Nature* **2007**, *446*, 778.

(13) Bucar, D.; MacGillivray, L. R. *J. Am. Chem.Soc.* **2007**, *129*, 32.

(14) Atwood, J. L.; Barbour, L. J.; Jerga, A.; Schottel, B. L. *Science* **2002**, *298*, 1000.

(15) Libri, S.; Mahler, M.; Espallargas, G. M.; Singh, D. C. N. G.; Soleimannejad, J.; Adams, H.; Burgard, M. D.; Rath, N. P.; Brunelli, M.; Brammer, L. *Angew. Chem., Int. Ed.* **2008**, *47*, 1693.

(16) Das, S. K.; Supriya, S. *J. Am. Chem. Soc.* **2007**, *129*, 3464-3465.

(17) Albrecht, M.; Lutz, M.; Spek, A. L.; van Koten, G. *Nature* **2000**, *406*, 970-974.

(18) Lennartson, A.; Håkansson, M.; Jagner, S. *New J. Chem.* **2007**, *31*, 344-347.

(19) In the case of **[Ir]-O$_2$** some crystal splitting is observed but the single crystal is not converted to a microcrystalline powder.

(20) Gordon, A. J.; Ford, R. A. *The Chemist's Companion* p 107, John Wiley & Sons, New York, **1972**.

(21) Ghosh, R.; Kanzelberger, M.; Emge, T. J.; Hall, G. S.; Goldman, A. S. *Organometallic*

2006, *25*, 5668.

(22) Göttker-Schnetmann, I.; White, P. S.; Brookhart, M. *Organometallic* **2004**, *23*, 1766.

(23) Kanzelberger, M.; Zhang, X.; Emge, T. J.; Goldman, A. S.; Zhao, J.; Incarvito, C.; Hartwig, J. F. *J. Am. Chem. Soc.* **2003**, *125*, 13644.

(24) Williams, D. B.; Kaminsky, W.; Mayer, J. M.; Goldberg, K. I. *Chem. Comm.* **2008**, 4195.

(25) Spek, A. L. *Platon, J. Appl. Cryst.* **2003**, *36*, 7.

(26) Batsanov, A. S.; Cornet, S. M.; Dillon, K. B.; Goeta, A. E.; Hazendonk, P.; Thompson, A. L. *Dalton Transactions* **2002**, 4622.

(27) Herde, J. L.; Lambert, J. C.; Senoff, C. V. *Inorganic Syntheses* **1974**, *15*, 18.